THE UNROOFING HISTORY OF THE FUNERAL MOUNTAINS METAMORPHIC CORE COMPLEX, CALIFORNIA

by

JAMES DAVID ROBERT APPLEGATE

B.S. Geology, Yale University
(1989)

Submitted to the Department of Earth, Atmospheric, and Planetary Sciences in Partial Fulfillment of the Requirements for the Degree of

DOCTOR OF PHILOSOPHY

at the MASSACHUSETTS INSTITUTE OF TECHNOLOGY

May, 1994

Signature of Author _____
Department of Earth, Atmospheric, and Planetary Sciences
May, 1994

Certified by _____
Kip V. Hodges
Thesis Advisor

Accepted by _____
Thomas H. Jordan
Department Head

THE UNROOFING HISTORY OF THE FUNERAL MOUNTAINS METAMORPHIC CORE COMPLEX, CALIFORNIA

by

James David Robert Applegate

Submitted to the Department of Earth, Atmospheric, and Planetary Sciences at the Massachusetts Institute of Technology on May 16, 1994, in Partial Fulfillment of the Requirements for the Degree of Doctor of Philosophy in Geology

ABSTRACT

High-grade metamorphic rocks are exposed in the northern Funeral Mountains, located on the eastern side of Death Valley in southeastern California. These rocks are in the footwall of a Late Miocene detachment system that separates them from unmetamorphosed Proterozoic to Recent sedimentary rocks in its hanging wall. A protracted tectonic history of burial and unroofing for this metamorphic core complex is reflected by multiple deformational phases and a complex thermal evolution for the high-grade rocks. This study combines field mapping and structural analysis with U-Pb and $^{40}Ar/^{39}Ar$ geochronology to determine the sequence and timing of deformation and cooling history for rocks in the footwall of the Funeral Mountains metamorphic core complex. The results indicate several discrete episodes of extension experienced by the core rocks since Early Cretaceous burial and metamorphism. These episodes took place in Late Cretaceous and Late Miocene to Recent time and are responsible for the exhumation of the core rocks from mid-crustal depths. A substantial amount of unroofing was accommodated by movement on extensional shear zones within the core in Late Cretaceous time long before extension took place on the core-bounding detachment system in Late Miocene to Recent time. The youngest deformation in the core has taken place over the past 6 My and may be related to a component of transform-normal extension on the right-lateral Northern Death Valley fault zone.

The timing of shear zone formation and associated ductile attenuation of the high-grade rocks is constrained by U-Pb zircon and monazite ages on pre/synkinematic and postkinematic pegmatite dikes. Deformation was taking place by 72 Ma and had ended by 70 Ma except for late-stage folding that may have continued into earliest Paleocene time. The thermal history experienced by high-grade rocks in the Funeral Mountains reflects the tectonic evolution of the complex. Cooling through the closure temperature for argon in hornblende took place in Late Cretaceous time synchronous with extensional deformation. A range of ages for muscovites and biotites indicates that slow cooling took place over much of the Tertiary Period. K-feldspar cooling ages are consistent with previously published fission-track data that indicate a period of rapid cooling in Late Miocene time, synchronous with brittle movement on the core-bounding detachment system. Rocks in the hanging wall of extensional shear zones within the core yield much older cooling ages, compatible with the interpretation that these structures represent a significant structural break within the core.

Thesis advisor: Kip V. Hodges, Professor of Geology

"The strata are greatly disturbed and dislocated..."

— G. K. Gilbert (1875) on his traverse through Boundary Canyon at the northern end of the Funeral Mountains

ACKNOWLEDGMENTS

This section represents a unique opportunity to make a small payment on the immense debt of gratitude that I owe to mentors, colleagues, friends, and family – a debt so large that even my student loans pale in comparison. Since I never showed much interest in rocks as a kid, except as a substrate on which to clamber about, my first thanks go to a diverse group of teachers who have been excellent guides along my serendipitous path to geology. I thank Sheldon Rabinowitz, James McKenrick, and Rodney Crawford, the first for letting my interest in geography run wild in fifth grade, the second for letting my interest in history run wild in high school, and the third just for letting me run. To them and to many other teachers in Chambersburg, Pennsylvania, I am grateful for a good start on this long road. I thank William Cronon at Yale for letting me write about geology as a history major and Mark Brandon for giving a history major a home in the geology department. Jeff Lacy and Bob Shrock at Shippensburg University helped to get me started in the right direction in chemistry and geology, respectively.

Hopefully to his credit, my pre-eminent mentor at M.I.T. has been my advisor, field boss, and good friend Kip Hodges, the thesis-smashing pig-dog himself. Kip has given me incredible freedom to pursue this project, but at the same time has always kept his door open, providing guidance and answering inane questions. This dissertation owes its genesis and much of the credit for its fruition to Kip. Any progress I have made in becoming a scientist and a scientific writer is thanks to him. Larky and Rachel Hodges (and Star!) are to be thanked for their hospitality over the years. Clark Burchfiel has been very generous in sharing his encyclopedic knowledge of the Cordillera (not to mention the rest of the Earth). John Grotzinger introduced me to stratigraphy (seeing as how I attended a heathen undergraduate institution that had no sedimentologists). Roger Burns attempted to salvage my woeful mineral identification skills, and he will be sorely missed. I thank Wiki Royden for being a fabulous teacher of fabulously long equations, and Sam Bowring for introducing me to the world of isotope geochemistry. Clark, Kip, Doug Walker, and Chris Marone are gratefully acknowledged for serving as my thesis committee and thanked for making the whole experience productive and (almost) pleasant. Chris also gets the good samaritan award for push-starting my car down Memorial Drive on a dark and stormy night two winters ago.

As much as I have learned from my teachers, I have no doubt learned more from my fellow graduate students. A great debt of gratitude goes to my former officemates and

current e-mail buddies Allison MacFarlane and Dave Dinter. They have been wonderful accomplices over the years and I hope will continue to be for many years to come (Greece yet beckons!). Early on, Larry McKenna showed me how to handle my advisor, and Julio Friedman provided a refreshing dose of pure entropy. Allison, Dave, and Larry (along with Jim Knapp) get special thanks for their theses, which have sat in a large heap (thanks for the desk space, Jen!), providing guidance in style and content for this next addition to the heap. I acknowledge Eric Buchovecky for his awesome insight and for his choice to share that insight with high-school physics students. Dave McCormick, Dawn Sumner, Beverly Saylor, Roy Adams, Pete & Paula, and Mark Simons have provided osmotic learning and good fellowship as fellow travelers over many years. The same goes for the present band of Kip students – Martha, Meg, Audrey, Anke, and Ellen (do you see any pattern here?). Thank you for everything, Martha! Dave Hawkins and C.J. Northrup, both of them geologist's geologists, have provided endless hours of discussion (scientific and otherwise). Martha and C.J. deserve extra credit for having read this entire thesis, correcting some of the more egregious blunders. Erchie Wang and Richard Beck have provided late-night companionship during the final push. Up on the 11th floor, Drew Coleman has been one big ray of sunshine, and I am grateful to him and Clark Isaksen for their U-Pb help. The Bills (Hames and Olszewski) have been a constant help on all matters noble (gaseous and otherwise). Pat Walsh and Nancy Dallaire both have been an immense help in unravelling the MIT bureaucracy as have Anita Killian and more recently Cindy Hanes. Thanks also to John Harbison and my fellow quartet members for providing a wonderful diversion, especially during this past semester.

Several months at the University of Kansas in (hilly!) Lawrence have produced another group of colleagues and friends. Doug Walker has been a second advisor on this project, and I am grateful for his scientific guidance, his hospitality, and his culinary adroitness. Larry McKenna (he turns up in the strangest places!) provided hospitality, his bicycle, and a great deal of clean lab help. Thanks also to the rest of the McSpiz household for putting me up that first April — Liz, Elise, Rebekah (two weeks old at the time), Paducah, and Amargosa. Mark Martin and Drew Coleman (again!) taught me the ins and outs of U-Pb geochronology. Thanks to them and Marlee Babinsky, Rob Fillmore, John Lynn, Lynn John, Dave Gonzalez, Steve Hoffine, and Sharon Stern. Also thanks to Doug, Daphne, Mark, Larry, and Rob for many excellent runs.

My other home away from home has been Death Valley and the Funeral Mountains. The geologic community there has been very helpful and welcoming to me over the years.

My greatest thanks go to Lauren Wright, whose recollection of areas he mapped thirty years ago puts to shame my recollection of areas I mapped the day before. His hospitality and help both in Shoshone and back in State College are gratefully acknowledged. I also acknowledge the help of Bennie Troxel, the other half of the dynamic duo that has contributed so much to the knowledge of the Death Valley region. Cathy Summa has provided repeated assistance on Johnnie Formation stratigraphy and desert logistics, and Tony Prave guided me on a wonderful journey into the (uncooked) Pahrump Group in southern Death Valley. I would like to acknowledge Tim Coonan and Doug Threloff at Death Valley National Monument for their logistical support (bureaucrax clamantis in deserto). George Hagle and Dave Glatstein provided aeronautical support for aerial photography of the Funeral Mountains. Former residents of FUMP and The Cottage, they are far better men than Ed Meese ever will be. Field assistance is crucial when one is foolish enough to work in the desert during May and June, and I would like to thank Erika Anderson, Martin Anderson, and Kyle (Anderson) Blasch for keeping me healthy and happy and for being wonderful sounding boards. I am particularly grateful to Kyle for choosing the Funeral Mountains as a training ground for boot camp.

For two field seasons and for twenty-four years before that, Martin Anderson has taught me what it means to be a scientist with his intense curiosity and openness to ideas. Now science has lost an extraordinary biologist but engineering has gained an equally extraordinary bio-mechanical engineer. Thank you, Martin, for your friendship — we will always have Chateau le Haute Fete. And thank you, Martin and Rachel, for introducing me to Heidi Stoltzfus. I owe her the past year of blissful happiness that I hope will bloom into a lifetime of the same.

Jeffrey Small, Meg Coleman (welcome back from Nepal!), Buckmaster DeWolf, Rosemary Ratcliff, Maria Masucci, and Shane Pelechaty have been my housemates over the past five years, and I thank them for providing a refuge from M.I.T. and for many shared meals at 14 Line Street and 657 Washington Street — first thing, let's dine with the lawyers!

I thank my family for more love and support than I can ever give back, and especially for the next generation, half of whom are the same age as this project: Virginia, Jesse, Jamey, Abigail, Cea, and Henry. Finally, I would like to acknowledge my namesake, James David Strait (1899-1993), for setting the example of a purposeful life.

To James and Joan Applegate
for their unconditional love and support

and to John Applegate
for suggesting a less-traveled road

TABLE OF CONTENTS

CHAPTER 1

INTRODUCTION

Geologists working in the Basin and Range early in this century recognized exposures of deep metamorphosed rocks separated from shallow unmetamorphosed rocks by low-angle faults (e.g. Emmons, 1907; Ransome et al., 1910). The significance of these structures, however, was not recognized because of the pre-eminence of G. K. Gilbert's block-faulting model, which held that Basin and Range extension was the result of movement on high-angle faults, producing small lateral displacements (Gilbert, 1874). For the next 50 years, geologists mapped these low-angle structures as thrust faults despite the younger over older relationships of hanging wall to footwall and normal-sense offset. During the early 1970's, the existence of low-angle extensional faults, referred to as detachments, was reconfirmed (e.g. Anderson, 1971; Armstrong, 1972; Wright and Troxel, 1973), and the term "metamorphic core complex" was first coined in 1974 by Peter Coney for these tectonic windows into the middle crust (Coney, 1974). It was not until the 1980's, however, that low-angle normal faulting became widely recognized as the mechanism for large amounts of Cenozoic extension (e.g. Wernicke, 1981), and the core complexes became the focus of widespread study. Since that time, much of the work on core complexes has focused on extensional unroofing accommodated by core-bounding detachment faults in Tertiary time. The earlier Mesozoic history of these core complexes was thought to comprise the burial and metamorphism of these rocks at mid-crustal depths during crustal thickening that accompanied the development of the Sevier fold-and-thrust belt (Armstrong, 1968). This two-stage evolution of Mesozoic burial followed by Cenozoic unroofing, however, does not account for a growing body of evidence which suggests that extension may have played an important role in the hinterland of the thrust belt during Mesozoic time (Hodges and Walker, 1992).

The Funeral Mountains metamorphic core complex in California is a compelling example of this more complicated unroofing history. Located on the eastern side of Death Valley, the northern part of the range is an exposure of mid-crustal rocks beneath a Late Miocene core-bounding detachment, part of the fault system first recognized by Spurr (1901) as a low-angle extensional fault. These rocks were tectonically emplaced at mid-crustal depths by Mesozoic thrust faults, undergoing metamorphism up to upper amphibolite facies conditions as a result. A significant component of the unroofing of these rocks, however, took place in Late Cretaceous time on extensional shear zones within the core complex. This extensional event was accompanied by the intrusion of a suite of granitoid dikes and sills, providing tight timing constraints on the age of extension. Ductile fabrics that dominate the core rocks are related to this early extensional event, which occurred more than 50 My before Late Miocene unroofing took place on the brittle core-bounding detachment.

This project in the Funeral Mountains metamorphic core complex began nearly a decade ago when Kip Hodges and Doug Walker started their investigation of the thermobarometric history of high-grade rocks within the core. Their Gibbs-method modeling of pressure-temperature paths combined with previously reported $^{40}Ar/^{39}Ar$ geochronology by Ed DeWitt suggested that a substantial amount of unroofing took place in Late Cretaceous time (Hodges and Walker, 1990; DeWitt et al., 1988). That possibility was the genesis of the current study, which combines detailed structural mapping with structural analysis to work out the sequence and style of deformational events within the core and relate those events to macroscopic structures present within and around the core complex. U-Pb geochronology was used to obtain precise ages on pegmatite dikes which constrain the age of several deformational events. It is also applied to determine the high-temperature end of the thermal history. $^{40}Ar/^{39}Ar$ thermochronology is used to work out the cooling history of rocks from several structural levels within the core. These techniques, combined with

earlier thermobarometry, provide a great deal of insight into the mechanisms and timing of unroofing within the footwall of the core complex.

This dissertation is arranged in four chapters beyond the introduction, each written as stand-alone papers intended for journal publication. Chapter 2 covers the structural evolution of the Funeral Mountains metamorphic core complex. When published, it will have Kip Hodges as a coauthor. Chapter 3 documents the age and significance of Late Cretaceous extensional shear zones within the core complex. It is only slightly modified from a *Geology* article with Doug Walker and Kip Hodges as co-authors (Applegate et al., 1992). The modifications are discussed in a brief preface to the chapter. Chapter 4 presents the results of U-Pb geochronology and $^{40}Ar/^{39}Ar$ thermochronology undertaken to deduce the time-temperature history of the core rocks, including the age of metamorphism, intrusion of the granitoid and pegmatite dikes, and the cooling history for the core rocks. When published, this chapter will have both Hodges and Walker as coauthors. Chapter 5 explores the possibility that Miocene to Recent, southwest-directed extension in the Funeral Mountains is related to oblique slip on the Northern Death Valley fault zone.

Geologic field work took place during three field seasons in May and June of 1990, 1991, and 1992. Some of the work at lower elevations took place during shorter seasons in January and February of 1991, 1992, and 1993. The results of field mapping are presented in Plate 1, which uses the Chloride Cliff 15-minute topographic sheet as a base map. The U-Pb analyses were carried out with Doug Walker at the University Kansas Isotope Geochemistry Laboratory. The $^{40}Ar/^{39}Ar$ analyses were carried out at the Cambridge Laboratory for Argon Isotope Research (CLAIR) at M.I.T. with the help of Kip Hodges, Bill Hames, and Bill Olszewski.

My work is only the most recent contribution to our understanding of the Funeral Mountains. Geologic work on the Funeral Mountains has a history spanning over 100 years with the earliest geological description of the Funeral Mountains coming from G. K.

Gilbert who passed through Boundary Canyon, leaving the epigram to this dissertation behind (Gilbert, 1875). The Funeral Mountains were first mapped by Levi Noble and Lauren Wright (Noble and Wright, 1954), and their mapping was incorporated into the Death Valley sheet of the Geologic Map of California in 1958 (Jennings, 1958). That map shows the core rocks bounded by extensional faults. Much earlier, Spurr (1901) mapped the adjacent Bullfrog Hills metamorphic terrain, arguing for the existence of a low-angle detachment, a surface correlative with the Boundary Canyon detachment (Maldonado, 1990). Hunt and Mabey (1966) recognized that the metamorphic rocks in the Funeral Mountains occurred in a fenster (i.e. tectonic window) and interpreted the low-angle, core-bounding structures to be thrust faults. The soon-to-be-published map of Wright and Troxel (1994) represents the seminal mapping in this area during the 1960's. Early geochronologic work in the area was done by Wasserberg et al. (1959), who dated muscovite from a pegmatite in Monarch Canyon using conventional K-Ar dating as part of a regional study of Proterozoic basement terrains. More recently, DeWitt et al. (1988) conducted a $^{40}Ar/^{39}Ar$ study of high-grade rocks, noting that argon systematics were greatly complicated by an excess component. Petrologic and thermobarometric studies have been done by Labotka (1980), Giaramita (1984), Hodges and Walker (1990), and Hoisch and Simpson (1993). Both Giaramita (1984) and Hoisch and Simpson (1993) also conducted structural studies of the core-bounding detachment and core rocks.

ACKNOWLEDGMENT OF SUPPORT

My graduate work has been supported by a National Science Foundation Graduate Fellowship, teaching assistantships, and by NSF grants EAR90-05238 and EAR92-18721 awarded to Kip Hodges. Partial laboratory support was provided by grant EAR-8904007 to Doug Walker and EAR 89-17150 and 91-06031 to Hodges. Additional support from a Geological Society of America student research grant and the Student Research Fund of the

Department of Earth, Atmospheric, and Planetary Sciences at M.I.T. are also gratefully acknowledged.

REFERENCES

Anderson, R. E., 1971, Thin skin distension in Tertiary rocks of southeastern Nevada: Geological Society of America Bulletin, v. 82, p. 43-58.

Applegate, J. D. R., Walker, J. D., and Hodges, K. V., 1992, Late Cretaceous extensional unroofing in the Funeral Mountains metamorphic core complex, California: Geology, v. 20, p. 519-522.

Armstrong, R. L., 1968, Sevier orogenic belt in Nevada and Utah: Geological Society of America Bulletin, v. 79, p. 429-458.

Armstrong, R. L., 1972, Low-angle (denudation) faults, hinterland of the Sevier orogenic belt, eastern Nevada and western Utah: Geological Society of America Bulletin, v. 83, p. 1729-1754.

Coney, P. J., 1974, Structural analysis of the Snake Range "décollement," east-central Nevada: Geological Society of America Bulletin, v. 85, p. 973-978.

DeWitt, E., Sutter, J. F., Wright, L. A. and Troxel, B. W., 1988, Ar-Ar chronology of early Cretaceous regional metamorphism, Funeral Mountains, California — A case study of excess argon: Geological Society of America Abstracts with Programs, v. 20, p. A16.

Emmons, W. H., 1907, Normal faulting in the Bullfrog district: Science, v. 26, p. 221.

Giaramita, M. J., 1984, Structural evolution and metamorphic petrology of the Monarch Canyon area, northern Funeral Mountains, Death Valley, California [M.S. thesis]: University of California, Davis, 145 pp.

Gilbert, G. K., 1874, Preliminary geologic report, expedition of 1872: U.S. geographical and geological survey west of the one hundredth meridian (Wheeler Survey) progress report, p. 48-52.

Gilbert, G. K., 1875, Report on the geology of portions of Nevada, Utah, California, and Arizona examined in the years 1871 and 1872, *in* Report on U.S. Geographical and Geological Surveys West of the 100th Meridian 3, Geology, Pt. 1, p. 17-187.

Hodges, K. V. and Walker, J. D., 1990, Petrologic constraints on the unroofing history of the Funeral Mountains metamorphic core complex, California: Journal of Geophysical Research, v. 95, p. 8437-8445.

Hodges, K. V., and Walker, J. D., 1992, Extension in the Cretaceous Sevier orogen, North American Cordillera: Geological Society of America Bulletin, v. 104, p. 560-569.

Hoisch, T. D., and Simpson, C., 1993, Rise and tilt of metamorphic rocks in the lower plate of a detachment fault in the Funeral Mountains, Death Valley, California: Journal of Geophysical Research, v. 98, p. 6805-6827.

Hunt, C. B., and Mabey, D. R., 1966, Stratigraphy and structure of Death Valley, California: U.S. Geological Survey Professional Paper 494-A, 165 pp.

Jennings, C. W., 1958, Geologic map of California, Death Valley sheet: California Division of Mines and Geology, scale 1:250,000.

Labotka, T. C., 1980, Petrology of a medium-pressure regional metamorphic terrane, Funeral Mountains, California: American Mineralogist, v. 65, p. 670-689.

Maldonado, F., 1990, Structural geology of the upper plate of the Bullfrog Hills detachment fault system, southern Nevada: Geological Society of America Bulletin, v. 102, p. 992-1006.

Noble, L. F. and Wright, L. A., 1954, Geology of the central and southern Death Valley region, California, *in* R. H. Jahns ed., Geology of southern California: California Division of Mines and Geology Bulletin 170, p. 143-160.

Ransome, F. L., Emmons, W. H. and Garrey, G. H., 1910, Geology and ore deposits of the Bullfrog district, Nevada: U.S. Geological Survey Bulletin, v. 407, 130 pp.

Spurr, J. E., 1901, Origin and structure of basin ranges: Geological Society of America Bulletin, v. 12, p. 217-270.

Wasserburg, G. J., Wetherill, G. W., and Wright, L. A., 1959, Ages in the Precambrian terrain of Death Valley, California: Journal of Geology, v. 67, p. 702-708.

Wernicke, B. P., 1981, Low-angle faults in the Basin and Range Province—Nappe tectonics in an extending orogen: Nature, v. 291, p. 645-648.

Wright, L. A., and Troxel, B. W., 1973, Shallow-fault interpretation of Basin and Range structure, southwestern Great Basin, *in* K. A. de Jong and R. Scholten ed., Gravity and tectonics: New York, John Wiley and Sons, p. 397-407.

Wright, L. A. and Troxel, B. W., 1994, Geologic map of the central and northern parts of the Funeral Mountains and adjacent areas, Death Valley region, southern California, scale 1:48,000: U.S. Geol. Surv. Misc. Invest. Ser. I-2305, in press.

CHAPTER 2

STRUCTURAL EVOLUTION OF THE FUNERAL MOUNTAINS METAMORPHIC CORE COMPLEX, CALIFORNIA

David Applegate
Department of Earth, Atmospheric, and Planetary Sciences
Massachusetts Institute of Technology

ABSTRACT

Several generations of ductile fabrics have affected high-grade metamorphic rocks in the Funeral Mountains metamorphic core complex, southeastern California. These fabrics developed during burial and subsequent unroofing of the core rocks during Mesozoic and Cenozoic time. An early foliation and associated isoclinal folding are related to burial and metamorphism at mid-crustal levels by thrust faulting in Early Cretaceous time. This early foliation has been transposed and overprinted by Late Cretaceous extensional deformation that produced the dominant foliation in the core rocks as well as mineral and stretching lineations. These fabrics formed in conjunction with movement on extensional shear zones within the core. Subsequent tight to isoclinal folding and crenulations represent a late stage of the same event. A second extensional event in Late Miocene time was accommodated by brittle movement on the core-bounding Boundary Canyon detachment. Doming of the core rocks is associated with mesoscopic dome-and-basin folding and boudinage, and it appears to have initiated before brittle movement on the detachment. The most recent extension postdates detachment movement and is in a direction orthogonal to that of both the earlier events. A diabase dike that cuts all ductile fabrics in the high-grade rocks yields a $^{40}Ar/^{39}Ar$ amphibole age of 33.2 ± 0.7 Ma. Late Cretaceous extension on the intracore shear zones is responsible for a substantial portion of the unroofing of rocks that represent the deepest exposure of Mesozoic crust in the Death Valley region. These high-grade rocks are juxtaposed across the shear zones beneath rocks from shallower structural levels in the

Mesozoic crust. The shear zones appear to have excised thrust plates and may represent reactivation of the décollement for the Mesozoic thrust belt. This extension may be the result of gravitationally driven spreading as compression waned due to a transpressional plate boundary.

INTRODUCTION

Cordilleran metamorphic core complexes are tectonic windows in which rocks that were at mid-crustal depths during Mesozoic time are exposed in the footwall of a Tertiary low-angle detachment system (Davis and Coney, 1979). This fault system separates brittlely deformed upper plate rocks from highly metamorphosed, mylonitic rocks in the lower plate (Armstrong, 1982). The fabric in these ductilely deformed rocks often parallels the detachment surface, and sense-of-shear indicators as well as stretching fabrics indicate transport parallel to motion on the detachment (Wernicke, 1992). As a result, numerous authors have viewed these ductile and brittle structures as part of a continuum associated with the progressive unroofing of mid-crustal rocks through the brittle-ductile transition in Tertiary time (e.g., Hodges et al., 1987; Davis and Lister, 1988). Although the kinematics are such that some of the footwall fabrics may be Tertiary and related to progressive unroofing, ductile footwall fabrics often are the product of long and complicated deformation histories, recording Mesozoic as well as Tertiary events (e.g., Miller and Gans, 1989; Hudec, 1992).

In the Funeral Mountains metamorphic core complex, located on the eastern side of Death Valley in California (Figure 1), ductile fabrics demonstrate a transport direction similar to that inferred for the core-bounding detachment, and previous authors have suggested that these fabrics represent a continuum of deformation (e.g., Hoisch and Simpson, 1993). These fabrics, however, are Late Cretaceous in age and represent a separate, high-temperature unroofing event at the end of Mesozoic time after the cessation of thrusting in the region (Applegate et al., 1992). This earlier extension was concentrated

along intracore shear zones that may have accommodated as much, if not more, of the unroofing than the core-bounding detachment. This chapter documents multiple deformational phases that record a history of tectonic burial and extensional unroofing events and presents constraints on the timing and kinematics of these phases as well as a possible model for the structural evolution of the Funeral Mountains since Mesozoic time.

GEOLOGIC SETTING

The Death Valley extensional terrain, which is bounded by the Spring Mountains to the east and by the Sierra Nevada to the west, has undergone as much as 160 km of extension since the end of Mesozoic thrusting in the area (Wernicke et al., 1988). This large amount of extension has produced a number of metamorphic core complexes in the region. In addition to the northern Funeral Mountains, core complexes bordering Death Valley include the Black Mountains (Figure 1; Holm and Wernicke, 1990) and the central and northern Panamint Mountains (Figure 1; Hodges et al., 1990; Hodges et al., 1987). The northern Funeral Mountains have been mapped by Giaramita (1984), Wright and Troxel (1994), and this study (1:15,000 scale mapping; Plate 1). Although only recently published, much of the seminal mapping by Wright and Troxel was conducted during the 1960's. The core rocks consist primarily of amphibolitic, granitic, and pelitic gneisses and metasedimentary rocks that appear to correlate with the Neoproterozoic Pahrump Group, Noonday Dolomite, Johnnie Formation, and Stirling Quartzite (Wright and Troxel, 1966; Troxel, 1988; Wright and Troxel, 1994; this study). These units have been intruded by several generations of granitic and mafic dikes and sills. Metamorphic conditions increase from southeast to northwest, reaching a maximum of upper amphibolite facies with extensive migmatization in Monarch Canyon (Labotka, 1980). Metamorphism, thought to peak by Early Cretaceous time (DeWitt et al., 1988), is due both to tectonic burial–as a result of Mesozoic thrusting–and to heating related to the emplacement of the Sierran arc (Labotka and Albee, 1988).

The high-grade metamorphic rocks are in fault contact below essentially unmetamorphosed Neoproterozoic to Tertiary sedimentary rocks, including those of the Stirling Quartzite, Neoproterozoic-Cambrian Wood Canyon Formation, and Oligocene-Miocene Titus Canyon Formation (Wright and Troxel, 1994). These rocks are separated by the Boundary Canyon detachment along the northern flank of the core complex and by the Keane Wonder fault along the southern flank (Figure 2). These two structures converge to the west, and it has been suggested that they represent two traces of the same surface (Hamilton, 1988). Other authors, however, have argued for a separate history for these faults (Wright and Troxel, 1994). The Boundary Canyon detachment is a regionally significant structure that has been correlated with the Bullfrog Hills and Fluorspar Canyon fault systems to the northeast (Figure 3; Carr and Monsen, 1988; Maldonado, 1990). It is thought to be part of the Miocene to Recent extensional event that resulted in the Death Valley extensional terrain. The eastern boundary of the core is less certain, as it is characterized by a diffuse set of normally faulted blocks carrying progressively lower-grade rocks in their hanging walls. Several of the contacts between units within the core are extensional shear zones that represent significant structural and metamorphic discontinuities. These shear zones include the Eastern shear zone, the Monarch Canyon shear zone, and the Chloride Cliff shear zone (Figure 4; Applegate et al., 1992).

TECTONIC STRATIGRAPHY

One of the problems encountered in metamorphic terrains is the correlation of highly metamorphosed rocks with their sedimentary equivalents found elsewhere in the region. The metamorphic rocks exposed in the northern Funeral Mountains have a well-defined stratigraphy comprising units of schist, gneiss, and marble that can be maintained throughout the mapping area (Figure 5). Wright and Troxel worked out the basic stratigraphy, correlating rocks in the footwall of the core complex with rift- and Windermere-related sedimentary rocks of the Pahrump Group, Johnnie Formation, and

Stirling Quartzite (Troxel, 1988; Wright and Troxel, 1994). Whereas their assignments are adopted in this study for the most part, some changes have been made to accommodate new geochronologic data. Although the protoliths of metasedimentary strata in the Funeral Mountains core comprise a relatively complete Neoproterozoic sequence in proper stratigraphic order, many contacts between units here are structural. Where they are not cut out by later brittle faults, the basal contact of the Stirling Quartzite is the Eastern shear zone, the basal contact of the Johnnie Formation is the Monarch Canyon shear zone, and the basal contact of the Kingston Peak Formation is the Chloride Cliff shear zone (Figure 5).

Neoproterozoic Crystal Spring and Beck Spring Formations

A thick sequence of gneisses, schists, quartzites, amphibolites, and marbles are correlated with the Crystal Spring Formation, which is the basal unit of the Pahrump Group, a sedimentary package related to rifting of the proto-Pacific margin. The minimum age of this unit is constrained regionally by 1.1 Ga diabase sills within the Crystal Spring Formation exposed in the Saratoga Springs area south of Death Valley (Heaman and Grotzinger, 1992).

The stratigraphically lowest rocks in the Funeral Mountains are amphibolitic gneisses with minor pelitic intercalations, both of which are exposed in the cores of two anticlinal culminations: one near the mouth of Monarch Canyon and the second located 0.5 km further to the southeast (Plate 1). They are assigned here to the basal member of the Crystal Spring Formation (Ycb). Pelitic gneisses from Monarch Canyon contain upper amphibolite facies assemblages (garnet + biotite + muscovite + kyanite ± sillimanite). These rocks are migmatitic and were intruded by an injection complex of Late Cretaceous granites and pegmatites that locally make up a significant fraction of the exposed rock (Labotka, 1980; Applegate et al., 1992). The assignment of these rocks to the Crystal Spring Formation is in keeping with earlier workers, including Giaramita (1984) and Labotka (1980). Several lines of evidence suggest this correlation. Elsewhere in the Death

Valley region, exposed basement is typically a megacrystic orthogneiss very unlike anything exposed in the Funeral Mountains (e.g., Hunt and Mabey, 1966; Wright, 1973). As noted above, the thick sequence of amphibolitic gneiss that dominates the exposures here could quite likely be the metamorphosed equivalent of the diabase sills found in the lower part of the Crystal Spring Formation elsewhere in the Death Valley region. Furthermore, the metamorphic grade of these rocks is identical to that in overlying rocks correlated with the Crystal Spring Formation, indicating that if these rocks had an earlier metamorphic history, they have totally reequilibrated during the metamorphism which also affected the overlying strata (Hodges and Walker, 1990).

Recently, Wright and Troxel (1994) assigned a pre-Pahrump Mesoproterozoic age to these gneisses based on a ~ 1.7 Ga $^{207}Pb/^{206}Pb$ zircon date for a granitic dike that intrudes the gneisses in Monarch Canyon (Zartman, written communication in Wright and Troxel, 1994). This date was obtained from a large fraction of zircon grains, and subsequent work indicates that the 1.7 Ga date probably represents an inherited component in the zircons and that the granitic bodies are of Late Cretaceous age (Chapter 4). Basement rocks, although not exposed, are likely to underlie the metamorphic core not far below the present surface exposure as indicated by the large inherited component in zircons analyzed from both igneous and metamorphic rocks (Chapter 4).

Units within the Crystal Spring Formation above the basal member have been broken out based on the alternation of schist and marble sequences (Figure 5), and they differ somewhat from the units used by Wright and Troxel (1994). The lower member (Ycl) is dominated by pelitic schists punctuated by quartzites, amphibolites, and several thin grey and tan calcite marble horizons. The base of the middle member (Ycm) is marked by a 2 m-thick, light- to dark-grey calcite marble overlain by a thick sequence of orange to brown calcite marbles, which are often dark grey on fresh surfaces. Within this marble unit are layers of micaceous calcsilicate rocks, amphibolites, pelitic schists, and minor interbedded quartzites. The top of the middle member (Ycmg) is defined by a cliff-forming, light-grey

calcite marble up to 5 m-thick, which forms the rim of Monarch Canyon and is a distinctive marker horizon. The upper member (Ycu) consists of brown arkosic quartzites with interbeds of psammitic schist, tan calcite marble, and garnet-bearing amphibolite sills. It is capped by another distinctive light grey calcite marble horizon, which is lithologically similar to the Ycmg grey marble. The lack of a more compelling reason to assign this unit to the Crystal Spring Formation, however, leads us to follow Wright and Troxel (1994) in assigning the upper grey marble to the Beck Spring Dolomite (Yb). This decision represents a change from Applegate et al. (1992).

Rocks of the Crystal Spring and Beck Spring Formations are exposed only in the structurally deepest level of the core complex, stretching from just east of Chloride Cliff to Boundary Canyon. The upper units are quite thin in the vicinity of Monarch Canyon due to later tectonic attenuation but are well-exposed in a much greater thickness in the vicinity of Chloride Cliff. The latter thickness more closely approximates thicknesses in the Panamint Range to the west (e.g., Miller, 1985). Pelitic schists of the lower Crystal Spring Formation in Monarch Canyon have assemblages including kyanite ± sillimanite, indicating upper amphibolite facies metamorphism. Schists in the upper Crystal Spring Formation contain garnet and biotite but lack either staurolite or an aluminum silicate polymorph, suggesting a lack of saturation in Al_2SiO_5 rather than a decrease in metamorphic grade. No dolomitic marbles have been found in the high-grade rocks of the northern Funeral Mountains, and it appears that all dolomites in this Neoproterozoic succession have been metamorphosed into calcite marbles. Many of these marbles contain phlogopite, which may have partitioned Mg in the calcification reactions.

Neoproterozoic Kingston Peak Formation

Overlying the Crystal Spring and Beck Spring Formations is a sequence of schists, marbles, and conglomerates correlated with the Kingston Peak Formation, the uppermost unit within the Pahrump Group. The upper part of this unit is thought be be related to a

glacial event at around 600 Ma, but the lower part is probably rift-related (Heaman and Grotzinger, 1992). The lower member (Ykl), which is best exposed around Chloride Cliff, is comprised of pelitic schists with minor quartzite and amphibolite as well as several horizons of orange and grey calcite marble. Ykl schists in Monarch Canyon contain staurolite and garnet, although both are heavily retrograded by hydrothermal activity associated with the Monarch Canyon and Chloride Cliff shear zones. To the east of Boundary Canyon, the Ykl is represented by a dark grey marble. The upper member (Yku) is dominated by a metadiamictite, correlative with the Wildrose Diamictite submember defined in the Panamint Mountains (Miller, 1985). The metadiamictite is composed of a dark brown calcareous matrix surrounding highly-strained clasts of orange calcite marble, quartzite, possible basement gneiss, and quartz veins. This submember alone is over 100 m-thick on the ridge east of Chloride Cliff, but the entire Kingston Peak Formation in Monarch Canyon is only 5 m-thick due to tectonic attenuation, and the diamictite is missing to the west of Monarch Canyon.

Neoproterozoic Noonday Dolomite

A thin layer of orange-weathering, sandy calcite marble and minor schist overlies the diamictite of the upper Kingston Peak Formation. This unit is at most 5 m-thick, but is almost continuously exposed from the western side of Monarch Canyon to well east of Chloride Cliff and the Keane Wonder millsite. It is always exposed directly in the footwall of the Monarch Canyon shear zone and hence is strongly deformed. Stratigraphically and lithologically, it is similar to the basal Sentinel Peak member of the Noonday Dolomite (Znsp) exposed in the northern Panamint Mountains (e.g., Labotka et al., 1980; Harding, 1987). Although Wright and Troxel (1966) argue that the Noonday Dolomite is unconformably omitted in the Funeral Mountains, Stewart (1970) noted that the Noonday, if present, is represented by a thin layer of sandy dolomite in the Funeral Mountains, an observation in agreement with our own.

Neoproterozoic Johnnie Formation

A thick sequence of green-weathering pelitic schists, quartzites, amphibolites, and dark grey marbles sits structurally above the Noonday Dolomite across the Monarch Canyon shear zone. These rocks are correlated to the stratigraphically overlying Johnnie Formation (Zj), the basal unit of the Cordilleran miogeocline. Unlike the lower units, rocks of the Johnnie Formation are found throughout the core complex from the very northwest end at Boundary Canyon for 35 km to the southeast (Figure 2). As a result, these rocks show an increase in metamorphism from lower-greenschist facies, biotite-grade phyllites at Echo Canyon to lower-amphibolite facies, staurolite-grade schists at Monarch Canyon.

Neoproterozoic Stirling Quartzite

A thick sequence of white to light-grey quartzite and quartz pebble conglomerate containing jasper pebbles overlies the rocks of the Johnnie Formation. This sequence is correlated with the basal member of the Stirling Quartzite (Zs), following the divisions used by Wright and Troxel (1994). Interbeds of light-green phyllite and calcite marble are also present. This unit is exposed along the eastern edge of the mapping area, where the phyllites (transitional to schist) contain garnet. The quartzites are also exposed in two klippen west of Chloride Cliff. Within the mapping area, these rocks are always separated from the underlying Johnnie Formation by the Eastern shear zone or, in the case of the klippen, other normal faults. As was the case with rocks of the Johnnie Formation, these rocks are found throughout the structurally higher levels of the core complex over a very broad area (Figure 2).

Igneous intrusions within the core

The metamorphosed Neoproterozoic rocks of the core are intruded by a number of younger igneous bodies. An injection complex of Late Cretaceous granitoid dikes and

sills, many of them pegmatitic, occurs in the deepest structural level of the core. These dikes make up as much as 20% of the basal Crystal Spring Formation exposed in lower Monarch Canyon and are found in decreasing volume up into the Kingston Peak Formation. They are exposed laterally from Boundary Canyon to east of Chloride Cliff and the Keane Wonder millsite. Although many of the dikes are 1 to 2 m-thick, several map-scale bodies are present and shown on Plate 1. The dikes are predominantly muscovite-rich monzogranites and granodiorites with ages in the range of ~ 65-72 Ma (Applegate et al., 1992; Chapter 3; Chapter 4). Several generations of Tertiary diabase dikes intrude the core rocks. The age for one of these dikes that cuts ductile fabrics in Monarch Canyon is presented later in this chapter.

Unmetamorphosed rocks in the hanging wall of the core complex

The hanging wall of the core-bounding detachment system in the northern Funeral Mountains often carries a sequence of unmetamorphosed orange- to brown-weathering dolomite and limestone correlated with the middle member of the Stirling Quartzite (Wright and Troxel, 1994). Quartzites with minor siltstone, dolomite, and arkose from the upper members of this unit are also found in the hanging wall overlain by brown to green dolomites and siltstones of the Wood Canyon Formation. Rocks of the Stirling and Wood Canyon Formations are unconformably overlain by the Titus Canyon Formation, a thick sequence of conglomerates and lake-bed sediments deposited in what was probably a local strike-slip basin (Saylor and Hodges, 1991). On the west side of the Funeral Mountains, the core rocks are structurally overlain by Miocene sedimentary rocks (Tsa of Wright and Troxel, 1994), consisting of arkosic sandstone, conglomerate, siltstone, limestone, and tuff horizons. In the vicinity of sulfur springs west of the Keane Wonder millsite, these beds are overlain by a white lacustrine limestone horizon.

STRUCTURAL DEVELOPMENT OF THE FUNERAL MOUNTAINS

Rocks in the metamorphic core of the Funeral Mountains have experienced a series of ductile deformational phases: three phases of folding, including a composite one, and a phase of extensional attenuation (Table 1). These ductile phases are followed by two phases of brittle deformation: the first associated with the Boundary Canyon detachment and the second with the Keane Wonder fault and low-angle faults within the core. Although several of these phases resulted in macroscopic structures shown on the accompanying map and cross sections (Plates 1 and 2), temporal relationships are most apparent at outcrop and microscopic scales.

This section covers descriptions of the various deformational phases, whereas the next section deals with kinematic analysis of these structures. In keeping with standard terminology for multiply deformed terrains, structures are numbered to correspond with the deformational phase during which they developed. For example, the first lineation, which developed during the third deformational phase, is termed L_3. Description of the folding phases follows the procedure outlined by Hansen (1971).

D_{1-2}: Isoclinal, recumbent folding

The earliest deformation recorded by rocks in the Funeral Mountains has no apparent macroscopic manifestation. An axial-planar schistosity (S_1) is defined by aligned micas in the hinges of mesoscopic folds that deform compositional layering (S_0). These folds are similar, inclined to recumbent, isoclinal, and have height-width ratios of five or greater. They are best exposed in marbles of the Pahrump Group and Noonday Dolomite where the compositional layering can be easily distinguished (Figure 6). In some areas, morphologically indistinguishable folds deform the S_1 schistosity, and all such folds are designated F_{1-2} and grouped into a composite D_{1-2} event. F_{1-2} fold axes show considerable scatter, although the majority plunge shallowly to the east (Figure 7).

In other lithologies, the S_1 foliation has been transposed by subsequent deformation into the regional foliation. An internal foliation defined by quartz inclusions is preserved in rotated garnet and staurolite porphyroblasts in pelitic schists, and it is inferred to be a relict manifestation of S_1 (Figure 8). The presence of S_1 as an internal foliation in prograde porphyroblasts suggests that S_1 predated or was synchronous with growth of these minerals, and hence predated or was synchronous with the peak of regional metamorphism. Labotka (1980) stated that the dominant foliation in lower-grade rocks to the southeast of the study area predates growth of prograde minerals. If that is the case, then S_1 may not have been overprinted by subsequent deformation at structurally higher levels.

D_3: Ductile attenuation and extensional shear zone development

One of the most distinctive features of the Funeral Mountains core complex is the presence of several intracore shear zones, in places subparallel to but separated from the core-bounding detachment. The Eastern shear zone places Stirling Quartzite on top of schists of the Johnnie Formation without a complete unit missing (Figure 4). Wright and Troxel (1994) mapped the Eastern shear zone in the area east of Chloride Cliff cutting down-section, from the upper to lower Johnnie Formation, towards the northwest in the footwall. The Monarch Canyon shear zone represents a clear stratigraphic break, placing rocks of the Johnnie Formation on the older Kingston Peak Formation, omitting all but the lowest part of the stratigraphically intervening Noonday Dolomite. The Chloride Cliff shear zone places rocks of the Kingston Peak Formation on the older Beck Spring Dolomite without a complete unit missing. In Monarch Canyon and to the west, the Monarch Canyon and Chloride Cliff shear zones dip 4 – 11° to the north. Further to the east, however, both shear zones dip 35 – 45° to the southeast in the area east of Chloride Cliff (Plate 1; cross-section A-A' in Plate 2). The Eastern shear zone is exposed in two klippen on peaks west of Chloride Cliff and along a ridge east of Chloride Cliff where it

dips gently to the northeast. It is the only one of the major D_3 shear zones that is truncated by the Boundary Canyon detachment. All three of the shear zones are truncated by the Keane Wonder fault: the Monarch Canyon and Chloride Cliff shear zones are truncated to the east of Boundary Canyon, and the Monarch Canyon and Eastern shear zones are cut off east of the Keane Wonder millsite. The D_3 shear zones are loci for subsequent CO_2- and Al-rich hydrothermal alteration and are marked by graphite-rich, blue, maroon, and red mylonitized schists along their length.

Rocks throughout the core show a well-developed foliation (S_3) related to shear zone development. At a mesoscopic scale, D_3 deformation has transposed the earlier S_1 foliation into the S_3 foliation. S_3 planes have a mean orientation of N6E; 20 SE, and their poles show great variability due to later folding (Figure 9). Petrographically, this coarse, continuous S_3 foliation is defined by micas and quartz ribbons. Most of the rocks in the mapping area can be described as L-S tectonites with well-developed lineations (L_3) associated with the S_3 foliation. A polycrystalline mineral stretching lineation (L_{3s}) is defined by elongated quartz aggregates in quartzites, granites, and amphibolites and by elongate calcite aggregates and opaques in marbles (Figure 10). A mineral grain lineation (L_{3m}) is defined by aligned kyanite and staurolite grains in pelitic schists and by amphiboles in amphibolites. L_{3s} and L_{3m} lineations cluster well in the southeast and northwest quadrants, with mean orientations of 35; S76E and 32; S64E, respectively (Figure 11). The difference between these mean orientations arises from the tendency of L_{3m} kyanite and staurolite lineations to be deformed by subsequent microfolds that are well-developed in the schists.

Figure 8 shows the S_3 foliation defined by biotite and muscovite being deflected around a garnet porphyroblast. This relationship indicates that D_3 deformation postdates prograde metamorphism.

D_4: Tight to isoclinal folding

Mesoscopic F_4 folds are inclined and isoclinal with sharp hinges and straight limbs (Figure 12), except in calc-silicate lithologies where hinges tend to be more rounded with broadly curved limbs. The height-width ratios of these folds vary from one to three, and the folds consistently verge to the west. F_4 fold axes in general plunge to the east with a mean orientation of 41; N73E (Figure 13). No macroscopic F_4 folds are present in the mapping area. The F_4 folds deform the S_3 regional foliation and, in places, the contacts of the extensional shear zones.

In some cases, F_4 folds have an associated axial-planar cleavage (S_4). Although the S_4 cleavage itself is poorly defined in outcrop, S_3-S_4 intersection lineations (L_4) are well-developed in places. In low-grade Stirling and Johnnie rocks to the southeast, a similar cleavage-cleavage intersection produces a well-developed pencil cleavage. In higher-grade rocks, the S_3-S_4 intersection lineation is developed in some quartzites, but the principal manifestation of L_4 is as a crenulation hinge lineation, particularly well-developed in schists and micaceous quartzites. L_4 lineations generally plunge to the southeast with a mean orientation of 33; S64E (Figure 14). In outcrop, L_4 lineations are often oriented sub-parallel to the orientation of mesoscale F_4 fold axes. In some outcrops, it appears that the earlier L_{3m} lineation is aligned parallel to the later crenulation hinges, but other outcrops show a distinct discordance between the alignment of kyanite and staurolite grains and the orientation of the crenulation hinges. In thin-section, crenulations are fairly symmetric without a well-developed associated crenulation cleavage (Figure 15). Kyanite and biotite grains from schists in the high-grade portion of the core are kinked (Labotka, 1980; Hodges and Walker, 1990). Discrete kink bands are also found in outcrop, especially in the lower-grade rocks of the Johnnie Formation. In both cases, the kinks may be evidence for a late-stage, steep foliation that deforms the earlier S_3 fabric, a relationship suggestive of a D_4 origin.

D_5: Doming

The high-grade rocks of the northern Funeral Mountains are exposed in a domal topographic high from east of Chloride Cliff to Boundary Canyon in the west. Wright and Troxel (1994) recognized this doming of the core rocks and described it as a doubly-plunging antiformal feature. Reynolds (1969) viewed the shape of the northern Funeral Mountains as part of a regional antiform that extended into the Grapevine Mountains. Section A-A' in Plate 2 shows that both the Monarch Canyon and Chloride Cliff shear zones change from a gentle northward dip to a moderate southward dip east of Chloride Cliff. Other cross-sections drawn perpendicular to A-A' show a northwest-southeast axial antiformal structure to the core rocks (Plate 2; location of cross-section lines shown on Figure 4 and Plate 1). Although doming clearly affects the Boundary Canyon detachment, suggesting at least some of its development postdates movement on that structure, associated ductile structures suggest that the initiation of doming predates brittle faulting. Doming is associated with second-order folds on the southwest limb of the northwest-axial anticline, dome-and-basin folding, and boudinage.

Sections C-C', D-D', and E-E' (Plate 2) show second-order, macroscopic F_5 folds that dominate the limb of the northwest-southeast axial anticline on the Death Valley side of the northern Funeral Mountains. These northwest-southeast axial folds are characterized by shallow, east-dipping limbs and steep, west-dipping limbs, resulting in a "stair step" effect (Troxel, 1988). Axes for 17 F_5 folds were measured with a mean orientation of 36, S46E (Figure 16a). It is a curious feature of the Funeral Mountains that these folds are only found on the crest and western limb of the dome. Unlike earlier deformational features which had no correlative structures in the hanging-wall of the core-bounding faults, folds similar to F_5 folds deform rocks in the hanging-wall of the core-bounding detachment system (Giaramita, 1984; Applegate, unpub. mapping).

D_5 structures at an outcrop scale differ substantially from their macroscopic counterparts but are grouped into the same phase because they appear to be small-scale

manifestations of doming. Two roughly orthogonal sets of broadly curved, open folds (F_{5DB}) form a dome-and-basin pattern, particularly common in marbles near the core of the dome (Figure 17). These folds have height-width ratios of 0.1 and gently deform the regional foliation. They do not display an associated axial-planar cleavage. F_{5DB} folds appear upright and symmetric and, consequently, do not show any vergence. When plotted on a stereographic projection, F_{5DB} fold axes plunge gently to both the northwest and northeast with no mean orientation (Figure 16b).

Boudinage, again on two axes, forms a chocolate-tablet structure in several lithologies throughout the core, including marble and the Late Cretaceous pegmatite dikes (Figure 18). Like the dome-and-basin folding, the boudinage is best expressed near the core of the dome. Boudinage axes were too sparce to establish mean orientations, but they appear to show a spread similar to that of F_{5DB} folds. The boudinage appears to be symmetric, pinching and swelling marble horizons at the expense of intervening schists that are in places entirely cut out between two marble horizons.

D_6: Development of Boundary Canyon Detachment

The northern edge of the metamorphic core is defined by the Boundary Canyon detachment, a low-angle, brittle structure that dips gently to the north. In a manner similar to other detachment faults in the region, a number of low-angle faults in the hanging-wall of the Boundary Canyon detachment show listric terminations against the detachment surface (Reynolds et al., 1986). Over much of its length in the study area, the detachment is underlain by Johnnie Formation schists, quartzites, and marble horizons. In numerous exposures of the schists, the S_3 foliation strikes obliquely into the detachment surface. Hoisch and Simpson (1993) attribute mylonitic fabrics in the calcite marbles to movement on the Boundary Canyon detachment, because calcite behaves plastically at temperatures consistent with brittle detachment motion. These marbles are quite thin, however, and the

Boundary Canyon detachment is predominantly a brittle structure with little manifestation in the ductile fabrics found in its footwall.

D_7: Development of the Keane Wonder fault and brittle faulting

The Keane Wonder fault forms the southern margin of the core rocks in the northern Funeral Mountains (Figure 4). It is a low-angle, brittle fault that dips gently to the southwest in this area. Hamilton (1988) has argued that the Keane Wonder fault represents part of a continuous, domal detachment surface with the Boundary Canyon detachment, and the two structures have been mapped as a continous structure at the northwestern termination of the core complex (e.g., Giaramita, 1984; Reynolds, 1976). Alluvium in Boundary Canyon, however, covers the area where the two faults meet, and Wright and Troxel (1994) argue for a separate evolution of the two faults because of the difference in structural features in the hanging walls of the two faults. Troxel (1988) argues that the Keane Wonder fault continues northwest into the Grapevine Mountains, and to the southwest it cuts into the footwall of the core complex (Wright and Troxel, 1994). Rocks along strike in the footwall of the two faults are different as well: rocks of the Johnnie Formation are consistently in the footwall of the Boundary Canyon detachment, whereas middle and lower Crystal Spring Formation rocks are found in the footwall of the Keane Wonder fault away from its northwestern end where the Keane Wonder fault cuts the Monarch Canyon shear zone (Figure 4; Plate 1). Rocks in the hanging wall of the two faults are also different: Tertiary sediments (unit Tsa of Wright and Troxel, 1994) not found in the hanging wall of the Boundary Canyon detachment are common above the Keane Wonder fault.

Unlike the Boundary Canyon detachment, which is associated with relatively little deformation within the core, the Keane Wonder fault is the southwestern limit of a zone of low- to moderate-angle, southwest-dipping normal faults that extends from the crest of the range towards Death Valley as first observed by Wright and Troxel (1994; Plate 1 and Plate

2: Sections D-D' and E-E'). These faults cut F_5 folds but also appear to have produced drag on some of the folds, increasing their apparent southwest vergence. Faults with normal-sense offset and similar orientation to the range-front faults are also found in the hanging wall of the core complex, and two of these structures cut the Boundary Canyon detachment between Boundary and Monarch Canyons (Figure 4). These structures are discussed more fully in Chapter 5.

KINEMATIC ANALYSIS

Up to this point, structures have been treated descriptively in an attempt to catalogue and arrange fabrics found in the core rocks into a coherent sequence. In this section, sense-of-shear indicators and fold vergence are used to determine the vergence of the five predominantly ductile deformation phases. In the case of D_4, it was possible to apply Hansen (1971) slip-line analysis to obtain a transport direction for F_4 folds. Strained carbonate clasts from rocks within the D_3 shear zones permitted some measure of the intensity of deformation associated with that phase.

$D_{1\text{-}2}$

The overprinting of subsequent deformation precludes analysis of $F_{1\text{-}2}$ folds. Their recumbent, isoclinal nature, as well as their very large height-width ratios appear to be the product of D_3 attenuation of the core rocks.

D_3

Schists within and adjacent to the shear zones exhibit asymmetric fabrics, and quartz crystals have undergone extensive recrystallization, displaying a mortar texture. Away from the shear zones, quartz crystals show undulose extinction, sutured grain boundaries, and subgrain development but do not have well-developed S-C fabrics. The stretching lineation, L_{3s}, indicates that the direction of transport for D_3 deformation is either to the

WNW or ESE. Fabrics within and in the footwall of the Monarch Canyon, Chloride Cliff, and Eastern shear zones show top-to-the-northwest shear sense using asymmetric porphyroclasts (Passchier and Simpson, 1986) and mica fish that form a Type II S-C fabric (Figure 19; Lister and Snoke, 1984). Hoisch and Simpson (1993) looked at sense-of-shear indicators in mylonitic rocks within 300 m beneath the Boundary Canyon detachment and Keane Wonder fault. They determined a similar top-to-the-northwest sense of motion for these mylonites, using asymmetric porphyroclasts, shear bands, mica fish, grain-shape preferred orientations, and crystallographic preferred orientations. Hoisch and Simpson (1993) ascribed these fabrics to progressive development of the detachment as lower plate rocks rose and cooled through the transition from ductile to brittle regimes. The fabrics, however, are identical to D_3 fabrics at these and lower structural levels that are unrelated to brittle detachment motion, with the only possible exception being calcite mylonites directly beneath the detachment.

Given the sense-of-shear information suggesting top-to-northwest movement on extensional structures that appear to have had shallow northwest dips when active, it is unusual that the majority of lineations in the core plunge toward the southeast rather than the northwest. The most obvious explanation is doming of the core in response to tectonic unloading, a process that appears to have warped the surfaces of the major extensional structures. If that is the case, then one would expect to see a geographic distribution of NW-plunging fabrics to the northwest and SE-plunging fabrics to the southeast across the dome. Figure 20 shows contoured stereographic plots of poles to S_3 planes, L_{3s} lineations, and L_4 lineations for the Monarch Canyon area, the Chloride Cliff area, and the area adjacent to the Keane Wonder fault, the latter dominated by SW-dipping planar fabrics. The plots in Figure 20 do not show a geographic progression in the plunge of the lineation data, suggesting that another explanation is needed. Figure 21 shows the contour plots of poles to F_4 axial planes and poles to S_3 foliations. The considerable overlap shown by these two data sets may indicate that the predominantly isoclinal F_4 folds, which

are consistently asymmetric toward the west, have resulted in the large number of SE-dipping foliation surfaces and hence SE-plunging lineations across the core. Whereas the enveloping surfaces for F_4 folds dip to the northwest, the asymmetry and frequent overturning of the folds creates a dominantly southeast dip in the foliation.

D_3 attenuation of strata is most intense in Monarch Canyon between the Monarch Canyon and Chloride Cliff shear zones, where units equivalent to the basal Sentinel Peak member of the Noonday Dolomite and the entire Kingston Peak Formation have been reduced in thickness from several hundred meters to less than ten meters. It is evident from the intensity of attenuation that strains associated with D_3 deformation and the intracore shear zones were very high. The upper Kingston Peak diamictite permits a minimum estimate of the extent of attenuation. The diamictite consists of a brown silty carbonate matrix supporting tan marble and basement orthogneiss clasts. Since the entire rock is predominantly calcite, dolomite having been replaced during metamorphism, no large strength contrast exists between the marble clasts and the matrix such that the marble clasts represent excellent passive strain markers (Figure 22). In contrast, the much stronger basement clasts are significantly less deformed. The marble clasts in unstrained areas are variable in dimension but are roughly equant and are assumed so for this analysis. Measurement of 42 clasts on faces both perpendicular and parallel to the D_3 transport direction produced a set of S_1/S_2 and S_2/S_3 ratios with an average $S_1 : S_2 : S_3$ stretch ratio (normalized to S_3) of 14 : 7.6 : 1. These data plot well into the flattening field, which is to be expected given the intense attenuation of units between the shear zones. Such flattening represents a significant component of pure shear, an observation that is corroborated by Hoisch and Simpson (1993), who found evidence for a large pure shear component using c-axis data from mylonitic middle Crystal Spring Formation marbles beneath the Keane Wonder fault.

Wright and Troxel (1994) mapped the Monarch Canyon shear zone as a low-angle normal fault but did not ascribe much stratigraphic omission to it because, in some areas

several tens of kilometers to the south of the Funeral Mountains, the Johnnie Formation unconformably overlies Pahrump Group strata. Nearby exposures in the Panamint Mountains (Figure 1), however, show no such unconformity (Stewart, 1970), suggesting that the Monarch Canyon shear zone omits on the order of 400 m of section (the approximate thickness of the Noonday Dolomite in the Panamint Mountains cited in Hodges et al., 1990). Although Applegate et al. (1992) ascribed stratigraphic throw to the Chloride Cliff shear zone based on the assumption that it omitted the Beck Spring Dolomite, the current stratigraphic correlation suggests that the Beck Spring Dolomite is present, and the Chloride Cliff shear zone represents the base of a zone of intense ductile attenuation, the top of which is the Monarch Canyon shear zone. The relatively small amount of stratigraphic omission on these structures assumes that the units juxtaposed across the shear zones are from the same structural level. The Discussion section presents arguments that rocks in the hanging wall of these two shear zones are from a very different level in the Mesozoic crust than those in their footwall.

D_4

Axes were measured for 138 F_4 folds, and 68 of these measured folds belonged to fold trains with a well-defined vergence, amenable to Hansen (1971) slip-line analysis. These folds are plotted in Figure 23 along with their vergence direction. The region of overlap between opposite vergences defines the separation angle, in this case 42°. This analysis suggests either a WNW or ESE transport direction. Similar analyses by Giaramita (1984) and Hoisch and Simpson (1993) corroborate these results. The consistent westward vergence of F_4 folds in conjunction with the separation angle analysis suggests that the transport direction for D_4 is towards the WNW. The bimodal clustering of F_4 folds in the southeast and northeast quadrangles (Figure 13) appears to be the result of a number of folds forming with axes parallel to the transport direction and a number of others forming at a discrete angle to the transport direction but verging in that direction. These characteristics

are typical of drag folds where subsequent simple shear rotates originally oblique hinges toward parallelism with the slip direction (e.g., Cobbold and Quinquis, 1980). It should be noted, however, that to some extent the southwest vergence of folds plotting in the SE quadrant may be the result of southwest-directed drag produced by later brittle faults.

The vast majority of the L_4 lineations plot within the separation angle defined by F_4 folds, a relationship that becomes very striking when the lineation data is contoured (Figure 14). Since L_4 lineations represent the intersection between the earlier foliation and a crenulation cleavage, their consistent orientation in the direction of transport suggests that a component of constrictional strain was oriented perpendicular to the extension direction.

D_5

The consistent southwest vergence of F_5 folds results from a combination of two factors. The measured folds are all on the western limb of the dome, and their asymmetry is in the direction expected for second-order folds on the limb of a first-order fold. The inference that these are second-order folds is further strengthened by a symmetric anticline-syncline pair (not measured) found at the crest of the first-order anticline (Plate 2: D-D'). Reynolds et al. (1986) noted that these southwest-vergent folds modify the first-order anticline, an observation compatible with this interpetation. The apparent southwest vergence of the F_5 folds has been enhanced by drag on southwest-vergent normal faults. Mesoscopic structures associated with D_5 do not lend themselves to kinematic analysis. The chocolate-tablet style of boudinage suggests, however, that the rocks were responding to a flattening strain without an appreciable component of simple shear.

D_6

Reynolds et al. (1986) inferred westward movement for the upper plate of the Boundary Canyon detachment. Maldonado (1990) argued for a similar sense of motion for the Bullfrog detachment fault system and Fluorspar Canyon fault system, which appear to

represent the northward trace of the detachment. If Hoisch and Simpson (1993) are correct that some calcite mylonitization is coeval with detachment motion, then these fabrics also indicate top-to-the-northwest motion on the detachment.

The amount of displacement on the Boundary Canyon detachment is not well known. Wright and Troxel (1994) state that the stratigraphic offset at the northwesternmost exposure of the detachment is on the order of 4 km, placing the upper Stirling Quartzite on the lower Johnnie Formation. The actual offset, however, must be greater, because the unmetamorphosed Stirling Quartzite unconformably underlies Oligocene-Miocene Titus Canyon Formation rocks, and thus was very near the surface before detachment movement, whereas the Johnnie Formation schists experienced staurolite-grade conditions and must have been at some depth prior to movement on the detachment. A minimum offset on the detachment can be etimated by the extent of its exposure parallel to the transport direction since rocks in the hanging wall cannot be matched with rocks in the footwall. Mapping by Wright and Troxel (1994) shows a klippe of the Boundary Canyon detachment located 33 km southeast of its northwesternmost exposure at Boundary Canyon (Figure 2). Snow and Wernicke (1988) estimated a minimum of 30 km offset on the Boundary Canyon detachment based on their correlations of Mesozoic structures.

D_7

The Keane Wonder fault and related normal faults show a minimum of 4.6 km of down-to-the-southwest separation with somewhat less than 4 km of that estimate accommodated by the Keane Wonder fault itself (Chapter 5). At its southern continuation in the southern Funeral Mountains, the Keane Wonder fault shows a minimum 5 km of right-lateral offset (Cemen and Wright, 1990). Thus, the Keane Wonder fault appears to be an oblique-slip fault with roughly equal components of right-lateral and normal motion, assuming the minimum estimates of offset.

TIMING OF DEFORMATIONAL EVENTS

D_{1-2}: Mesozoic compressional event

The principal episode of metamorphism that affected rocks in the Funeral Mountains is syn- to postkinematic with respect to D_{1-2} deformation. DeWitt et al. (1988) suggested an Early Cretaceous age for metamorphism in the Funeral Mountains based on $^{40}Ar/^{39}Ar$ dates from amphibole in Monarch Canyon. Metamorphic zircons from lower Crystal Spring schists in Monarch Canyon yield a lower intercept age of 127 ± 9 Ma for the growth of these minerals during prograde metamorphism (Chapter 3), and amphiboles from Chloride Cliff yield $^{40}Ar/^{39}Ar$ cooling ages that suggest peak metamorphism is older than 113 Ma (Hoisch and Simpson, 1993; Applegate and Hodges, 1993). Labotka (1980) argues that burial and metamorphism of the Funeral Mountains were the result of Mesozoic thrusting in the region combined with thermal effects from Sierran arc emplacement. As a consequence, it is reasonable to assume that D_{1-2} deformation is the result of Early Cretaceous or older thrusting in the area.

D_3 and D_4: Late Cretaceous extensional event

Hodges and Walker (1990) first suggested the existence of Late Cretaceous extension in the Funeral Mountains on the basis of isothermal decompression paths for pelitic samples from Monarch Canyon in conjunction with Late Cretaceous $^{40}Ar/^{39}Ar$ cooling ages for muscovites at temperatures below those for which isothermal decompression was indicated (DeWitt et al., 1988). Applegate et al. (1992 and Chapter 4) provided more direct evidence for extensional deformation in that time interval, obtaining U-Pb zircon ages for granitic pegmatites with cross-cutting relationships to D_3 fabrics. A pegmatite with both an S_3 foliation and L_{3s} lineation was dated at 72 ± 1 Ma, and a pegmatite which cross-cut the S_3 foliation and was itself unaffected by D_3 fabrics was dated at 70 ± 1 Ma. These two ages continue to be the best available constraint on the timing of D_3 deformation, indicating that deformation was ongoing at 72 Ma and had ceased by 70 Ma.

Kinematic analysis of the transport direction for F_4 folds indicates its similarity to that for D_3 fabrics, suggesting a possible association of these two phases. Pegmatite dikes are both deformed by and cross-cut F_4 folds in lower Monarch Canyon and just east of Monarch Canyon. The dikes are from the Late Cretaceous injection complex, but the cross-cutting dikes may be as young as 65 Ma (Chapter 4), suggesting possible diachroneity between D_3 and D_4. The two phases nevertheless appear to represent two stages of a single, progressive extensional event in Late Cretaceous time, possibly extending into earliest Paleocene time.

A further minimum age constraint on ductile fabrics within the core is provided by a new $^{40}Ar/^{39}Ar$ amphibole age on a cross-cutting diabase dike. Sample 613-1 is from a north-south-trending, near-vertical, fine-grained diabase dike that cuts all ductile fabrics in basal and lower Crystal Spring strata (location on Figure 4). Similar dikes cut the Late Cretaceous shear zones, but efforts to date these dikes have been unsuccessful due to a large excess ^{40}Ar component that produces ages older than the shear zones. Further analyses will be attempted to constrain this excess component and obtain an age for these dikes. Sample description, separation procedures, and analytical techniques are discussed in the appendix. A regression age for sample 613-1 was obtained using the least squares regression technique of York (1969) on the individual subsample results (Table 2).

For sample 613-1, the model ages for individual subsamples (assuming an initial $^{40}Ar/^{36}Ar$ ratio of 295.5 similar to that of modern atmosphere) range from 5 to 33 Ma (Table 2.1). When plotted on an inverse isotope correlation diagram (Figure 24), all ten steps yield a regression age of 32.6 ± 0.6 Ma with a MSWD of 2.1 and an initial $^{40}Ar/^{36}Ar$ ratio of 200 ± 70, lower than that for modern atmosphere. Removing points 4 and 5, which are outliers with very little gas, one obtains a regression age of 33.2 ± 0.7 Ma with a MSWD of 1.0 and an initial $^{40}Ar/^{36}Ar$ ratio of 190 ± 70, which is the preferred age. The spread of data on the diagram is suggestive of mixing between multiple trapped components with variable $^{40}Ar/^{36}Ar$ ratios, making it difficult to determine the radiogenic

intercept. The first subsample with a model age of 32.1 ± 0.6 Ma controlled the x-intercept of the regression, and hence the age, because of its high $^{39}Ar/^{40}Ar$ ratio, indicative of a large radiogenic component. This date indicates that ductile deformation at structurally deep levels of the core was over by Oligocene time.

D_5: Core complex doming, a response to several events?

One of the most notable topographic expressions of Cordilleran core complexes is their domal appearance. Numerous authors have suggested that doming is the result of footwall flexure in response to tectonic unloading of the hanging wall by movement on the core-bounding detachment (e.g., Spencer, 1984). The broad warps of F_{5DB} folds and their dome-and-basin interference patterns suggest a non-directional driving force such as isostatic rebound rather than the strongly directional northwest transport of earlier extension. Doming appears to have affected the Boundary Canyon detachment, rotating it from its original northwest dip in the direction of transport to its present shallow dip to the northeast along much of its trace (see Plate 1). Thus it appears that doming at least partially represents an isostatic response to movement on the core-bounding detachment. Several lines of evidence, however, suggest that doming may have a more protracted history. Many of the outcrop-scale features associated with doming and D_5 are indicative of rocks deforming plastically, but the temperature interval over which Late Miocene deformation took place (~560 to 400 K; Holm and Dokka, 1991) is consistent with brittle behavior in quartz-rich rocks. The only upper age constraint on D_5 deformation is that 70 Ma pegmatite dikes in Monarch Canyon are deformed by D_5 boudinage, and that boudinage deforms isoclinal folds correlative with F_4 folds in this classification (Giaramita, 1984). The majority of the boudinage and dome-and-basin folding is found in the footwall of the Monarch Canyon and Chloride Cliff shear zones, and doming itself is restricted to the high-grade areas of the core, showing little expression east of the Eastern shear zone. A broad northeast-axial anticline (shown in Section A-A' on Plate 2) that rotates the intracore shear

zones from shallow northeastward dips similar to the Boundary Canyon detachment to moderate southeastward dips does not have any expression in the trace of the detachment. For these reasons, much of the doming and associated D_5 deformation appears to predate Late Miocene extension, and only a broad warping clearly postdates movement on the Boundary Canyon detachment.

D_6: Tertiary extensional event: the core-bounding detachment system

Reynolds et al. (1986) estimated that active top-to-the-northwest motion on the Boundary Canyon detachment took place from 9 to 5 Ma based in part on the presence of rocks as young as 7 Ma in its hanging wall. Subsequent fission-track and $^{40}Ar/^{39}Ar$ K-feldspar data indicate rapid cooling during Late Miocene time, consistent with tectonic unroofing at that time. Fission-track dates on titanite, zircon, and apatite from Late Cretaceous pegmatite dikes indicate rapid cooling of the core rocks through the closure temperatures for those minerals, approximately 560 K to 400 K, between 11 and 6 Ma (Holm and Dokka, 1991). K-feldspar from several pegmatites in the same injection complex dated using the $^{40}Ar/^{39}Ar$ method yield 11 to 9 Ma dates for a similar temperature range (Applegate and Hodges, 1993; Chapter 3). Thus it appears that movement on the Boundary Canyon detachment is responsible for Late Miocene unroofing and cooling of the metamorphic core rocks.

D_7: Post-detachment extensional event

The timing of movement on the Keane Wonder fault and related intracore normal faults is not well constrained except that it is younger than movement on the Boundary Canyon detachment and hence is younger than ~ 6 Ma. The resulting extension produced by dip-slip on these structures is in a direction perpendicular to the earlier northwest extension direction. The possibility that this southwest-oriented extension may be evidence for

young, oblique motion on the Furnace Creek/ Northern Death Valley fault zone (Figure 3) is discussed in Chapter 5.

DISCUSSION

The Funeral Mountains metamorphic core – an intact block of Mesozoic crust?

Although the Eastern and Monarch Canyon shear zones have been previously mapped as normal faults (Wright and Troxel, 1994), they were not considered to be important structures with significance beyond their relatively small stratigraphic throw. As a consequence, previous workers have viewed extension in the Funeral Mountains as a one-stage process accommodated by the Boundary Canyon detachment system in Tertiary time (e.g., Hoisch and Simpson, 1993). Such a scenario requires that the metamorphic rocks in the Funeral Mountains act as an intact block of Mesozoic crust in the hanging wall of the Schwaub Peak thrust exposed east of Echo Canyon in the southern Funeral Mountains (Figure 3). One of the most puzzling features of the core rocks is that they change from lowest-greenschist facies conditions above the thrust at Echo Canyon to migmatitic, upper-amphibolite facies conditions over a fairly narrow stratigraphic interval. In particular, rocks of the Johnnie Formation and Stirling Quartzite are exposed over a distance of 30 km orthogonal to strike, increasing from chlorite-grade phyllites to staurolite-grade schists across that interval. Hoisch and Simpson (1993) present a model in which the rocks were metamorphosed in Mesozoic time as an intact west-dipping block that subsequently has been rotated into its present subhorizontal position as an isostatic response to unroofing by the Boundary Canyon detachment. Although this model accounts for the large increase in metamorphic grade from southeast to northwest over a restricted stratigraphic interval, it fails to account for the overburden necessary to achieve the depths associated with metamorphism at Chloride Cliff and Monarch Canyon. Both Labotka and Albee (1988) and Wernicke et al. (1988) place the Funeral and Grapevine Mountains in the footwall of the Last Chance thrust system, which they correlate with the Grapevine thrust across the

Northern Death Valley-Furnace Creek fault zone (Figure 3). The Last Chance thrust system, which may be as old as Permian (Snow et al., 1991) but is traditionally thought to be of Early Jurassic or Late Triassic age (Burchfiel et al., 1970), carries Cambrian rocks in its hanging-wall and can account for 6 km of overburden. Including the rocks stratigraphically above the Johnnie Formation in the footwall of the Last Chance thrust adds another 7 km of overburden. In order to account for the large increase in metamorphic grade over a narrow stratigraphic interval, Hoisch and Simpson (1993) show the core rocks dipping 30° to the west during burial and metamorphism, but this geometry only accounts for an additional 3 km of overburden, bringing the total to ~ 15 km. This depth is consistent with pressure estimates for Indian Pass (Figure 2) where Hoisch and Simpson (1993) estimated a minimum pressure of 360 MPa, or ~ 12 km depth (assuming a nominal lithostatic pressure gradient of 30 MPa/km). It is not, however, consistent with the 27-33 km depths estimated thermobarometrically for the rocks at Chloride Cliff and Monarch Canyon (Hodges and Walker, 1990; Hoisch, 1991). No higher thrust plates have been identified above the Last Chance system; thus, in order to account for these depths, one must consider the possibility that the intracore shear zones have omitted structurally lower thrusts including the Schwaub Peak thrust plate (Figure 3).

The metamorphic core complex at Tucki Mountain at the northern end of the Panamint Mountains sits in the footwall of the Lemoigne thrust, correlated with the Clery thrust in the southern Funeral Mountains (Figure 3; Wernicke et al., 1988). Those rocks, however, were metamorphosed at a depth of only 10 km, much shallower than the high-grade rocks in the Funeral Mountains (Labotka and Albee, 1988). Even if one stacked both the Schwaub Peak and Clery thrust plates on top of the northern Funeral Mountains, their combined stratigraphic throw only accounts for an additional 6 km of overburden (Snow and Wernicke, 1989). In order to account for the mid-crustal depths for rocks in the northern Funeral Mountains, one must stack a number of thrust plates, in effect locating these rocks in the footwall of the regional décollement for the thrust belt. Such a scenario

is fundamentally incompatible with the view that the Funeral Mountains represent an intact crustal section, and it supports the possibility, first introduced by Hodges and Walker (1990), that additional thrust plates were excised by subsequent extension on intracore shear zones.

If an extensional shear zone has excised thrust plates, then rocks beneath that shear zone should belong to a very different structural level than stratigraphically proximal rocks above. Consequently, one would expect to see a significant break in metamorphic grade across the zone. Although the structurally highest Eastern shear zone is not a major metamorphic discontinuity, the combined Monarch Canyon and Chloride Cliff shear zones place staurolite-grade rocks of the Johnnie Formation on top of kyanite-grade rocks of the Pahrump Group. A further argument that these shear zones represent a significant structural break is provided by $^{40}Ar/^{39}Ar$ data. Hornblendes from amphibolite sills in the Johnnie Formation give Paleozoic to Proterozoic K-Ar and $^{40}Ar/^{39}Ar$ ages (Hoisch and Simpson, 1993; Applegate and Hodges, 1993), suggesting that Mesozoic metamorphic temperatures were insufficiently high to cause resetting. In contrast, all $^{40}Ar/^{39}Ar$ and K-Ar mineral ages for samples collected beneath the Monarch Canyon and Chloride Cliff shear zones yield Mesozoic or Cenozoic ages (Hoisch andSimpson, 1993; Applegate and Hodges, 1993).

Model for unroofing of the Funeral Mountains

The cartoon in Figure 25 illustrates a possible explanation for the development of the Funeral Mountains core complex since Mesozoic time. This highly schematic cross-section runs roughly parallel to the California-Nevada border from the Grapevine Mountains in the northwest to the Spring Mountains in the southeast (Figure 1). The width of this section in Mesozoic time is based on the palinspastic reconstruction of Wernicke et al. (1988). Figure 25a represents the time period after Mesozoic thrusting and regional metamorphism but before the initiation of Late Cretaceous extension. The thrust belt at this latitude appears to

have stopped moving in the foreland by approximately 90 Ma, according to a recent study in the Clark Mountains of Nevada (Walker et al., in preparation). In Figure 25a, rocks at Chloride Cliff and Monarch Canyon lie beneath the regional thrust belt décollement and are separated from rocks at Indian Pass and Echo Canyon by a substantial wedge of crust. Figure 25b represents the setting in Late Cretaceous time. In response to the waning of compression in the thrust belt coupled with a high regional heat flow associated with the adjacent Sierra Nevada batholith, an extensional regime develops in the middle crust, reactivating a portion of the regional décollement and moving a mid-crustal wedge (cf. Hodges and Walker, 1992) off towards the northwest. By removing this wedge, the rocks at Monarch Canyon and Chloride Cliff are juxtaposed across the combined Monarch Canyon and Chloride Cliff shear zones against the much shallower Indian Pass/Echo Canyon block (Figure 25c). Hodges and Walker (1992) argued that such a mid-crustal wedge could form if a strong layer of middle crust existed between two weak layers and was ejected in order to accommodate isostatic spreading of an overthickened crust. The portion of the décollement east of the wedge is labelled with a question mark because it is not known whether it was reactivated or was simply inactive at this time. The depths shown for Early Tertiary time are probably greater than was actually the case, because the erosional surface upon which the Titus Canyon Formation was deposited was the Stirling Quartzite and Wood Canyon Formation (Wright and Troxel, 1994), indicating that the entire Paleozoic section had been removed by earlier erosion, possibly as a result of an isostatic response to the Late Cretaceous unroofing event. Figure 25d represents the setting in Late Miocene time after movement on the Boundary Canyon detachment and subsequent doming of the footwall rocks due to isostatic rebound. Note that one feature of this model is that the extensional shear zone is dipping at a moderate angle toward the southeast between Chloride Cliff and Indian Pass, consistent with the observed geometry of the Monarch Canyon and Chloride Cliff shear zones east of Chloride Cliff (Plate 1 and A-A' in Plate 2). Both Monarch Canyon and Chloride Cliff are shown at some depth beneath the

surface in order to account for subsequent movement on the Keane Wonder fault, which may account for the final exhumation of these rocks since 6 Ma (Chapter 5).

Possible driving forces and regional significance of Late Cretaceous extension

A possible driving force for the extension discussed above is gravitationally-driven spreading brought on by a slowing of compression, indicated by the lack of Late Cretaceous thrusting in the region, coupled with a regionally high heat flow. Extension synchronous with or soon after compression has generally been ascribed to gravitationally driven spreading of an orogen as is seen in the Himalayas today (Burchfiel and Royden, 1985). Early Cenozoic extension in the Basin and Range has been attributed to gravitational collapse of an overthickened crustal welt accompanied by a high geothermal gradient associated with magmatism (Coney and Harms, 1984). Wernicke et al. (1987) observed a close temporal relationship between magmatism and subsequent extension. In areas where maximum crustal thickening coincided most closely with Cretaceous batholiths, for example the Shuswap complex in southern British Columbia (Carr, 1992), extension occurred soon after compression due to initial weakness of the lithosphere (Wernicke, 1992). This scenario has been used to explain the lack of extension earlier in Tertiary time for the Death Valley region, because it is an area of relatively minor Tertiary plutonism (Wernicke et al., 1987). In Late Cretaceous time, however, the Death Valley region lay adjacent to the Sierran arc, and metamorphism in both the Funeral Mountains and Panamint Mountains has been ascribed at least in part to regional contact metamorphism (Labotka and Albee, 1988). The last major pulse of Sierran magmatism ended at 80 Ma (Burchfiel et al., 1992) and may have had a dominant effect on regional heat flow in Late Cretaceous time.

Whether Late Cretaceous extension is essentially a local phenomenon or represents a regionally significant event remains to be seen. Both the Panamint Mountains on the western side of Death Valley and the Old Woman Mountains in southeastern California are

core complexes affected by Late Cretaceous plutonism: the Panamint Mountains by the Sierran arc and the Old Woman Mountains by the Old Woman-Piute Range batholith (Foster et al., 1989; Labotka and Albee, 1988). Late Cretaceous extension is well documented in the Old Woman Mountains (Carl et al., 1991), where the western Old Woman Mountains shear zone postdates 73 Ma intrusive rocks and is associated with rapid cooling between 73 Ma and 65 Ma. Late Cretaceous extension is also a possibility in the Panamint Mountains, where the earliest generation of normal faults may be responsible for cooling through greenschist-facies temperatures in Late Cretaceous to Eocene time (Hodges and Walker, 1992). These examples are part of a growing body of evidence that the areas of overthickened crust adjacent to the Sierran arc and other Cretaceous plutons may have undergone substantial extension in Late Cretaceous time.

An alternative explanation for Late Cretaceous extension is suggested by plate motions at that time and, in particular, on the location of the Kula-Farallon plate boundary. The Kula plate formed by breaking off from the Farallon plate around 85 Ma, but the latitude of the break is not well constrained (Woods and Davies, 1982). Within the uncertainty, the break may be either north of the western United States during Late Cretaceous and Paleocene time, in which case the Farallon plate would be adjacent to the Death Valley region, or to the south, in which case the Kula plate would be adjacent to the region (Engebretson et al., 1985). Farallon-North America convergence is very rapid and almost purely orthogonal during the period from 85 to 56 Ma (Engebretson et al., 1984). Kula-North America convergence is also rapid but very oblique with a significant right-lateral component (Engebretson et al., 1985). This component, which peaked around 75 Ma, may represent an alternative hypothesis to gravitational spreading for Late Cretaceous extension. If the plate boundary was transpressional and at least locally transtensional, then extension could have formed in a manner analogous to the modern Basin and Range province.

CONCLUSIONS

Multiple episodes of ductile fabrics are exposed in the rocks of the Funeral Mountains metamorphic core complex. These fabrics show evidence of Mesozoic compression followed by diachronous extension. Early unroofing of very deep rocks in Late Cretaceous time was accommodated by ductile shear zones within the core. This extensional event was followed by a considerable hiatus and then another extensional unroofing event in Late Miocene time accommodated by movement on the Boundary Canyon detachment. Both the Late Cretaceous and Miocene unroofing events may have been accompanied by doming. The youngest extension is oriented perpendicular to the regional extension direction and was accommodated by movement on the Keane Wonder fault and related normal faults within the core.

Models that show the Funeral Mountains as an intact structural block in Mesozoic time do not provide enough overburden to account for the depths of rocks exposed at the northwest end of the core. Instead, it appears that several thrust plates have been excised by the intracore shear zones, most likely the Monarch Canyon shear zone, which may represent a reactivated segment of the basal décollement for the Mesozoic thrust belt. This model suggests that Late Cretaceous extension within the core was responsible for a substantial component of the unroofing of the deepest rocks.

Late Cretaceous extensional unroofing of the core complex may be the result of a waning of compression, which allowed gravitationally controlled spreading of overthickened crust. In this model, flow of a mid-crustal wedge was facilitated by a high regional heat flow as a result of emplacement of large volumes of Late Cretaceous magma in the Sierran arc. This extensional episode may represent a regionally significant event along the margins of the arc and related plutonic bodies. Alternatively, extension may be related to a significant transpressional component to plate interactions at that time, a driving force similar to that for more recent extension. In either case, the documentation of an early extensional event accommodated by structures within the core complex rather than the core-

bounding detachment may have significant implications for the evolution of other metamorphic core complexes where such intracore shear zones are present, such as the Bitterroot core complex in Montana-Idaho and the Arizona core complexes (e.g., House and Hodges, in preparation; Davis and Lister, 1988).

REFERENCES

Applegate, J. D. R. and Hodges, K. V., 1993, Episodic unroofing of the Funeral Mountains metamorphic core complex, Death Valley, California: Geological Society of America Abstracts with Programs, v. 25, p. A411.

Applegate, J. D. R., Walker, J. D. and Hodges, K. V., 1992, Late Cretaceous extensional unroofing in the Funeral Mountains metamorphic core complex, California: Geology, v. 20, p. 519-522.

Armstrong, R. L., 1982, Cordilleran metamorphic core complexes – From Arizona to southern Canada: Annual Reviews of Earth and Planetary Science, v. 10, p. 129-154.

Burchfiel, B. C., Cowan, D. S. and Davis, G. A., 1992, Tectonic overview of the Cordilleran orogen in the western United States, *in* Burchfiel, B. C., and others, eds., The Cordilleran Orogen: Conterminous U.S., v. G-3, The Geology of North America: Boulder, CO, Geological Society of America, p. 407-479.

Burchfiel, B. C., Pelton, P. J. and Sutter, J., 1970, An early Mesozoic deformation belt in south-central Nevada–southeastern California: Geological Society of America Bulletin, v. 81, p. 211-215.

Burchfiel, B. C. and Royden, L. R., 1985, North-south extension within the convergent Himalayan region: Geology, v. 13, p. 679-682.

Carl, B. S., Miller, C. F. and Foster, D. A., 1991, Western Old Woman Mountains shear zone: Evidence for late ductile extension in the Cordilleran orogenic belt: Geology, v. 19, p. 893-896.

Carr, M. D. and Monsen, S. A., 1988, A field trip guide to the geology of Bare Mountain, *in* Weide, D. L., and Faber, M. L., eds., This extended land; Geological journeys in the southern Basin and Range; Geological Society of America Cordilleran Section Field Trip Guide: University of Nevada at Las Vegas Geosciences Department Special Publication 2, p. 50-57.

Carr, S. D., 1992, Tectonic setting and U-Pb geochronology of the Early Tertiary Ladybird Leucogranite Suite, Thor-Odin-Pinnacles area, southern Omineca Belt, British Columbia: Tectonics, v. 11, p. 258-278.

Cebula, G. T., Kunk, M. J., Mehnert, H. H., Naeser, C. W., Obradovich, J. D. and Sutter, J. F., 1986, The Fish Canyon tuff, a potential standard for the ^{40}Ar-^{39}Ar and fission-track methods: Terra Cognita, v. 6, p. 139-140.

Cemen, I. and Wright, L. A., 1990, Effect of Cenozoic extension on Mesozoic thrust surfaces in the central and southern Funeral Mountains, Death Valley, California, *in* Wernicke, B. P., ed., Basin and Range extensional tectonics near the latitude of Las Vegas: Geological Society of America Memoir 176, p. 305-316.

Cobbold, P. R. and Quinquis, H., 1980, Development of sheath folds in shear regimes: Journal of Structural Geology, v. 2, p. 119-126.

Coney, P. J. and Harms, T. A., 1984, Cordilleran metamorphic core complexes: Cenozoic extensional relics of Mesozoic compression: Geology, v. 12, p. 550-554.

Davis, G. A. and Lister, G. S., 1988, Detachment faulting in continental extension; Perspectives from the Southwestern U.S. Cordillera, *in* Clark, S. P., and others, eds., Processes in Continental Lithospheric Deformation: Boulder, CO, Geological Society of America Special Paper 218, p. 133-159.

Davis, G. H. and Coney, P. J., 1979, Geologic development of the Cordilleran metamorphic core complexes: Geology, v. 7, p. 120-124.

DeWitt, E., Sutter, J. F., Wright, L. A. and Troxel, B. W., 1988, Ar-Ar chronology of early Cretaceous regional metamorphism, Funeral Mountains, California – A case study of excess argon: Geological Society of America Abstracts with Programs, v. 20, p. A16.

Engebretson, D. C., Cox, A., and Gordon, R. G., 1985, Relative motions between oceanic and continental plates in the Pacific basin: Boulder, CO, Geological Society of America Special Paper 206, 59 pp.

Engebretson, D. C., Cox, A., and Thompson, G. A., 1984, Correlation of plate motions with continental tectonics: Laramide to Basin-Range: Tectonics, v. 3, p. 115-119.

Foster, D. A., Harrison, T. M. and Miller, C. F., 1989, Age, inheritance, and uplift history of the Old Woman-Piute batholith, California, and implications for K-feldspar age spectra: Journal of Geology, v. 97, p. 232-243.

Giaramita, M. J., 1984, Structural evolution and metamorphic petrology of the Monarch Canyon area, northern Funeral Mountains, Death Valley, California [M.S. thesis]: University of California, Davis, 145 pp.

Hamilton, W. B., 1988, Detachment faulting in the Death Valley region, California and Nevada: U.S. Geological Survey Bulletin, v. 1790, p. 51-85.

Hansen, E., 1971, Strain Facies: New York, Springer-Verlag, 207 pp.

Harding, M. B., 1987, Geology of the Wildrose Peak area, Death Valley region, California [M.S. thesis]: University of Wyoming, 196 pp.

Hawthorne, F. C., 1981, Crystal chemistry of the amphiboles, *in* Veblen, D. R., ed., Amphiboles and other hydrous pyriboles – mineralogy: Mineralogical Society of America Reviews in Mineralogy, v. 9A, p. 1-102.

Heaman, L. M. and Grotzinger, J. P., 1992, 1.08 Ga diabase sills in the Pahrump Group, California: Implications for development of the Cordilleran miogeocline: Geology, v. 20, p. 637-640.

Hodges, K. V., Hames, W. E., Olszewski, W., Burchfiel, B. C., Royden, L. H., and Chen, Z., 1994, Thermobarometric and 40Ar/39Ar geochronologic constraints on Eohimalayan metamorphism in the Dinggyê area, southern Tibet: Contributions to Mineralogy and Petrology, in press.

Hodges, K. V., McKenna, L. W. and Harding, M. B., 1990, Structural unroofing of the central Panamint Mountains, Death Valley region, southeastern California, *in*

Wernicke, B. P., ed., Basin and Range extensional tectonics near the latitude of Las Vegas, Nevada, v. Boulder, Colorado, Geological Society of America Memoir 176, p. 377-389.

Hodges, K. V. and Walker, J. D., 1990, Petrologic constraints on the unroofing history of the Funeral Mountains metamorphic core complex, California: Journal of Geophysical Research, v. 95, p. 8437-8445.

Hodges, K. V. and Walker, J. D., 1992, Extension in the Cretaceous Sevier orogen, North American Cordillera: Geological Society of America Bulletin, v. 104, p. 560-569.

Hodges, K. V., Walker, J. D. and Wernicke, B. P., 1987, Footwall structural evolution of the Tucki Mountain detachment system, Death Valley region, southeastern California, *in* Coward, M. P., and others, eds., Continental Extensional Tectonics: Geological Society of London Special Publication 28, p. 393-408.

Hoisch, T. D., 1991, Equilibria within the mineral assemblage quartz + muscovite + biotite + garnet + plagioclase, and implications for the mixing properties of octahedrally-coordinated cations in muscovite and biotite: Contributions to Mineralogy and Petrology, v. 108, p. 43-54.

Hoisch, T. D. and Simpson, C., 1993, Rise and tilt of metamorphic rocks in the lower plate of a detachment fault in the Funeral Mountains, Death Valley, California: Journal of Geophysical Research, v. 98, p. 6805-6827.

Holm, D. K. and Dokka, R. K., 1991, Major Late Miocene cooling of the middle crust associated with extensional orogenesis in the Funeral Mountains, California: Geophysical Research Letters, v. 18, p. 1775-1778.

Holm, D. K. and Wernicke, B. P., 1990, Black Mountains crustal section, Death Valley extended terrain, California: Geology, v. 18, p. 520-523.

Hudec, M. R., 1992, Mesozoic structural and metamorphic history of the central Ruby Mountains metamorphic core complex, Nevada: Geological Society of America Bulletin, v. 104, p. 1086-1100.

Hunt, C. B. and Mabey, D. R., 1966, Stratigraphy and structure, Death Valley, California: U.S. Geological Survey Professional Paper 494-A, 162 pp.

Labotka, T. C., 1980, Petrology of a medium-pressure regional metamorphic terrane, Funeral Mountains, California: American Mineralogist, v. 65, p. 670-689.

Labotka, T. C. and Albee, A. L., 1988, Metamorphism and tectonics of the Death Valley region, California, *in* Ernst, W. G., ed., Metamorphism and Crustal Evolution of the Western United States, v. Englewood Cliffs, N.J., Prentice-Hall, p. 714-736.

Labotka, T. C., Albee, A. L., Lanphere, M. A. and McDowell, S. D., 1980, Stratigraphy, structure, and metamorphism in the central Panamint Mountains, Telescope Peak quadrangle, Death Valley area, California: Geological Society of America Bulletin, v. 91, part 2, p. 843-933.

Lister, G. S. and Snoke, A. W., 1984, S-C mylonites: Journal of Structural Geology, v. 6, p. 617-638.

Maldonado, F., 1990, Structural geology of the upper plate of the Bullfrog Hills detachment fault system, southern Nevada: Geological Society of America Bulletin, v. 102, p. 992-1006.

Miller, E. L. and Gans, P. B., 1989, Cretaceous crustal structure and metamorphism in the hinterland of the Sevier thrust belt, western U.S. Cordillera: Geology, v. 17, p. 59-62.

Miller, J. M. G., 1985, Glacial and syntectonic sedimentation: The Upper Proterozoic Kingston Peak Formation, southern Panamint Range, eastern California: Geological Society of America Bulletin, v. 96, p. 1537-1553.

Passchier, C. W. and Simpson, C., 1986, Porphyroclast systems as kinematic indicators: Journal of Structural Geology, v. 8, p. 831-843.

Reynolds, M. W., 1976, Geology of the Grapevine Mountains, Death Valley, California: A summary, *in* Troxel, B. W., and Wright, L. A., eds., Geologic Features, Death Valley, California, Special Reports California Division of Mines and Geology v. 106: p. 19-25.

Reynolds, M. W., Wright, L. A. and Troxel, B. W., 1986, Geometry and chronology of late Cenozoic detachment faulting, Funeral and Grapevine Mountains, Death Valley, California: Geological Society of America Abstracts with Programs, v. 18, p. 175.

Samson, S. D. and Alexander, E. C., 1987, Calibration of the interlaboratory $^{40}Ar/^{39}Ar$ dating standard, MMhb-1: Chemical Geology, v. 66, p. 27-34.

Saylor, B. Z. and Hodges, K. V., 1991, The Titus Canyon Formation: Evidence for Early Oligocene extension in the Death Valley area, CA: Geological Society of America Abstracts with Programs, v. 23, p. A82.

Snow, J. K., Asmerom, Y., and Lux, D. R., 1991, Permian-Triassic plutonism and tectonics, Death Valley region, California and Nevada: Geology, v. 19, p. 629-632.

Snow, J. K. and Wernicke, B., 1989, Uniqueness of geological correlations: An example from the Death Valley extended terrain: Geological Society of America Bulletin, v. 101, p. 1351-1362.

Spear, F. S. and Kimball, K. L., 1984, RECAMP - A Fortran IV program for estimating Fe^{3+} contents in amphiboles: Computers and Geosciences, v. 10, p. 317-325.

Spencer, J. E., 1984, Role of tectonic denudation in warping and uplift of low-angle normal faults: Geology, v. 12, p. 95-98.

Stewart, J. H., 1970, Upper Precambrian and Lower Cambrian strata in the southern Great Basin, California and Nevada: U.S.Geological Survey Professional Paper 620, 206 pp.

Troxel, B. W., 1988, A geologic traverse of the northern Funeral Mountains, Death Valley, California, *in* Weide, D. L., and Faber, D. L., eds., This extended land; Geological journeys in the southern Basin and Range; Geological Society of America Cordilleran Section Field Trip Guide: University of Nevada at Las Vegas Geosciences Department Special Publication 2, p. 45-49.

Wernicke, B., 1992, Cenozoic extensional tectonics of the U.S. Cordillera, *in* Burchfiel, B. C., and others, eds., The Cordilleran Orogen: Conterminous U.S., v. G-3, The Geology of North America: Boulder, CO, Geological Society of America, p. 553-581.

Wernicke, B., Axen, G.J., and Snow, J.K., 1988, Basin and Range extensional tectonics at the latitude of Las Vegas, Nevada: Geological Society of America Bulletin, v. 100, p. 1738-1757.

Wernicke, B., Christiansen, R. L., England, P. C. and Sonder, L. J., 1987, Tectonomagmatic evolution of Cenozoic extension in the North American Cordillera, *in* Coward, M. P., and others, eds., Continental Extensional Tectonics: Geological Society of London Special Publication 28, p. 203-221.

Woods, M. T., and Davies, G. F., 1982, Late Cretaceous genesis of the Kula plate: Earth and Planetary Science Letters, v. 58, p. 161-166.

Wright, L. A., 1973, Geology of the SE1/4 of Tecopa 15-minute quadrangle, San Bernardino and Inyo Counties, California: California Division of Mines and Geology Map Sheet 20.

Wright, L. A. and Troxel, B. W., 1966, Strata of Late Precambrian-Cambrian age, Death Valley region, California-Nevada: Bulletin of the American Association of Petroleum Geologists, v. 50, p. 846-857.

Wright, L. A. and Troxel, B. W., 1994 in press, Geologic map of the central and northern parts of the Funeral Mountains and adjacent areas, Death Valley region, southern California, scale 1:48,000: U.S. Geol. Surv. Misc. Invest. Ser. I-2305.

York, D., 1969, Least squares fitting of a straight line with correlated errors: Earth and Planetary Science Letters, v. 5, p. 320-324.

APPENDIX

Sample Descriptions and Analytical Procedures for $^{40}Ar/^{39}Ar$ Geochronology

Based on electron microprobe data recalculated using the approach of Spear and Kimball (1984), amphibole from sample 613-1 has a formula of $(K_{0.192}Na_{0.621})$ $(Na_{0.127}Ca_{1.778})$ $(Mn_{0.020}Fe^{2+}_{1.073}Ti_{0.476}Fe^{3+}_{0.338}Al_{0.076})$ $(Al_{2.051}Si_{5.949})$ O_{22} $(OH)_2$. Using the classification scheme of Hawthorne (1981), this sample is magnesio-hastingsite. Separation procedures and analytical techniques are described more fully in Chapter 3 as well as in Hodges et al. (1994, in press). The amphibole separate was hand-picked grain-by-grain, resulting in at least 99.9% purity. The separate was irradiated for 15 hours in the core of the research reactor at McMaster University in Hamilton, Ontario as part of irradiation package CLAIR 12. The fast neutron flux was monitored with MMhb-1 hornblende (520.4 Ma; Samson and Alexander, 1987) and Fish Canyon sanidine (20.4 Ma; Cebula et al., 1986). The samples were analyzed at the Cambridge Laboratory for Argon Isotope Research at the Massachusetts Institute of Technology using a MAP 215-50 mass spectrometer and a Coherent 10 W argon-ion laser. Laser fusion analyses were conducted by exposing 5- to 10-grain subsamples to the continuous emission of the laser operating for 10 seconds at approximately 4 W. Additional details of laboratory procedures, descriptions of facilities, and propagation of uncertainties can be found in Hodges et al. (1994, in press). The average laser M/e blank for this sample was 5×10^{-16} moles.

Table 1. Sequence of deformational phases in the metamorphic rocks of the Funeral Mtns.

Phase	Structural elements	Inferred vergence or transport direction	Age
D_{1-2}	Recumbent folds (F_{1-2}) Axial-planar foliation (S_1)	—	>112 Ma (pre- or syn-peak Mm.)
D_3	Extensional intracore shear zones Regional foliation (S_3) Stretching lineation (L_{3s}) Mineral lineation (L_{3m})	WNW	72-65 Ma
D_4	Tight to isoclinal folds (F_4) Axial-planar foliation (S_4) Crenulation hinge and S_3-S_4 intersection lineation (L_4)	WNW	72-65 Ma
D_5	Doming of core rocks "Stair-step" upright folds (F_5) Dome-and-basin folds (F_{5DB}) Boudinage	—	<70 Ma (continues after D_6)
D_6	Boundary Canyon detachment	WNW	<11 Ma
D_7	Keane Wonder fault Brittle low-angle faults within the core	SW	? 2-3 Ma ?

Table 2. $^{40}Ar/^{39}Ar$ Laser-fusion Analytical Data for sample 613-1, amphibole

Subsample	$^{39}Ar/^{40}Ar$	$^{36}Ar/^{40}Ar$	$^{39}Ar_K$ (x 10^{-14})	$^{40}Ar^*$(%)	K/Ca	Age (Ma) (± 2σ)
1 +	0.1891	0.0003	3.6	90.8	0.1	32.1 ± 0.6
2 +	0.1164	0.0018	2.4	45.5	0.1	26.2 ± 0.5
3 +	0.1554	0.0017	7.9	51.2	0.2	22.1 ± 0.4
4	0.1671	0.0027	4.0	20.0	0.1	8.0 ± 0.2
5	0.1870	0.0029	3.6	14.7	0.1	5.3 ± 0.1
6 +	0.1286	0.0020	3.0	40.8	0.1	21.3 ± 0.4
7 +	0.1422	0.0010	2.7	71.8	0.1	33.7 ± 0.7
8 +	0.1620	0.0006	2.5	81.8	0.1	33.7 ± 0.7
9 +	0.1467	0.0022	3.2	35.8	0.1	16.4 ± 0.3
10 +	0.1412	0.0014	2.1	58.1	0.1	27.5 ± 0.5

York 2 regression age = 33.2 ± 0.7 Ma. MSWD = 1.0. $(^{40}Ar/^{36}Ar)_0$ = 190 ± 70. J = 0.003735 ± 0.00003735. Subsamples used in regression are marked with a plus sign. $^{39}Ar_K$ — moles of irradiation-produced ^{39}Ar released during laser fusion. $^{40}Ar^*$ (%) — percentage of measured ^{40}Ar derived from natural decay of ^{40}K.

FIGURE CAPTIONS

Figure 1 Regional map of Death Valley extensional corridor including features described in text. Box in inset shows location of Figure 1. Dashed boxes on main figure show locations of Figures 2 and 3. Stippled pattern indicates outcrop of pre-Tertiary rocks. Heavy lines show major Tertiary faults: strike-slip faults are shown with arrows, and normal faults are unornamented. Abbreviations refer to: DVF–Death Valley fault, GF–Garlock fault, NDF–Northern Death Valley fault zone (also referred to as the Furnace Creek fault zone), PVF–Panamint Valley fault, and SDF–Southern Death Valley fault zone. Map modified from Wernicke et al., 1988.

Figure 2 Simplified tectonic map of the central and northern Funeral Mountains with locations discussed in text. Dashed box shows area of Figure 4 (and Plate 1). Map modifed from Wright and Troxel (1994).

Figure 3 Map of northern Death Valley showing location of Mesozoic thrusts and correlations across the Northern Death Valley-Furnace Creek fault zone after Wernicke et al. (1988). Pre-Tertiary outcrop is shown by stippled pattern. Geographic features are labeled in Figure 1.

Figure 4 Simplified tectonic map of mapping area in northern Funeral Mountains including sample localities. More detail is shown on Plate 1. Lines of cross-sections found in Plate 2 are marked.

Figure 5 Tectonic stratigraphy of the metamorphic core rocks exposed in the northern Funeral Mountains, showing the placement of the intracore shear zones. Units are same as in Plate 1 and are discussed in text.

Figure 6 Photograph of F_{1-2} folds in marble of the Crystal Spring Formation east of Monarch Canyon. Hammer for scale.

Figure 7 Lower hemisphere, equal area stereonet plots of F_{1-2} fold axes. (a) F_{1-2} scatter plot. (b) F_{1-2} contour plot; contour interval = 4%/1% area.

Figure 8 Sketch of garnet porphyroblast from Lower Crystal Spring Formation pelitic schist in Monarch Canyon. Internal foliation (S_i) is defined by aligned quartz inclusions in the garnet. Subsequent S_3 foliation is defined by muscovite and biotite grains and goes around garnet.

Figure 9 Lower hemisphere, equal area stereo plots of poles to S_3 foliation planes. (a) S_3 scatter plot with mean vector and great circle. (b) S_3 contour plot; contour interval = 4%/1% area.

Figure 10 Photograph of L_{3s} stretching lineations in outcrop of Beck Spring marble at Chloride Cliff. Pencil is aligned with lineation which is defined by elongate calcite aggregates.

Figure 11 Lower hemisphere, equal area stereonet plots of L_3 lineations. (a) Scatter plot of L_{3s} stretching lineations with mean vector. (b) L_{3s} contour plot; contour interval = 4%/1% area. (c) Scatter plot of L_{3m} mineral lineations with mean vector. (d) L_{3m} contour plot; contour interval = 4%/1% area.

Figure 12 Photograph of F_4 folds in silty marble of the lower Kingston Peak Formation east of Monarch Canyon. Northwest is to the left in photograph. Hammer for scale.

Figure 13 Lower hemisphere, equal area stereonet plots of F_4 fold axes. (a) F_4 scatter plot with mean vector. (b) F_4 contour plot; contour interval = 4%/1% area.

Figure 14 Lower hemisphere, equal area stereonet plots of L_4 lineations. (a) L_4 scatter plot with mean vector. (b) L_4 contour plot; contour interval = 4%/1% area. Dashed lines indicate separation angle obtained for F_4 folds from Hansen (1971) analysis shown in Figure 24.

Figure 15 Photomicrograph of L_4 crenulation hinges in pelitic schist of upper Crystal Spring Formation from Monarch Canyon. Crenulation is defined by biotite and muscovite. Field of view is 4 mm across.

Figure 16 Lower hemisphere, equal area stereonet scatter plot of F_5 and F_{5DB} fold axes. (a) F_5 fold axes. (b) F_{5DB} fold axes.

Figure 17 Photograph of meter-scale F_{5DB} dome-and-basin folding in Middle Crystal Spring calcite marble exposed in Monarch Canyon. Field assistant (1.8 m) and hammer (0.3 m) for scale.

Figure 18 Photograph of D_5 boudinage affecting Late Cretaceous pegmatite dike in Monarch Canyon. Note the "bow-tie" effect caused by boudinage along orthogonal axes. Hammer for scale.

Figure 19 Photomicrograph of Type II S-C mylonitic fabric in pelitic schist from Monarch Canyon. Northwest is to right in this photograph. Mica "fish" indicate transport direction top-to-the-right. Field of view is 2 mm.

Figure 20 Lower hemisphere, equal area contour plots for three regions within the core complex: Monarch Canyon, Chloride Cliff, and adjacent to the Keane Wonder fault. Plots are superimposed on map from Figure 4. Contour interval = 4%/1% area. (a) Poles to S_3 foliation planes. (b) L_{3S} stretching lineations. (c) L_4 lineations.

Figure 21 Lower hemisphere, equal area contour plots comparing poles to F_4 axial planes to poles to S_3 foliation planes; contour interval = 4%/1% area. (a) F_4 poles to axial planes. (b) S_3 poles to planes.

Figure 22 Photograph of highly-strained metadiamictite of upper Kingston Peak Formation between Monarch Canyon and Chloride Cliff shear zones near Chloride Cliff. Tan marble clasts in carbonate matrix have become highly stretched, whereas clasts of basement orthogneiss are less deformed, showing much greater strength. Hammer for scale.

Figure 23 Lower hemisphere, equal area stereonet plot showing Hansen (1971) analysis of F_4 fold axes showing distinct vergence. Curved arrows show sense of overturning in either clockwise or counterclockwise direction relative to the plunge of the axis. Shaded area represents separation angle of 42°. Large arrow shows transport direction inferred from kinematic indicators.

Figure 24 Inverse isotope correlation diagram showing results of $^{40}Ar/^{39}Ar$ laser fusion analysis of amphiboles from sample 613-1, a diabase dike in Monarch Canyon that cuts all ductile fabrics in the high-grade core rocks. Sample location in Figure 4. Numbers correspond to the individual subsamples listed in Table 2. Filled symbols are those used in regression analyses, the results of which are indicated by solid line.

Figure 25 Cartoon showing model for development of the Funeral Mountains metamorphic core complex. (a) Early Cretaceous: metamorphism of core rocks and thrust belt active. (b) Late Cretaceous: extrusion of mid-crustal wedge along extensional shear zones which react portion of thrust belt décollement. (c) Early Tertiary: shear zones are inactive and detachment system has not yet become active. (d) Late Miocene: after movement on Boundary Canyon detachment and major regional extension.

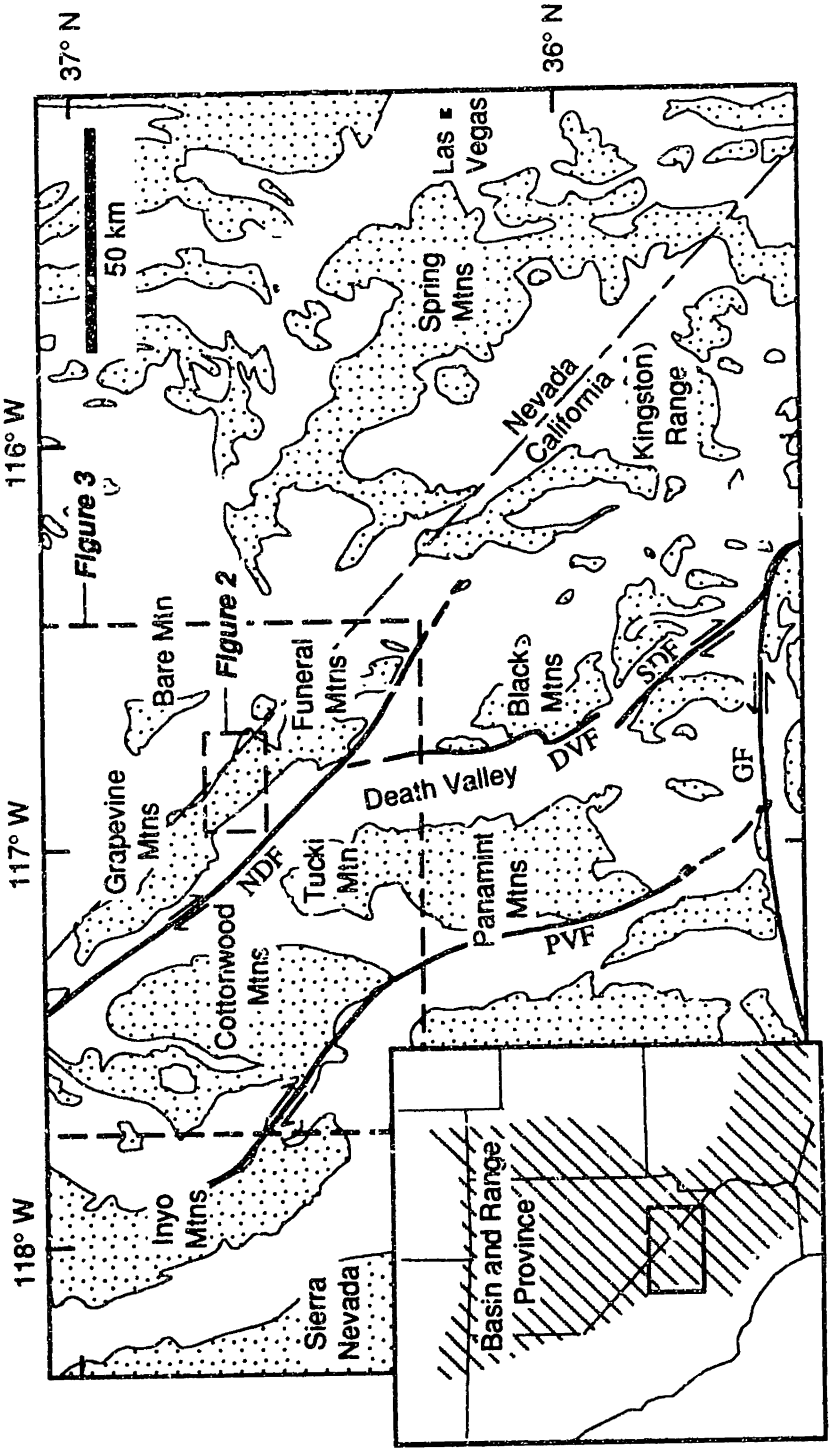
37° N
36° N
116° W
117° W
118° W
50 km
Figure 3
Figure 2
Las Vegas
Spring Mtns
Nevada
California
Kingston Range
Bare Mtn
Funeral Mtns
Black Mtns
SFF
DVF
GF
Death Valley
Grapevine Mtns
NDF
Tucki Mtn
Panamint Mtns
PVF
Cottonwood Mtns
Inyo Mtns
Sierra Nevada
Basin and Range Province

Figure 1

116°45'
36°45'
N
0
5
km
Cover rocks
Quaternary deposits
Precambrian-Tertiary sedimentary rocks
Core rocks
Proterozoic Stirling Quartzite
Proterozoic Johnnie Formation
Proterozoic Noonday & Kingston Peak Fms.
Proterozoic Beck Spring & Crystal Spring Fms.
Figure 4
NV
CA
Indian Pass
Death Valley
117°00'
Boundary Canyon detachment
Keane Wonder fault
Tertiary normal faults
Intracore extensional shear zones
Garnet isograd (Labotka, 1980)
Staurolite + biotite isograd (Labotka, 1980)

Figure 2

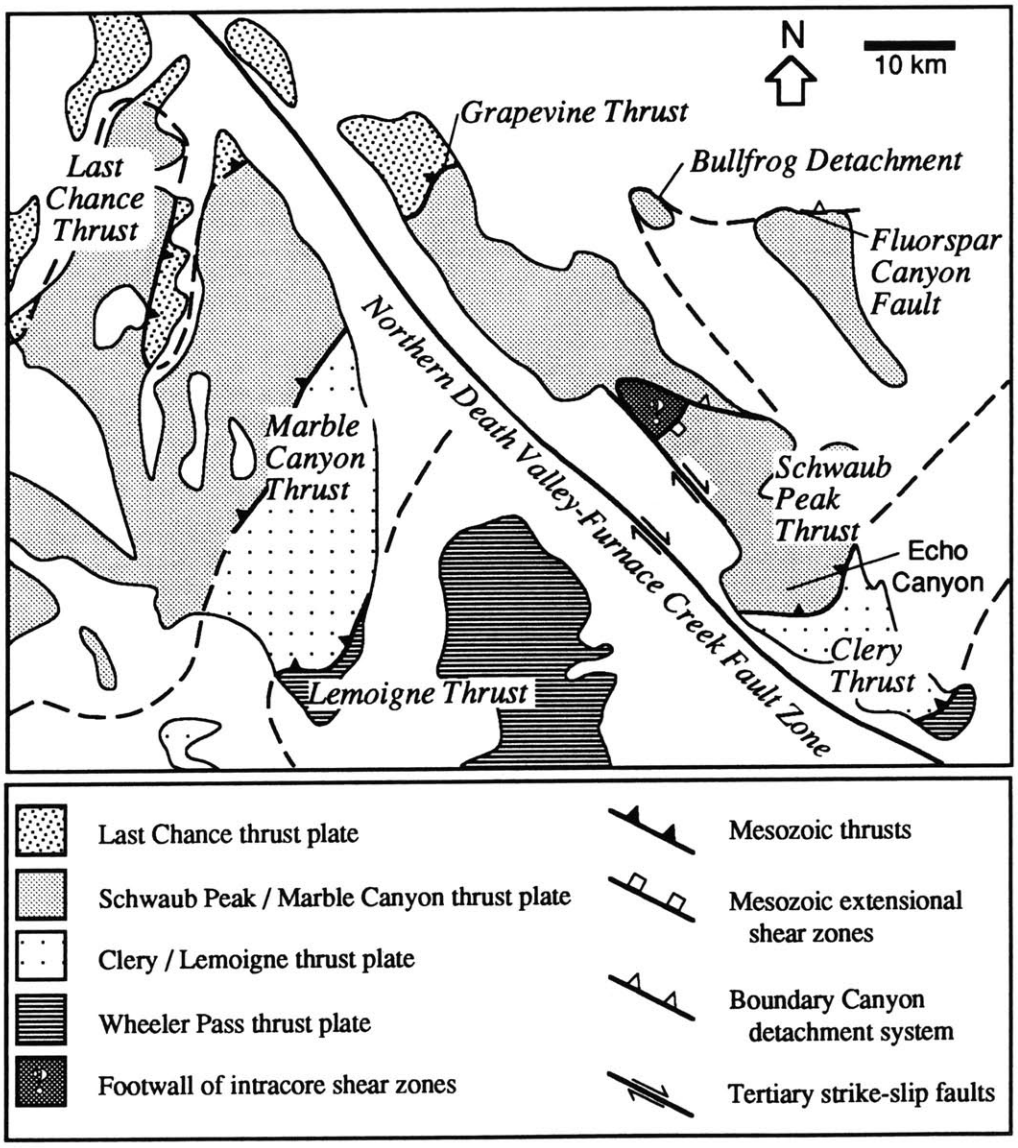
N
10 km
Grapevine Thrust
Bullfrog Detachment
Last Chance Thrust
Fluorspar Canyon Fault
Northern Death Valley-Furnace Creek Fault Zone
Marble Canyon Thrust
Schwaub Peak Thrust
Echo Canyon
Clery Thrust
Lemoigne Thrust
Last Chance thrust plate
Schwaub Peak / Marble Canyon thrust plate
Clery / Lemoigne thrust plate
Wheeler Pass thrust plate
Footwall of intracore shear zones
Mesozoic thrusts
Mesozoic extensional shear zones
Boundary Canyon detachment system
Tertiary strike-slip faults

Figure 3

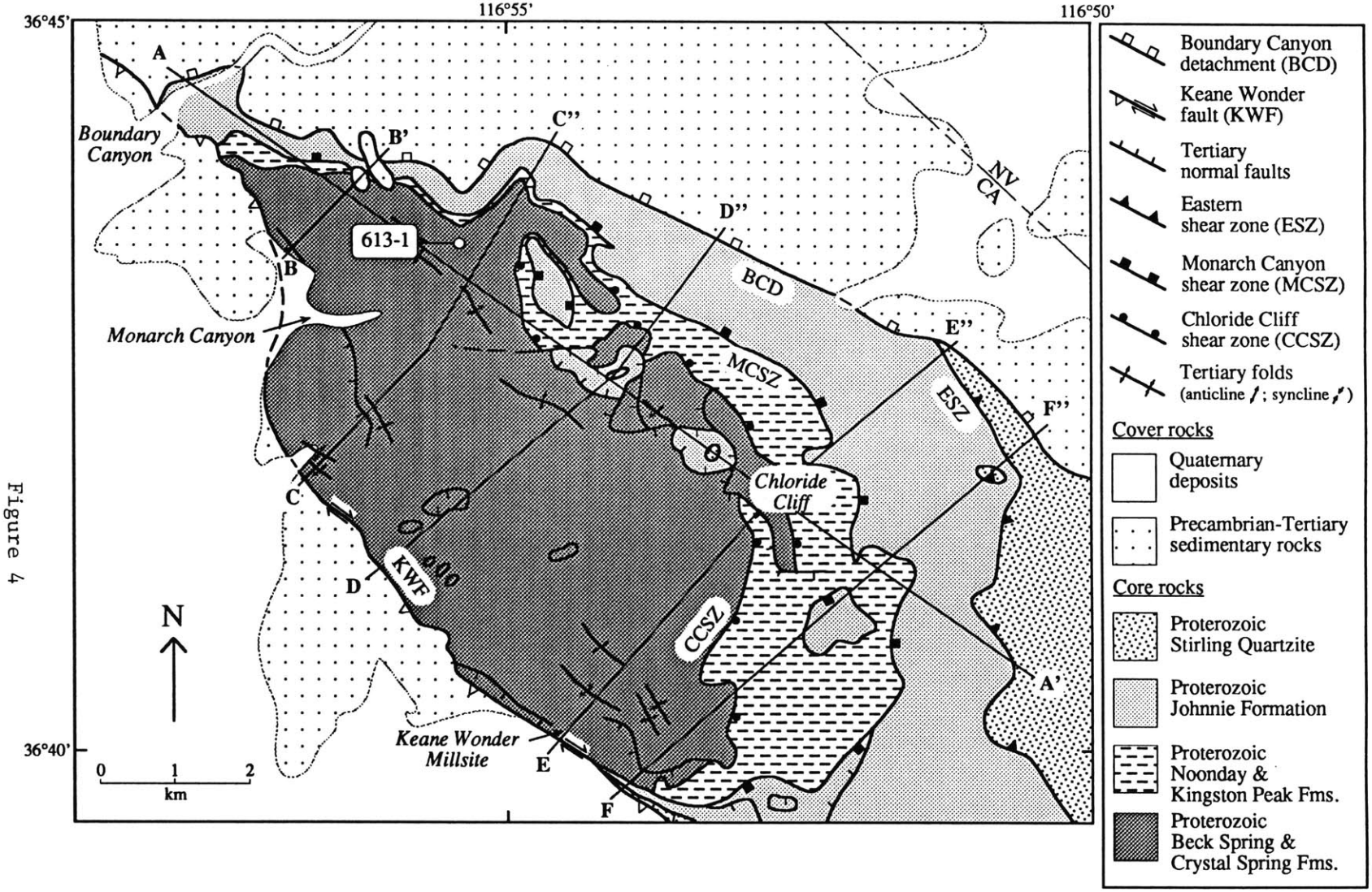
36°45'
116°55'
116°50'
36°40'
A
A'
B
B'
C
C''
D
D''
E
E''
F
F''
Boundary Canyon
Monarch Canyon
613-1
BCD
MCSZ
ESZ
CCSZ
KWF
NV
CA
Chloride Cliff
Keane Wonder Millsite
N
0
1
2
km
Boundary Canyon detachment (BCD)
Keane Wonder fault (KWF)
Tertiary normal faults
Eastern shear zone (ESZ)
Monarch Canyon shear zone (MCSZ)
Chloride Cliff shear zone (CCSZ)
Tertiary folds (anticline ; syncline)
Cover rocks
Quaternary deposits
Precambrian-Tertiary sedimentary rocks
Core rocks
Proterozoic Stirling Quartzite
Proterozoic Johnnie Formation
Proterozoic Noonday & Kingston Peak Fms.
Proterozoic Beck Spring & Crystal Spring Fms.

Figure 4

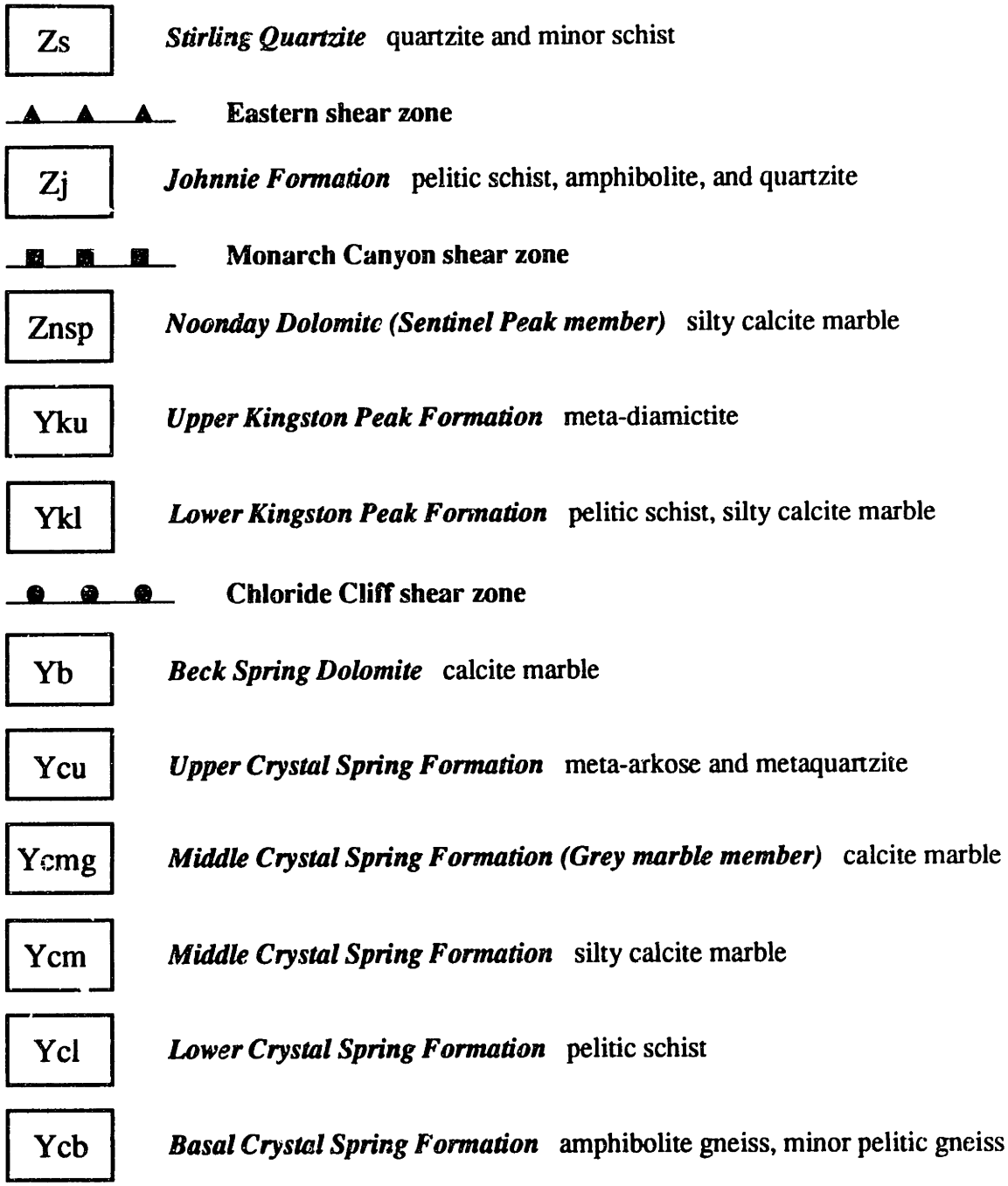
Zs
Stirling Quartzite quartzite and minor schist
Eastern shear zone
Zj
Johnnie Formation pelitic schist, amphibolite, and quartzite
Monarch Canyon shear zone
Znsp
Noonday Dolomite (Sentinel Peak member) silty calcite marble
Yku
Upper Kingston Peak Formation meta-diamictite
Ykl
Lower Kingston Peak Formation pelitic schist, silty calcite marble
Chloride Cliff shear zone
Yb
Beck Spring Dolomite calcite marble
Ycu
Upper Crystal Spring Formation meta-arkose and metaquartzite
Ycmg
Middle Crystal Spring Formation (Grey marble member) calcite marble
Ycm
Middle Crystal Spring Formation silty calcite marble
Ycl
Lower Crystal Spring Formation pelitic schist
Ycb
Basal Crystal Spring Formation amphibolite gneiss, minor pelitic gneiss

Figure 5

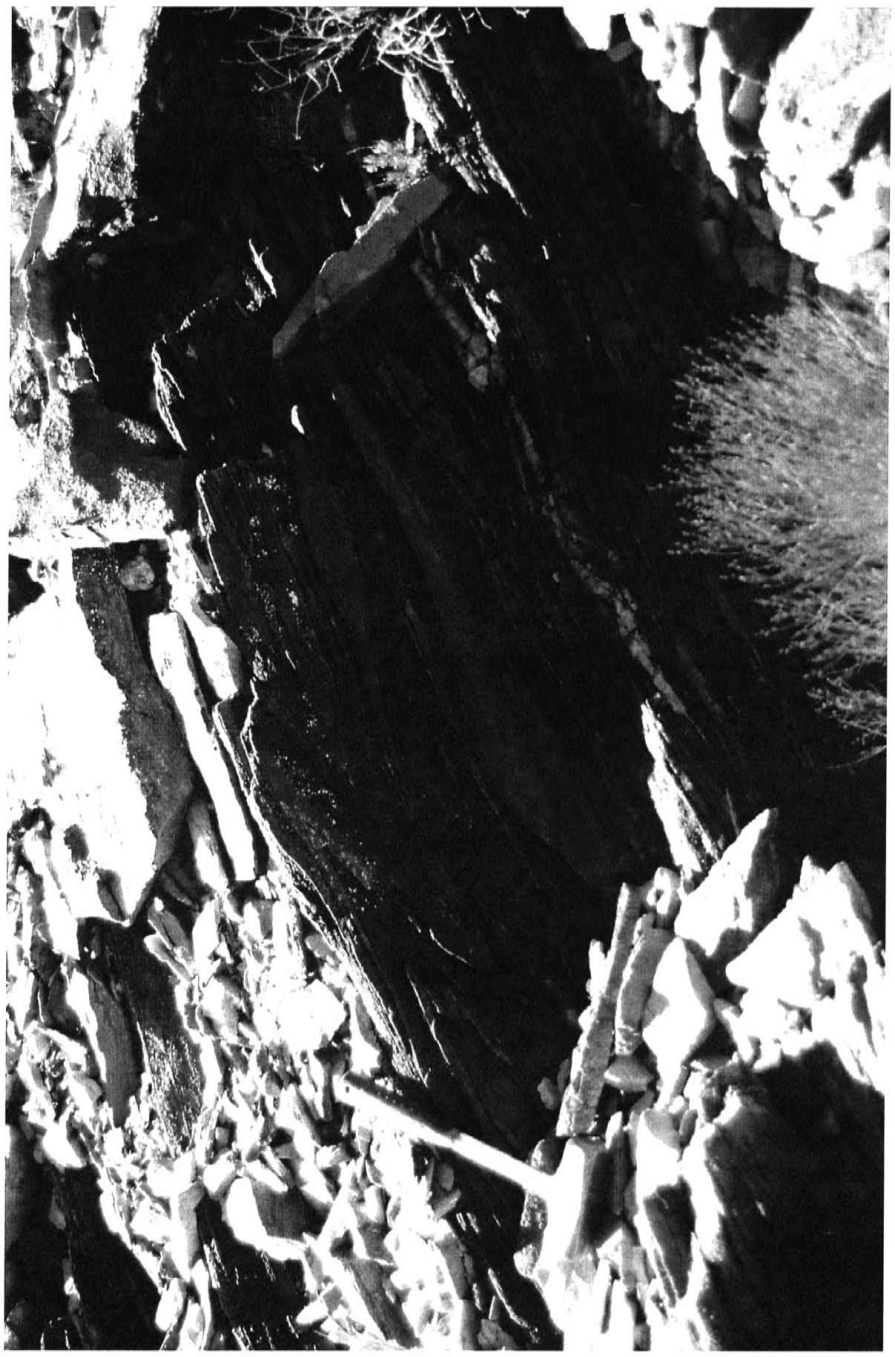

Figure 6

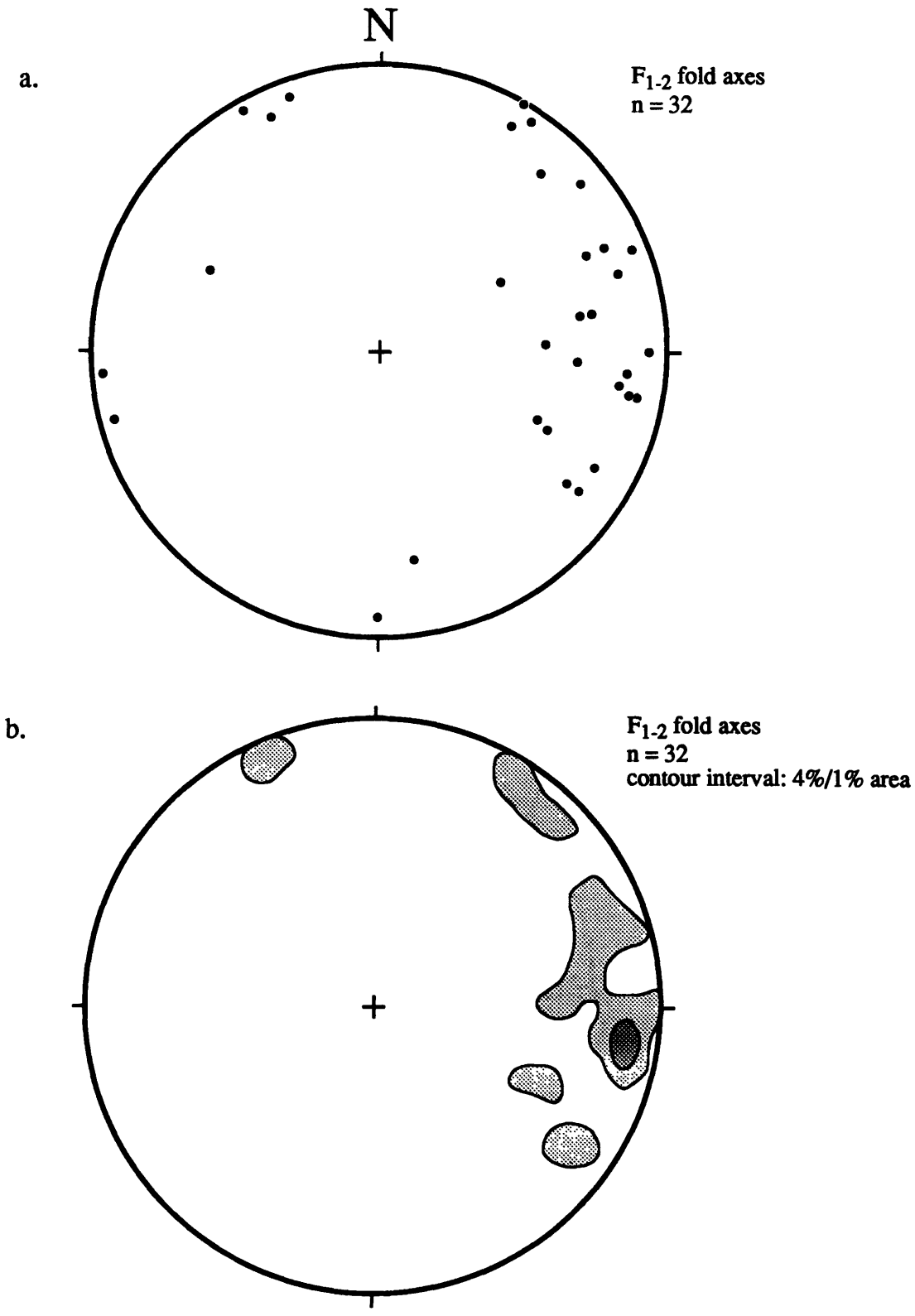
a.
N
F_{1-2} fold axes
n = 32
b.
F_{1-2} fold axes
n = 32
contour interval: 4%/1% area

Figure 7

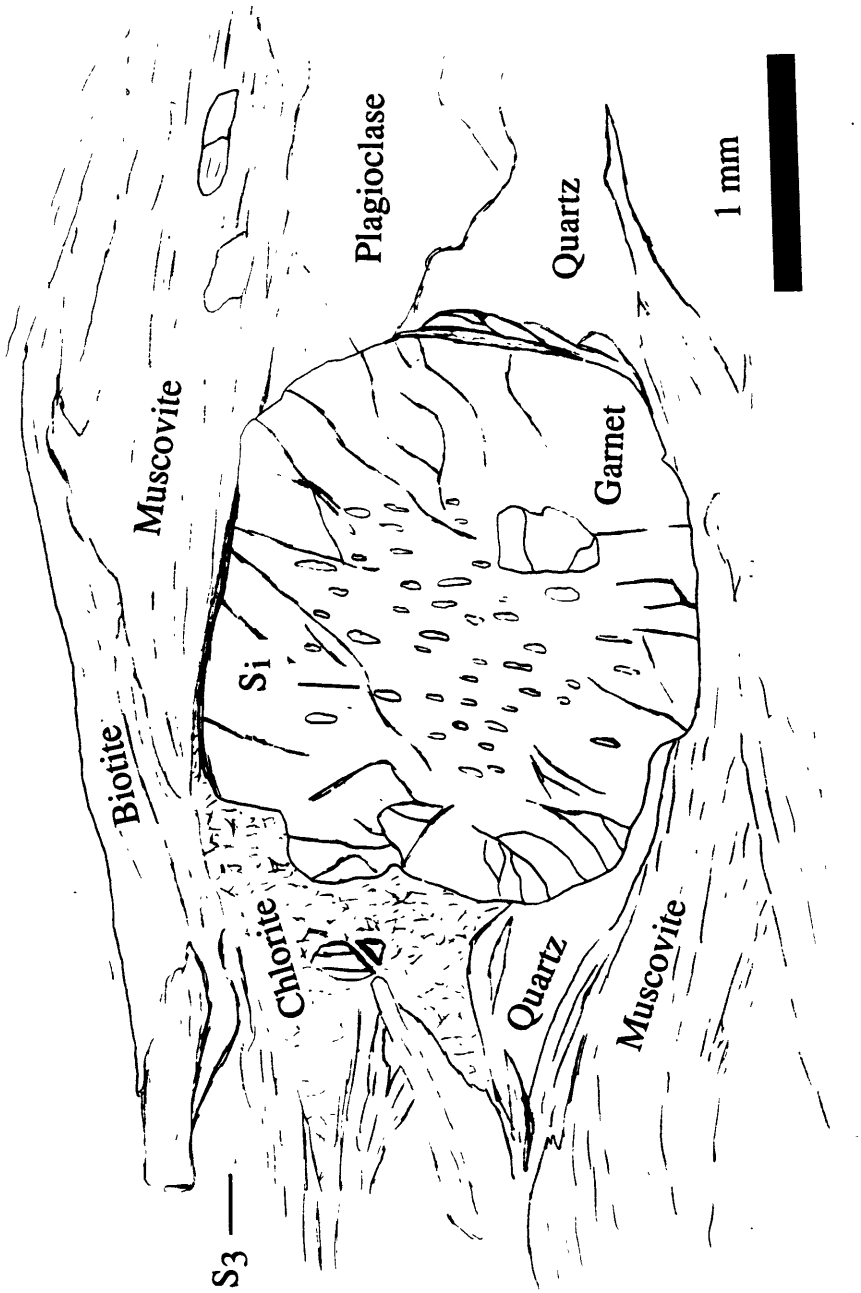
Biotite
Muscovite
Si
Plagioclase
Quartz
Garnet
1 mm
Chlorite
Quartz
Muscovite
S3

Figure 8

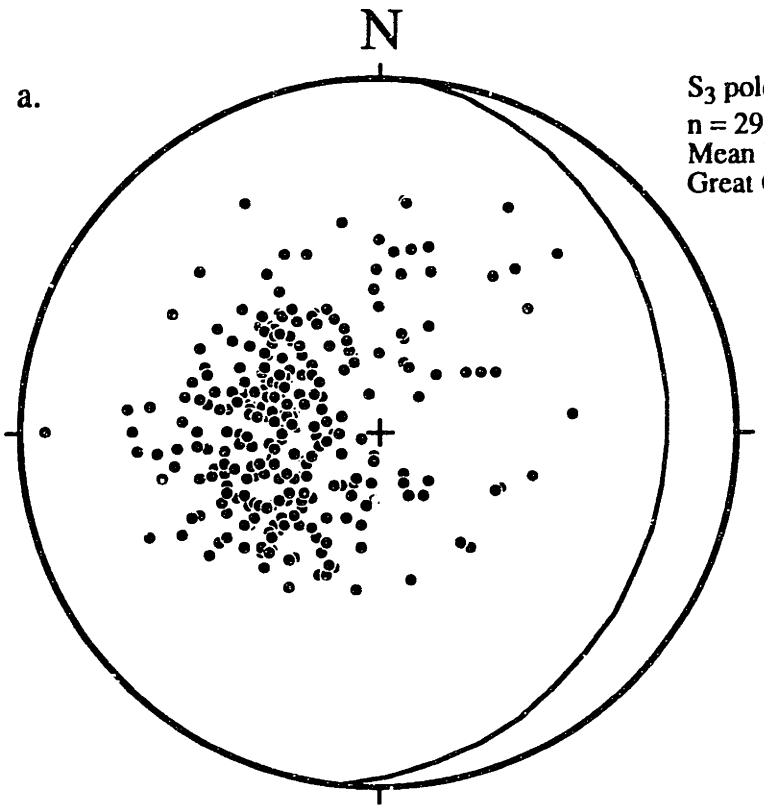
N
a.
S_3 poles to foliations
n = 293
Mean Vector: 70, N84W
Great Circle: N6E, 20 SE

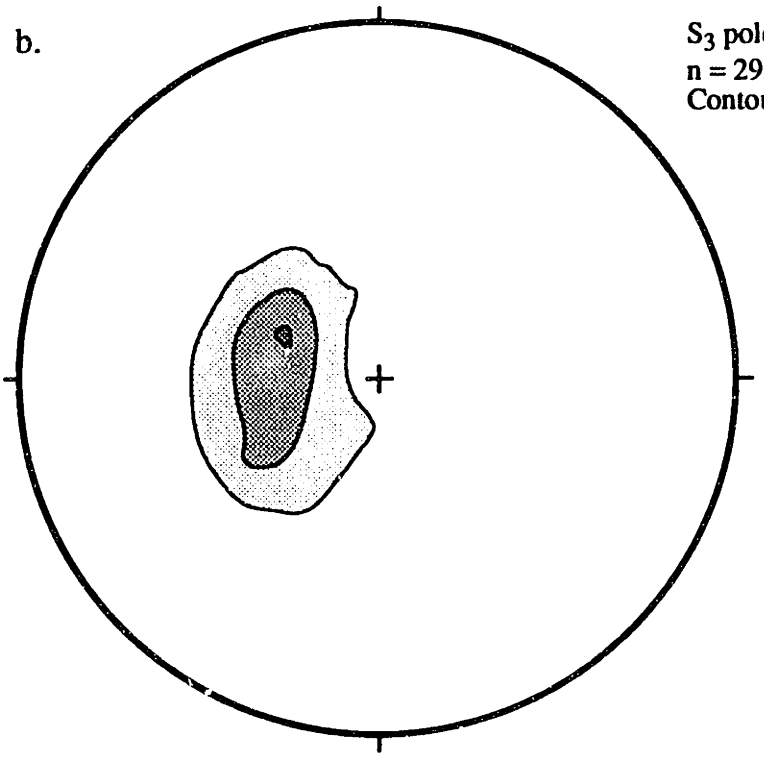
b.
S_3 poles to foliations
n = 293
Contour interval: 4% / 1% area

Figure 9

Figure 10

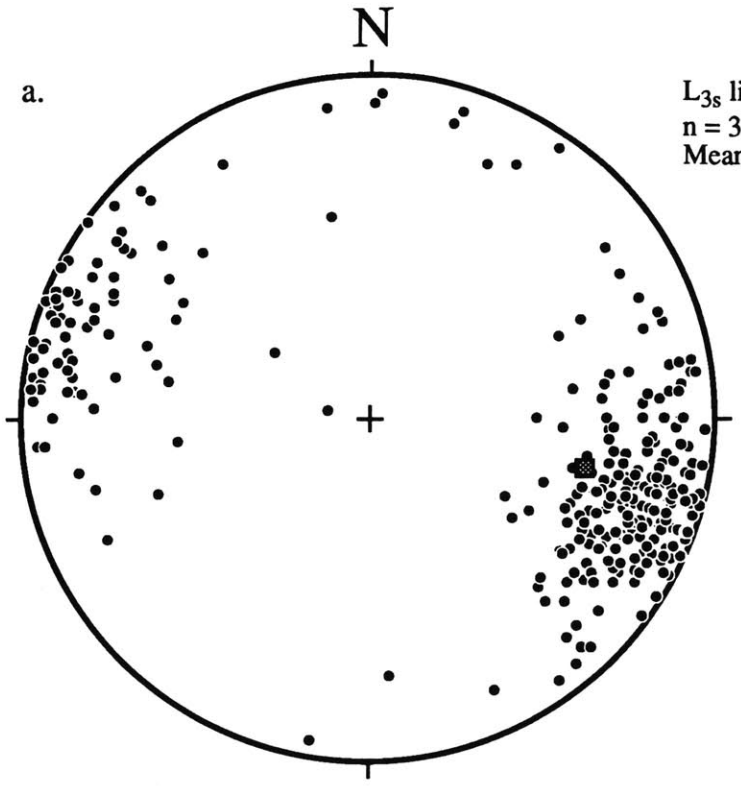

a.

L_{3s} lineations
n = 301
Mean Vector: 35, S76E

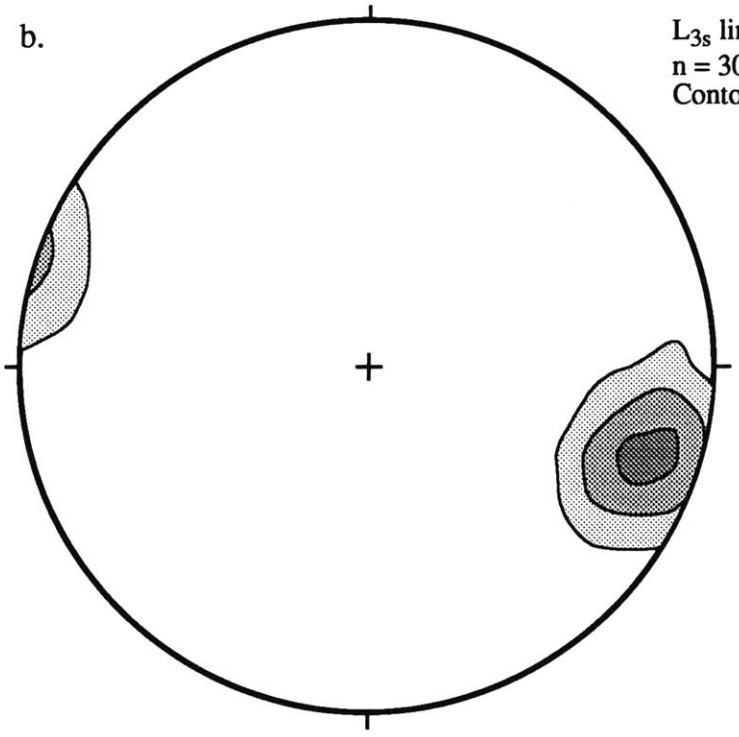

b.

L_{3s} lineations
n = 301
Contour interval: 4% / 1% area

Figure 11

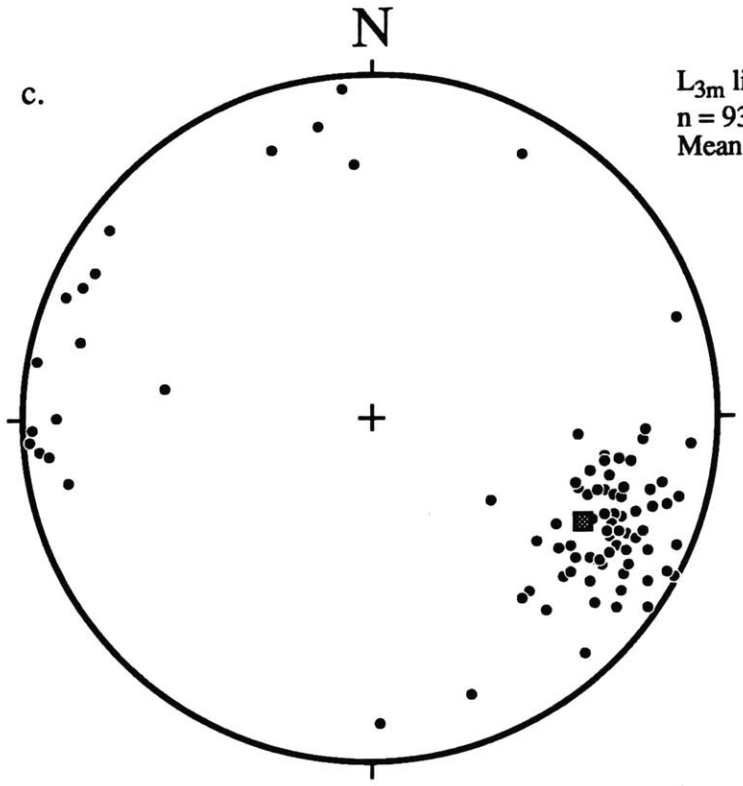

c.

L_{3m} lineations
n = 93
Mean Vector: 32, S64E

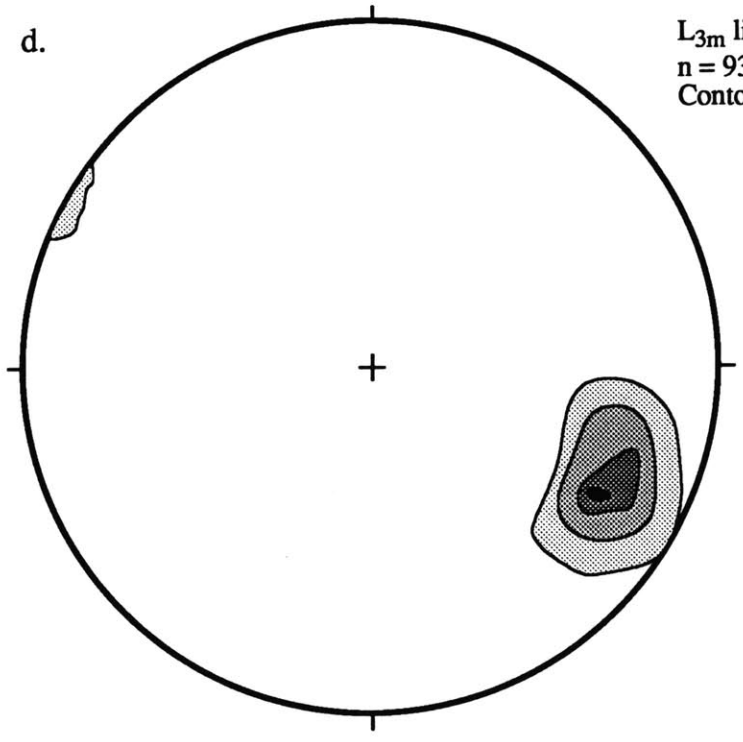

d.

L_{3m} lineations
n = 93
Contour interval: 4% / 1% area

Figure 11

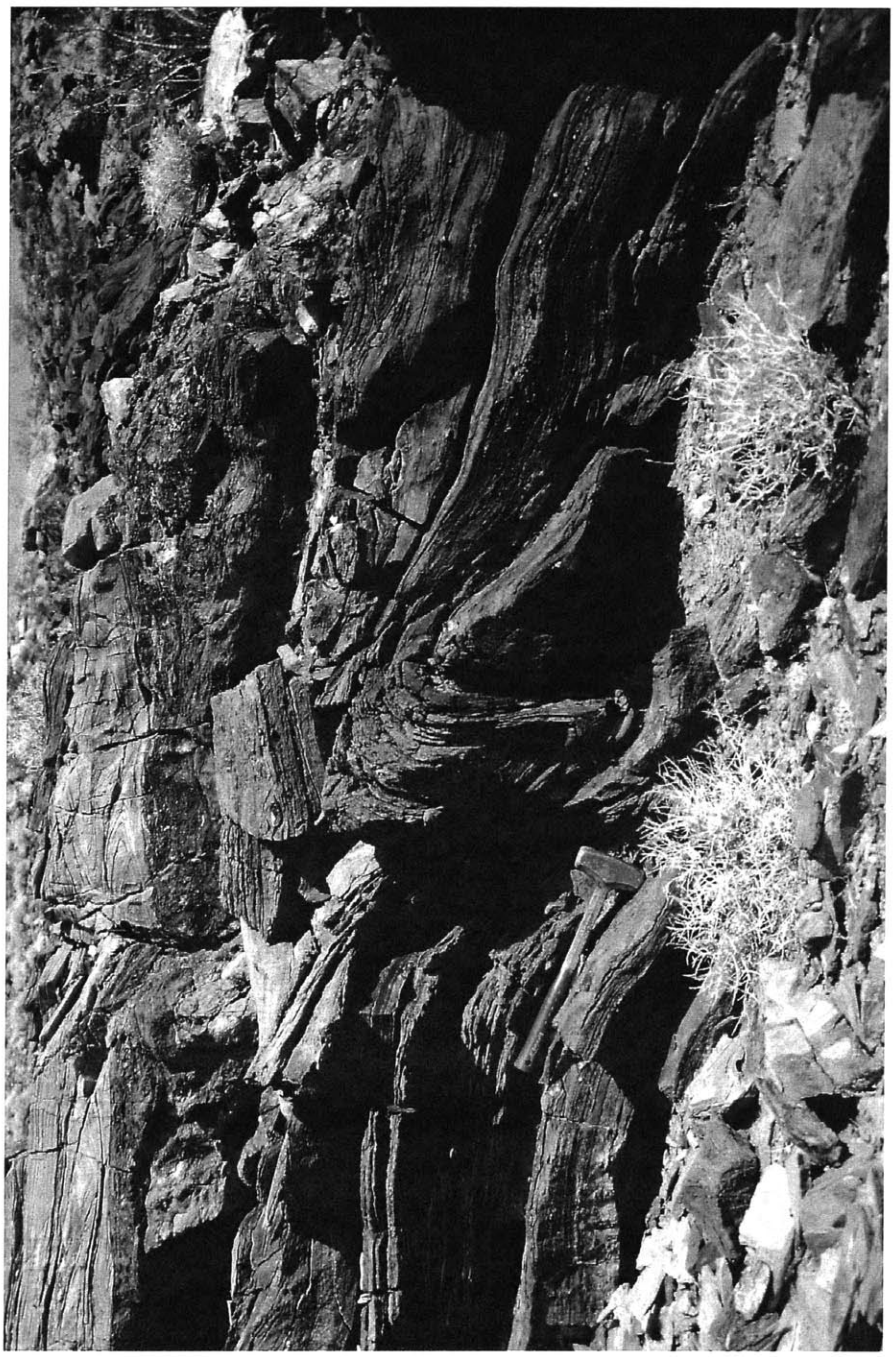

Figure 12

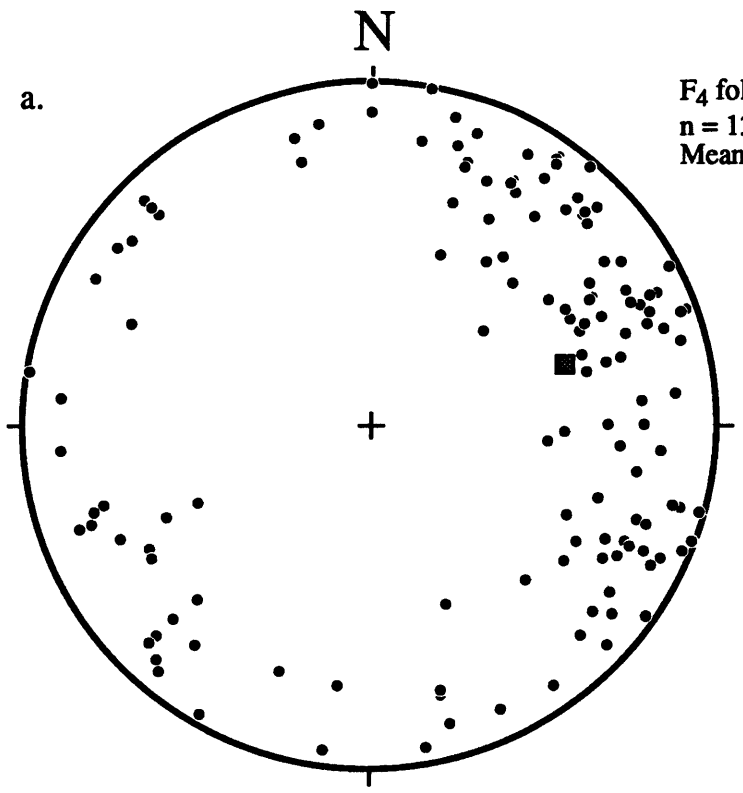
N
a.
F_4 fold axes
n = 138
Mean Vector: 41, N73E

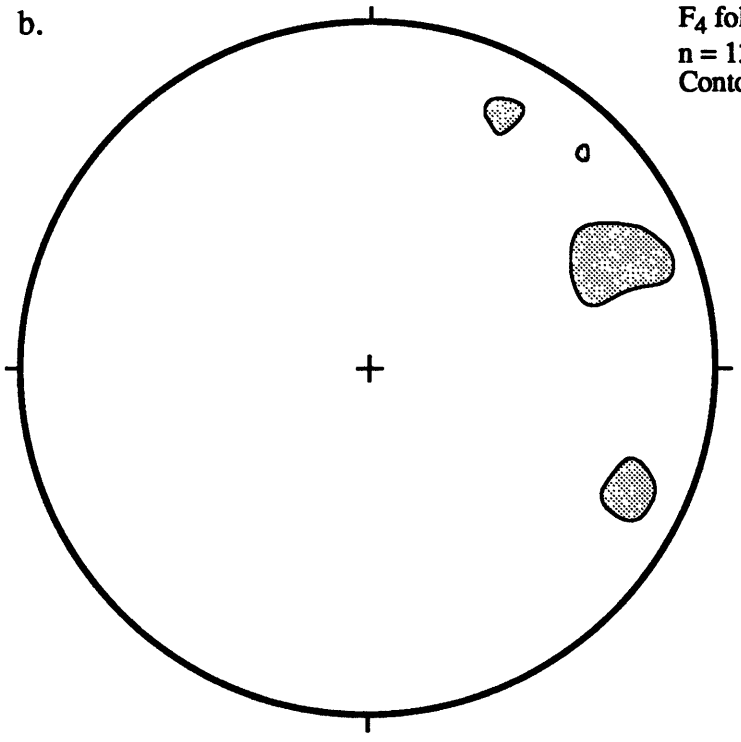
b.
F_4 fold axes
n = 138
Contour interval: 4% / 1% area

Figure 13

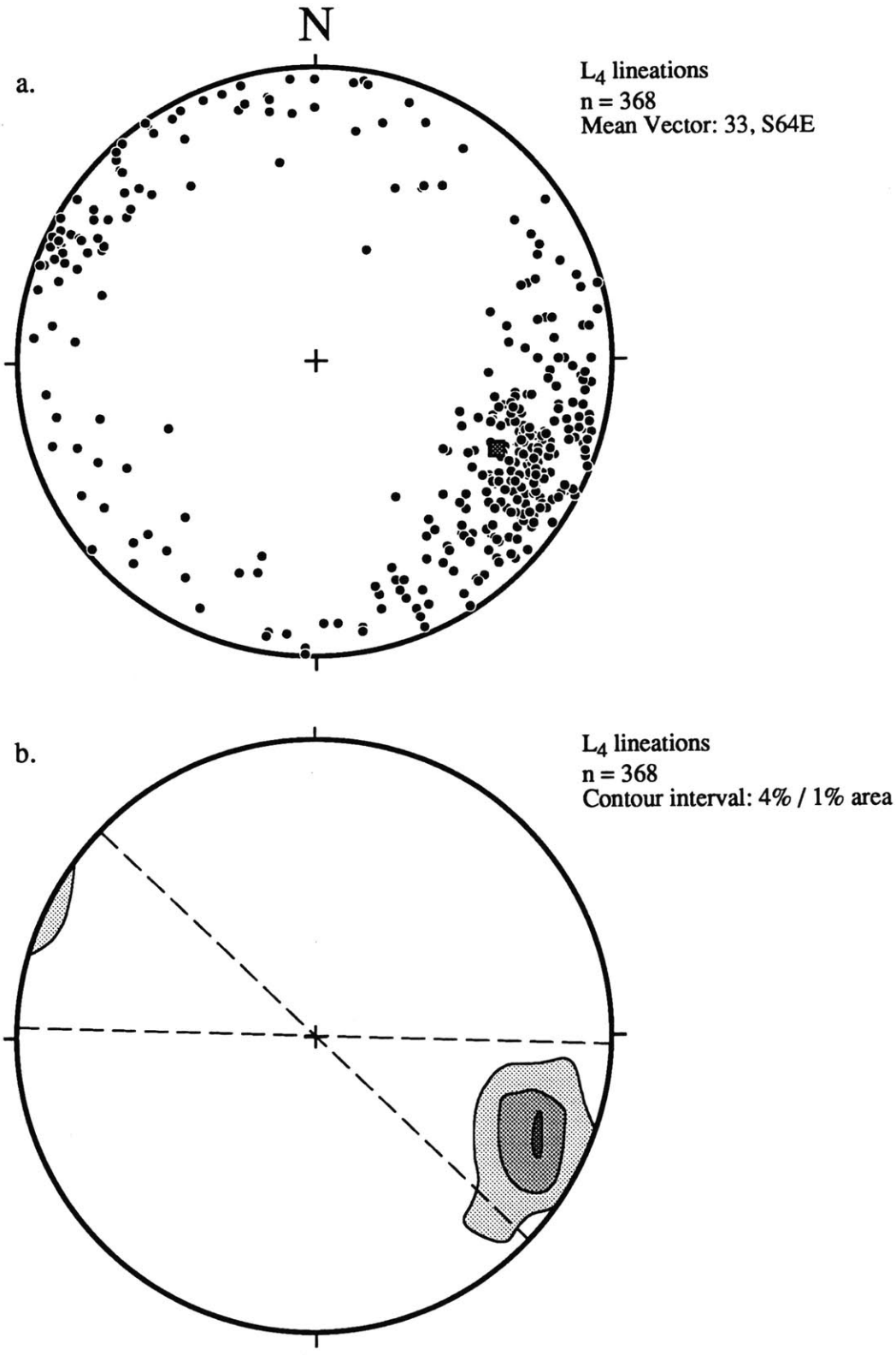
N
a.
L_4 lineations
n = 368
Mean Vector: 33, S64E
b.
L_4 lineations
n = 368
Contour interval: 4% / 1% area

Figure 14

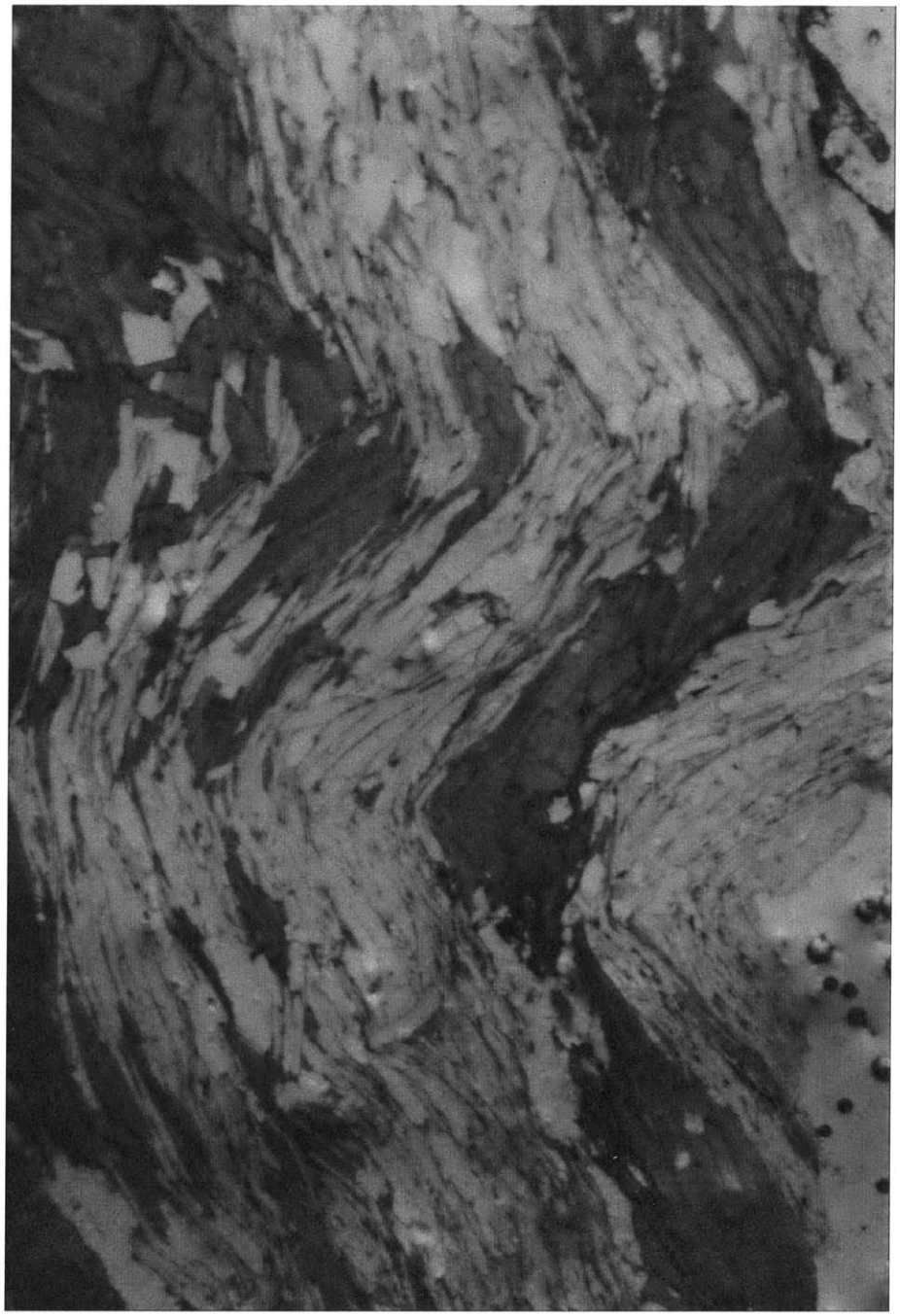

Figure 15

a.

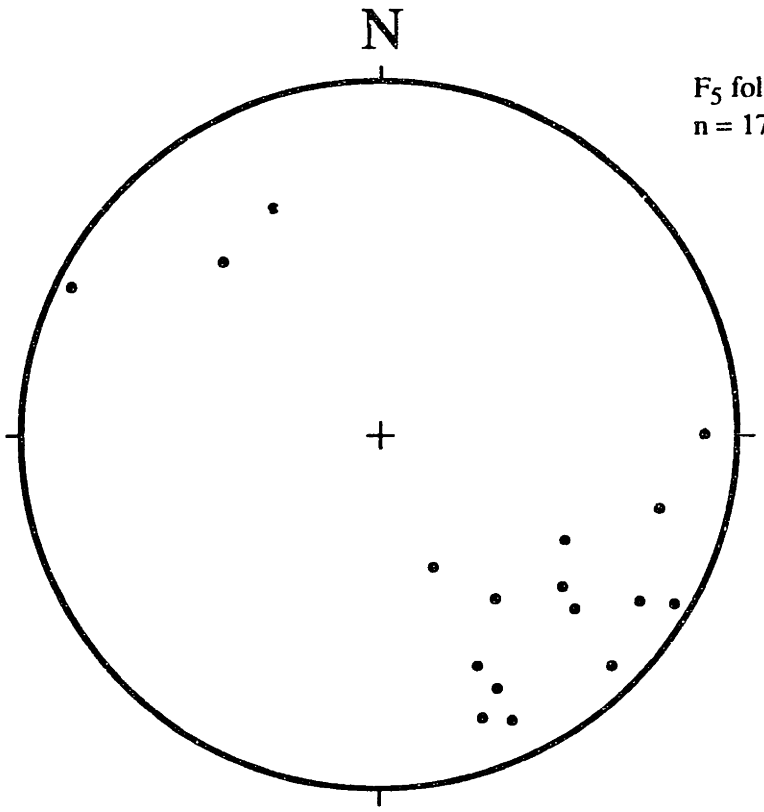

F_5 fold axes
n = 17

b.

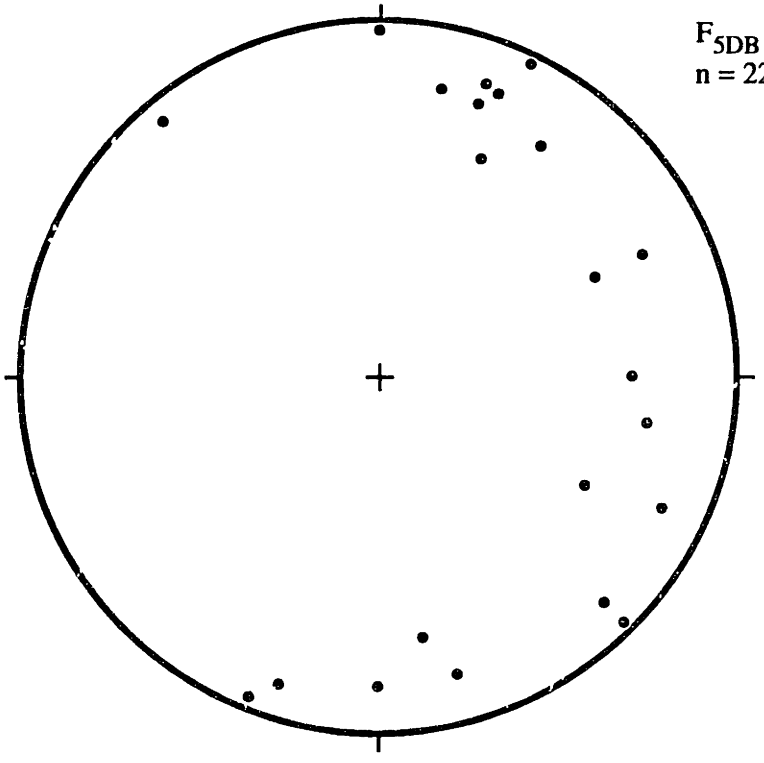

F_{5DB} fold axes
n = 22

Figure 16

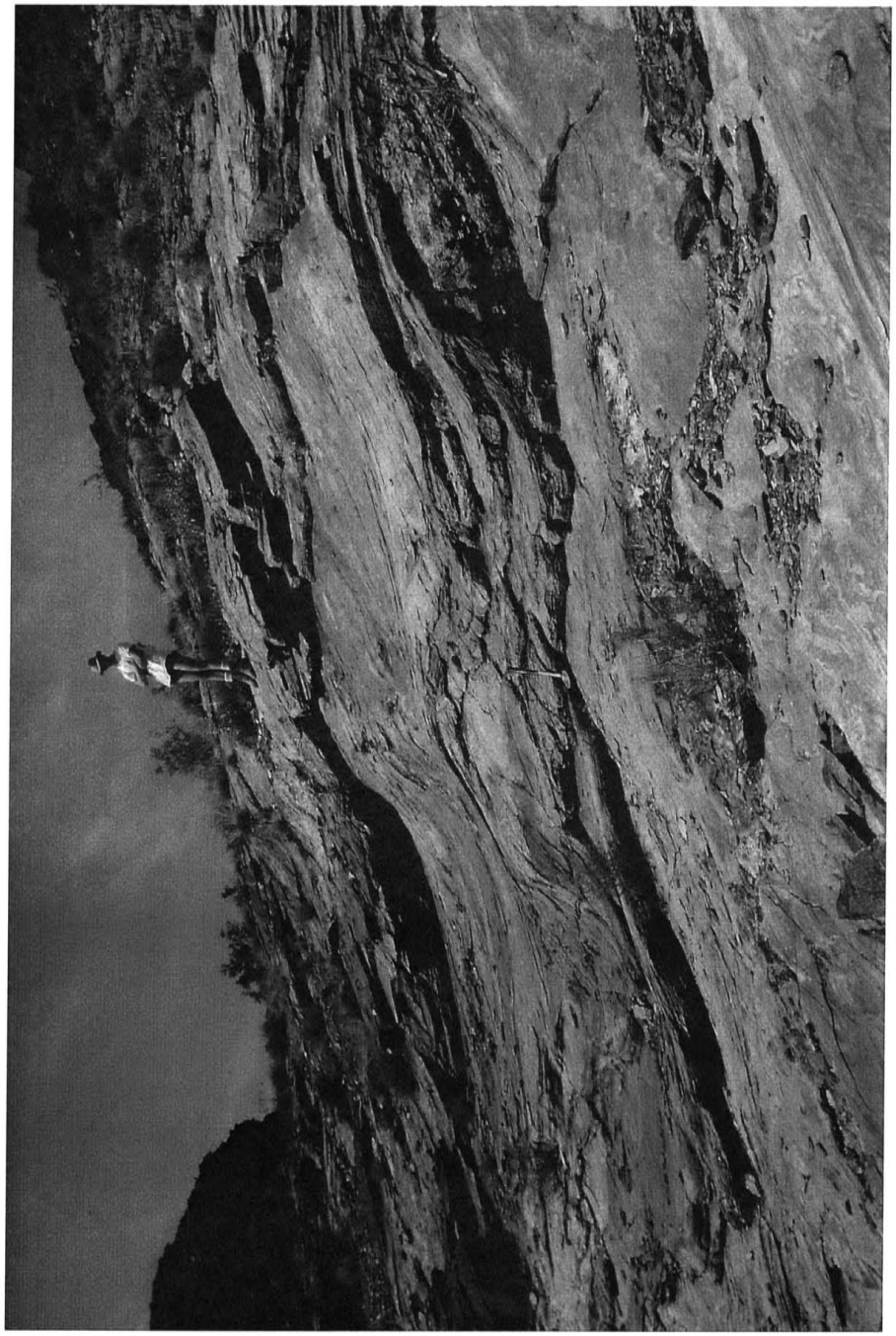

Figure 17

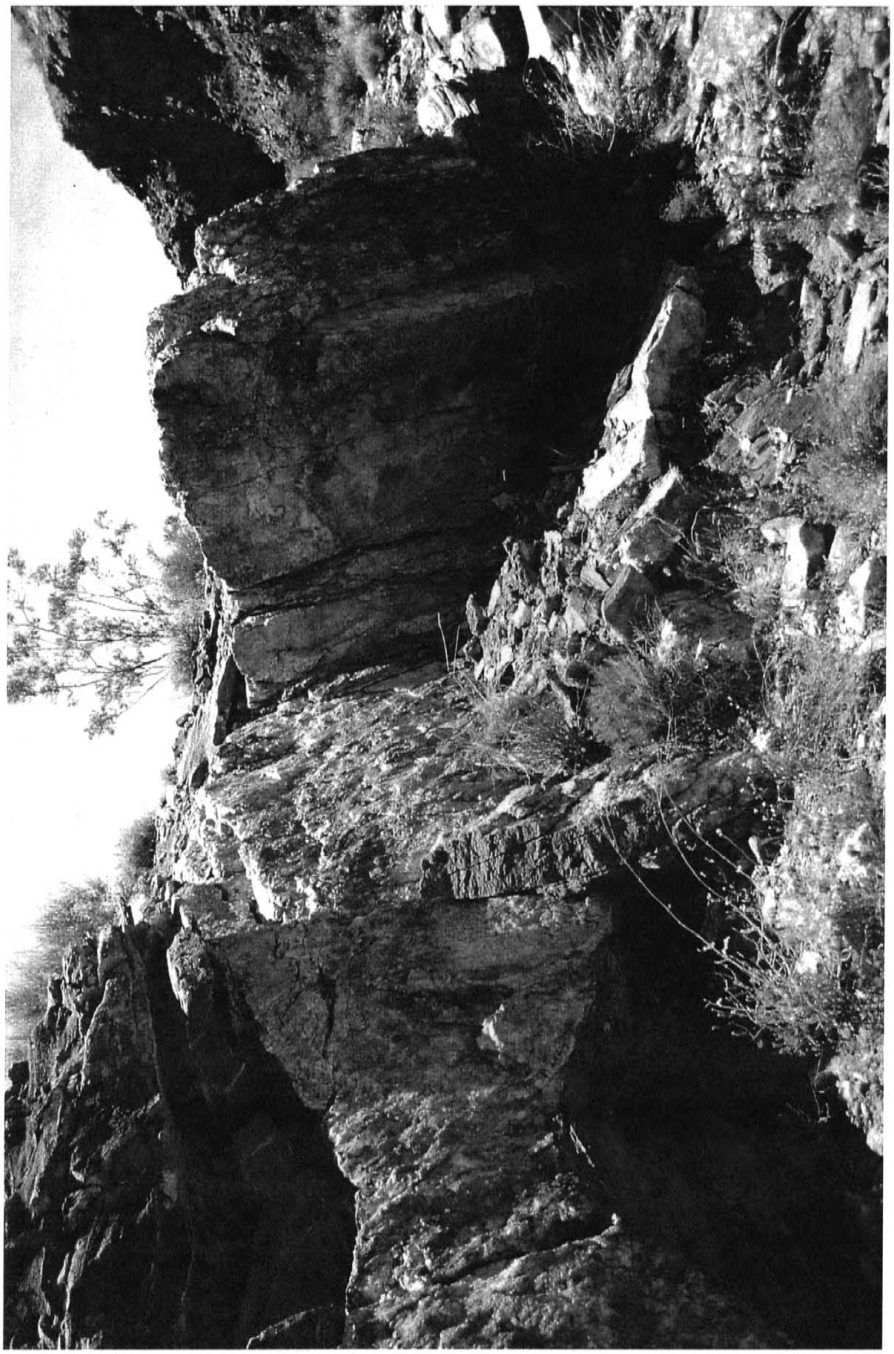

Figure 18

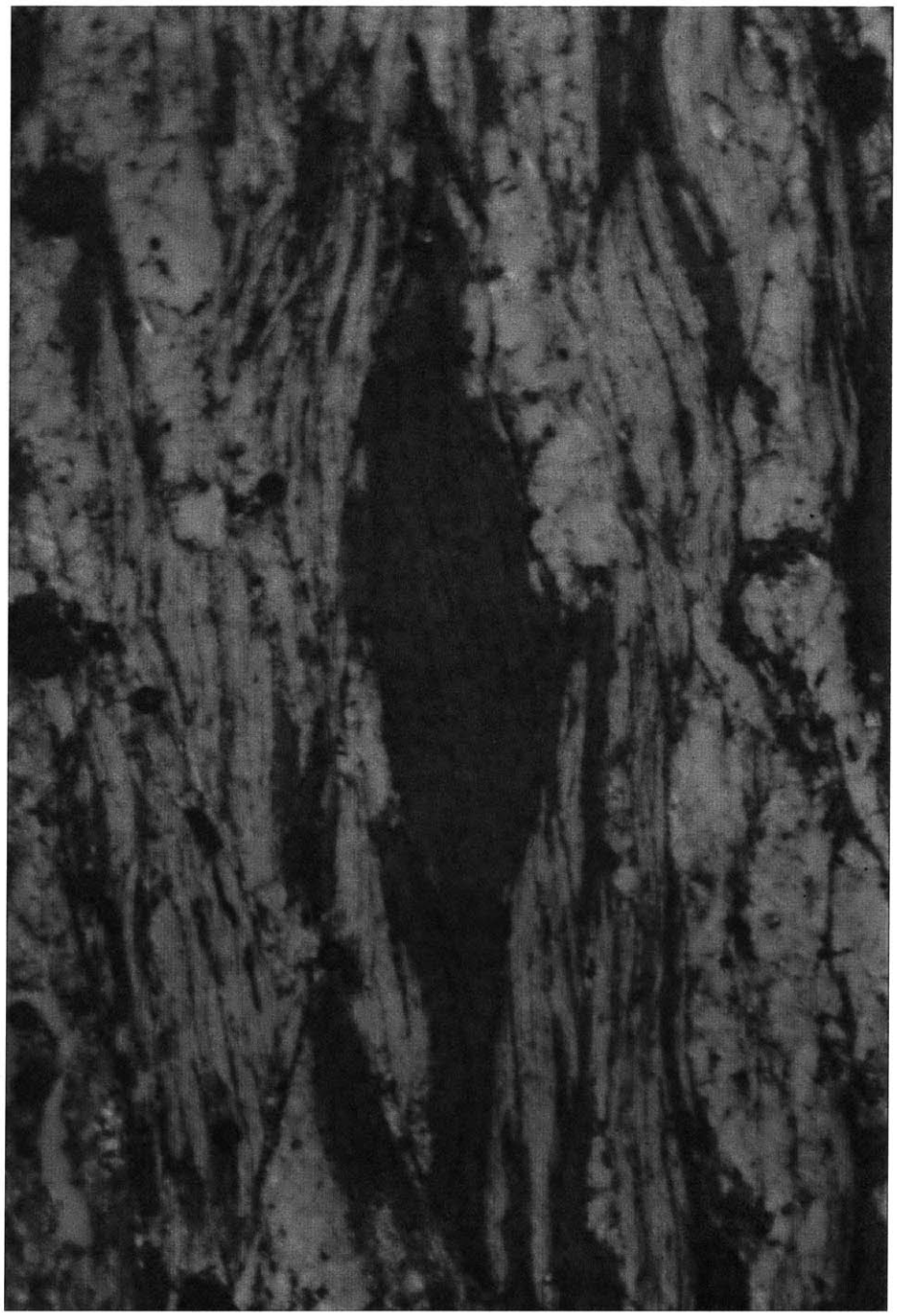

Figure 19

a.

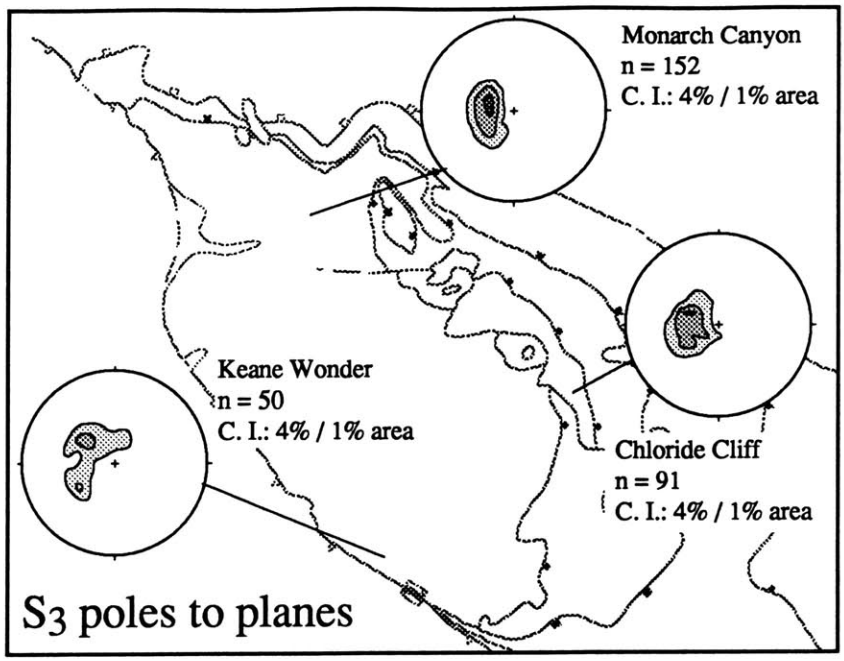
Monarch Canyon
n = 152
C. I.: 4% / 1% area
Keane Wonder
n = 50
C. I.: 4% / 1% area
Chloride Cliff
n = 91
C. I.: 4% / 1% area
S3 poles to planes

b.

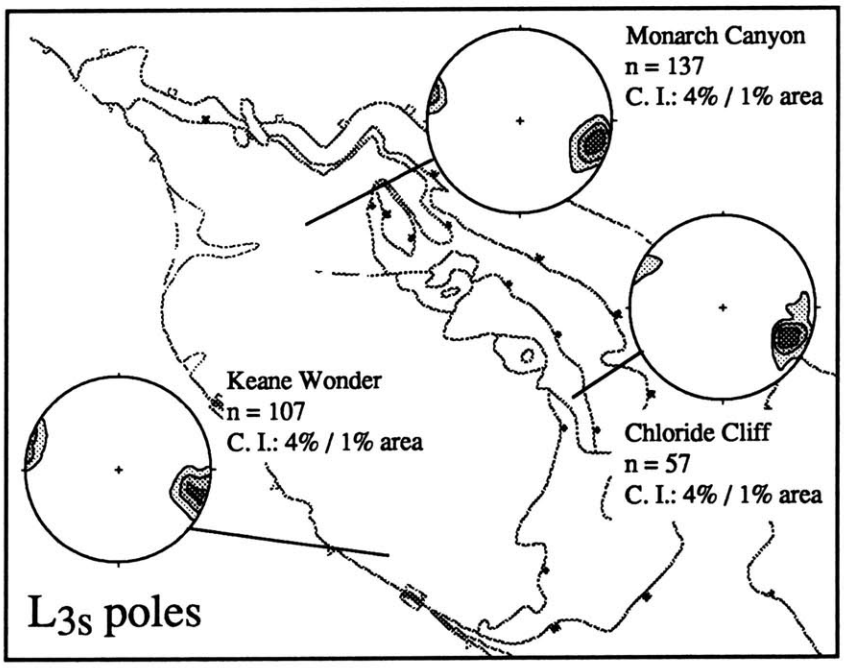
Monarch Canyon
n = 137
C. I.: 4% / 1% area
Keane Wonder
n = 107
C. I.: 4% / 1% area
Chloride Cliff
n = 57
C. I.: 4% / 1% area
L3s poles

Figure 20

c.

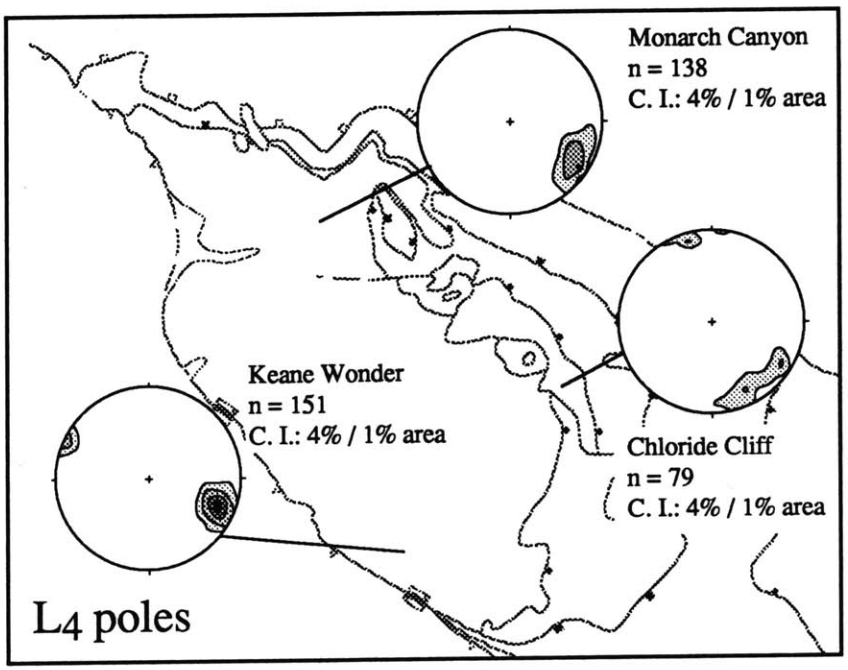
Monarch Canyon
n = 138
C. I.: 4% / 1% area
Keane Wonder
n = 151
C. I.: 4% / 1% area
Chloride Cliff
n = 79
C. I.: 4% / 1% area
L4 poles

Figure 20

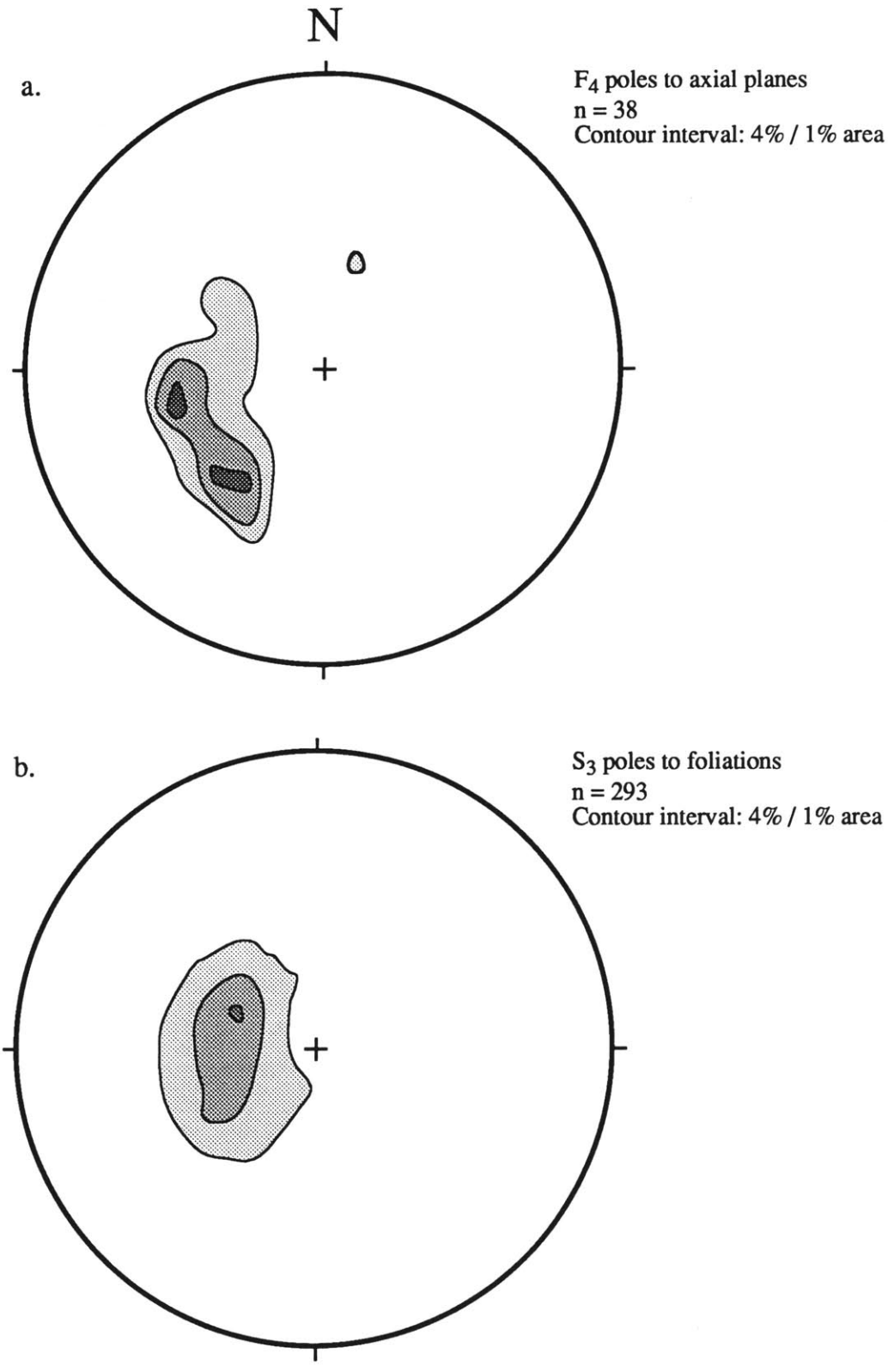
N
a.
F_4 poles to axial planes
n = 38
Contour interval: 4% / 1% area
b.
S_3 poles to foliations
n = 293
Contour interval: 4% / 1% area

Figure 21

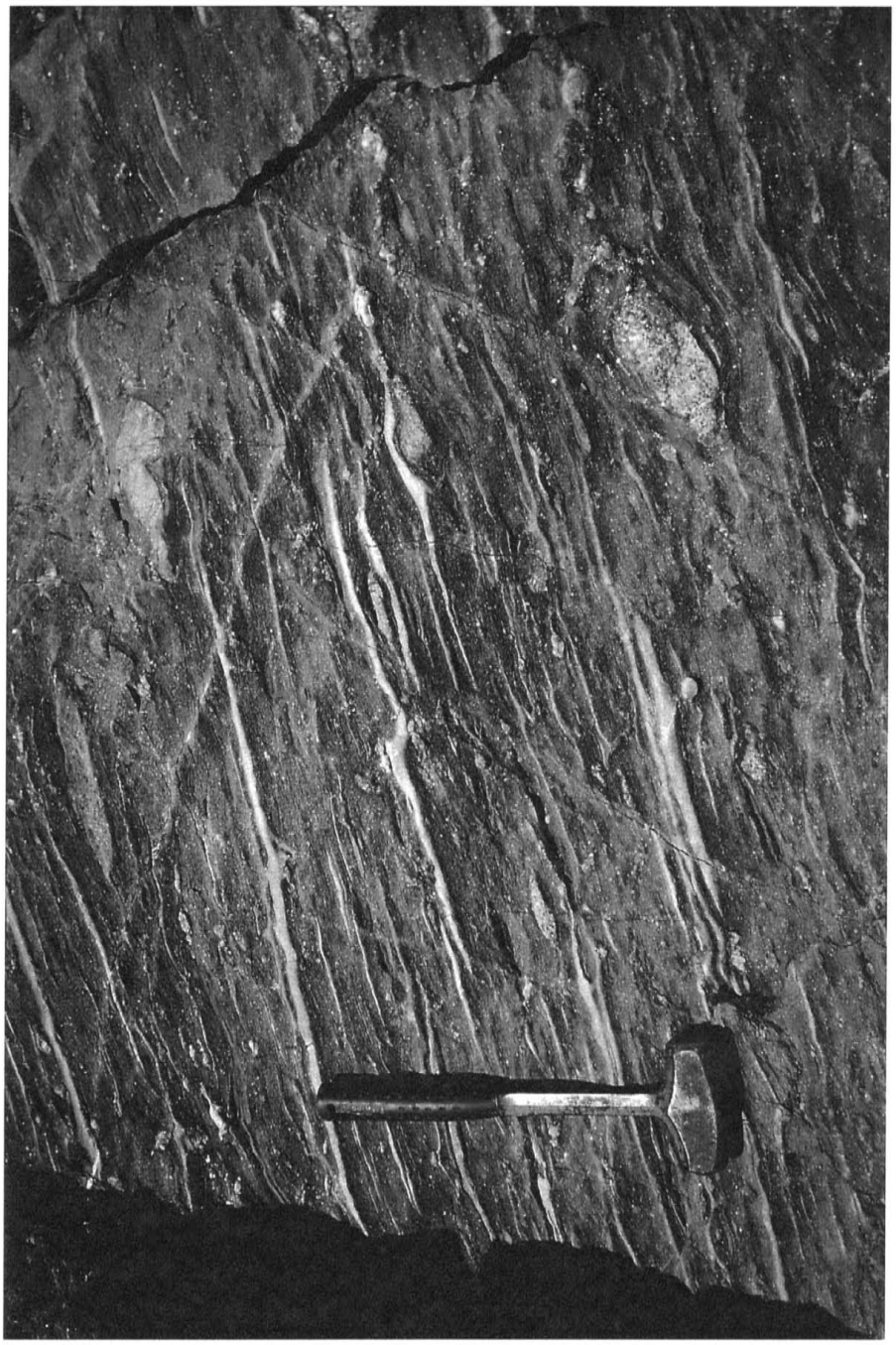

Figure 22

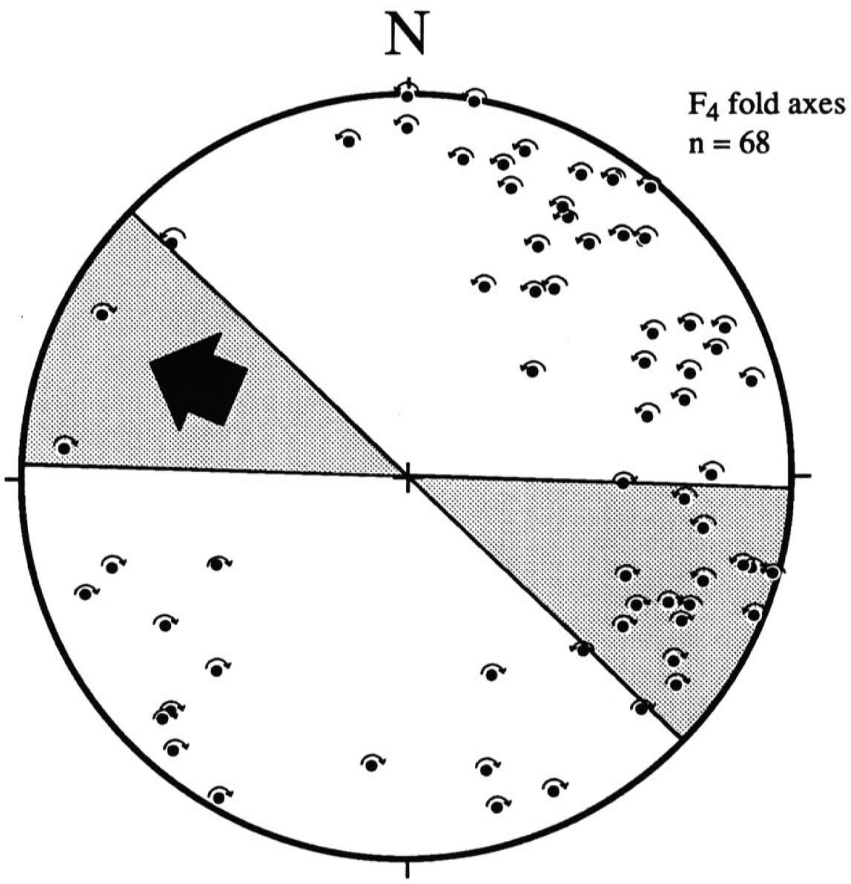

Figure 23

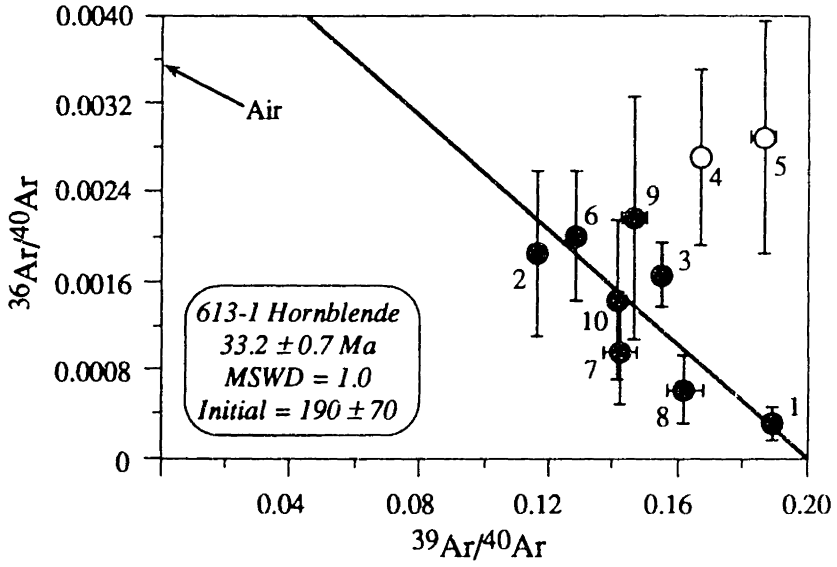
0.0040
0.0032
0.0024
0.0016
0.0008
0
$^{36}Ar/^{40}Ar$
Air
613-1 Hornblende
33.2 ± 0.7 Ma
MSWD = 1.0
Initial = 190 ± 70
1
2
3
4
5
6
7
8
9
10
0.04
0.08
0.12
0.16
0.20
$^{39}Ar/^{40}Ar$

Figure 24

Last Chance/ Grapevine Thrust
Schwaub Peak Thrust
Clery Thrust
NW
SE
EC
IP
Basal decollement of thrust belt
Incipient extensional shear zone
CC
MC
10 km
10 km
A. Early Cretaceous
NW
SE
EC
IP
?
Extensional shear zones
CC
MC
10 km
10 km
B. Late Cretaceous

Figure 25

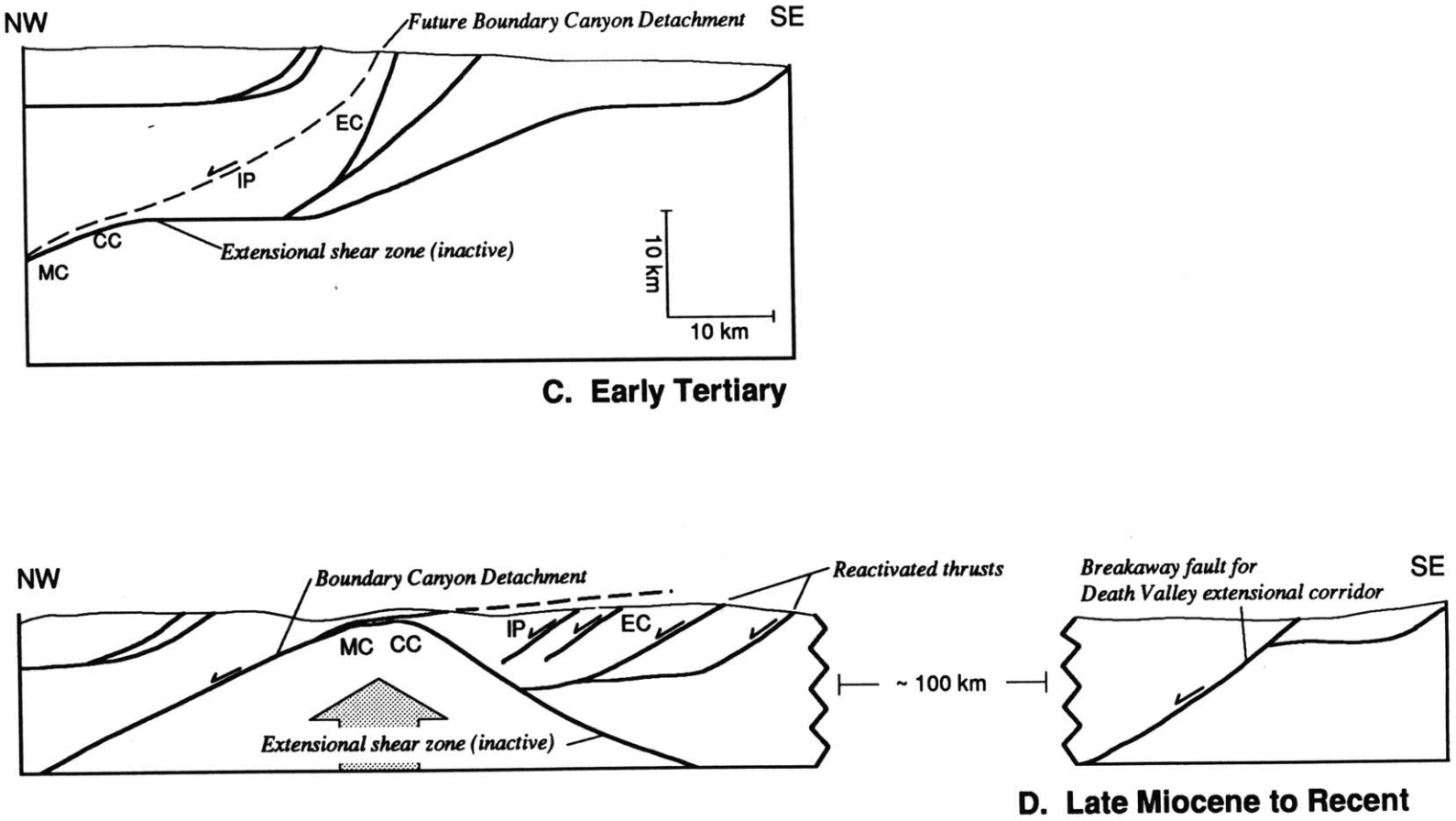
NW
Future Boundary Canyon Detachment
SE
EC
IP
CC
MC
Extensional shear zone (inactive)
10 km
10 km
C. Early Tertiary
NW
Boundary Canyon Detachment
Reactivated thrusts
Breakaway fault for
Death Valley extensional corridor
SE
IP
EC
MC
CC
~ 100 km
Extensional shear zone (inactive)
D. Late Miocene to Recent

Figure 25

CHAPTER 3

LATE CRETACEOUS EXTENSIONAL UNROOFING IN THE FUNERAL MOUNTAINS METAMORPHIC CORE COMPLEX, CALIFORNIA

David Applegate
Department of Earth, Atmospheric, and Planetary Sciences
Massachusetts Institute of Technology

PREFACE

This chapter was published two years ago† at a preliminary stage in the investigation, and some of the interpretations have changed over the intervening time, my own thinking being not nearly so immutable as the rocks. Nevertheless, the U-Pb results presented in this article still represent the best available constraints on the timing of early ductile extensional fabrics within the core. The chapter is presented as published with the exception of typographic corrections and substitutions for wording that initially was intended but mistakenly altered at some stage in the publication process. Changes in interpretation include the reinterpretation of basement rocks as the basal Crystal Spring Formation and the assertion that the Chloride Cliff shear zone removed the entire Beck Spring Dolomite. As discussed in Chapter 2, that shear zone does not cut out an entire unit, and its significance derives more as the base of a zone of intense attenuation topped by the Monarch Canyon shear zone than as a discrete fault surface. Subsequent work on pegmatites that are involved in F_4 folding suggests that this event continued after 65 Ma and is not constrained to be older than 70 Ma as indicated in this chapter (see Chapter 4).

†Applegate, J. D. R., Walker, J. D., and Hodges, K. V., 1992, Late Cretaceous unroofing in the Funeral Mountains metamorphic core complex, California: Geology, v. 20, p. 519-522.

ABSTRACT

New field and geochronologic data document the existence of Late Cretaceous extensional structures in the Death Valley region, California-Nevada. We have mapped two major, low-angle, ductile shear zones that omit stratigraphy in the footwall of the Funeral Mountains metamorphic core complex. Intervening strata have been strongly attenuated. Although stratigraphic offset across the shear zones is only 1.5 km, the presence of a large metamorphic discontinuity suggests that the amount of unroofing must be much greater. The timing of shear zone formation, attenuation, and subsequent northwest-vergent folding is constrained by U-Pb geochronology on pre/synkinematic and postkinematic pegmatites. Deformation was taking place by 72 Ma and had ended by 70 Ma. These results support earlier petrologic and geochronologic data that suggested substantial unroofing of the Funeral Mountains in Late Cretaceous time, and add to a growing body of evidence for widespread Mesozoic extension in the hinterland of the Sevier thrust belt.

INTRODUCTION

The western U.S. Cordillera underwent Mesozoic compressional deformation followed by Tertiary to Recent extension (e.g., Burchfiel and Davis, 1972). This sequence of compression and extension has been responsible for the polygenetic evolution of Cordilleran metamorphic core complexes, which formed in a belt of tectonically thickened crust coinciding with the hinterland of the Mesozoic Sevier thrust belt (Armstrong, 1982). As a consequence, ductile compressional structures in the footwalls of these core complexes are generally considered to be Mesozoic (e.g., Miller and Gans, 1989) while ductile extensional structures are commonly thought to be Tertiary (e.g., Davis and Lister, 1988). In this paper, we document the existence of Late Cretaceous ductile *extensional* structures in the Funeral Mountains metamorphic core complex of southeastern California. Coupled with previously published petrologic evidence for substantial synmetamorphic

tectonic denudation of the Funeral metamorphic core (Hodges and Walker, 1990a), these data reinforce the idea that Mesozoic extension may have been widespread in the Sevier hinterland (e.g., Allmendinger et al., 1984; Hodges and Walker, 1990b; Livaccari, 1991; Hodges and Walker, 1992).

GEOLOGIC SETTING

The northern Funeral Mountains have been mapped by Troxel and Wright (1989) and Applegate (1:10,000 scale unpublished mapping). The core rocks consist primarily of Late Proterozoic age amphibolitic, granitic, and pelitic basement gneisses and metasedimentary rocks that comprise the Pahrump Group, Noonday Dolomite, Johnnie Formation, and Stirling Quartzite (Wright and Troxel, 1966; Troxel, 1988). These units have been intruded by several generations of granitic dikes and sills. Metamorphic grade increases from southeast to northwest, reaching a maximum of upper amphibolite facies in Monarch Canyon (Labotka, 1980).

The high-grade metamorphic Precambrian rocks are in fault contact below essentially unmetamorphosed upper Proterozoic to Tertiary sedimentary rocks (e.g., Labotka, 1980; Troxel and Wright, 1989). Metamorphism, thought to have peaked by Early Cretaceous time (DeWitt et al., 1988), is due both to tectonic burial as a result of Mesozoic thrusting and to heating related to the emplacement of the Sierran arc (Labotka and Albee, 1988). Unroofing of the Funeral Mountains core on the flanking Boundary Canyon detachment (BCD in Fig. 1B) and Keane Wonder fault (KWF; Fig. 1) began at 9 Ma, on the basis of stratigraphic and geochronologic constraints (Reynolds et al., 1986). Recent fission track data (Holm and Dokka, 1991) also indicate an unroofing event in Miocene time. Early Oligocene extension may be recorded by the deposition of the Titus Canyon Formation in the hanging-wall of the core complex (Reynolds, 1969; Saylor and Hodges, 1991), although the significance of this extension to unroofing of the core is not clear.

DUCTILE EXTENSIONAL STRUCTURES WITHIN THE CORE

Two extensional shear zones have been mapped in the core rocks of the northern Funeral Mountains. The upper shear zone, which we have named the Monarch Canyon shear zone (MCSZ; Fig. 1), places rocks of the Johnnie Formation on older Pahrump Group strata, omitting all but the lowest part of the stratigraphically intervening Noonday Dolomite. The lower shear zone, named here the Chloride Cliff shear zone (CCSZ; Fig. 1), places rocks of the Kingston Peak Formation on older Crystal Spring Formation (?) strata, apparently omitting the entire Beck Spring Dolomite (Fig. 1).

We consider the Monarch Canyon and Chloride Cliff shear zones to be major structures responsible for a minimum of 1 km of unroofing in the core. Both shear zones dip gently to the north and are marked by altered graphitic schists indicative of CO_2-rich fluid flow. Sense-of-shear indicators, including mica fish, asymmetric pressure shadows, asymmetric augen, and s-c mylonitic fabrics, suggest down-dip (top to the northwest) displacement. The shear zones bracket the most intensely deformed and strongly attenuated units. Troxel and Wright (1989) mapped the Monarch Canyon shear zone as a low-angle normal fault but did not ascribe much stratigraphic omission to it because, in some areas far to the south of the Funeral Mountains, the Johnnie Formation unconformably overlies Pahrump Group strata (Wright and Troxel, 1966). Nearby exposures in the Panamint Mountains (Figure 1), however, show no such unconformity (Stewart, 1970). We think that the Monarch Canyon shear zone omits on the order of 400m of section (the approximate thickness of the Noonday Dolomite in the Panamint Mountains; Hodges et al., 1990).

Our interpretation of the significance of the Chloride Cliff shear zone stems from our belief that the Beck Spring Dolomite does not occur in the northern Funeral Mountains. In the vicinity of Chloride Cliff, Troxel and Wright (1989) interpreted a 30-m-thick calcite marble-arkose-calcite marble sequence to be the Beck Spring Dolomite. However, exposures of the Beck Spring Dolomite elsewhere in the Death Valley region contain only minor arkosic layers (Gutstadt, 1968; Stewart, 1970). Since the arkosic unit is similar to

beds commonly found in the upper part of the Crystal Spring Formation, we have reinterpreted it as such and consider the Beck Spring Dolomite (~ 0.5 km thick; Stewart, 1970) to have been excised by the Chloride Cliff shear zone.

Core rocks have undergone several episodes of ductile deformation. Early deformation included the development of two generations of isoclinal folds (F_1 and F_2) and an axial-planar schistosity (S_1). S_1 can be seen in outcrop as well as in rotated inclusion trails in garnets. D_1 and D_2 were followed by a ductile attenuation event (D_3) during which the Monarch Canyon shear zone and Chloride Cliff shear zone developed. D_3 structures found throughout the core include distinctive stretching and mineral lineations (L_3) and the regional foliation (S_3). The stretching lineations are best defined in quartzites, granites, amphibolites, and carbonates, whereas the mineral lineations are defined by aligned kyanite grains in pelitic schists. Least-squares analysis of 264 mineral and stretching lineations in the northern Funeral Mountains resulted in a mean orientation of 33°; S69°E. We consider this northwest-southeast trend to be representative of the bulk displacement direction during D_3 simple shear, but the present southeasterly plunge of L_3 probably reflects folding of F_4 structures (with axes roughly orthogonal to L_3) rather than the original plunge. D_3 attenuation of strata is most evident in Monarch Canyon between the Boundary Canyon detachment and the Chloride Cliff shear zone where units equivalent to the lowermost Sentinel Peak member of the Noonday Dolomite and the entire Kingston Peak Formation (Fig. 1) have been reduced in thickness from several hundred metres to as little as ten metres. The attenuation appears to be associated with subsequent drag folds (F4) that are tight to isoclinal and verge to the northwest. Unlike F_1 and F_2 folds, these folds have not been attenuated substantially and retain height:width ratios of 5:1 or less. Least squares analysis of 50 F_4 fold axes in the vicinity of Monarch Canyon and Chloride Cliff resulted in a mean orientation of 26° to N43°E. These deformational events were followed by a later northwest-axial folding event (F_5) and by brittle extensional faulting thought to be of Tertiary age.

AGE CONSTRAINTS ON ATTENUATION AND FOLDING

The Monarch Canyon shear zone is loosely constrained to be pre-Oligocene by diabase dikes dated at 34.4 Ma (K-Ar biotite; Troxel and Wright, 1989) which cut the shear zone east of Chloride Cliff. A tighter constraint derives from the observation that pegmatitic intrusions within the rocks of the Crystal Spring Formation in Monarch Canyon that are both pre- or synkinematic (Suite I) and postkinematic (Suite II) with respect to D_3 attenuation. Pegmatites of Suite I are foliated, lineated, and deformed by F_4 folds. Pegmatites of Suite II are neither foliated nor lineated and can be seen to crosscut the S_3 fabric and F_4 folds in surrounding rocks. All pegmatite bodies have been affected by F_5 folds, minor symmetric boudinage, and brittle faulting. While none of these pegmatites has been dated previously, a conventional K-Ar date of 30 Ma was reported for a pegmatite that crosscuts deformed basement rocks further south in the canyon (Wasserburg et al., 1959), and DeWitt et al. (1988) inferred a Late Cretaceous age for granitic rocks lower in the canyon on the basis of resetting of $^{40}Ar/^{39}Ar$ ages in adjacent basement gneisses.

Samples of both suites of pegmatites were collected in upper Monarch Canyon for U-Pb geochronology. The Suite I pegmatite is large-grained and composed primarily of feldspar and quartz with abundant muscovite. A 50 kg sample (2190-1) was collected at lat 36°43.5'N, long 116°54.9'W (Fig. 1). The Suite II pegmatite is petrographically similar to the Suite I pegmatite except for the absence of any deformational fabrics. A 50 kg sample (YG) was collected at lat 36°43.8'N, long 116°55'W (Fig. 1).

Two zircon morphologies were present in both samples: clear, equant crystals and cloudy crystals. Clear, equant monazite fractions were also analyzed for sample YG. Figures 2 and 3 show concordia plots for the two samples, and analytical data are presented in Table 1. Sample 2190-1 shows what are interpreted to be the effects of inherited xenocrystic zircon (Fig. 2). The most concordant points yield a lower intercept of 72 ±1 Ma (MSWD = 8.7; model 2 of Ludwig, 1983). A concordant point at 72 Ma was obtained

from an air-abraded fraction. Owing to the high U concentrations in these fractions and deformation in the rock, however, we consider lead-loss has probably occurred and interpret 72 Ma to represent a minimum age.

The systematics for sample YG are simpler (Table 1). A clear zircon fraction showed signs of extensive inheritance, giving Paleozoic to Proterozoic U-Pb and Pb-Pb ages. The cloudy zircon fraction, however, was nearly concordant at 70 Ma (Fig. 3). The monazite fractions plotted above concordia, indicating excess ^{206}Pb. The $^{207}Pb/^{235}U$ age is interpreted to reflect more closely the crystallization age (see Parrish, 1990), 70.2 Ma and 69.4 Ma, respectively, for the two monazite fractions. Hence, we interpret the crystallization age of sample YG to be 70 ±1 Ma (average of zircon and monazite ages).

The similarity in petrology and setting of the two pegmatites suggests that they formed during the same magmatic event. Pegmatites in the study areas are isolated, rootless bodies, and thus may be the result of anatectic melting, possibly triggered by unroofing. This interpretation is supported by the presence of migmatitic textures in Lower Crystal Spring schists in Monarch Canyon. Note also that the pegmatites are found only at the deepest structural levels in Monarch Canyon. For these reasons we consider pegmatites of both suites to be close in age. Therefore, the simplest interpretation of U-Pb mineral dates is that the age of Suite I pegmatites is 72 Ma, or only slightly older than that of the Suite II pegmatites (70 Ma).

DISCUSSION

Late Cretaceous Unroofing Event

The geochronologic data indicate that attenuation was taking place by 72 Ma and that both the D_3 attenuation and F_4 folding were over by 70 Ma. The timing of extensional deformation corroborates the inference made by Hodges and Walker (1990a), on the basis of their thermobarometric data in conjunction with thermochronologic data of DeWitt et al. (1988), that tectonic denudation of the metamorphic core was occurring in Late Cretaceous

time. The pressure-temperature-time paths presented by Hodges and Walker (1990a) are from rocks in the footwall of the Monarch Canyon shear zone and Chloride Cliff shear zone; presumably, at least some of the unroofing recorded by the thermobarometric data was accommodated by these structures. Note that stratigraphic omission associated with the shear zones is relatively small compared to discontinuities in metamorphic grade. For example, the hanging wall of the Monarch Canyon shear zone comprises staurolite-grade Johnnie Formation schists while the footwall of the Chloride Cliff shear zone comprises kyanite ± sillimanite grade schists of the Crystal Spring Formation. Comparative thermobarometry is in progress to better characterize the offsets.

Implications for the Death Valley region

The sequence of ductile deformation in the Funeral Mountains is very similar to that found on the west side of Death Valley at Tucki Mountain (Hodges et al., 1987). Extensional deformation there is considered to be younger than the Skidoo granite which has been dated at ~100 Ma (Rb/Sr whole rock; Hodges et al., 1990), and it is possible that some of the deformation there may be Cretaceous and linked to that in the Funeral Mountains.

The Wernicke et al. (1988) reconstruction of Mesozoic thrusts at the latitude of Las Vegas argues for 247 ±56 km of extension in the Neogene. This estimate is based on the assumption that, except for possible extension related to deposition of the Titus Canyon Formation in the early Oligocene, extension in the Death Valley region did not begin until mid-Miocene time (Wernicke et al., 1988). These estimates may require refinement to account for the component of total extension that is Cretaceous in age.

REFERENCES CITED

Allmendinger, R.W., Miller, D.M. and Jordan, T.E., 1984, Known and inferred Mesozoic deformation in the hinterland of the Sevier belt, northwest Utah, *in* Kerns, G.J. and

Kerns, R.L., eds., Geology of northwest Utah, southern Idaho, and northeast Nevada: Utah Geological Association Publication, p. 21-34.

Armstrong, R.L., 1982, Cordilleran metamorphic core complexes — From Arizona to southern Canada: Annual Review of Earth and Planetary Sciences, v. 10, p. 129-154.

Burchfiel, B.C., and Davis, G.A., 1972, Structural framework and evolution of the southern part of the Cordilleran orogen, western United States: American Journal of Science, v. 272, p. 97-118.

Davis, G.A., and Lister, G.S., 1988, Detachment faulting in continental extension; Perspectives from the Southwestern U.S. Cordillera, *in* Clark, S.P., Jr., Burchfiel, B.C., and Suppe, J., eds., Processes in continental lithospheric deformation: Geological Society of America Special Paper 218, p. 133-159.

DeWitt, E., Sutter, J.F., Wright, L.A. and Troxel, B.W., 1988, Ar-Ar chronology of early Cretaceous regional metamorphism, Funeral Mountains, California — A case study of excess argon: Geological Society of America Abstracts with Programs, v. 20, p. A16.

Gutstadt, A.M., 1968, Petrology and depositional environments of the Beck Spring Dolomite (Precambrian), Kingston Range, California: Journal of Sedimentary Petrology, v. 38, p. 1280-1289.

Hodges, K.V., McKenna, L.W., and Harding, M.B., 1990, Structural unroofing of the central Panamint Mountains, Death Valley region, southeastern California, in Wernicke, B.P., ed., Basin and Range extensional tectonics near the latitude of Las Vegas, Nevada: Geological Society of America Memoir 176, p. 377-390.

Hodges, K.V., and Walker, J.D., 1990a, Petrologic constraints on the unroofing history of the Funeral Mountains metamorphic core complex, California: Journal of Geophysical Research, v. 95, p. 8437-8445.

——1990b, Widespread evidence for Cretaceous extensional collapse in the hinterland of tne Sevier orogen of western North America: Geological Society of America Abstracts with Programs, v. 22, p. A276.

—— 1992, Extension in the Cretaceous Sevier Orogen, North American Cordillera: Geological Society of America Bulletin, in press.

Hodges, K.V., Walker, J.D. and Wernicke, B.P., 1987, Footwall structural evolution of the Tucki Mountain detachment system, Death Valley region, southeastern California, *in* Coward, M.P., Dewey, J.F. and Hancock, P.L., eds., Continental extensional tectonics: Geological Society of London, p. 393-408.

Holm, D.K., and Dokka, R.K., 1991, Major Late Miocene cooling of the middle crust associated with extensional orogenesis in the Funeral Mountains, California: Geophysical Research Letters, v. 18, p. 1775-1778.

Krogh, T.E., 1973, A low-contamination method of hydrothermal decomposition of zircon and extraction of U and Pb for isotopic age determinations: Geochimica et Cosmochimica Acta, v. 37, p. 485-494.

—— 1982, Improved accuracy of U-Pb ages by the creation of more concordant systems using an air abrasion technique: Geochimica et Cosmochimica Acta, v. 46, p. 637-649.

Labotka, T.C., 1980, Petrology of a medium-pressure regional metamorphic terrane, Funeral Mountains, California: American Mineralogist, v. 65, p. 670-689.

Labotka, T.C., and Albee, A.L., 1988, Metamorphism and tectonics of the Death Valley region, California, *in* Ernst, W.G., ed., Metamorphism and crustal evolution of the western United States: Englewood Cliffs, New Jersey, Prentice-Hall, p. 714-736.

Livaccari, R.F., 1991, Role of crustal thickening and extensional collapse in the tectonic evolution of the Sevier-Laramide orogeny, western United States: Geology, v. 19, p. 1104-1107.

Ludwig, K.R., 1983, Plotting and regression programs for isotope geochemists, for use with HP 86/87 microcomputers: U.S. Geological Survey Open-File Report 83-849, 102 p.

Miller, E.L., and Gans, P.B., 1989, Cretaceous crustal structure and metamorphism in the hinterland of the Sevier thrust belt, western U.S. Cordillera: Geology, v. 17, p. 59-62.

Parrish, R.R., 1987, An improved micro-capsule for zircon dissolution in U-Pb geochronology: Chemical Geology (Isotope Geoscience Section), v. 66, p. 99-102.

—— 1990, U-Pb dating of monazite and its application to geological problems: Canadian Journal of Earth Sciences, v. 27, p. 1431-1450.

Reynolds, M.W., 1969, Stratigraphy and structural geology of the Titus and Titanothere Canyons area, Death Valley, California (Ph.D. thesis): Berkeley, University of California, 310 p.

Reynolds, M.W., Wright, L.A. and Troxel, B.W., 1986, Geometry and chronology of late Cenozoic detachment faulting, Funeral and Grapevine Mountains, Death Valley, California: Geological Society of America Abstracts with Programs, v. 18, p. 175.

Saylor, B.Z. and Hodges, K.V., 1991, The Titus Canyon Formation: Evidence for Early Oligocene extension in the Death Valley area, California: Geological Society of America Abstracts with Programs, v. 23, p. A82.

Stacey, J.S., and Kramers, J.D., 1975, Approximation of terrestrial lead isotope evolution by a two-stage model: Earth and Planetary Science Letters, v. 26, p. 207-221.

Steiger, R.H., and Jäger, E., 1977, Subcommission on geochronology: Convention on the use of decay constants in geo- and cosmochronology: Earth and Planetary Science Letters, v. 1, p. 369-371.

Stewart, J.H., 1970, Upper Precambrian and Lower Cambrian strata in the southern Great Basin, California and Nevada: U.S. Geological Survey Professional Paper 620, 206 p.

Troxel, B.W., 1988, A geologic traverse of the northern Funeral Mountains, Death Valley, California, *in* Weide, D.L. and Faber, M.L., eds., This extended land, geological journeys in the southern Basin and Range, Geological Society of America Cordilleran Section Field Trip Guidebook: Las Vegas, University of Nevada, Department of Geological Science, p. 45-49.

Troxel, B.W., and Wright, L.A., 1989, Geologic map of the central and northern Funeral Mountains and adjacent areas, Death Valley region, southern California: U. S. Geological Survey Open-File Report, v. 89-348.

Wasserburg, G.J., Wetherill, G.W. and Wright, L.A., 1959, Ages in the Precambrian terrain of Death Valley, California: Journal of Geology, v. 67, p. 702-708.

Wernicke, B., Axen, G.J., and Snow, J.K., 1988, Basin and Range extensional tectonics at the latitude of Las Vegas, Nevada: Geological Society of America Bulletin, v. 100, p. 1738-1757.

Wright, L.A., and Troxel, B.W., 1966, Strata of Late Precambrian-Cambrian age, Death Valley region, California-Nevada: American Association of Petroleum Geologists Bulletin, v. 50, p. 846-857.

ACKNOWLEDGMENTS

JDRA would like to thank E. Anderson, D. Coleman, C. Isachsen, M. Martin, and L. McKenna for help and guidance in sample collection and preparation; T. Coonan at Death Valley National Monument for logistical support; and L. Wright for helpful discussions. We would also like to thank T. Harms and R. Schweikert for their careful and helpful reviews. This work was supported by National Science Foundation (NSF) grant EAR-9005238 awarded to KVH and a GSA student research grant awarded to JDRA. JDRA's graduate studies are supported in large part by an NSF Graduate Fellowship. Partial laboratory support was provided by NSF grant EAR-8904007 awarded to JDW.

TABLE 1. ANALYTIC DATA FOR FUNERAL MOUNTAINS GRANITES

Fraction	Sample wt. (μg)	U (ppm)	Measured ratios‡			Radiogenic ratios			Ages (Ma)		
			$^{206}Pb^*$ (ppm)	$^{206}Pb/^{204}Pb$	$^{207}Pb/^{206}Pb$	$^{208}Pb/^{206}Pb$	$^{206}Pb^*/^{238}U$	$^{207}Pb^*/^{235}U$	$^{207}Pb^*/^{206}Pb^*$	$^{206}Pb^*/^{238}U$	$^{207}Pb^*/^{235}U$	$^{207}Pb^*/^{206}Pb^*$ †
Sample YG												
nm(1) <100	10 (z)	642.9	23.90	139.1	0.1877	0.3784	0.04328	0.5186	0.08690	273.1	424.2	1358 (19)
m(2) <100 c	89 (z)	8443	78.77	742.0	0.06742	0.06039	0.01086	0.07121	0.04755	69.6	69.8	77.2 (7)
m(10) >60	135 (m)	6037	57.41	466.9	0.07851	1.893	0.01107	0.07159	0.4691	71.0	70.2	44.5 (12)
m(10) >60	459 (m)	5925	55.76	2052	0.05404	2.064	0.01095	0.07075	0.04684	70.2	69.4	41.3 (4)
Sample 2190-1												
nm(0) c aa	5 (z)	6296	69.91	70.27	0.2632	0.5510	0.01293	0.09895	0.05552	82.8	95.8	433.3 (29)
nm(0) g aa	4 (z)	2550	54.84	357.9	0.1542	0.2673	0.02503	0.4021	0.1165	159.4	343.2	1903 (6)
nm(2) b	10 (z)	2792	42.93	142.0	0.1713	0.3185	0.01790	0.1738	0.07043	114.4	162.7	940.9 (8)
nm(2) g	60 (z)	6099	61.42	514.9	0.07791	0.08526	0.01172	0.07976	0.04935	75.1	77.9	164.3 (4)
nm(2) c	84 (z)	5754	56.11	684.1	0.07010	0.06220	0.01135	0.07602	0.04858	72.8	74.4	127.4 (3)
nm(2) g aa	5 (z)	1248	44.81	528.2	0.1287	0.1549	0.04180	0.5915	0.1026	264.0	471.9	1672 (5)
nm(3) c aa	14 (z)	4353	42.08	559.7	0.07373	0.07150	0.01125	0.07346	0.04734	72.1	72.0	66.3 (8)
nm(3) g aa	7 (z)	2687	28.04	411.8	0.08774	0.1006	0.01215	0.08724	0.05209	77.8	84.9	289.5 (30)

Note: nm = nonmagnetic, m = magnetic on Frantz separator at angle of tilt (degrees, in parentheses); >200 = size in standard mesh; aa = air abraded fraction; g = clear fraction; c = cloudy fraction; b = bulk fraction; (z) = zircon; (m) = monazite. Zircon dissolution followed the methods of Krogh (1973) and Parrish (1987). Elemental separation was done with a HBr anion column chemistry for lead and HCl column chemistry for uranium. Mixed ^{205}Pb-^{235}U spike used for zircon fractions. Air abrasion followed the methods of Krogh (1982). Decay constants used were $^{238}U = 0.15513 \times 10^{-9}$ yr^{-1} and $^{235}U = 0.98485 \times 10^{-9}$ yr^{-1} (Steiger and Jäger, 1977). Isotopic analyses were determined on a VG Sector multicollector thermal ionization mass spectrometer. A mass fractionation correction of 0.10%/amu, as determined by standard runs on NBS 981 (common lead) and NBS 982 (equal atom lead), was applied to the lead data. Errors on $^{206}Pb/^{204}Pb$ were minimized by use of a Daly multiplier. Common lead corrections were made using values determined from Stacey and Kramers (1975) for the crystallization age. Values used for YG are $^{206}Pb/^{204}Pb = 18.60$, $^{207}Pb/^{204}Pb = 15.62$, and $^{208}Pb/^{204}Pb = 38.50$; values used for 2190-1 are $^{206}Pb/^{204}Pb = 18.59$, $^{207}Pb/^{204}Pb = 15.62$, and $^{208}Pb/^{204}Pb = 38.49$.

* Radiogenic component.

† Numbers in parentheses are analytical errors on age (in m.y., 2 sigma). Errors were computed using data reduction program PBDAT of Ludwig (1983).

‡ Ratios corrected for spike and mass fractionation only.

FIGURE CAPTIONS

Figure 1. A: Map of northern Death Valley extended region, showing major extensional faults. B: Simplified tectonic map of northern Funeral Mountains, showing locations of samples YG and 2190-1. Structures discussed in text are Boundary Canyon Detachment (BCD), Keane Wonder Fault (KWF), Monarch Canyon Shear Zone (MCSZ), and Chloride Cliff Shear Zone (CCSZ).

Figure 2. Concordia diagram for U-Pb analyses of zircons in sample 2190-1. Ellipses show propagated analytical uncertainty at 2 sigma level. Numbers along concordia indicate age in Ma.

Figure 3. Concordia diagram for U-Pb analyses of zircons (z) and monazites (m) in sample YG. Ellipses show propagated analytical uncertainty at 2 sigma level. Numbers along concordia indicate age in Ma.

B
117°56'
36°44'
KWF
BCD
YG
2190-1
Monarch
Canyon
117°56'
MCSZ
CCSZ
36°42'
Chloride
Cliff
117°54'
117°52'
0
1
km
Tertiary strike-separation faults
Tertiary low-angle normal faults
Mesozoic extensional shear zones
Unmetamorphosed Precambrian and Tertiary cover rocks
Precambrian Stirling/Johnnie strata
Precambrian Noonday/Kingston Peak strata
Precambrian Crystal Spring strata & undiff. basement
N
A
0
km
50
Area of
Fig 1B
GRAPEVINE MTNS
COTTONWOOD MTNS
FUNERAL MTNS
PANAMINT MTNS
DEATH VALLEY
BLACK MTNS
NV
CA

Figure 1

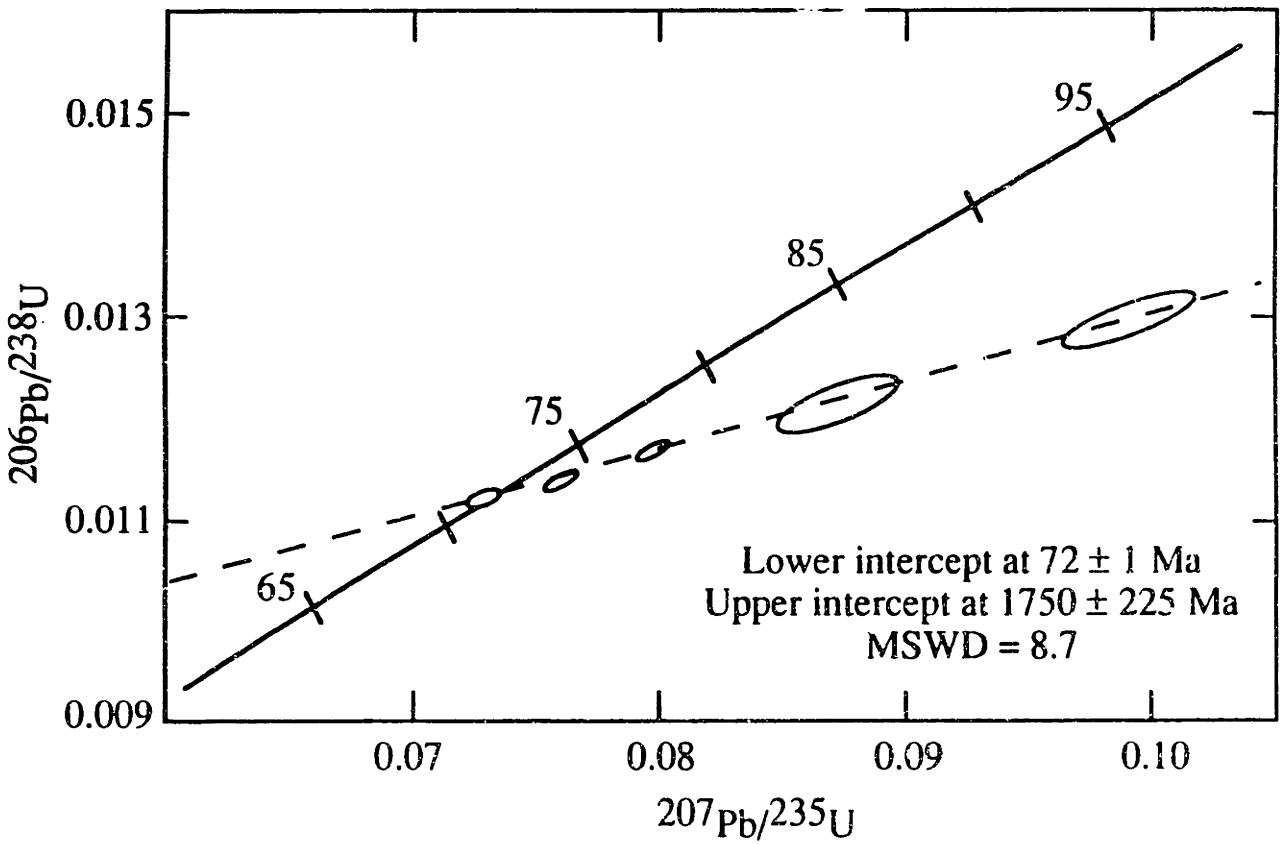
0.015
0.013
0.011
0.009
$^{206}Pb/^{238}U$
95
85
75
65
Lower intercept at 72 ± 1 Ma
Upper intercept at 1750 ± 225 Ma
MSWD = 8.7
0.07
0.08
0.09
0.10
$^{207}Pb/^{235}U$

Figure 2

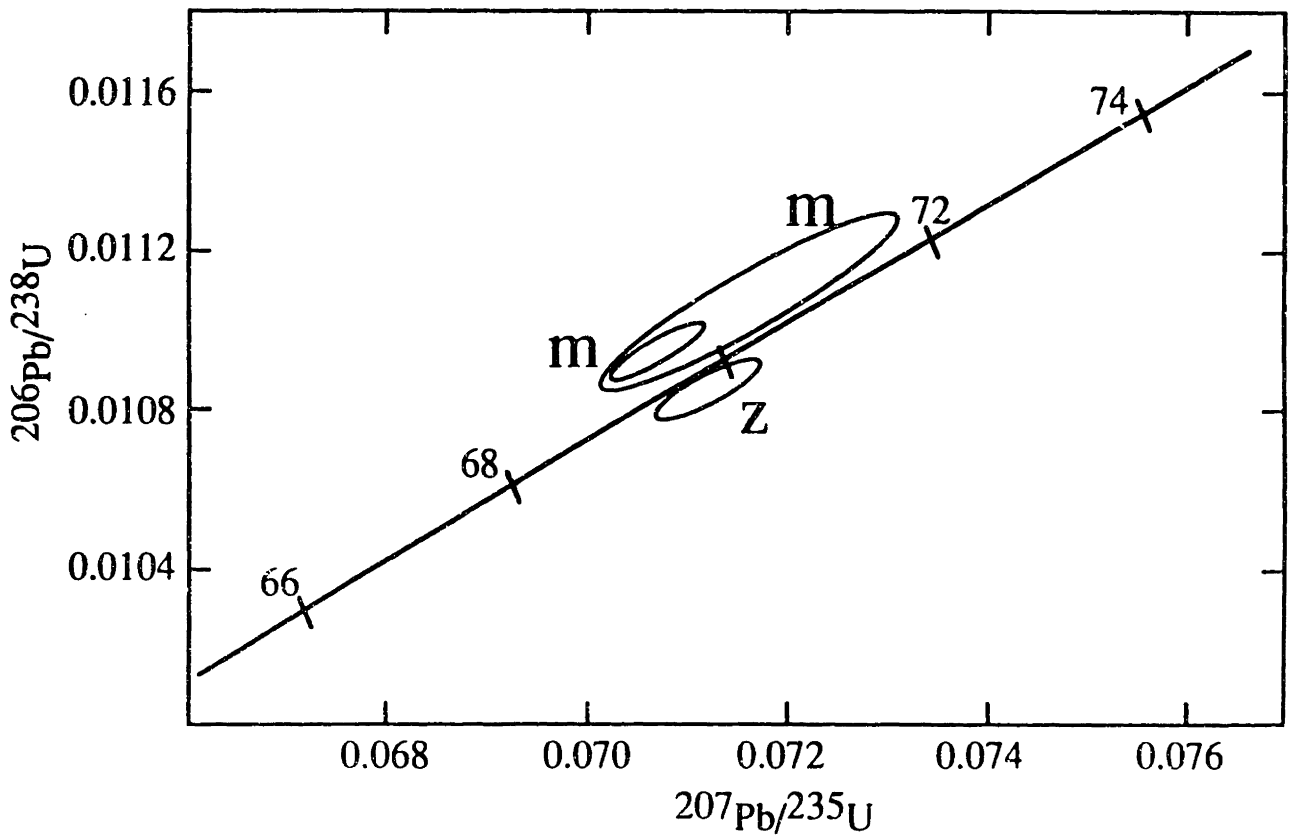
0.0116
0.0112
0.0108
0.0104
$^{206}Pb/^{238}U$
74
72
68
66
m
m
z
0.068
0.070
0.072
0.074
0.076
$^{207}Pb/^{235}U$

Figure 3

CHAPTER 4

GEOCHRONOLOGIC CONSTRAINTS ON METAMORPHISM, PLUTONISM, AND SUBSEQUENT COOLING OF THE FUNERAL MOUNTAINS METAMORPHIC CORE COMPLEX, CALIFORNIA

David Applegate
Department of Earth, Atmospheric, and Planetary Sciences
Massachusetts Institute of Technology

ABSTRACT

The thermal history experienced by high-grade rocks in the Funeral Mountains metamorphic core complex, California, reflects the tectonic evolution of the complex. Results of a combined U-Pb and $^{40}Ar/^{39}Ar$ geochronologic study yield useful constraints on the burial and unroofing of these rocks, despite complications by inherited lead and unsupported argon components. Metamorphic zircons from a pelitic schist support an Early Cretaceous age for peak metamorphism. In conjunction with earlier thermobarometric modeling, hornblende cooling ages of ~70 Ma indicate cooling in Late Cretaceous time synchronous with extensional deformation and the intrusion of a suite of pegmatite and granitoid dikes. Zircon ages for these dikes constrain the age of ductile deformational events within the core. A span of muscovite, rutile, and biotite ages indicates slow cooling over much of the Tertiary Period. K-feldspars are less affected by excess argon than mica and hornblende separates and are consistent with previously published fission-track data that indicate a period of rapid cooling in Late Miocene time, synchronous with brittle movement on the core-bounding detachment system. Rocks in the hanging wall of extensional shear zones within the core yield much older cooling ages, compatible with the interpretation that these structures represent a significant structural break within the core.

INTRODUCTION

Rocks in the footwall of the Funeral Mountains metamorphic core complex in southeastern California were taken to mid-crustal depths in Mesozoic time as the result of regional contraction and have since been brought to the surface by extensional processes. Unroofing took place during two pulses of extension, the first in Late Cretaceous time and the second in Late Miocene time. The Late Cretaceous event was accompanied by the intrusion of granitoids and pegmatite dikes at deep structural levels in the core. The episodic nature of the unroofing history for the core rocks should be reflected in their cooling history. Although this history has been constrained at its low-temperature end by fission-track data (Holm and Dokka, 1991), attempts to constrain the middle and upper portions of the cooling history using $^{40}Ar/^{39}Ar$ thermochronology have been complicated by unsupported ("excess") ^{40}Ar components that produce artificially old ages when plotted on release spectrum diagrams (e.g. DeWitt et al., 1988).

This paper presents results from $^{40}Ar/^{39}Ar$ analyses of hornblende, muscovite, biotite, and K-felspar and from U-Pb analyses of zircon and rutile in an effort to constrain the Mesozoic to Tertiary thermal evolution of the core complex. Despite the effects of excess argon and inherited lead components, useful constraints have been obtained on the age of metamorphism, igneous intrusion, and subsequent cooling history of the deepest structural levels of the core. Because early extension took place on shear zones within the core, the cooling history of rocks in the hanging-wall of those structures was also studied, yielding much older ages indicative of a substantially different high-temperature cooling history. High-grade rocks in the footwall of the shear zones underwent prograde metamorphism in Early Cretaceous time followed by rapid cooling in Late Cretaceous time synchronous with unroofing. Slow cooling took place over much of Tertiary time until Late Miocene unroofing produced a second episode of rapid cooling.

TECTONIC SETTING

High-grade metamorphic rocks are exposed at the northern end of the Funeral Mountains, located on the eastern side of Death Valley in the center of the Death Valley extensional corridor of the southern Basin and Range (Figure 1). This corridor is a broad zone of deformation that has undergone as much as 250% extension since the end of Mesozoic thrusting (Wernicke et al., 1988). Most extension in the corridor took place over the last 15 My, and that traditionally has been the interpretation for the Funeral Mountains as well (Reynolds et al., 1986). Our work, however, has documented a component of extension that took place in Late Cretaceous time in addition to previously documented Miocene extension (Applegate et al., 1992). Miocene extension was primarily accommodated by the core-bounding structures: the Boundary Canyon detachment, a low-angle normal fault; and the Keane Wonder fault, a low-angle oblique-slip fault (Figure 2). In contrast, Late Cretaceous extension was accommodated by movement on low-angle, extensional shear zones within the core: the Chloride Cliff shear zone, Monarch Canyon shear zone, and Eastern shear zone (Figure 2). Ductile extensional fabrics in the footwall of these shear zones are cut by a 70 ± 1 Ma pegmatite dike (Applegate et al., 1992). The Monarch Canyon and Chloride Cliff shear zones represent the upper and lower bounds, respectively, of a zone of intense deformation, and together they represent a significant structural discontinuity within the core (Chapter 2).

Metamorphic rocks within the core complex consist of pelitic schists, calcite marbles, micaceous quartzites, and amphibolitic gneisses correlated with the Middle to Late Proterozoic Pahrump Group —including, from older to younger, the Crystal Spring Formation, Beck Spring Dolomite, and Kingston Peak Formation — and the Late Proterozoic Noonday Dolomite, Johnnie Formation, and Stirling Quartzite (Wright and Troxel, 1994; Chapter 2). The Eastern shear zone places Stirling Quartzite rocks on Johnnie Formation rocks. The Monarch Canyon shear zone carries Johnnie Formation rocks in its hanging-wall and the footwall of the Chloride Cliff shear zone is comprised of

Crystal Spring Formation rocks. In Monarch Canyon, where the highest-grade rocks are exposed, the two shear zones are separated by only 10 m of lowermost Noonday Formation and Kingston Peak Formation rocks that at Chloride Cliff to the southeast are well over 100 m in thickness, indicating a large amount of ductile attenuation (Figure 2). The two shear zones converge just to the west of Monarch Canyon. The Boundary Canyon detachment and the Keane Wonder fault separate the core rocks from unmetamorphosed Proterozoic, Paleozoic, and Tertiary units (Figure 2).

The core rocks have undergone a number of deformational events. An early foliation (S_1) and composite folding event (F_{1-2}) are synchronous with regional metamorphism. The S_1 foliation is transposed and overprinted by the regionally-present foliation (S_3), which is accompanied by stretching and mineral lineations (L_3). These fabrics are associated with movement on the intracore shear zones and are Late Cretaceous in age (Applegate et al., 1992). A subsequent folding event (F_4) also appears to be of Late Cretaceous age. Later events, all occurring in the Cenozoic Era, include doming of the core rocks and brittle movement on the Boundary Canyon detachment and then later on the Keane Wonder fault and associated normal faults within the core.

The degree of metamorphism increases from lowest greenschist facies, chorite-grade conditions to the southeast in the central Funeral Mountains to upper amphibolite facies, kyanite ± sillimanite grade conditions to the northwest in Monarch Canyon. Rocks in the footwall of the Chloride Cliff shear zone in Monarch Canyon contain sillimanite and have undergone extensive migmatization (Labotka, 1980). Thermobarometric estimates for these rocks indicate maximum pressures as high as 1000 MPa (Hodges and Walker, 1990), equivalent to over 30 km depth, and temperatures as high as 975 K (Hoisch, 1991). These conditions are thought to be the result of regional metamorphism associated with crustal contraction and a high heat flow associated with the emplacement of the Sierra Nevada batholith to the west (Labotka and Albee, 1988). Labotka (1980) was the first to suggest that metamorphism in the Funeral Mountains was Mesozoic in age and contemporaneous

with metamorphism in the nearby Panamint Mountains (Figure 1). Evidence to support this inference was provided by DeWitt et al. (1988), who obtained Cretaceous $^{40}Ar/^{39}Ar$ ages from hornblendes and muscovites in Monarch Canyon that were complicated, however, by significant excess argon contamination. They obtained plateau ages of 130-115 Ma from hornblendes with high-K_2O contents that were thought to minimize the effects of excess argon. They also obtained plateau ages of 110-55 Ma for muscovites that appeared to them to contain no excess argon. Dewitt et al. (1988) interpreted these results to indicate that the core rocks had cooled below 775 K in Neocomian time and below 625 K by Albian time, assuming nominal closure temperatures for hornblende and muscovite, respectively. They went on to suggest that these rocks experienced a reheating event in Late Cretaceous time related to emplacement of leucocratic muscovite granites and subsequently cooled through 625 K by Eocene time (DeWitt et al., 1988).

Other previously reported thermochronologic work in the Funeral Mountains includes conventional K-Ar biotite ages from rocks below the shear zones that range from 21 Ma up to 74 Ma (Hoisch and Simpson, 1993). Conventional K-Ar dates for muscovites in rocks of the basal Crystal Spring formation yield ages of 21.0 ± 0.5 and 44 ± 1 Ma (Hoisch and Simpson, 1993), and a muscovite schist from the Johnnie Formation in Monarch Canyon yielded a 63 ± 2 Ma conventional K-Ar date (Hoisch and Simpson, 1993).

The present study seeks to shed more light on the complicated thermal history of these rocks, taking advantage of an improved ability to address complex argon systematics as well as the capability of U-Pb geochronology to obtain more direct age constraints on the age of metamorphism and granite emplacement.

ANALYTICAL METHODS

Sample selection

Samples were collected in Monarch Canyon except for sample CC13 which was collected at Chloride Cliff (Figure 2). The U-Pb samples and all but two of the $^{40}Ar/^{39}Ar$ samples were obtained from the footwall of the combined Monarch Canyon and Chloride Cliff shear zones. The remaining two, 22-4 and CC19, are from the Johnnie Formation in the hanging-wall of the Monarch Canyon shear zone. Mineral separates were obtained from three different rock types: hornblende, biotite, zircon and/or rutile from amphibolites; muscovite, biotite, and/or zircon from pelitic schists; and K-feldspar, muscovite, biotite, and/or zircon from pegmatites and granitoids. For seven of the samples, two or more different minerals were analyzed.

Sample preparation

Samples were trimmed of weathered surfaces, then crushed and sieved at M.I.T. following standard practices. In general, fairly coarse grain sizes (> 150 μm) were used for mica and feldspar separates, representing the actual grain size in the rock. Hornblende separates were finer-grained (< 150 μm) in order to minimize composite grains. U-Pb samples were separated hydraulically on a Wilfley table. Separates were purified using a combination of heavy liquid, magnetic, and paper shaking techniques. Hornblendes were subjected to an ultrasonic purifier in order to remove composite grains. All mineral separates for argon analysis were picked clean to achieve >99% purity, then washed consecutively in distilled water, acetone, and ethanol. Laser argon separates and U-Pb separates were hand-picked grain by grain in ethanol, resulting in at least 99.9% purity.

U-Pb analyses

Zircon fractions were divided into separates of 10-50 grains based on crystal size, morphology, and clarity. Some zircon separates were air-abraded for a minimum of 8

hours following the methods of Krogh (1982) in an effort to reduce the effects of surficial lead loss. Separates were leached in a warm nitric acid bath for 15 minutes to remove pyrite and other surficial contaminants. They were then rinsed, weighed, and spiked with a mixed ^{205}Pb-^{235}U spike before dissolution. Some large samples were analyzed using a 208Pb spike on post-dissolution aliquot. Zircon dissolution followed the methods of Krogh (1973) and Parrish (1987). Elemental separation was done with a HBr anion column chemistry for lead and HCl column chemistry for uranium. Procedures for rutile fractions were similar, but a ^{208}Pb-^{235}U spike was used. Isotopic analyses were determined on a VG Sector multicollector thermal ionization mass spectrometer at the University of Kansas Isotope Geochemistry Laboratory, and errors on $^{206}Pb/^{204}Pb$ were minimized by use of a Daly multiplier. A mass fractionation correction of 0.10%/amu, as determined by standard runs on NBS 981 (common lead) and NBS 982 (equal atom lead), was applied to the lead data. Common lead corrections were made using values determined from Stacey and Kramers (1975) for the crystallization age of each sample (Table 1). Decay constants used were $^{238}U = 0.15513 \times 10^{-9}$ yr^{-1} and $^{235}U = 0.98485 \times 10^{-9}$ yr^{-1} (Steiger and Jäger, 1977). The data were reduced using the data reduction program PBDAT of Ludwig (1988a). Analyses were carried out in April, 1992 with blanks of 15-20 pg total Pb and 10 pg total U, and in February, 1994 with blanks of 5-20 pg total Pb and 10 pg total U. Analytical data for U-Pb analyses are presented in Table 1, and concordia plots are shown for each sample. Age estimates for samples showing discordant behavior of one or more fractions were obtained through linear regression analysis following the approach of Ludwig (1988b) with uncertainties reported at the 95% confidence level.

$^{40}Ar/^{39}Ar$ analyses

Samples were placed in aluminum foil packets, weighed, and then placed in stacked aluminum disks that form the irradiation package. Muscovite furnace samples 22-1A, 22-

1B, 614-2, 616-1, and 620-2 were part of package CLAIR 10, which was irradiated for 7 hours in the core of the Omega West research reactor at Los Alamos National Laboratory. The remaining samples were in CLAIR 12, which was irradiated for 15 hours in the core of the research reactor at McMaster University in Hamilton, Ontario. Ca and K production factors during irradiation were established by including reagent grade K_2SO_4 and CaF_2 in each package. The fast neutron flux was monitored with MMhb-1 hornblende (520.4 Ma; Samson and Alexander, 1987) and Fish Canyon sanidine (20.8 Ma; Cebula et al., 1986). J-values varied linearly from layer to layer along the length of the package, ranging from 0.00551 to 0.00556 for the samples in CLAIR 10, and from 0.0036 to 0.0038 for the samples in CLAIR 12, with a minimum precision in any given layer of 1%. All samples were analyzed at the Cambridge Laboratory for Argon Isotopic Research (CLAIR) at the Massachusetts Institute of Technology using a MAP 215-50 mass spectrometer. Laser work was done with a Coherent 10 W argon-ion laser. Laser fusion analyses were conducted by exposing 5- to 10-grain subsamples to the continuous emission of the laser operating for 10 seconds at approximately 4 W. Laser incremental-heating experiments were conducted by bathing single crystals with a defocused beam for 2 minutes at successively higher power levels until all Ar was released. The average laser M/e blank for these samples was 4×10^{-16} moles. The total system M/e blank for incremental heating varied between 1×10^{-15} and 2×10^{-14} moles. Additional details of laboratory procedures, descriptions of facilities, and propagation of uncertainties can be found in Hodges et al. (1994, in press).

Compiled age data and sample data for argon analyses are presented in Table 2, and the raw data for incremental heating schedules and individual laser analyses are presented in Table 3. Age estimates are based on linear regression analysis of inverse isotope correlation diagrams (Roddick et al., 1980). We used the mean squared weighted deviation (MSWD) of data from the best-fit line to determine our choice of regression treatment. If the calculated MSWD for a particular data set was within 2σ of the expected value of 1 (as

calculated using the approach of Wendt and Carl, 1991), then we used the regression treatment of York (1969), which provides errors in fit parameters (and ultimately estimated ages) that are based largely on the magnitude of analytical uncertainties. Values of MSWD $> 1 + 2\sigma$ were obtained for many samples, indicating that the scatter of points about the best-fit line was too large to be explained by analytical imprecision alone. In these cases, we used the regression treatment of York (1966), which yields errors based largely on data scatter. All uncertainties are reported at the 2σ level.

SAMPLE DESCRIPTIONS AND RESULTS

Granitoid and pegmatite dikes

An injection complex of muscovite-bearing pegmatite and granitoid dikes intrudes rocks in the footwall of the intracore shear zones. The dikes are most common as intrusions in amphibolite gneisses of the basal Crystal Spring formation. In lower Monarch Canyon, these dikes make up as much as 20% of the total exposure (Hoisch and Simpson, 1993). Although dikes intrude Crystal Spring Formation rocks east of Chloride Cliff and the Keane Wonder millsite several kilometers away, no dikes are present above the Monarch Canyon shear zone.

The crystallization ages of two pegmatites have been constrained by U-Pb zircon and monazite ages obtained earlier in this study (Applegate et al., 1992; Chapter 3). A pegmatite that cuts across the S_3 foliation yielded an age of 70 ± 1 Ma, and a pegmatite that contains the S_3 foliation as well as L_3 lineations yielded a concordant point at 72 Ma, and a lower intercept for discordant points of 72 ± 1 Ma. We have dated several other pegmatite and granitoid dikes in order to further constrain the age of the intrusive event as well as the age of F_4 folding.

In order to characterize the minerals analyzed for 40Ar/39Ar thermochronology, electron microprobe analyses were done on the JEOL 733 Superprobe at M. I. T. Muscovites from granitoid samples 614-2, 614-1, and 620-2 are all quite similar with

$(Fe_{TOTAL} + Mg)/Al^{VI}$ ratios of 0.217 - 0.266, $Si^{IV}/(Si^{IV} + Al^{IV})$ ratios of 0.691 - 0.861, and Na/(Na + K) ratios of 0.027 - 0.047, indicating a significant phengite component but a very low paragonite component. Sample 628-1 has a low $(Fe_{TOTAL} + Mg)/Al^{VI}$ ratio of 0.060, but a high $Si^{IV}/(Si^{IV} + Al^{IV})$ ratio of 0.868 and a high Na/(Na + K) ratio of 0.222, indicating significant phengite and paragonite components. The Mg/(Mg + Fe) ratio in biotites from sample 614-1 is 0.349. K-feldspars from samples 614-2, 614-1, 616-1, and 620-2 are all binary K-Na solid solutions with X_{Or} ranging from 0.900 to 0.934.

Sample 614-2

Sample 614-2 is from a muscovite-bearing pegmatite dike that intrudes basal Crystal Spring Formation amphibolite gneisses in Monarch Canyon (Figure 2). The dike is unfoliated but is involved in an outcrop-scale F_4 fold (Figure 3). Six fractions of zircon were analyzed, and the results are given in Table 1 and shown on a concordia diagram in Figure 4a. All of the fractions plot on or very close to concordia and show no evidence of inheritance. They yield $^{206}Pb/^{238}U$ and $^{207}Pb/^{235}U$ ages between 64 and 66 Ma. This spread of ages along concordia may indicate bulk Pb-loss due to radiation damage of the zircon crystals, a hypothesis supported by the fact that all but one of the fractions have >2000 ppm U. The one fraction with a lower U concentration gave a signal not much above background and thus has very large uncertainties associated with it. One sample was air-abraded for over 40 hours in an effort to minimize the effects of surficial Pb-loss. It plots just below concordia and yields a $^{206}Pb/^{238}U$ age of 65.5 ± 0.3 Ma and a $^{207}Pb/^{235}U$ age of 65.7 ± 0.3 Ma (uncertainties given at 2σ level). We consider these ages to represent a minimum estimate for the crystallization age of the pegmatite. It should be noted that these analyses were not corrected for ^{232}Th disequilibrium effects.

Two muscovite separates from sample 614-2 were analyzed by step heating: a 150 - 250 μm size fraction in the furnace and a 250-500 μm size fraction with the laser (Tables 2, 3.1, and 3.2. In the age spectrum diagram for the furnace sample (Figure 4b), no plateau

exists and the steps show a "saddle-shaped" morphology. Plotted on an isotope correlation diagram (Figure 4c), the points show a reasonably linear trend indicative of mixing between a radiogenic component and one with an inital $^{40}Ar/^{36}Ar$ ratio close to that of air. An MSWD of 6.9 precluded the application of a York II fit, but a York I regression yields an age of 20 ± 2 Ma with an initial $^{40}Ar/^{36}Ar$ ratio of 370 ± 60. Only four steps were obtained for the laser step-heating analysis of the coarser fraction with the majority of gas coming off on the second step (Figure 4d). Eliminating the first point, which represents less than 1% of the total $^{39}Ar_K$ released, from the York II regression yields an age of 35.1 ± 0.7 Ma with an MSWD of 0.3 and an initial $^{40}Ar/^{36}Ar$ ratio of 200 ± 300 (Figure 4e). Owing to its large uncertainty, this ratio is within uncertainty of air.

K-feldspars from 614-2 were analyzed in the resistance furnace with an increased number of steps in order to elucidate the complicated patterns of gas release in K-feldspars. The first several percent of gas released yield old ages characterized by an excess component, then ages drop to a minimum, or "saddle", and slowly climb to a second relatively flat near-plateau (Figure 4f). Several authors have argued that the presence of multiple near-plateau segments is indicative of multiple diffusion domains within the K-feldspar grains (Heizler and Harrison, 1988; Lovera et al., 1991). In this interpretation, the flat "saddle" at low-temperature steps would represent the least-retentive domain in K-feldspar, whereas the near-plateau at higher-temperature steps would represent a more-retentive domain. The young ages of the lower-temperature saddle are a reflection of the lower closure temperature for this domain, and the older ages in the higher-temperature near-plateau reflect a higher closure temperature for that domain. When plotted on an isotope correlation diagram (Figure 4g), however, the points show a good deal of scatter, suggestive of mixing between multiple argon components, including an excess component. This scattering suggests a second explanation for the second, older near-plateau: that old ages obtained for higher-temperature steps could be the result of an excess argon component trapped in a more-retentive diffusion domain (Foster et al., 1990). The two

explanations can be tested by regressing the steps from each of the two near-plateaus. If the two domains have different closure temperatures, i.e. if the different model ages are meaningful, then the two sets of points should plot along two separate mixing lines with different x-intercepts and hence different ages. The initial $^{40}Ar/^{36}Ar$ ratios for these mixing lines may be the same or different. In the other case, the higher-temperature steps should lie on a mixing line with an appreciably higher initial $^{40}Ar/^{36}Ar$ ratio than a mixing line for the low-temperature steps, but both lines would have a similar x-intercept. Steps 5-10 yield a York II regression age of 11.7 ± 0.2 Ma with an MSWD of 0.9 and an initial $^{40}Ar/^{36}Ar$ ratio of 360 ± 70. Points 12-15, which define a second relatively flat portion of the release spectrum, yield a York II regression age of 23.4 ± 0.5 Ma with an MSWD of 2.9 and an initial $^{40}Ar/^{36}Ar$ ratio of 360 ± 40. The presence of two distinct age domains within the sample, both with virtually identical initial ratios, suggests that there are two domains with different closure temperatures. The intermediate steps between the two flat portions of the release spectrum all plot between the two regression lines on the isotope correlation diagram, suggesting that those steps represent mixing between the two domains.

Sample 614-1

Sample 614-1 is from the same outcrop as sample 614-2 (Figure 2). It is from a muscovite- and biotite-bearing granodiorite dike that cuts across the S_3 foliation as well as the F_4 fold that deforms sample 614-2 (Figure 3). Eight fractions of zircon were analyzed from this sample, and the results are given in Table 1 and shown in Figure 5a. In strong contrast to sample 614-2, none of the fractions yield concordant points. Instead, all plot along a discordia line, suggesting variable amounts of inheritance. When all fractions are regressed, they yield an upper intercept of 1700 ± 100 Ma and a lower intercept of 80 ± 70 Ma with a MSWD of 87. The lower intercept is poorly constrained in part because the point closest to the lower intercept has a large uncertainty associated with it (Fraction 3 on

Figure 5a). Although the lower intercept age of 80 Ma is older than that for 614-2, the large uncertainty makes it consistent with a younger age as indicated by the structural relations of the two dikes.

Figure 5b is an isotope correlation diagram obtained for four groups of muscovite grains from sample 614-1 that were fused with the laser. Total fusion ages are equivalent to conventional K-Ar dating, although with much higher precision. These analyses yielded model ages of 11-19 Ma individually. Regressing all four points yields a York II age of 14.2 ± 0.3 Ma with an MSWD = 0.9 and an initial $^{40}Ar/^{36}Ar$ ratio of 330 ± 20, slightly higher than air. Because of the large uncertainties associated with the second analysis and the similar plotting positions of the third and fourth analyses, this regression is effectively a two-point isochron.

Biotite from sample 614-1 yields a relatively flat release spectrum but no plateau (Figure 5c). On an isotope correlation diagram (Figure 5d), the points define a regression line with a York II age of 17.5 ± 0.2 Ma, an MSWD = 0.8, and an initial $^{40}Ar/^{36}Ar$ ratio of 280 ± 20 within uncertainty of air. The 614-1 biotite age is much younger than the conventional K-Ar biotite ages reported in Hoisch and Simpson (1993) for other samples below the shear zones, suggesting that their samples were heavily contaminated with excess ^{40}Ar. The presence of a poorly constrained excess component in our sample may explain the fact that the biotite age is greater than the muscovite age even though the nominal closure temperature for the latter is higher.

The release spectrum for the K-feldspar separate from sample 614-1 (Figure 5e) shows a similar morphology to that of 614-2. A flat saddle is evident in the low-temperature increments. Because fewer steps were analyzed, however, it is not possible to define a second, higher-temperature domain. When plotted on an isotope correlation diagram (Figure 5f), the individual steps that form a minimum on the release spectrum (points 3-12) plot along a mixing line with a York II regression age of 9.7 ± 0.2 Ma, an MSWD of 0.9, and an initial $^{40}Ar/^{36}Ar$ ratio of 320 ± 20, only slightly higher than air. Some idea of the

age of a possible higher-temperature domain is given by the model age of 18.4 ± 0.3 Ma for step 14, which represents the final 38.7 % of the total gas released.

Sample 616-1

Sample 616-1 is from a muscovite-bearing pegmatite dike that intrudes middle Crystal Spring Formation marbles in a side canyon east of Monarch Canyon (Figure 2). Like sample 614-1, this dike is unfoliated and cuts an F_4 fold. Only one zircon fraction was obtained from this sample (Figure 6a; Table 1). It shows a significant component of inheritance and plots well off of concordia, providing no useful constraint on the age of the dike. If the fraction is forced through an upper intercept of 1700 Ma, equivalent to that obtained for sample 614-1, one obtains a lower intercept of ~ 70 Ma, consistent with other ages obtained for pegmatite dikes in Monarch Canyon.

K-feldspar from this sample yields a release spectrum diagram that is similar to the other K-feldspar analyses (Figure 6b). Steps 3-5 yield a York II regression age of 9.8 ± 0.4 Ma with an MSWD of 0.1 and an initial $^{40}Ar/^{36}Ar$ ratio of 300 ± 100 when plotted on an isotope correlation diagram (Figure 6c). Steps 14-19, representing over 50% of the total $^{39}Ar_K$ released, yield a York II regression age of 18.3 ± 0.7 Ma with an MSWD = 0.5 and an initial $^{40}Ar/^{36}Ar$ ratio of 280 ± 50. The presence of two near-plateaus with similar initial $^{40}Ar/^{36}Ar$ ratios suggests that two distinct age domains are present in this sample.

Sample 620-2

Sample 620-2 is a garnet-bearing granodiorite dike in lower Monarch Canyon that intrudes the basal Crystal Spring amphibolite gneisses (Figure 2). The dike is unfoliated and does not appear to have been affected by subsequent deformation. A single, cloudy zircon fraction from the sample plots above concordia with a $^{206}Pb/^{238}U$ age of 53.5 ± 0.3 Ma and a 207Pb/235U age of 52.1 ± 0.6 Ma (Figure 7a; Table 1). This fraction contains >4000 ppm U and may have undergone significant bulk Pb-loss. The apparent ages for the

dike must be considered minima and are consistent with either a Late Cretaceous or Early Tertiary age for the dike.

A muscovite separate from sample 620-2 was analyzed in the furnace and yielded a saddle-shaped age spectrum with no apparent plateau (Figure 7b). On an isotope correlation diagram (Figure 7c), the individual steps plot along a mixing line that yields a York I age of 17 ± 1 Ma, an MSWD = 3.9, and an initial $^{40}Ar/^{36}Ar$ ratio of 300 ± 60, within uncertainty of the atmospheric value.

K-feldspar from sample 620-2 yields a low-temperature saddle at about 10 Ma, with higher temperature steps climbing to ages of greater than 12 Ma (Figure 7d). Regressing points 4-10, which define a flat minimum on the release spectrum, one obtains a York II regression age of 10.4 ± 0.2 Ma with an MSWD of 0.1 and an initial $^{40}Ar/^{36}Ar$ ratio of 300 ± 100 (Figure 7e). Step 14 contains the final 41.3 % of the total gas released and has a model age of 16.1 ± 0.2 Ma, which may suggest the age of a higher-temperature domain.

Sample 628-1

Sample 628-1 is a muscovite-bearing pegmatite dike that intrudes upper Crystal Spring strata less than 10 m beneath the Chloride Cliff shear zone. The dike contains an S_3 foliation and has been deformed by movement on the shear zone. No zircons were obtained from this dike, but it is petrologically similar to the other pegmatites and is assumed to be of a similar age. A muscovite separate from sample 628-1 was analyzed by laser step-heating and produced a flat release spectrum (Figure 8a) except for the first step which represents less than 1% of the total $^{39}Ar_K$ released. When plotted on an isotope correlation diagram (Figure 8b), the four steps yield a York II regression age of 81 ± 2 Ma with an MSWD of 0.5 and an initial $^{40}Ar/^{36}Ar$ ratio of 800 ± 700. This anomalously old age is 10 My older than the ages obtained for the crystallization of this suite of pegmatites. Although it is possible that the pegmatite is older than 81 Ma, it is more likely that the sample contains a much higher excess argon component than is apparent from the analysis,

especially given the fact that rocks at equivalent structural depths yield substantially younger $^{40}Ar/^{39}Ar$ muscovite ages. If one forces the regression through an x-intercept equivalent to a 70 Ma age, the inital $^{40}Ar/^{36}Ar$ ratio rises to 3000, albeit with a very large uncertainty.

Metamorphic rocks beneath the Chloride Cliff shear zone

A wide range of minerals was studied from metamorphic rocks in the footwall of the shear zones: zircon and rutile by the U-Pb method, and muscovite, biotite, and hornblende by the $^{40}Ar/^{39}Ar$ method. Muscovites from pelitic schists in the Crystal Spring Formation have $(Fe_{TOTAL} + Mg)/Al^{VI}$ ratios of 0.062 - 0.114, $Si^{IV}/(Si^{IV} + Al^{IV})$ ratios of 0.793 - 0.909, and Na/(Na + K) ratios of 0.090 - 0.223, indicating a significant phengite component and a range of paragonite components. The Mg/(Mg + Fe) ratio in biotites from sample 628-2 is 0.380. The method of Spear and Kimball (1984) was used to recalculate hornblende formulas based on electron microprobe data. Amphiboles from samples 22-2, KW13, and CC13 have formulae of $(K_{0.188}Na_{0.320})$ $(Na_{0.159}Ca_{1.840})$ $(Mn_{0.019}Fe^{2+}_{1.682}Ti_{0.059}Fe^{3+}_{0.003}Al_{0.854})$ $(Al_{1.324}Si_{6.676})$ O_{22} $(OH)_2$, $(K_{0.140}Na_{0.439})$ $(Na_{0.114}Ca_{1.793})$ $(Mn_{0.021}Fe^{2+}_{2.214}Ti_{0.121}Fe^{3+}_{0.330}Al_{0.667})$ $(Al_{1.704}Si_{6.296})$ O_{22} $(OH)_2$, and $(K_{0.033}Na_{0.011})$ $(Na_{0.073}Ca_{1.845})$ $(Mn_{0.021}Fe^{2+}_{2.214}Ti_{0.009}Fe^{3+}_{0.035}Al_{0.463})$ $(Al_{0.486}Si_{7.514})$ O_{22} $(OH)_2$, respectively. Using the classification scheme of Hawthorne (1981), sample 22-2 is edenitic hornblende, KW13 is ferroan pargasitic hornblende, and CC13 is actinolite/actinolitic hornblende.

Sample 22-1

Sample 22-1 is from a kyanite-garnet-mica schist in the lower Crystal Spring Formation in Monarch Canyon. Six fractions of clear, euhedral to subhedral zircons from three diamagnetic splits were analyzed, and the results are presented in Table 1. In each diamagnetic split, one separate contained optically-visible cores and inclusions, and the

other did not. None of the six fractions yielded concordant points when plotted on a concordia diagram (Figure 9a). Instead, all show evidence of an inherited component, and they plot along a discordia line. When all six fractions are regressed, they yield an upper intercept of 1700 ± 400 Ma and a lower intercept of 130 ± 60 Ma with an MSWD of 270. If the two fractions with the largest uncertainty (Fractions 5 and 6 in Figure 9a) are removed from the regression, the remaining four fractions yield much better regression statistics: an upper intercept of 1570 ± 60, a lower intercept of 128 ± 9, and an MSWD = 5.1. The intercepts can be interpreted in one of two ways; either: 1) the lower intercept represents the age of a thermal disturbance of zircons whose age is equivalent to the upper intercept; or 2) the lower intercept represents the growth of metamorphic zircons that nucleated on older detrital zircons with ages equivalent to the upper intercept, and hence the analyses plot along a mixing line. The presence of visible cores in some fractions suggests that the latter interpretation is correct.

Muscovites define the S_3 foliation in sample 22-1. Two muscovite separates were analyzed in the furnace: a coarser, 250 - 500 μm size fraction (22-1A; Table 3.3) and a finer, 150 - 250 μm size fraction (22-1B; Table 3.4). Both samples yield age spectra with very similar morphologies (Figures 9b and 9d), neither yielding a plateau and both showing a saddle in their higher-temperature steps. On an isotope correlation diagram (Figure 9c), the data are highly clustered and do not provide a good linear fit (MSWD = 19.3). Most gas fractions, however, plot sufficiently close to the $^{39}Ar/^{40}Ar$ axis that the apparent age (57 ± 1 Ma) is relatively insensitive to the slope of the line or the $^{36}Ar/^{40}Ar$ initial intercept. The initial $^{40}Ar/^{36}Ar$ ratio for the best-fit line is 500 ± 200, suggesting the presence of an unsupported ^{40}Ar component. The isotope correlation diagram for sample 22-1B (Figure 9e) shows a similar clustering with a York I regression age of 45 ± 2 Ma, an MSWD of 13.3, and an initial $^{40}Ar/^{36}Ar$ ratio of 500 ± 400.

Sample 22-2

Sample 22-2 is from an orthoamphibolite gneiss within the basal Crystal Spring Formation exposed in Monarch Canyon (Figure 2). This sample displays a well-developed S_3 foliation defined by biotite and a L_3 mineral lineation defined by amphibole. The sample was collected more than 10 m from the nearest granitic dike in order to minimize the thermal effects of these intrusions noted by DeWitt et al. (1988). Both zircon and rutile were analyzed, and the results are presented in Table 1. When plotted on a concordia diagram (Figure 10a), one of the zircon fractions plots above concordia and the other shows a large component of inheritance. The two plot on a line with an upper intercept of 1656 Ma and a lower intercept of 114 Ma. The upper intercept age is similar to those obtained for other samples. The fraction which plots above concordia suggests the presence of young, metamorphic zircons that grew during Mesozoic metamorphism.

Rutiles from this rock also display inheritance (inset of Figure 10a), possibly suggesting that they are primary igneous rutile that have been overgrown during metamorphism. One fraction plots just below concordia, yielding a $^{206}Pb/^{238}U$ age of 38 $\pm$ 3 Ma and a $^{207}Pb/^{235}U$ age of 44 $\pm$ 7 Ma. The $^{206}Pb/^{238}U$ age is taken to represent a minimum estimate of the cooling age for rutile in this sample, because this ratio is less sensitive to the common Pb correction, which is quite large for rutile.

A hornblende separate from sample 22-2 was analyzed in the furnace. On an age spectrum diagram (Figure 10b), it does not show a plateau, and model ages for individual steps range from 22 Ma to 140 Ma. When plotted on an isotope correlation diagram (Figure 10c), these data define a field indicative of three-component mixing between a radiogenic component, an atmospheric component, and a high $^{40}Ar/^{36}Ar$ ratio component signaling the presence of excess argon. As a first attempt at determining the age of this sample, one can obtain minimum and maximum ages based on the edges of the field of points. This approach yields a minimum age of 53 Ma and a maximum age of 89 Ma. Step 8, the most radiogenic point with the highest $^{39}Ar/^{40}Ar$ ratio, yields a model age of 85 Ma

when forced through the modern atmospheric $^{40}Ar/^{36}Ar$ value, similar to the maximum age for the sample (Table 3.1). Excluding the first four steps, which represent less than 6% of the total gas and plot as outliers, one obtains a York II regression age of 70 ± 3 Ma with a MSWD of 1.7 and a high initial $^{40}Ar/^{36}Ar$ ratio of 1000 ± 300.

Sample KW13

Sample KW13 is another orthoamphibolite gneiss within the basal Crystal Spring Formation exposed in Monarch Canyon (Figure 2). Like Sample 22-2, this sample is foliated and lineated. It also was collected over 10 m from the nearest granitic dike. Two zircon fractions were analyzed from this sample, and both fractions show evidence of a large inherited component and may represent detrital zircons that have only been slightly overgrown by metamorphic rims (Figure 11a). The two points plot on a line with a Mesoproterozoic upper intercept and a Paleozoic lower intercept, and hence they do not appear to provide any useful age information.

A hornblende separate from sample KW13 was analyzed in the furnace. It does not yield a plateau (Figure 11b) and shows a great deal of scatter on the isotope correlation plot (Figure 11c), defining a field consistent with mixing of three separate components. Determining a minimum and maximum age from the edges of the field, one obtains a minimum age of 31 Ma and a maximum age of 76 Ma. The maximum age is comparable to the model age for the most radiogenic point, step 6 (Table 3.2). This sample yields a York I regression age of 70 ± 10 Ma for a mixing line with a MSWD of 6.3 and a high excess component as indicated by the initial $^{40}Ar/^{36}Ar$ ratio of 800 ± 400. This age is consistent with the age obtained for sample 22-2 as well as a 68 ± 2 Ma K-Ar date obtained for hornblende from a biotite hornblende schist in the basal Crystal Spring Formation (Hoisch and Simpson, 1993).

Sample 628-2

Sample 628-2 was obtained from an orthoamphibolite body less than 10 m beneath the Chloride Cliff shear zone, and it has been very intensely deformed by that structure. The amphibolite has an S_3 foliation defined by biotites and a L_3 mineral lineation defined by amphibole. A biotite separate from sample 628-2 was analyzed in the furnace. It does not yield a plateau (Figure 12a), and the points cluster on an isotope correlation diagram (Figure 12b). A York I regression line yields an age of 36 ± 5 Ma with a MSWD of 14.6 and an initial $^{40}Ar/^{36}Ar$ ratio of 300 ± 200, again within uncertainty of air.

Sample 628-3

Sample 628-3 is a garnet-mica schist in the upper Crystal Spring Formation adjacent to Sample 628-2 and 10 m from Sample 628-1. Ten subsamples of muscovite that defines the S_3 foliation in this rock were analyzed by laser total fusion. Model ages for the individual subsamples range from 42.9 ± 0.9 Ma to 50 ± 1 Ma with a mean model age of 47 ± 5 Ma (Table 2; Table 3.16). The subsamples cluster very tightly when plotted on an inverse isotope correlation diagram, preventing the determination of a regression line (Figure 13). Because the subsamples were all highly radiogenic, however, the age is relatively insensitive to the slope of a regression line, and the model ages represent a reasonable estimate of the cooling age for this sample.

Sample CC13

Hornblendes were obtained from a sample collected just below the Chloride Cliff shear zone at Chloride Cliff (Figure 2). Sample CC13 is from a garnetiferous orthoamphibolite body in the upper Crystal Spring formation. Metamorphic conditions for rocks at Chloride Cliff were not as high as for those from the same stratigraphic level in Monarch Canyon, suggesting a westward dip to these units when they were metamorphosed (Hoisch and Simpson, 1993). As a consequence, one would expect an older cooling age for samples

from this area. Sample CC13 shows a saddle-shaped age spectrum (Figure 14a) with a near-plateau defined by steps 6-8. When these points are regressed they yield a York II regression age of 110 ± 4 Ma. On an isotope correlation diagram (Figure 14b), all the steps define a three-component field. Regressing points along the edges of this field yields a minimum age of 95 Ma and a maximum age of 117 Ma. Regressing all the steps combined yields a York II age of 104 ± 4 Ma with an MSWD of 1.7 and a high initial $^{40}Ar/^{36}Ar$ ratio of 1000 ± 400. Hoisch and Simpson (1993) obtained a 112.9 ± 0.8 Ma plateau age for hornblendes from the same body.

Metamorphic rocks above the Monarch Canyon shear zone

Sample 22-4

In contrast to the Mesozoic ages obtained for amphiboles from rocks in the footwall of the intracore shear zones, amphibole obtained from an orthoamphibolite sill in the Johnnie Formation above the Monarch Canyon shear zone in Monarch Canyon yields very different ages ranging from Paleozoic to Proterozoic. Sample 22-4 is a ferroan pargasite based on the Hawthorne (1981) classification, with a formula of $(K_{0.127}Na_{0.388})$ $(Na_{0.100}Ca_{1.846})$ $(Mn_{0.008}Fe^{2+}_{2.129}Ti_{0.056}Fe^{3+}_{0.192}Al_{1.084})$ $(Al_{1.803}Si_{6.197})$ O_{22} $(OH)_2$, calculated as above. Like the hornblende analyses, sample 22-4 does not yield a plateau (Figure 15a), and the data scatter on an isotope correlation diagram (Figure 15b) is suggestive of multiple reservoirs. Although this plot is for the most part uninterpretable, a York II regression age of 580 ± 30 Ma is obtained for the first six steps, representing the first 35% of the gas released. This regression has an MSWD of 1.9 and an initial $^{40}Ar/^{36}Ar$ ratio of 270 ± 40, within uncertainty of the value for modern atmosphere. Such an age is consistent with the time of deposition of the Johnnie Formation. It is also similar to a conventional K-Ar date of 540 ± 10 Ma reported by Hoisch and Simpson (1993) for hornblende for a similar amphibolite body in the Johnnie Formation in Monarch Canyon.

Sample CC19

Sample CC19 is a staurolite-garnet-mica schist in the Johnnie Formation. Although these schists have undergone substantial retrogression with abundant chlorite, we were able to obtain a clean muscovite separate. Muscovite from this sample has a $(Fe_{TOTAL} + Mg)/Al^{VI}$ ratio of 0.044, a $Si^{IV}/(Si^{IV} + Al^{IV})$ ratio of 0.908, and a Na/(Na + K) ratio of 0.320, indicating large phengite and paragonite components. Laser fusion analysis of ten subsamples yielded individual model ages of 57 ± 1 Ma to 69 ± 1 Ma with a mean model age of 63 ± 7 Ma (Table 2; Table 3.19). As with sample 628-3, these subsamples all cluster very tightly, preventing determination of a mixing line, but because they are all highly radiogenic, the model ages are a reasonable estimate of the actual cooling age (Figure 16).

DISCUSSION

Closure temperature

The nominal closure temperatures for argon in hornblende, muscovite, and biotite define a down-temperature progression: 800 ± 50 K for hornblende, 650 ± 50 K for muscovite, and 620 ± 50 K for biotite (McDougall and Harrison, 1988). The U-Pb closure temperature for rutile is strongly grain-size dependent, and Mezger et al. (1989) found that rutiles with diameters < 180 μm yielded a closure temperature of 650 K, the same as the nominal closure temperature for muscovite. Rutiles from sample 22-2 are < 75 μm and predictably yield younger ages than muscovite from nearby samples (e.g. sample 22-1). Hornblende analyses yielded consistently older ages than the other systems, as expected by its higher closure temperature. In sample 614-1, from which both biotite and muscovite were analyzed, the biotite age of 17.5 ± 0.2 Ma is older than the muscovite age of 14.2 ± 0.3 Ma, implying that the biotite cooled through its closure temperature before the muscovite did. DeWitt et al. (1988) report a similar phenomenon for biotite-muscovite pairs that they analyzed from Monarch Canyon. The closure temperatures for these two

minerals overlap within uncertainty, and this apparent inversion may simply be an artifact of that overlap. Another explanation is that the biotite may contain an excess component despite its fairly flat release spectrum (Figure 5c). Numerous studies have documented anomalously old ages, sometimes older than the age of the Earth, for biotites with flat release spectra (e.g. Pankhurst et al., 1973). The clustering of points on the isotope correlation diagram for this sample (Figure 5d) is indicative of sample homogenization with respect to radiogenic argon at a low temperature in the step-heating experiment as the biotite becomes unstable during heating *in vacuo* due to dehydration and delamination reactions (Hanson et al., 1975). This homogenization makes it impossible to determine whether an excess component was present in the sample and will produce a flat release spectrum.

Calculation of K-feldspar closure temperature

Unlike other minerals commonly used for $^{40}Ar/^{39}Ar$ thermochronology, K-feldspar is an anhydrous mineral that remains essentially stable throughout much of a step-heating experiment until it melts at relatively high temperature (~1326 K; Montana et al., 1991). This stability and the resulting absence of other reactions that could affect the mechanism of argon release make it possible to model the argon release as the result of simple, thermally-activated volume diffusion and thus obtain closure temperatures for individual samples (Berger and York, 1981).

In order to obtain a closure temperature, T_C [K], we use Dodson's equation (Dodson, 1973):

$$T_C = \frac{E}{R \ln [-ART_C D_0/l^2 E(dT/dt)]} \qquad (1)$$

where E [J/mol] is the activation energy, A is a geometric constant relating the ratio of surface area per unit volume for a given shape, R [J/K/mol] is the gas constant, D_0 [second^{-1}] is diffusivity at infinite temperature, l [m] is the characteristic diffusion dimension, and dT/dt [K/second] is the cooling rate. K-feldspar traditionally is modeled

with a plane sheet geometry, in which case A = 8.7 and l is the half-width of the sheet (Dodson, 1973). A cooling rate can be assumed based on other thermochronologic information. In the case here, fission track data indicates rapid cooling over the temperature interval usually associated with closure for K-feldspar (Holm and Dokka, 1991), and consequently we assume a cooling rate of 100 K/Ma. The remaining variables to be determined are E, D_0, and l. The first two are defined by the Arrhenius relationship for simple volume diffusion:

$$D = D_0 \exp(-E/RT) \qquad (2)$$

where D is the diffusivity [second^{-1}]. Note that in order to solve equation 1, one actually needs the quantites E and D_0/l^2. By dividing both sides of equation 2 by l^2, both quantities appear:

$$D/l^2 = D_0/l^2 \exp(-E/RT) \qquad (2a)$$

McDougall and Harrison (1988) provide exact and approximate solutions for the diffusion equation using the results from step-heating experiments. Using the approximate solution for a plane sheet geometry, one obtains D/l^2 for each individual step with T being the temperature for that step:

$$D/l^2 = f_i^2\pi/4t_i \qquad 0 \le f_i < 0.45 \qquad (3a)$$

$$D/l^2 = (-4/\pi^2 t_i) \ln(0.125\pi^2 (1 - f_i)) \qquad 0.45 \le f_i \le 1 \qquad (3b)$$

where f_i is the cumulative percentage of argon released after a given step and t_i is the duration in seconds of that step. By taking the natural logarithm of both sides of equation 2a, it can now be rewritten in y = mx + b form and solved for each step:

$$\ln D/l^2 = -E/RT + \ln D_0/l^2 \qquad (2b)$$

The resulting plot is known as an Arrhenius diagram. A line can be regressed through points for each individual step to obtain the slope (-E/R) and the y-intercept ($\ln D_0/l^2$). Equation 1 can be solved iteratively for T_c using assumed values for A and dT/dt and the values for E and D_0/l^2 obtained from the linear regression. The results of these calculations

for each of the four K-feldspar samples are shown in Table 4, and plots of the regressions are shown in Figure 17.

Figure 17a shows the Arrhenius diagram for sample 614-1. Increments between 775 K and 900 K (corresponding to steps 3-8) form a linear trend. The two lower temperature increments, which showed evidence for a strong excess component, plot off this linear trend as do higher temperature increments. The regression results (shown in Table 4) yield a closure temperature of 490 ± 60 K, assuming a cooling rate of 100 K/Ma. A closure temperature of 490 K is within the range generally obtained for K-feldspar (Lovera et al., 1989). The choice of a slower cooling rate, for example 10 K/Ma, would have the effect of lowering the apparent closure temperature by approximately 30 K, well within the uncertainty of the estimates obtained.

Interpretation of the age significance for closure temperatures derived in this method is complicated in many K-feldspar samples by the presence of multiple diffusion domains of varying size, each with its own age and closure temperature (Lovera et al., 1989). Lovera et al. (1989) demonstrated that different size domains can produce local plateaus in the age spectrum. The age of the local plateau depends on the domain size and its position with respect to the percentage of ^{39}Ar released, with small domains yielding lower closure temperatures and large domains yielding higher closure temperatures (Lovera et al., 1989). Consequently, the departure of higher-temperature increments on an Arrhenius diagram from a single linear trend reflects the exhaustion of gas coming from the smallest domain size (Lovera et al., 1989). Thus the closure temperature derived from the Arrhenius plot only pertains to the smallest domain and thus only to the lowest flat portion of the release spectrum in each case. In the case of sample 614-1, the closure temperature of 490 K obtained above applies to the 9.7 ± 0.2 Ma age obtained for the younger plateau, a result that is consistent with ages of 14.2 ±0.3 Ma for muscovite and 17.5 ± 0.2 Ma for biotite, both of which have higher nominal closure temperatures.

Figure 17b is the Arrhenius diagram for sample 614-2. In this case, increments of 725-925 K form a linear trend that result in a closure temperature of 370 ± 40 K at a cooling rate of 100 K/Ma. This temperature is below the range generally obtained for K-feldspar and is surprising given that an age of 11.7 ± 0.2 Ma was obtained for this sample, 2 My older than was obtained for the adjacent sample 614-1 with its much higher calculated closure temperature.

For sample 616-1, increments 675 - 875 K yield regression results that produce an apparent closure temperature of 500 ± 100 K at a cooling rate of 100 K/Ma (Figure 17c). The large uncertainty is the result of poor regression statistics produced by a poor fit of the data to a linear trend. This closure temperature is similar to that obtained for sample 614-1, and the two samples yielded ages that are identical within uncertainty.

The final sample, 620-2, shows a good fit to the data for increments 725 -850 K, resulting in a closure temperature of 470 ± 40 K at a cooling rate of 100 K/Ma, within uncertainty of that obtained for sample 614-1 (Figure 17d). Its age of 10.4 ± 0.2 Ma is slightly older than those obtained for 614-1 and 616-1 and may reflect a slightly higher closure temperature.

All four of the K-feldspar samples analyzed in this study show evidence for two flat portions in their release spectra (Figures 4e, 5e, 6b, 7d). In the two cases where enough increments existed to regress lines for each flat portion, the higher-temperature flat portions yield different regression ages but similar initial $^{40}Ar/^{36}Ar$ ratios to the lower-temperature saddles, indicating that the older age is not simply an artifact of an excess component released at higher temperatures. Without a known closure temperature for the higher temperature portion of the release spectrum, however, we do not know the significance of the age obtained for that portion with respect to a time-temperature history. Lovera and others have developed sophisticated techniques to model these multiple domains (Lovera et al., 1989; Lovera et al., 1991). Although such techniques may be applicable to some of these samples, they require a greater number of steps and cycling of closure temperatures to

a greater degree than was attempted here. Some idea of the closure temperature for the higher-temperature increments can be derived from their ages relative to other phases studied. In the case of sample 614-2, the regression age of 23.4 ± 0.5 Ma obtained for the higher-temperature steps is similar to the younger of the muscovite ages obtained for that sample (20 ± 2 Ma), suggesting that if that age represents a second domain, its closure temperature may be as high as ~650 K.

Age of metamorphism

Zircon becomes a closed system with respect to U and Pb at temperatures greater than 1025 K (Ghent et al., 1988), higher than the maximum temperatures reported for the Funeral Mountains. As a result, it is unlikely that the zircon ages represent a "cooling" age but instead represent the age of prograde metamorphism, i.e. the time at which these minerals grew. The lower intercept age of ~130 Ma for zircons from sample 22-1 indicates that these zircons grew in Early Cretaceous time during kyanite-grade metamorphism of the schist, overgrowing detrital zircons derived from Early Proterozoic basement. A minimum age for metamorphism is provided by hornblende from sample CC13 at Chloride Cliff which yielded a 104 ± 4 Ma cooling age. Peak temperatures for the rocks at Chloride Cliff are 850 - 875 K as determined by Hoisch and Simpson (1993). These temperatures are only 50 -75 K above the nominal closure temperature for hornblende, indicating that these rocks would not have had to cool very much before reaching the hornblende closure temperature.

Age of granitoid injection complex

Pegmatite and granodiorite dikes appear to have intruded over a span of several million years at the end of the Late Cretaceous Epoch. Results reported in Applegate et al. (1992; Chapter 3) remain the best constrained ages for these intrusions. Those results indicated that D_3 deformation was ongoing at 72 ± 1 Ma and over by 70 ± 1 Ma. The results

presented here are consistent with these constraints on D_3 deformation and may provide additional constraints on the age of D_4 deformation. Sample 614-2, which is deformed by F_4 folds, has a minimum age of ~65 Ma, suggesting that D_4 deformation continued into earliest Paleocene time. Other pegmatite dikes, however, cut F_4 folds, including one that may be part of the same body as the 70 Ma pegmatite dated by Applegate et al. (1992; Chapter 3). If that is the case, then folding may be diachronous or, alternatively, the 65 Ma age for sample 614-2 is an artifact of lead loss and the actual age of the pegmatite is somewhat older.

The upper intercept age for these dikes is consistent with the 1.7 Ga age of crystalline basement rocks in the Death Valley region. Although not exposed in the Funeral Mountains, basement rocks directly underlie the Crystal Spring Formation elsewhere in the region (Wright, 1973) and are a likely source for the anatectic melting that produced these dikes.

Cooling history for Monarch Canyon

Figure 18 presents the thermochronologic results from this study in the form of a time-temperature diagram for the structurally deepest rocks in the core complex, those from Monarch Canyon in the footwall of the intracore shear zones. This plot also includes previously published fission-track data of Holm and Dokka (1991) obtained from one of the pegmatites that intrude the basal Crystal Spring formation in lower Monarch Canyon. The K-feldspar ages are generally consistent with sphene and zircon fission-track ages, indicating rapid Late Miocene cooling. The low closure temperatures for sample 614-2, however, is not consistent with the 7 ± 3 Ma fission-track age obtained by Holm and Dokka (1991) for apatite. The 11.7 ± 0.2 Ma age for sample 614-2 is older than those obtained from the other K-feldspar samples, perhaps suggesting that its closure temperature is higher than calculated using the Arrhenius diagram..

Holm and Dokka (1991) suggested that rapid, Late Miocene cooling was associated with tectonic denudation of the core complex by the core-bounding Boundary Canyon Detachment, and Reynolds et al. (1986) postulated that the detachment developed at ~10 Ma, synchronous with rapid cooling, based on rough stratigraphic constraints. Recent $^{40}Ar/^{39}Ar$ results from tuffs within the Tertiary Titus Canyon Formation, which is cut by the Boundary Canyon Detachment, indicate an unconformity after 16 Ma, suggesting that the detachment may have been active at that time (Saylor and Hodges, 1994). If that is the case, then it is quite possible that cooling represents thermal reequilibration of these rocks as a response to the unroofing rather than strictly synchronous with it (House and Hodges, 1994, submitted).

Rutile, muscovite, and biotite results indicate a protracted period of slow cooling over much of Tertiary time prior to the rapid Late Miocene cooling indicated by the K-feldspar and fission-track data. There is a general progression in the muscovite data from structurally higher to lower rocks: the oldest ages come from schists directly beneath the Chloride Cliff shear zone (628-3) and in the lower Crystal Spring Formation (22-1A and 22-1B), and younger ages come from pegmatites intruding the basal Crystal Spring formation (614-1, 614-2, and 620-2). Likewise the older biotite age is from an amphibolite directly below the shear zones (628-2), and the younger age is from a granite intruding the basal Crystal Spring formation (614-1). It also appears that grain size plays some role in the closure temperature for muscovite. In the two samples for which two grain size fractions of muscovite were analyzed, the larger grain size (250 to 500 μm) yielded older ages than the smaller grain size (150 to 250 μm). In the case of sample 614-2, that variation was on the order of 15 My.

On the face of it, the hornblende results for samples KW13 and 22-2 are also consistent with slow cooling extending back through Late Cretaceous time to the time of peak metamorphism. Such a conclusion, however, is strongly at odds with thermobarometry and thermodynamic modeling of garnet zonation performed by Hodges and Walker (1990).

Their data indicate that the rocks now exposed in lower Monarch Canyon underwent 400 to 600 MPa of near-isothermal decompression at temperatures above the nominal closure temperature for hornblende. Such decompression paths are consistent with paths derived from numerical modeling of extensional unroofing (e.g. Ruppel et al., 1988; Ruppel and Hodges, 1994). The 70 Ma hornblende ages for samples KW13 and 22-2 imply that this decompression predates 70 Ma, making it synchronous with ductile extensional fabrics related to the intracore shear zones (Applegate et al., 1992). Thus, the hornblende cooling ages appear to represent cooling of the footwall of the intracore shear zones after extensional unroofing accommodated by those structures.

Whereas zircon and hornblende results support an Early Cretaceous age for peak metamorphism consistent with earlier estimates, our data from Monarch Canyon do not support Early Cretaceous cooling through either the hornblende or even lower muscovite closure temperatures at that structural level as reported by DeWitt et al. (1988) from plateau ages. Both of the hornblende analyses from Monarch Canyon yield regression ages of 70 Ma and evidence of a large excess component. Because of this large excess component, model ages and hence plateau ages will be artificially old. For example, sample 22-2 yields a total gas model age of 108 ± 2 Ma and sample KW13 yields a total gas model age of 85 ± 2 Ma. These ages are similar to the plateau ages obtained by DeWitt et al. (1988). In contrast to DeWitt, our results from Monarch Canyon indicate a cooling history that extended from Late Cretaceous through Miocene time.

Age of ductile extensional deformation and significance of intracore shear zones

Several authors have argued that at least some of the ductile extensional fabrics in the footwall of the Funeral Mountains core complex are Tertiary in age and related to movement on the core-bounding detachment (e.g. Holm and Dokka, 1991; Hoisch and Simpson, 1993). The cooling history derived above suggests that this is not the case, at least for the quartz-rich lithologies which dominate the core rocks. Hoisch and Simpson

(1993) estimated that mylonitization in quartz *ended* within the temperature range of 750 - 600 K (dashed lines on Figure 18). Our data indicate that the deepest rocks in the core had cooled to temperatures within this range by early Tertiary time. Thus, whereas Late Cretaceous unroofing took place at much higher temperatures consistent with the development of mylonitic fabrics, Late Miocene unroofing took place for the most part over a temperature range below the lower limit for mylonitization. Moreover, it is important to note that rocks in the footwall of the core-bounding Boundary Canyon detachment are at a structurally higher level that would have cooled even sooner than the rocks for which the cooling history in Figure 18 was derived, further suggesting an entirely brittle history for quartz-rich lithologies during Late Miocene unroofing. Some ductile fabrics may have formed, however, in calcite marble lithologies during Late Miocene deformation, since calcite behaves ductilely at temperatures where quartz behaves brittlely.

The decompression paths calculated by Hodges and Walker (1990) indicate that as much as 20 km of unroofing took place during Late Cretaceous extension. Consistent with this result are very low equilibration pressures for samples adjacent to granites that are synchronous with and postdate the Late Cretaceous deformation. These pressures correspond to depths of 15 to 18 km, equivalent to the amounts of unroofing estimated for Late Miocene extension that would have brought them to near-surface depths (Holm and Dokka, 1991). Thus, the evidence suggests that more than half of the unroofing of the deepest rocks exposed in the Funeral Mountains took place in Late Cretaceous time.

If indeed significant amounts of Late Cretaceous extensional unroofing were accommodated by the Monarch Canyon and Chloride Cliff shear zones, the implication is that rocks in the hanging-wall and footwall of these structures are from very different levels in the crust. As a result, rocks in the hanging-wall of the Monarch Canyon shear zone should have experienced a significantly different thermal history from that discussed above for rocks in the footwall of the shear zones, particularly for the higher-temperature portion of the cooling history prior to the Late Cretaceous unroofing event. Although the data are

complicated by significant retrogression and hydrothermal alteration of these rocks, they are nevertheless consistent with a significantly different cooling history. The mean model age of 63 ± 7 Ma for muscovites in sample CC19 is significantly older than muscovite ages from below the Monarch Canyon shear zone and may indicate cooling after movement on the structurally higher Eastern shear zone. Hornblende from sample 22-4 yields a 580 ± 30 Ma date, and none of the individual steps yielded Mesozoic ages. What is clear from these data is that there is no indication that these rocks experienced the same high-grade Mesozoic metamorphic event as rocks in the footwall of the shear zones, an observation consistent with a distinct metamorphic discontinuity – staurolite-grade Johnnie Formation across the shear zones from kyanite-grade Crystal Spring Formation – and indicative of an important structural break at that location.

CONCLUSIONS

Constructing a thermal history for the Funeral Mountains is complicated by the presence of significant amounts of isotopic inheritance in both the U-Pb and $^{40}Ar/^{39}Ar$ geochronologic systems. With the aid of other sources of geologic information, however, it is possible to constrain these data and produce meaningful results. Despite inheritance produced by overgrowth of Early Proterozoic detrital zircon grains, metamorphic zircons that grew during prograde regional metamorphism provide an upper age constraint of approximately 130 Ma for that event. Hornblende cooling ages from Chloride Cliff, where peak temperatures did not exceed the closure temperature for argon by more than 75 K, indicate that peak metamorphism had been reached by at least 104 Ma and possibly earlier. Rocks in the footwall of the intracore shear zones cooled through the closure temperature for argon in hornblende after undergoing substantial Late Cretaceous extensional unroofing. A spread of muscovite and biotite ages suggests that the core rocks cooled slowly during much of Tertiary time, compatible with slow, erosion-controlled unroofing. In Late Miocene time, the core rocks underwent rapid cooling through closure temperatures

for individual K-feldspar samples consistent with previously-reported fission-track data. This cooling is related to movement on the core-bounding Boundary Canyon detachment.

Our earlier finding of a Late Cretaceous age for ductile extensional fabrics in the core is consistent with evidence from the cooling history presented here that the core rocks had cooled within the temperature range for the lower limit of mylonitization calculated by Hoisch and Simpson (1993) by early Tertiary time, after Late Cretaceous extensional deformation but well before initiation of movement on the core-bounding detachment. A different cooling history for rocks in the hanging-wall of the Monarch Canyon shear zone is consistent with our earlier interpretation that this structure and the Chloride Cliff shear zone together represent a major structural discontinuity in the core and are responsible for a significant portion, perhaps more than half, of the unroofing of mid-crustal rocks in their combined footwall.

REFERENCES

Applegate, J. D. R., Walker, J. D. and Hodges, K. V., 1992, Late Cretaceous extensional unroofing in the Funeral Mountains metamorphic core complex, California: Geology, v. 20, p. 519-522.

Berger, G. W., and York, D., 1981, Geothermometry from $^{40}Ar/^{39}Ar$ dating experiments: Geochimica et Cosmochimica Acta, v. 45, p. 795-811.

Cebula, G. T., Kunk, M. J., Mehnert, H. H., Naeser, C. W., Obradovich, J. D. and Sutter, J. F., 1986, The Fish Canyon tuff, a potential standard for the ^{40}Ar-^{39}Ar and fission-track methods: Terra Cognita, v. 6, p. 139-140.

DeWitt, E., Sutter, J. F., Wright, L. A. and Troxel, B. W., 1988, Ar-Ar chronology of early Cretaceous regional metamorphism, Funeral Mountains, California – A case study of excess argon: Geological Society of America Abstracts with Programs, v. 20, p. A16.

Dodson, M. H., 1973, Closure temperature in cooling geochronological and petrological systems: Contributions to Mineralogy and Petrology, v. 40, p. 259-274.

Foster, D. A., Harrison, T. M., Copeland, P. and Heizler, M. T., 1990, Effects of excess argon with large diffusion domains on K-feldspar age spectra: Geochimica et Cosmochimica Acta, v. 54, p. 1699-1708.

Ghent, E. D., Stout, M. Z. and Parrish, R. R., 1988, Determination of metamorphic pressure-temperature-time (PTt) paths, in E. G. Nisbet and C. M. R. Fowler ed., Short Course on Heat, Metamorphism, and Tectonics, v. St. John's, Mineralogical Association of Canada, p. 155-188.

Hanson, G. N., Simmons, K. R. and Bence, A. E., 1975, $^{40}Ar/^{39}Ar$ spectrum ages for biotite, hornblende and muscovite in a contact metamorphic zone: Geochimica et Cosmochimica Acta, v. 39, p. 1269-1277.

Heizler, M. T., and Harrison, T. M., 1988, Multiple trapped argon isotope components revealed by $^{40}Ar/^{39}Ar$ isochron analysis: Geochimica et Cosmochimica Acta, v. 52, p. 1295-1303.

Hodges, K. V., Hames, W. E., Olszewski, W., Burchfiel, B. C., Royden, L. H., and Chen, Z., 1994, Thermobarometric and $^{40}Ar/^{39}Ar$ geochronologic constraints on Eohimalayan metamorphism in the Dinggyê area, southern Tibet: Contributions to Mineralogy and Petrology, in press.

Hodges, K. V., and Walker, J. D., 1990, Petrologic constraints on the unroofing history of the Funeral Mountains metamorphic core complex, California: Journal of Geophysical Research, v. 95, p. 8437-8445.

Hoisch, T. D., 1991, Equilibria within the mineral assemblage quartz + muscovite + biotite + garnet + plagioclase, and implications for the mixing properties of octahedrally-coordinated cations in muscovite and biotite: Contributions to Mineralogy and Petrology, v. 108, p. 43-54.

Hoisch, T. D., and Simpson, C., 1993, Rise and tilt of metamorphic rocks in the lower plate of a detachment fault in the Funeral Mountains, Death Valley, California: Journal of Geophysical Research, v. 98, p. 6805-6827.

Holm, D. K., and Dokka, R. K., 1991, Major Late Miocene cooling of the middle crust associated with extensional orogenesis in the Funeral Mountains, California: Geophysical Research Letters, v. 18, p. 1775-1778.

Krogh, T. E., 1973, A low-contamination method of hydrothermal decomposition of zircon and extraction of U and Pb for isotopic age determinations: Geochimica et Cosmochimica Acta, v. 37, p. 485-494.

Krogh, T. E., 1982, Improved accuracy of U-Pb ages by the creation of more concordant systems using an air abrasion technique: Geochimica et Cosmochimica Acta, v. 46, p. 637-649.

Labotka, T. C., 1980, Petrology of a medium-pressure regional metamorphic terrane, Funeral Mountains, California: American Mineralogist, v. 65, p. 670-689.

Labotka, T. C., and Albee, A. L., 1988, Metamorphism and tectonics of the Death Valley region, California, in W. G. Ernst ed., Metamorphism and Crustal Evolution of the Western United States, v. Englewood Cliffs, N.J., Prentice-Hall, p. 714-736.

Lovera, O. M., Richter, F. M. and Harrison, T. M., 1989, The $^{40}Ar/^{39}Ar$ thermochronometry for slowly cooled samples having a distribution of diffusion domain sizes: Journal of Geophysical Research, v. 94, p. 17917-17935.

Lovera, O. M., Richter, F. M. and Harrison, T. M., 1991, Diffusion domains determined by ^{39}Ar released during step heating: Journal of Geophysical Research, v. 96, p. 2057-2069.

Ludwig, K. R., 1988a, PBDAT for MS-DOS: a computer program for IBM-PC compatibles for processing raw Pb-U-Th isotope data: U.S. Geological Survey Open File Report 88-542.

Ludwig, K. R., 1988b, ISOPLOT for MS-DOS: a plotting and regression program for radiogenic-isotope data, for IBM-PC compatible computers: U.S. Geological Survey Open File Report 88-557.

McDougall, I., and Harrison, T. M., 1988, Geochronology and Thermochronology by the $^{40}Ar/^{39}Ar$ Method: New York, Oxford University Press, 212 pp.

Mezger, K., Hanson, G. N., and Bohlen, S. R., 1989, High-precision U-Pb ages of metamorphic rutile: application to the cooling history of high-grade terranes: Earth and Planetary Science Letters, v. 96, p. 106-118.

Montana, A., Luth, R. W., White, B. S., Boettcher, S. L., McBride, K. S. and Rice, J. F., 1991, Complications in the melting of silicate minerals from atmospheric to high pressures, in L. L. Perchuk ed., Progress in Metamorphic and Magmatic Petrology, v. New York, Cambridge University Press, p. 351-368.

Pankhurst, R. J., Moorbath, S., Rex, D. C. and Turner, G., 1973, Mineral age patterns in ca. 3700 my old rocks from West Greenland: Earth and Planetary Science Letters, v. 20, p. 157-170.

Parrish, R. R., 1987, An improved micro-capsule for zircon dissolution in U-Pb geochronology: Chemical Geology (Isotope Geoscience Section), v. 66, p. 99-102.

Reynolds, M. W., Wright, L. A. and Troxel, B. W., 1986, Geometry and chronology of late Cenozoic detachment faulting, Funeral and Grapevine Mountains, Death Valley, California: Geological Society of America Abstracts with Programs, v. 18, p. 175.

Roddick, J. C., Cliff, R. A. and Rex, D. C., 1980, The evolution of excess argon in alpine biotites—a $^{40}Ar/^{39}Ar$ analysis: Earth and Planetary Science Letters, v. 48, p. 945-960.

Ruppel, C., and Hodges, K. V., 1994, Pressure-temperature-time paths from two-dimensional thermal models: Prograde, retrograde, and inverted metamorphism: Tectonics, v. 13, p. 17-44.

Ruppel, C., Royden, L., and Hodges, K. V., 1988, Thermal modeling of extensional tectonics: Application to pressure-temperature-time histories of metamorphic rocks: Tectonics, v. 7, p. 947-957.

Samson, S. D., and Alexander, E. C., 1987, Calibration of the interlaboratory $^{40}Ar/^{39}Ar$ dating standard, MMhb-1: Chemical Geology, v. 66, p. 27-34.

Saylor, B. Z., and Hodges, K. V., 1994, $^{40}Ar/^{39}Ar$ age constraints on the depositional history of the Oligocene Titus Canyon Formation, Death Valley, CA: Geological Society of America Abstracts with Programs, v. 26, in press.

Stacey, J. S., and Kramers, J. D., 1975, Approximation of terrestrial lead isotope evolution by a two-stage model: Earth and Planetary Science Letters, v. 26, p. 207-221.

Steiger, R. H., and Jäger, E., 1977, Subcommision on geochronology: Convention on the use of decay constants in geo- and cosmochronology: Earth and Planetary Science Letters, v. 1, p. 369-371.

Wendt, I., and Carl, C., 1991, The statistical distribution of the mean squared weighted deviation: Chemical Geology, v. 86, p. 275-285.

Wernicke, B., Axen, G.J., and Snow, J.K., 1988, Basin and Range extensional tectonics at the latitude of Las Vegas, Nevada: Geological Society of America Bulletin, v. 100, p. 1738-1757.

Wright, L. A., 1973, Geology of the SE1/4 of Tecopa 15-minute quadrangle, San Bernardino and Inyo Counties, California: California Division of Mines and Geology Map Sheet 20.

Wright, L. A., and Troxel, B. W., 1994, in press, Geologic map of the central and northern parts of the Funeral Mountains and adjacent areas, Death Valley region, southern California, scale 1:48,000: U.S. Geol. Surv. Misc. Invest. Ser. I-2305.

York, D., 1966, Least-squares fitting of a straight line: Canadian Journal of Physics, v. 44, p. 1079-1086.

York, D., 1969, Least squares fitting of a straight line with correlated errors: Earth and Planetary Science Letters, v. 5, p. 320-324.

Table 1. U-Pb Analytical Data and Results

Fractions and Properties	Weight (mg)	Concentrations U (ppm)	Concentrations Pb* (ppm)	Atomic ratios 206 Pb† / 204 Pb	206 Pb‡ / 238 U	% err	207 Pb‡ / 235 U	% err	207 Pb‡ / 206 Pb	% err	Age (Ma) 206 Pb / 238 U	207 Pb / 235 U	207 Pb / 206 Pb	corr. coef.	Total common Pb (pg)
614-2															
nm(0)-240	0.057	3266.9	30.7	2985	0.010264	(0.48)	0.067104	(0.53)	0.047417	(0.22)	**65.8**	**65.9**	**70.3**	0.908	41
nm(0)-100	0.208	3042.7	27.6	7831	0.010019	(0.59)	0.065478	(0.59)	0.047399	(0.08)	**64.3**	**64.4**	**69.4**	0.991	31
nm(1)-240	0.075	3450.3	31.8	4008	0.010142	(1.16)	0.066053	(1.18)	0.047235	(0.25)	**65.1**	**64.9**	**61.1**	0.978	27
nm(-1)-240 aa(16)	0.007	686.1	8.4	120.4	0.010155	(4.31)	0.066337	(6.63)	0.047376	(4.86)	**65.1**	**65.2**	**68.2**	0.681	31
nm(0)-240 aa(16)	0.027	2321.5	24.4	382.7	0.010006	(0.58)	0.065004	(1.02)	0.047117	(0.82)	**64.2**	**63.9**	**55.2**	0.603	110
nm(0)-100 aa(40)	0.107	3404.9	31.5	6895	0.010209	(0.51)	0.066824	(0.53)	0.047474	(0.12)	**65.5**	**65.7**	**73.1**	0.976	34
614-1															
nm(0)-240	0.090	340.7	43.7	7408	0.128292	(0.55)	1.809890	(0.58)	0.102318	(0.16)	**778.1**	**1049.0**	**1666.6**	0.961	31
nm(0)-100	0.655	425.4	67.3	57314	0.161356	(0.48)	2.276110	(0.48)	0.102307	(0.05)	**964.3**	**1204.9**	**1666.4**	0.994	25
nm(0)-240 g	0.005	234.0	7.8	114	0.033149	(8.73)	0.320271	(9.28)	0.070073	(2.48)	**210.2**	**282.1**	**930.5**	0.964	24
nm(-1) g	0.001	417.4	50.5	70.83	0.080355	(14.40)	1.076440	(15.20)	0.097158	(4.49)	**498.2**	**741.9**	**1570.3**	0.956	36
nm(1)-240	0.094	422.3	52.0	17560	0.124209	(0.56)	1.754920	(0.57)	0.102471	(0.08)	**754.7**	**1029.0**	**1669.4**	0.991	16
nm(0)-240 aa(8)	0.011	313.0	61.8	5226	0.204176	(0.58)	2.904900	(0.64)	0.103187	(0.26)	**1197.7**	**1383.2**	**1682.2**	0.915	8
nm(0)-240 g	0.011	181.5	13.0	502.1	0.068874	(1.35)	0.927802	(1.91)	0.097701	(1.22)	**429.4**	**666.5**	**1580.7**	0.774	18
nm(1)240 aa(16)	0.035	413.4	45.3	6712	0.111748	(0.49)	1.598240	(0.49)	0.103729	(0.08)	**682.9**	**969.5**	**1691.9**	0.987	15
616-1															
nm(-1,0) -100 c	0.010	1846.8	77.3	361.7	0.035324	(0.85)	0.414938	(0.90)	0.085195	(0.28)	**223.8**	**352.4**	**1320.0**	0.949	120
620-2															
m(2) -100 c	0.045	4047.2	33.0	711.4	0.008329	(0.64)	0.052643	(1.10)	0.045840	(0.88)	**53.5**	**52.1**	**-10.8**	0.609	140
22-1															
nm(0)-100 aa(16)	0.014	832.8	25.1	268.7	0.026231	(1.03)	0.221756	(1.13)	0.061314	(0.45)	**166.9**	**203.4**	**650.3**	0.918	78
nm(0)-100	0.015	721.4	28.9	1622	0.039726	(0.59)	0.409395	(0.62)	0.074743	(0.17)	**251.1**	**348.4**	**1061.6**	0.960	17
m(0)-100 g	0.009	509.9	26.4	1115	0.050672	(0.81)	0.563378	(0.89)	0.080636	(0.34)	**318.7**	**453.7**	**1212.6**	0.925	13
nm(-1)-100 g	0.022	527.4	23.1	1244	0.043082	(0.75)	0.454094	(0.77)	0.076445	(0.14)	**271.9**	**380.1**	**1106.7**	0.984	26
m(0)-100 aa(16)	0.006	713.6	23.7	367.7	0.032444	(2.16)	0.352918	(2.26)	0.078892	(0.62)	**205.8**	**306.9**	**1169.4**	0.962	25
nm(0)-100 g	0.001	1370.7	78.6	431.7	0.056504	(2.09)	0.697501	(2.27)	0.089529	(0.82)	**354.3**	**537.3**	**1415.5**	0.933	12

Table 1. U-Pb Analytical Data and Results (continued)

Fractions and Properties	Weight (mg)	Concentrations U (ppm)	Concentrations Pb* (ppm)	Atomic ratios 206 Pb† / 204 Pb	206 Pb‡ / 238 U	% err	207 Pb‡ / 235 U	% err	207 Pb‡ / 206 Pb	% err	Age (Ma) 206 Pb / 238 U	207 Pb / 235 U	207 Pb / 206 Pb	corr. coef.	Total common Pb (pg)
22-2															
nm(6)-200	0.092 (r)	19.4	1.0	23.6	0.005850	(7.92)	0.044118	(15.30)	0.054692	(12.20)	**37.6**	**43.8**	**399.7**	0.616	?
nm(6)+200	0.312 (r)	29.9	497.7	211.2	0.014256	(1.74)	0.148721	(2.08)	0.075661	(1.06)	**91.3**	**140.8**	**1086.1**	0.862	41
nm(6)+140	0.738 (r)	37.5	650.0	201.7	0.013663	(1.01)	0.153165	(1.27)	0.081305	(0.73)	**87.5**	**144.7**	**1228.8**	0.822	98
m(.75A) -100	1.346 (r)	27.2	820.7	59.4	0.012198	(0.74)	0.106732	(4.21)	0.063460	(3.86)	**78.2**	**103.0**	**723.7**	0.532	700
nm(0)-100 split 1	0.060	354.0	58.4	4403	0.166955	(0.52)	2.281240	(0.53)	0.099099	(0.06)	**995.3**	**1206.5**	**1607.2**	0.994	52
nm(0)-100 split 2	0.011	111.3	2.7	47.6	0.012607	(12.60)	0.042936	(42.70)	0.024701	(39.10)	**80.8**	**42.7**	**-1801.6**	0.421	30
KW13															
nm(0)-100 split 1	0.014	86.4	16.5	221.9	0.149526	(4.36)	1.8108	(4.38)	0.087832	(0.38)	**898.3**	**1049.4**	**1378.8**	0.996	57
nm(0)-100 split 2	0.005	161.4	43.1	1092	0.255828	(6.29)	3.4824	(6.30)	0.098726	(0.38)	**1468.5**	**1523.2**	**1600.2**	0.998	12

Note: nm = nonmagnetic, m = magnetic on Frantz separator at angle of tilt (degrees in parentheses); -100 = size in standard mesh; aa = air abraded fraction (duration in hours in parentheses; 8 hours unless otherwise noted); g = clear fraction, c = cloudy fraction, b = bulk fraction; (r) = rutile; all other samples are zircons. Common lead corrections were made using values determined from Stacey and Kramers (1975) for the crystallization age. Values used for 614-2 are $^{206}Pb/^{204}Pb = 18.60$, $^{207}Pb/^{204}Pb = 15.62$, and $^{208}Pb/^{204}Pb = 38.50$; values used for 614-1 are $^{206}Pb/^{204}Pb = 15.76$, $^{207}Pb/^{204}Pb = 15.32$, and $^{208}Pb/^{204}Pb = 35.40$; values used for 616-1 are $^{206}Pb/^{204}Pb = 18.60$, $^{207}Pb/^{204}Pb = 15.62$, and $^{208}Pb/^{204}Pb = 38.50$; values used for 620-2 are $^{206}Pb/^{204}Pb = 18.70$, $^{207}Pb/^{204}Pb = 15.63$, and $^{208}Pb/^{204}Pb = 38.63$; values used for 22-1 are $^{206}Pb/^{204}Pb = 18.60$, $^{207}Pb/^{204}Pb = 15.62$, and $^{208}Pb/^{204}Pb = 38.50$; values used for 22-2 are $^{206}Pb/^{204}Pb = 16.89$, $^{207}Pb/^{204}Pb = 15.49$, and $^{208}Pb/^{204}Pb = 36.57$; and values used for KW13 are $^{206}Pb/^{204}Pb = 18.70$, $^{207}Pb/^{204}Pb = 15.63$, and $^{208}Pb/^{204}Pb = 38.63$.

*Radiogenic Pb.

†Ratios corrected for mass fractionation only

‡Ratios corrected for fractionation, spike, blank, and initial common Pb.

Table 2. Summary of $^{40}Ar/^{39}Ar$ Results

Sample	Rock Type	Mineral	Grain size (μm)	Extraction Method	Isochron age (Ma)	Fit	$^{39}Ar_i$ (%)	$(^{40}Ar/^{36}Ar)_0$	MSWD
Granitoid and pegmatite dikes									
614-2	pegmatite	Kfs	250-500	Furnace	11.7 ± 0.2	II	38	360 ± 70	0.9
		"	"	"	23.4 ± 0.5	II	49	360 ± 40	2.9
		Ms	150-250	Furnace	20 ± 2	I	100	370 ± 60	6.9
		Ms	250-500	Laser	35.1 ± 0.7	II	100	200 ± 300	0.3
614-1	granite	Kfs	150-250	Furnace	9.7 ± 0.2	II	46	320 ± 20	0.9
		Ms	250-500	Laser	14.2 ± 0.3	II	N/A	330 ± 20	0.9
		Bt	250-500	Furnace	17.5 ± 0.2	II	100	280 ± 20	0.8
616-1	pegmatite	Kfs	250-500	Furnace	9.8 ± 0.4	II	14	300 ± 100	0.1
		"	"	"	18.3 ± 0.7	II	53	280 ± 50	0.5
620-2	granite	Kfs	250-500	Furnace	10.4 ± 0.2	II	24	300 ± 100	0.1
		Ms	150-250	Furnace	17 ± 1	I	100	300 ± 60	3.9
628-1	pegmatite	Ms	250-500	Laser	81 ± 2	II	100	800 ± 700	0.5
Metamorphic rocks beneath the Chloride Cliff shear zone									
22-1A	schist	Ms	250-500	Furnace	51 ± 1	I	100	500 ± 200	19.3
22-1B		Ms	150-250	Furnace	45 ± 2	I	100	500 ± 400	13.3
22-2	amphibolite	Hbl	125-150	Furnace	70 ± 3	II	95	1000 ± 300	1.7
KW13	amphibolite	Hbl	125-150	Furnace	70 ± 10	I	100	800 ± 400	6.3
628-2	amphibolite	Bt	250-500	Furnace	36 ± 5	I	100	300 ± 100	14.6
628-3	schist	Ms	250-500	Laser	47 ± 5	M	N/A	295.5	N/A
CC13	amphibolite	Hbl	125-150	Furnace	104 ± 4	II	100	1000 ± 400	1.7

Table 2. Summary of $^{40}Ar/^{39}Ar$ Results (continued)

Sample	Rock Type	Mineral	Grain size (μm)	Extraction Method	Isochron age (Ma)	Fit	$^{39}Ar_i$ (%)	$(^{40}Ar/^{36}Ar)_0$	MSWD
Metamorphic rocks above the Monarch Canyon shear zone									
22-4	amphibolite	Hbl	125-150	Furnace	580 ± 30	II	35	270 ± 40	1.9
CC19	schist	Ms	250-500	Laser	63 ± 7	M	N/A	295.5	N/A

Abbreviations: Ms = muscovite, Bt = biotite, Hbl = hornblende, and Ksp = K-feldspar.
Isochron ages were calculated using fitting algorithms designated in the "Fit" column: I – least-squares linear regression (York, 1966); II – least-squares linear regression with correlated errors (York, 1969); and M – mean model age. The column "$^{39}Ar_i$" shows the percentage of total ^{39}Ar in the heating steps used for the regression. The MSWD (mean squared weighted deviation) is shown for Fit I and II regressions only. All uncertainties are quoted at the 2 σ confidence level. Multiple entries for 614-2 and 616-1 K-feldspar samples reflect our interpretation of the presence of multiple trapped Ar domains.

Table 3.1 $^{40}Ar/^{39}Ar$ Furnace Analytical Data for Sample 614-2, Muscovite

T(K)	$^{39}Ar/^{40}Ar$	$^{36}Ar/^{40}Ar$	^{39}Ar (%)	$^{40}Ar^{*}$ (%)	Ca/K	Age (Ma) (± 2σ)
900	0.2259	0.0019	2.7	43.2	0.0335	19.1 ± 0.4
950	0.2800	0.0014	3.7	57.7	0.0093	20.6 ± 0.4
1000	0.1862	0.0018	7.7	47.1	0.0050	25.2 ± 0.5
1050	0.2653	0.0012	28.5	65.8	0.0014	24.7 ± 0.5
1100	0.3760	0.0006	40.3	82.3	0.0056	21.8 ± 0.4
1150	0.3770	0.0008	55.2	77.4	0.0041	20.5 ± 0.4
1200	0.3263	0.0011	61.9	66.0	0.0025	20.2 ± 0.4
1250	0.3605	0.0008	75.2	77.8	0.0001	21.5 ± 0.4
1350	0.4019	0.0004	98.8	89.5	0.0012	22.2 ± 0.4
1550	0.3834	0.0009	100.0	72.4	0.0136	18.8 ± 0.4

York 1 regression age = 20 ± 2 Ma. MSWD = 6.9. $(^{40}Ar/^{36}Ar)_0$ = 370 ± 60. J = 0.00556 ± 0.0001112. All steps used in regression. All steps are of 5 minutes duration. $^{40}Ar^{*}$ (%) — percentage of measured ^{40}Ar derived from natural decay of ^{40}K.

Table 3.2 $^{40}Ar/^{39}Ar$ Laser Step-Heating Analytical Data for Sample 614-2, Muscovite

Increment (Amperes)	$^{39}Ar/^{40}Ar$	$^{36}Ar/^{40}Ar$	^{39}Ar (%)	$^{40}Ar^{*}$(%)	Ca/K	Age (Ma) (± 2σ)
10.5	0.0669	0.0003	0.8	92.4	8.205	87 ± 2
12	0.1524	0.0007	75.5	78.3	0.353	33.0 ± 0.7
14	0.1112	0.0018	93.2	47.0	6.894	27 ± 1
20	0.1371	0.0008	100.0	77.7	5.262	36.3 ± 0.7

York 2 regression age = 35.1 ± 0.7 Ma. MSWD = 0.3. $(^{40}Ar/^{36}Ar)_0$ = 200 ± 300. J = 0.00359 ± 0.0000359. All increments used in regression. $^{40}Ar^{*}$ (%) — percentage of measured ^{40}Ar derived from natural decay of ^{40}K.

Table 3.3 $^{40}Ar/^{39}Ar$ Furnace Analytical Data for Sample 614-2, K-feldspar

T(K)	$^{39}Ar/^{40}Ar$	$^{36}Ar/^{40}Ar$	^{39}Ar (%)	$^{40}Ar^*$ (%)	Ca/K	Age (Ma) (± 2σ)
675	0.0017	0.0018	0.5	46.3	0.0506	1250 ± 10
725	0.0390	0.0019	2.8	42.8	0.0107	69.6 ± 0.8
775	0.0821	0.0023	5.6	33.3	0.0091	26.1 ± 0.3
825	0.0762	0.0024	8.8	28.9	0.0075	24.4 ± 0.3
875 +	0.1568	0.0021	13.7	38.0	0.0106	15.6 ± 0.2
925 +	0.1877	0.0018	19.4	48.3	0.0128	16.6 ± 0.2
975 +	0.2208	0.0017	24.4	50.4	0.0064	14.7 ± 0.2
1025 +	0.2218	0.0019	28.8	45.1	0.0055	13.1 ± 0.1
1075 +	0.2090	0.0016	33.2	53.1	0.0056	16.4 ± 0.2
1125 +	0.1531	0.0020	47.2	41.2	0.0103	17.4 ± 0.2
1175	0.1192	0.0020	48.8	40.6	0.0030	21.9 ± 0.2
1225 *	0.1096	0.0019	52.3	42.8	0.0174	25.1 ± 0.3
1275 *	0.1062	0.0018	58.5	47.2	0.0122	28.6 ± 0.3
1325 *	0.1160	0.0016	69.1	53.7	0.0097	29.7 ± 0.3
1375 *	0.1442	0.0013	97.6	60.7	0.0068	27.1 ± 0.3
1300	0.1139	0.0005	97.9	85.8	0.0982	48.1 ± 0.5
1350	0.1043	0.0013	98.3	62.7	0.0870	38.5 ± 0.4
1400	0.0915	0.0025	98.6	26.8	0.0757	18.8 ± 0.2
1450	0.0592	0.0015	98.9	54.6	0.0851	58.7 ± 0.6
1500	0.0230	0.0030	99.1	12.5	0.1401	34.8 ± 0.4
1550	0.0238	0.0027	99.4	21.1	0.0397	56.5 ± 0.6
1875	0.0098	0.0029	100.0	13.4	0.3427	85.9 ± 0.9

York 2 regression age (Low-T domain) = 11.7 ± 0.2 Ma (MSWD = 0.9). $(^{40}Ar/^{36}Ar)_0$ = 360 ± 70. York 2 regression age (High-T domain) = 23.4 ± 0.5 Ma (MSWD = 2.9). $(^{40}Ar/^{36}Ar)_0$ = 360 ± 40. J = 0.00359 ± 0.0000359. Steps used in regressions are marked with plus sign for Low-T domain and with asterisk for High-T domain. All steps of 10 minutes duration except 1125 K and 1375 K, each 40 minutes. $^{40}Ar^*$ (%) — percentage of measured ^{40}Ar derived from natural decay of ^{40}K.

Table 3.4 $^{40}Ar/^{39}Ar$ Laser Fusion Analytical Data for Sample 614-1, Muscovite

Subsample	$^{39}Ar/^{40}Ar$	$^{36}Ar/^{40}Ar$	$^{39}Ar_K$ (x 10^{-14})	$^{40}Ar^*$(%)	Ca/K	Age (Ma) (± 2σ)
1	0.1016	0.0024	11.7	29.7	0.1287	18.9 ± 0.4
2	0.4326	0.0008	2.0	75.7	0.7386	11.4 ± 0.2
3	0.4238	0.0001	15.3	96.8	0.0985	14.8 ± 0.3
4	0.4526	0.0001	24.9	97.9	0.0604	14.0 ± 0.3

York 2 regression age = 14.2 ± 0.3 Ma. MSWD = 0.9. $(^{40}Ar/^{36}Ar)_0$ = 330 ± 20. J = 0.00361 ± 0.0000361. All subsamples used in regression. $^{39}Ar_K$ — moles of irradiation-produced ^{39}Ar released during laser fusion. $^{40}Ar^*$ (%) — percentage of measured ^{40}Ar derived from natural decay of ^{40}K.

Table 3.5 $^{40}Ar/^{39}Ar$ Furnace Analytical Data for Sample 614-1, Biotite

T(K)	$^{39}Ar/^{40}Ar$	$^{36}Ar/^{40}Ar$	^{39}Ar (%)	$^{40}Ar^*$ (%)	Ca/K	Age (Ma) (± 2σ)
900	0.2261	0.0014	14.2	59.1	0	16.8 ± 0.2
950	0.3066	0.0007	18.2	80.6	0.1793	16.9 ± 0.2
1000	0.3275	0.0004	26.4	88.1	0	17.3 ± 0.2
1050	0.3312	0.0004	36.1	88.9	0.0186	17.3 ± 0.2
1100	0.3124	0.0005	43.7	86.0	0.0901	17.7 ± 0.2
1150	0.3229	0.0004	51.0	88.1	0.1114	17.6 ± 0.2
1200	0.3284	0.0004	57.1	87.2	0	17.1 ± 0.2
1250	0.3367	0.0004	70.9	87.4	0	16.7 ± 0.2
1350	0.3299	0.0003	96.2	89.9	0.0799	17.6 ± 0.2
1550	0.3103	0.0007	100.0	79.7	0.0571	16.6 ± 0.2

York 2 regression age = 17.5 ± 0.2 Ma (MSWD = 0.8). $(^{40}Ar/^{36}Ar)_0 = 280 \pm 20$. J = 0.00359 ± 0.0000359. All steps used in regression. All steps are of 5 minutes duration. Ca/K ratios of zero indicate that amount of $^{37}Ar_{Ca}$ was less than the ^{37}Ar blank. $^{40}Ar^*$ (%) — percentage of measured ^{40}Ar derived from natural decay of ^{40}K.

Table 3.6 $^{40}Ar/^{39}Ar$ Furnace Analytical Data for Sample 614-1, K-feldspar

T(K)	$^{39}Ar/^{40}Ar$	$^{36}Ar/^{40}Ar$	^{39}Ar (%)	$^{40}Ar^*$ (%)	Ca/K	Age (Ma) (± 2σ)
725	0.0002	0.0033	0.0	1.5	0	413 ± 4
750	0.0159	0.0029	0.5	13.9	2.8201	55.7 ± 0.6
775 +	0.0749	0.0026	1.5	22.1	1.6822	19.0 ± 0.2
800 +	0.1505	0.0024	2.7	29.9	0	12.8 ± 0.1
825 +	0.1070	0.0028	4.2	18.4	1.1840	11.1 ± 0.1
850 +	0.0932	0.0028	6.0	17.3	0	12.0 ± 0.1
875 +	0.0917	0.0027	8.3	21.5	0.2893	15.1 ± 0.2
900 +	0.2380	0.0019	11.5	43.1	0.2516	11.7 ± 0.1
950 +	0.1984	0.0022	17.4	36.2	0.0323	11.8 ± 0.1
1000 +	0.2308	0.0020	24.8	41.1	0.0956	11.5 ± 0.1
1100 +	0.2433	0.0020	36.1	40.0	0	10.6 ± 0.1
1200 +	0.2963	0.0017	46.9	50.0	0	10.9 ± 0.1
1300	0.1723	0.0020	61.3	40.4	0.0673	15.1 ± 0.2
1500	0.1790	0.0017	100.0	51.2	0.0531	18.4 ± 0.3

York 2 regression age (Low-T domain) = 9.7 ± 0.2 Ma (MSWD = 0.9). $(^{40}Ar/^{36}Ar)_0 = 320 \pm 20$. J = 0.00359 ± 0.0000359. Steps used in regressions are marked with plus sign. All steps are of 10 minutes duration. Ca/K ratios of zero indicate that amount of $^{37}Ar_{Ca}$ was less than the ^{37}Ar blank. $^{40}Ar^*$ (%) — percentage of measured ^{40}Ar derived from natural decay of ^{40}K.

Table 3.7 $^{40}Ar/^{39}Ar$ Furnace Analytical Data for Sample 616-1, K-feldspar

T(K)	$^{39}Ar/^{40}Ar$	$^{36}Ar/^{40}Ar$	^{39}Ar (%)	$^{40}Ar^*$ (%)	Ca/K	Age (Ma) (± 2σ)
675	0.0126	0.0019	0.5	45.1	0.0152	221 ± 4
725	0.3107	0.0008	3.8	76.4	0.0023	16.0 ± 0.3
775 +	0.5208	0.0008	8.5	77.6	0.0035	9.7 ± 0.2
825 +	0.4104	0.0013	13.2	62.3	0.0004	9.9 ± 0.2
875 +	0.5880	0.0004	17.7	88.8	0.0021	9.8 ± 0.2
925	0.4873	0.0004	20.8	86.8	0.0025	11.6 ± 0.2
975	0.4422	0.0007	23.2	78.6	0.0063	11.6 ± 0.2
1025	0.4400	0.0007	25.5	80.1	0.0034	11.9 ± 0.2
1075	0.4155	0.0006	28.2	82.1	0.0030	12.9 ± 0.3
1125	0.3634	0.0008	39.4	75.3	0.0013	13.5 ± 0.3
1175	0.3341	0.0005	40.4	86.1	0.0083	16.8 ± 0.3
1225	0.3272	0.0007	43.3	80.2	0.0000	16.0 ± 0.3
1275	0.3322	0.0007	47.4	80.3	0.0028	15.7 ± 0.3
1325 *	0.2908	0.0006	53.5	81.1	0.0014	18.1 ± 0.4
1375 *	0.2850	0.0007	92.2	79.8	0	18.2 ± 0.6
1400 *	0.2784	0.0007	94.1	78.1	0.0033	18.3 ± 0.4
1450 *	0.2794	0.0010	95.7	70.2	0.0029	16.4 ± 0.3
1550 *	0.2968	0.0007	97.8	79.7	0.0036	17.5 ± 0.3
1875 *	0.1896	0.0017	99.9	51.2	0.0276	17.6 ± 0.3
1900	0.0137	0.0030	100.0	12.1	0.8182	57 ± 1

York 2 regression age (Low-T domain) = 9.8 ± 0.4 Ma (MSWD = 0.1). $(^{40}Ar/^{36}Ar)_0 = 300 \pm 100$. York 2 regression age (High-T domain) = 18.3 ± 0.7 Ma (MSWD = 0.5). $(^{40}Ar/^{36}Ar)_0 = 280 \pm 50$.
J = 0.003625 ± 0.0000725. Steps used in regressions are marked with plus sign for Low-T domain and with asterisk for High-T domain. All steps are of 10 minutes duration except 1125 K and 1375 K, each 40 minutes. Ca/K ratios of zero indicate that amount of $^{37}Ar_{Ca}$ was less than the ^{37}Ar blank. $^{40}Ar^*$ (%) — percentage of measured ^{40}Ar derived from natural decay of ^{40}K.

Table 3.8 $^{40}Ar/^{39}Ar$ Furnace Analytical Data for Sample 620-2, Muscovite

T(K)	$^{39}Ar/^{40}Ar$	$^{36}Ar/^{40}Ar$	^{39}Ar (%)	$^{40}Ar^*$ (%)	Ca/K	Age (Ma) (± 2σ)
900	0.2151	0.0024	4.2	28.3	0.1064	13.2 ± 0.3
950	0.4044	0.0016	5.5	52.7	0.0188	13.0 ± 0.3
1000	0.2570	0.0018	9.4	45.9	0.0157	17.8 ± 0.4
1050	0.3618	0.0012	26.6	65.3	0.0104	18.0 ± 0.4
1100	0.4849	0.0006	44.3	81.5	0.0106	16.8 ± 0.3
1150	0.4921	0.0010	56.2	71.6	0.0144	14.5 ± 0.3
1200	0.4547	0.0009	66.3	73.7	0.0072	16.2 ± 0.3
1250	0.4948	0.0006	81.2	81.9	0.0033	16.5 ± 0.3
1350	0.4845	0.0004	95.4	87.4	0.0097	18.0 ± 0.4
1550	0.4591	0.0003	100.0	91.1	0.0188	19.8 ± 0.4

York 1 regression age = 17 ± 1 Ma (MSWD = 3.9). $(^{40}Ar/^{36}Ar)_0 = 300 \pm 60$. J = 0.00556 ± 0.0001112. All steps used in regression. All steps are of 5 minutes duration. $^{40}Ar^*$ (%) — percentage of measured ^{40}Ar derived from natural decay of ^{40}K.

Table 3.9 $^{40}Ar/^{39}Ar$ Furnace Analytical Data for Sample 620-2, K-feldspar

T(K)	$^{39}Ar/^{40}Ar$	$^{36}Ar/^{40}Ar$	^{39}Ar (%)	$^{40}Ar^*$ (%)	Ca/K	Age (Ma) (± 2σ)
725	0.0151	0.0014	1.6	58.9	0	237 ± 3
750	0.2813	0.0010	2.6	71.7	1.1507	16.4 ± 0.2
775	0.3567	0.0011	4.4	68.6	0	12.4 ± 0.1
800 +	0.4492	0.0010	7.1	69.5	0.0979	10.0 ± 0.1
825 +	0.4437	0.0012	10.2	64.9	0	9.4 ± 0.1
850 +	0.3336	0.0018	13.5	48.2	0.0800	9.3 ± 0.1
875 +	0.4510	0.0010	15.3	70.4	0	10.1 ± 0.1
900 +	0.4461	0.0011	18.8	66.1	0.3267	9.6 ± 0.1
950 +	0.4623	0.0009	23.7	72.6	0	10.1 ± 0.1
1000 +	0.4072	0.0012	28.0	65.5	0.1875	10.4 ± 0.1
1100	0.3148	0.0014	33.3	59.0	0	12.1 ± 0.1
1200	0.3192	0.0014	41.7	59.1	0.1471	12.0 ± 0.1
1300	0.2851	0.0014	58.7	58.5	0.0193	13.2 ± 0.1
1500	0.2840	0.0010	100.0	70.9	0.0120	16.1 ± 0.2

York 2 regression age (Low-T domain) = 10.4 ± 0.2 Ma (MSWD = 0.1). $(^{40}Ar/^{36}Ar)_0 = 300 \pm 100$. J = 0.00359 ± 0.0000359. Steps used in regressions are marked with plus sign. All steps are of 10 minutes duration. Ca/K ratios of zero indicate that amount of $^{37}Ar_{Ca}$ was less than the ^{37}Ar blank. $^{40}Ar^*$ (%) — percentage of measured ^{40}Ar derived from natural decay of ^{40}K.

Table 3.10 $^{40}Ar/^{39}Ar$ Laser Step-Heating Analytical Data for Sample 628-1, Muscovite

Increment (Amperes)	$^{39}Ar/^{40}Ar$	$^{36}Ar/^{40}Ar$	^{39}Ar (%)	$^{40}Ar^*$(%)	Ca/K	Age (Ma) (± 2σ)
10.5	0.0367	0.0012	0.5	65.4	12.151	113 ± 2
12	0.0736	0.0001	55.1	97.0	0.0230	84 ± 2
14	0.0772	0.0000	87.2	99.0	0.7177	82 ± 2
20	0.0719	0.0001	100.0	97.3	0.4773	86 ± 2

York 2 regression age = 81 ± 2 Ma. MSWD = 0.5. $(^{40}Ar/^{36}Ar)_0 = 800 \pm 700$. J = 0.00362 ± 0.0000362. All increments used in regression. $^{40}Ar^*$ (%) — percentage of measured ^{40}Ar derived from natural decay of ^{40}K.

Table 3.11 $^{40}Ar/^{39}Ar$ Furnace Analytical Data for Sample 22-1A, Muscovite

T(K)	$^{39}Ar/^{40}Ar$	$^{36}Ar/^{40}Ar$	^{39}Ar (%)	$^{40}Ar^*$ (%)	Ca/K	Age (Ma) (± 2σ)
900	0.1340	0.0014	5.1	59.0	0.0119	43.6 ± 0.9
950	0.1489	0.0008	9.2	77.5	0.0040	52 ± 1
1000	0.1709	0.0002	37.3	92.9	0.0014	54 ± 1
1050	0.1925	0.0001	58.2	97.2	0.0019	50 ± 1
1100	0.2005	0.0001	67.9	96.8	0.0049	47.8 ± 0.9
1150	0.2010	0.0003	72.7	91.3	0.0077	45.0 ± 0.9
1200	0.1941	0.0002	77.0	93.3	0.0091	47.6 ± 0.9
1250	0.1932	0.0002	81.7	94.7	0.0067	49 ± 1
1350	0.1985	0.0002	93.2	95.1	0.0058	47.4 ± 0.9
1550	0.1911	0.0000	100.0	99.4	0.0045	51 ± 1

York 1 regression age = 51 ± 1 Ma (MSWD = 19.3). $(^{40}Ar/^{36}Ar)_0 = 500 \pm 200$. J = 0.00556 ± 0.0001112. All steps used in regression. All steps are of 5 minutes duration. $^{40}Ar^*$ (%) — percentage of measured ^{40}Ar derived from natural decay of ^{40}K.

Table 3.12 $^{40}Ar/^{39}Ar$ Furnace Analytical Data for Sample 22-1B, Muscovite

T(K)	$^{39}Ar/^{40}Ar$	$^{36}Ar/^{40}Ar$	^{39}Ar (%)	$^{40}Ar^*$ (%)	Ca/K	Age (Ma) (± 2σ)
900	0.1473	0.0014	3.3	57.2	0.0095	38.2 ± 0.8
950	0.1791	0.0010	7.4	69.5	0.0079	38.2 ± 0.8
1000	0.1794	0.0003	35.1	91.0	0.0012	50 ± 1
1050	0.2105	0.0001	56.5	96.5	0.0018	45.0 ± 0.9
1100	0.2239	0.0001	66.2	96.7	0.0038	42.4 ± 0.8
1150	0.2242	0.0002	71.1	93.2	0.0110	40.9 ± 0.8
1200	0.2172	0.0004	75.7	89.1	0.0117	40.3 ± 0.8
1250	0.2170	0.0002	81.1	93.0	0.0105	42.1 ± 0.8
1350	0.2138	0.0001	94.1	96.5	0.0130	44.3 ± 0.9
1550	0.2023	0.0000	100.0	99.0	0.1105	48.0 ± 0.9

York 1 regression age = 45 ± 2 Ma (MSWD = 13.3). $(^{40}Ar/^{36}Ar)_0$ = 500 ± 400. J = 0.00551 ± 0.0001102. All steps used in regression. All steps are of 5 minutes duration. $^{40}Ar^*$ (%) — percentage of measured ^{40}Ar derived from natural decay of ^{40}K.

Table 3.13 $^{40}Ar/^{39}Ar$ Furnace Analytical Data for Sample 22-2, Hornblende

T(K)	$^{39}Ar/^{40}Ar$	$^{36}Ar/^{40}Ar$	^{39}Ar (%)	$^{40}Ar^*$ (%)	Ca/K	Age (Ma) (± 2σ)
1100	0.0369	0.0024	2.0	28.7	4.6768	53 ± 1
1150	0.0459	0.0019	3.1	44.1	8.9268	65 ± 1
1175	0.0410	0.0029	4.1	13.6	12.159	22.6 ± 0.4
1200	0.0481	0.0019	5.4	42.9	15.106	60 ± 1
1225 +	0.0503	0.0011	8.4	68.9	17.098	92 ± 2
1250 +	0.0351	0.0009	15.6	74.4	18.454	140 ± 3
1275 +	0.0446	0.0005	49.6	84.5	17.072	125 ± 2
1300 +	0.0710	0.0003	80.9	90.5	16.139	85 ± 2
1350 +	0.0542	0.0004	87.3	87.3	16.927	107 ± 2
1550 +	0.0427	0.0007	98.4	79.7	17.063	124 ± 2
1725 +	0.0455	0.0005	100.0	86.6	17.123	126 ± 2

York 2 regression age = 70 ± 3 Ma (MSWD = 1.7). $(^{40}Ar/^{36}Ar)_0$ = 1000 ± 300. J = 0.0038 ± 0.000076. Steps used in regression are marked with plus sign. All steps are of 5 minutes duration. $^{40}Ar^*$ (%) — percentage of measured ^{40}Ar derived from natural decay of ^{40}K.

Table 3.14 $^{40}Ar/^{39}Ar$ Furnace Analytical Data for Sample KW13, Hornblende

T(K)	$^{39}Ar/^{40}Ar$	$^{36}Ar/^{40}Ar$	^{39}Ar (%)	$^{40}Ar^*$ (%)	Ca/K	Age (Ma) (± 2σ)
1100	0.0238	0.0022	0.7	35.0	20.950	98 ± 2
1150	0.0381	0.0002	1.4	93.1	0.0495	160 ± 3
1200	0.0392	0.0012	3.6	64.4	26.567	110 ± 2
1250	0.0574	0.0007	14.8	80.4	15.062	94 ± 2
1275	0.0718	0.0003	62.7	92.5	13.153	86 ± 2
1300	0.0837	0.0002	88.6	94.6	12.511	76 ± 2
1350	0.0723	0.0004	89.6	87.8	17.621	81 ± 2
1400	0.0696	0.0006	95.3	82.2	16.648	79 ± 2
1450	0.0678	0.0002	98.0	94.2	17.906	93 ± 2
1550	0.0632	0.0010	99.1	71.0	18.298	76 ± 2
1725	0.0577	0.0012	100.0	64.8	18.225	75 ± 2

York 1 regression age = 70 ± 10 Ma. $(^{40}Ar/^{36}Ar)_0$ = 800 ± 400. J = 0.0038 ± 0.000076. All steps used in regression. All steps are of 5 minutes duration. $^{40}Ar^*$ (%) — percentage of measured ^{40}Ar derived from natural decay of ^{40}K.

Table 3.15 $^{40}Ar/^{39}Ar$ Furnace Analytical Data for Sample 628-2, Biotite

T(K)	$^{39}Ar/^{40}Ar$	$^{36}Ar/^{40}Ar$	^{39}Ar (%)	$^{40}Ar^*$ (%)	Ca/K	Age (Ma) (± 2σ)
900	0.1203	0.0012	16.5	63.7	0.0892	35.9 ± 0.7
950	0.1302	0.0008	21.9	76.1	0.0222	39.6 ± 0.8
1000	0.1275	0.0007	28.8	78.0	0.0207	41.5 ± 0.8
1050	0.1297	0.0007	34.7	79.1	0.0204	41.3 ± 0.8
1100	0.1299	0.0007	41.2	78.6	0.0229	41.0 ± 0.8
1150	0.1329	0.0009	48.7	72.1	0.0301	36.8 ± 0.7
1200	0.1409	0.0009	63.5	73.5	0.0436	35.4 ± 0.7
1250	0.1470	0.0007	77.6	78.1	0.1156	36.1 ± 0.7
1350	0.1396	0.0007	94.0	78.9	0.0641	38.3 ± 0.8
1550	0.1218	0.0009	100.0	72.8	0.2981	40.5 ± 0.8

York 1 regression age = 36 ± 5 Ma (MSWD = 14.6). $(^{40}Ar/^{36}Ar)_0$ = 300 ± 100. J = 0.0038 ± 0.000076. All steps used in regression. All steps are of 5 minutes duration. $^{40}Ar^*$ (%) — percentage of measured ^{40}Ar derived from natural decay of ^{40}K.

Table 3.16 $^{40}Ar/^{39}Ar$ Laser Fusion Analytical Data for Sample 628-3, Muscovite

Subsample	$^{39}Ar/^{40}Ar$	$^{36}Ar/^{40}Ar$	$^{39}Ar_K$ (x 10^{-14})	$^{40}Ar^*$(%)	Ca/K	Age (Ma) (± 2σ)
1	0.1291	0.0003	180.4	91.7	0.0019	46 ± 1
2	0.1339	0.0002	92.2	93.6	0.0034	45.1 ± 0.9
3	0.1253	0.0005	23.3	84.4	0.0197	43.5 ± 0.9
4	0.1303	0.0005	10.3	86.6	0.0289	42.9 ± 0.9
5	0.1270	0.0003	21.1	90.0	0.0174	45.7 ± 0.9
6	0.1202	0.0003	24.6	89.8	0.0187	48 ± 1
7	0.1309	0.0002	111.3	92.6	0.0047	46 ± 1
8	0.1205	0.0003	65.1	91.9	0.0057	49 ± 1
9	0.1219	0.0002	45.8	93.9	0.0090	50 ± 1
10	0.1285	0.0003	163.7	92.0	0.0020	46 ± 1

Mean model age = 47 ± 5 Ma. J = 0.00362 ± 0.0000362. $^{39}Ar_K$ — moles of irradiation-produced ^{39}Ar released during laser fusion. $^{40}Ar^*$ (%) — percentage of measured ^{40}Ar derived from natural decay of ^{40}K.

Table 3.17 $^{40}Ar/^{39}Ar$ Furnace Analytical Data for Sample CC13, Hornblende

T(K)	$^{39}Ar/^{40}Ar$	$^{36}Ar/^{40}Ar$	^{39}Ar (%)	$^{40}Ar^*$ (%)	Ca/K	Age (Ma) (± 2σ)
1100	0.0396	0.0017	1.3	50.5	4.9750	86 ± 2
1150	0.0428	0.0008	4.2	76.9	14.404	120 ± 2
1175	0.0448	0.0005	6.3	86.3	19.200	128 ± 3
1200	0.0450	0.0006	9.0	82.3	16.300	121 ± 2
1225	0.0437	0.0003	18.0	91.7	16.872	139 ± 3
1250	0.0544	0.0001	64.4	95.7	.7.067	117 ± 2
1275	0.0563	0.0002	69.9	95.1	18.008	112 ± 2
1300	0.0504	0.0005	73.5	86.4	18.873	114 ± 2
1350	0.0438	0.0004	83.0	89.3	19.172	134 ± 3
1550	0.0404	0.0003	97.5	91.5	18.924	149 ± 3
1725	0.0416	0.0008	100.0	77.7	18.660	124 ± 2

York 2 regression age = 104 ± 4 Ma (MSWD = 1.7). $(^{40}Ar/^{36}Ar)_0$ = 1000 ± 400. J = 0.0038 ± 0.000076. All steps used in regression. All steps are of 5 minutes duration. $^{40}Ar^*$ (%) — percentage of measured ^{40}Ar derived from natural decay of ^{40}K.

Table 3.18 $^{40}Ar/^{39}Ar$ Furnace Analytical Data for Sample 22-4, Hornblende

T(K)	$^{39}Ar/^{40}Ar$	$^{36}Ar/^{40}Ar$	^{39}Ar (%)	$^{40}Ar^*$ (%)	Ca/K	Age (Ma) (± 2σ)
1100 +	0.0063	0.0014	4.0	57.6	35.113	540 ± 10
1150 +	0.0069	0.0008	6.2	76.0	44.368	630 ± 10
1175 +	0.0074	0.0009	8.4	74.5	43.761	580 ± 10
1200 +	0.0086	0.0007	11.1	79.3	42.592	540 ± 10
1225 +	0.0086	0.0005	18.3	86.4	41.908	580 ± 10
1250 +	0.0086	0.0005	36.7	83.8	45.260	570 ± 10
1275	0.0131	0.0006	51.6	82.5	45.647	387 ± 9
1300	0.0120	0.0008	53.4	77.6	44.626	395 ± 9
1350	0.0067	0.0005	67.0	84.3	47.490	700 ± 10
1550	0.0053	0.0005	97.1	85.3	46.886	860 ± 20
1725	0.0075	0.0007	100.0	79.4	33.841	610 ± 10

York 2 regression age = 580 ± 30 Ma (MSWD = 1.9). $(^{40}Ar/^{36}Ar)_0$ = 270 ± 40. J = 0.0038 ± 0.000076. Steps used in regression are marked with plus sign. All steps are of 5 minutes duration. $^{40}Ar^*$ (%) — percentage of measured ^{40}Ar derived from natural decay of ^{40}K.

Table 3.19 $^{40}Ar/^{39}Ar$ Laser Fusion Analytical Data for Sample CC19, Muscovite

Subsample	$^{39}Ar/^{40}Ar$	$^{36}Ar/^{40}Ar$	$^{39}Ar_K$ (x 10^{-14})	$^{40}Ar^*$(%)	Ca/K	Age (Ma) (± 2σ)
1	0.0895	0.0002	17.8	93.9	0.0118	68 ± 1
2	0.0879	0.0006	18.9	83.7	0.0147	61 ± 1
3	0.1010	0.0003	33.9	89.8	0.0069	57 ± 1
4	0.0928	0.0004	24.8	89.1	0.0168	62 ± 1
5	0.1042	0.0002	19.9	93.3	0.0205	58 ± 1
6	0.0896	0.0002	74.3	94.2	0.0051	68 ± 1
7	0.0935	0.0002	46.1	93.5	0.0029	65 ± 1
8	0.0861	0.0003	85.7	92.0	0.0047	69 ± 1
9	0.0958	0.0002	44.7	93.9	0.0031	63 ± 1

Mean model age = 63 ± 7 Ma. J = 0.00364 ± 0.0000364. $^{39}Ar_K$ — moles of irradiation-produced ^{39}Ar released during laser fusion. $^{40}Ar^*$ (%) — percentage of measured ^{40}Ar derived from natural decay of ^{40}K.

Table 4. Derived Closure Temperatures for K-feldspars

Sample	Increments	ln (D_0/a^2) (s^{-1})	E (kJ/mol)	T_c (K)
614-1	775 - 900 K	13 (2)	180 (10)	490 (60)
614-2	725 - 925 K	4 (1)	107 (7)	370 (40)
616-1	725 - 925 K	3 (3)	90 (20)	340 (120)
620-2	725 - 850 K	15 (2)	180 (10)	470 (40)

Values for kinetic parameters ln (D_0/a^2) and E (where D_0 is the frequency factor, E is the activation energy, and a is the characteristic diffusion dimension) were derived by simple linear regression of kinetic parameters for low-temperature increments (identified in the "Increments" column) as discussed in the text. Closure temperatures (T_c) were calculated from the diffusion data following the methods of Dodson (1973) and assuming a cooling rate of 100 K/My. Numbers in parentheses indicate 2 σ uncertainties based on regression statistics.

FIGURE CAPTIONS

Figure 1 Regional map of Death Valley extensional corridor including features described in text. Box in inset shows location of Figure 1. Dashed box on main figure shows location of Figure 2. Shaded areas indicate outcrop of pre-Tertiary rocks. Heavy lines show major Tertiary faults: strike-slip faults are shown with arrows, and normal faults are unornamented. Map modified from Wernicke et al. (1988).

Figure 2 Simplified tectonic map of the northern Funeral Mountains including sample localities.

Figure 3 Photograph showing relationship of dikes to F_4 folding in lower Monarch Canyon. Sample 614-2 is from pegmatite involved in fold at far right. Sample 614-1 is from granodiorite dike that cuts vertically across fold at left. The dikes intrude amphibolite gneisses of the basal Crystal Spring Formation. View is to the northeast. Area shown is approximately 10 m high by 15 m across.

Figure 4 Geochronologic results for sample 614-2. Concordia diagram for U-Pb analyses of zircons (a). For all concordia diagrams, ellipses show propagated analytical uncertainty at 2 σ level, and numbers along concordia indicate age in Ma. $^{40}Ar/^{39}Ar$ release spectra and inverse isotope correlation diagrams for muscovite furnace analyses (b and c), muscovite laser analyses (d and e), and K-feldspar furnace analyses (f and g). For all isotope correlation diagrams and release spectra, numbers correspond to the sequence of release increments. Filled symbols are those used in regression analyses, the results of which are indicated by solid lines. "Air" represents the $^{36}Ar/^{40}Ar$ ratio of modern air, indicated for reference. The solid line in

frame (f) is the best fit to steps 5-10 (filled symbols), whereas the dashed line is the best fit to steps 12-15 (shaded symbols).

Figure 5 Geochronologic results for sample 614-1. Concordia diagram for U-Pb analyses of zircons (a). $^{40}Ar/^{39}Ar$ inverse isotope correlation diagram for laser fusion analyses of muscovite (b). Release spectra and inverse isotope correlation diagrams for furnace analyses of biotite (c and d) and K-feldspar (e and f).

Figure 6 Geochronologic results for sample 616-1. Concordia diagram for U-Pb analyses of zircons (a). $^{40}Ar/^{39}Ar$ release spectrum and inverse isotope correlation diagram for K-feldspar feldspar analyses (b and c). The solid line in frame (b) is the best fit to steps 3-5 (filled symbols), whereas the dashed line is the best fit to steps 14-19 (shaded symbols).

Figure 7 Geochronologic results for sample 620-2. Concordia diagram for U-Pb analyses of zircons (a). $^{40}Ar/^{39}Ar$ release spectra and inverse isotope correlation diagrams for furnace analyses of muscovite (b and c) and K-feldspar (d and e).

Figure 8 Geochronologic results for sample 628-1. $^{40}Ar/^{39}Ar$ release spectrum and inverse isotope correlation diagram for muscovite laser analyses (a and b).

Figure 9 Geochronologic results for sample 22-1. Concordia diagram for U-Pb analyses of zircons (a). $^{40}Ar/^{39}Ar$ release spectra and inverse isotope correlation diagrams for furnace analyses of muscovite: 22-1A (b and c) and 22-1B (d and e).

Figure 10 Geochronologic results for sample 22-2. Concordia diagram for U-Pb analyses of zircons [z] and rutiles [r] (a). Inset shows enlargement of area

shown by dashed box. $^{40}Ar/^{39}Ar$ release spectrum and inverse isotope correlation diagram for furnace analyses of hornblende (b and c). Dashed lines on isotope correlation diagram indicate curves that correspond to the maximum and minimum ages possible from these data.

Figure 11 Geochronologic results for sample KW13. Concordia diagram for U-Pb analyses of zircons (a). $^{40}Ar/^{39}Ar$ release spectrum and inverse isotope correlation diagram for furnace analyses of hornblende (b and c). Dashed lines on isotope correlation diagram indicate curves that correspond to the maximum and minimum ages possible from these data.

Figure 12 Geochronologic results for sample 628-2. $^{40}Ar/^{39}Ar$ release spectrum and inverse isotope correlation diagram for biotite furnace analyses (a and b).

Figure 13 Geochronologic results for sample 628-3. $^{40}Ar/^{39}Ar$ inverse isotope correlation diagram for muscovite laser fusion analyses.

Figure 14 Geochronologic results for sample CC13. $^{40}Ar/^{39}Ar$ release spectrum and inverse isotope correlation diagram for hornblende furnace analyses (a and b). Dashed lines on isotope correlation diagram indicate curves that correspond to the maximum and minimum ages possible from these data.

Figure 15 Geochronologic results for sample 22-4. $^{40}Ar/^{39}Ar$ release spectrum and inverse isotope correlation diagram for hornblende furnace analyses (a and b).

Figure 16 Geochronologic results for sample CC19. $^{40}Ar/^{39}Ar$ inverse isotope correlation diagram for muscovite laser fusion analyses.

Figure 17 Arrhenius diagrams derived from the incremental heating experiments on K-feldspars from samples 614-1 (a), 614-2 (b), 616-1 (c), and 620-2 (d). Filled circles indicate the steps used in regression analysis, and the solid line represents the best linear fit.

Figure 18 Interpreted time-temperature evolution of rocks in Monarch Canyon beneath the intracore shear zones. Symbols correspond to best estimates of closure age plotted against estimated closure temperature (T_c). T_c's for hornblende, muscovite, rutile, and biotite (800 ± 50 K, 650 ± 50 K, 650 ± 50 K, and 620 ± 50 K) are nominal estimates. T_c's for K-feldspars are estimated from the step-heating experiments (Table 4). Fission-track data for titanite, zircon, and apatite from Holm and Dokka (1991) are also included with nominal closure temperature estimates of 560 ± 50 K, 480 ± 50 K, and 400 ± 50 K, respectively. The dashed lines indicate the range for the lower temperature limit of mylonitization (Hoisch and Simpson, 1993).

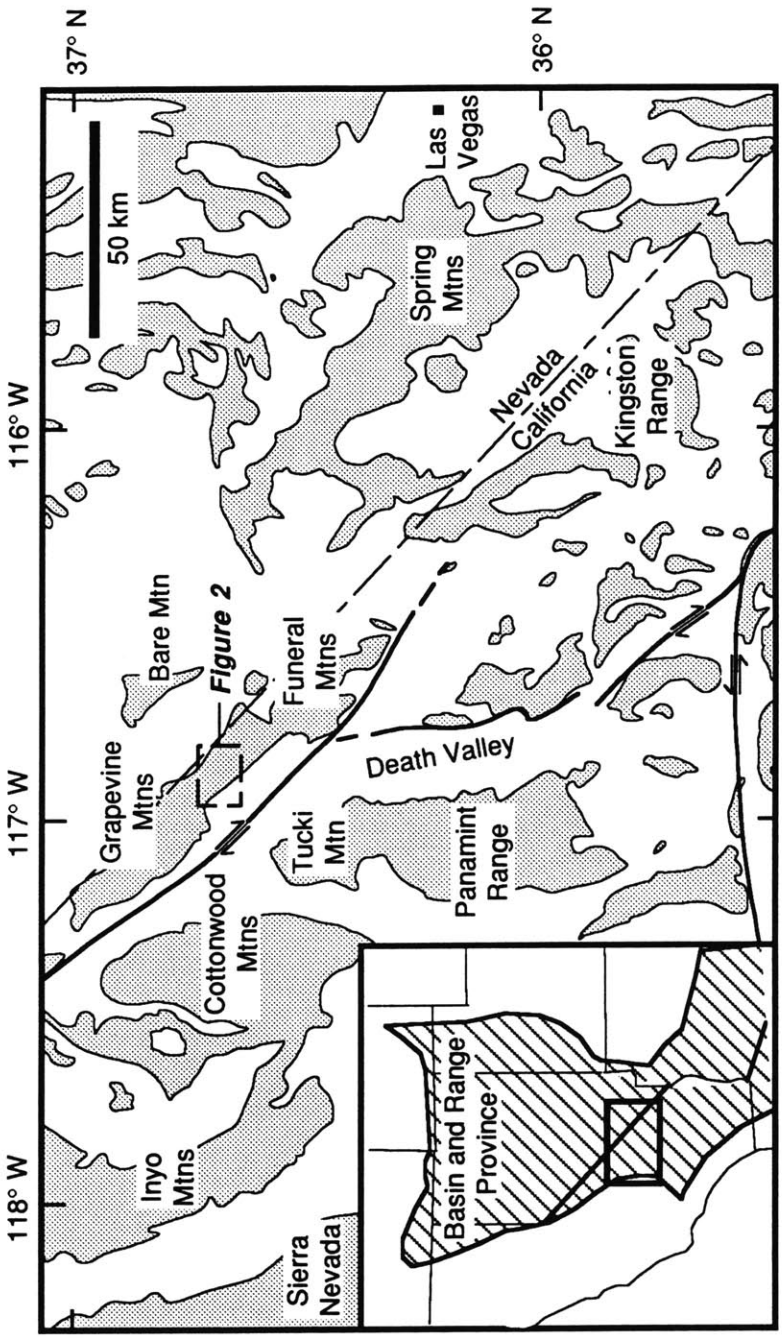
37° N
36° N
118° W
117° W
116° W
50 km
Las Vegas
Spring Mtns
Nevada
California
Kingston Range
Bare Mtn
Figure 2
Funeral Mtns
Grapevine Mtns
Death Valley
Tucki Mtn
Panamint Range
Cottonwood Mtns
Inyo Mtns
Sierra Nevada
Basin and Range Province

Figure 1

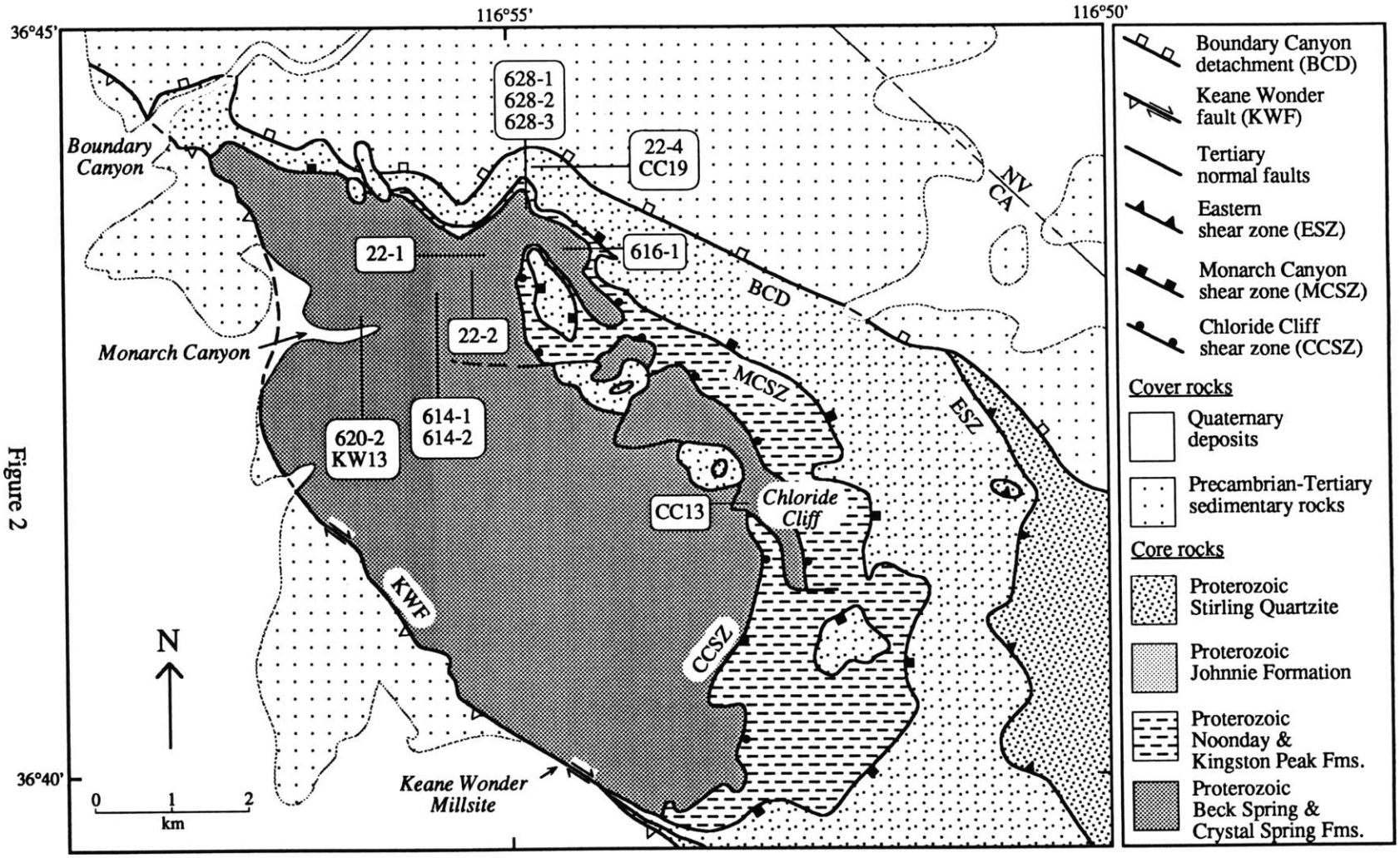
116°55'
116°50'
36°45'
36°40'
628-1
628-2
628-3
22-4
CC19
Boundary
Canyon
NV
CA
22-1
616-1
BCD
22-2
Monarch Canyon
MCSZ
ESZ
620-2
KW13
614-1
614-2
CC13
Chloride
Cliff
KWF
CCSZ
N
0
1
2
km
Keane Wonder
Millsite
Boundary Canyon detachment (BCD)
Keane Wonder fault (KWF)
Tertiary normal faults
Eastern shear zone (ESZ)
Monarch Canyon shear zone (MCSZ)
Chloride Cliff shear zone (CCSZ)
Cover rocks
Quaternary deposits
Precambrian-Tertiary sedimentary rocks
Core rocks
Proterozoic Stirling Quartzite
Proterozoic Johnnie Formation
Proterozoic Noonday & Kingston Peak Fms.
Proterozoic Beck Spring & Crystal Spring Fms.

Figure 2

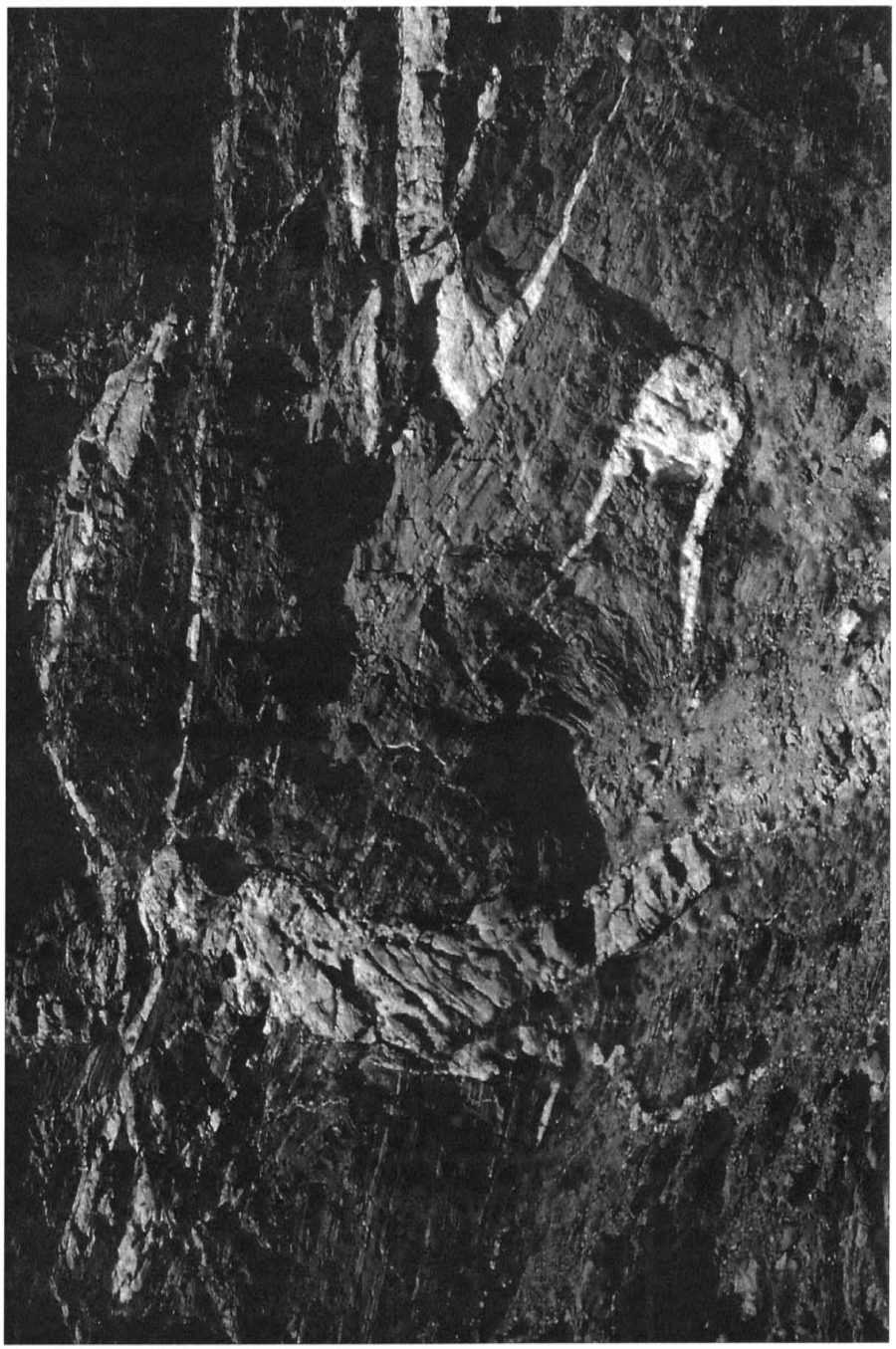

Figure 3

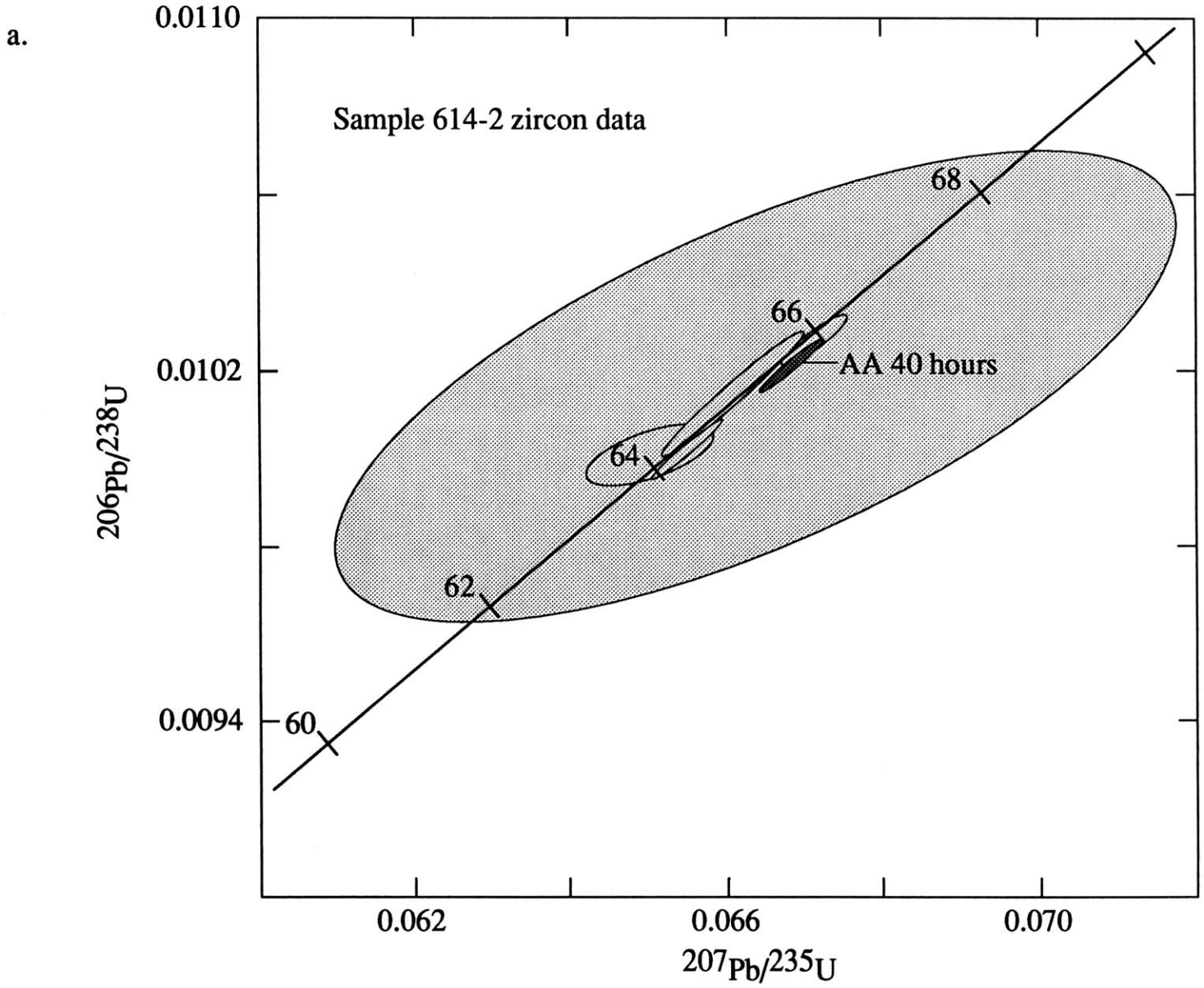
a.
Sample 614-2 zircon data
AA 40 hours
68
66
64
62
60
0.0110
0.0102
0.0094
0.062
0.066
0.070
$^{206}Pb/^{238}U$
$^{207}Pb/^{235}U$

Figure 4

b.

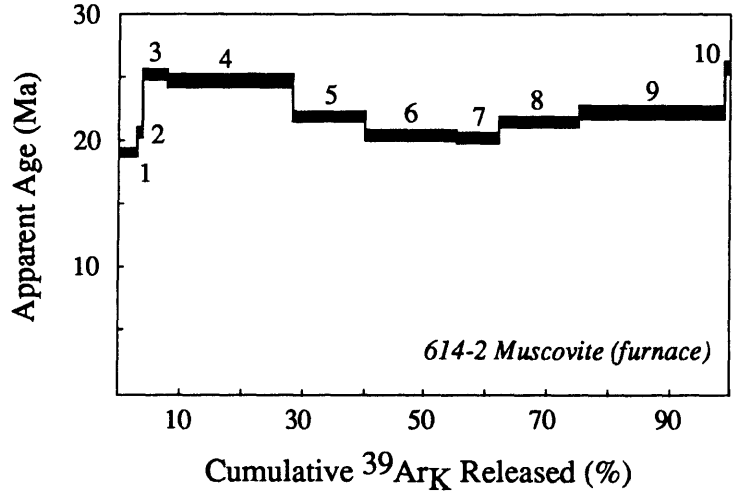
30
20
10
Apparent Age (Ma)
1
2
3
4
5
6
7
8
9
10
614-2 Muscovite (furnace)
10
30
50
70
90
Cumulative $^{39}Ar_K$ Released (%)

c.

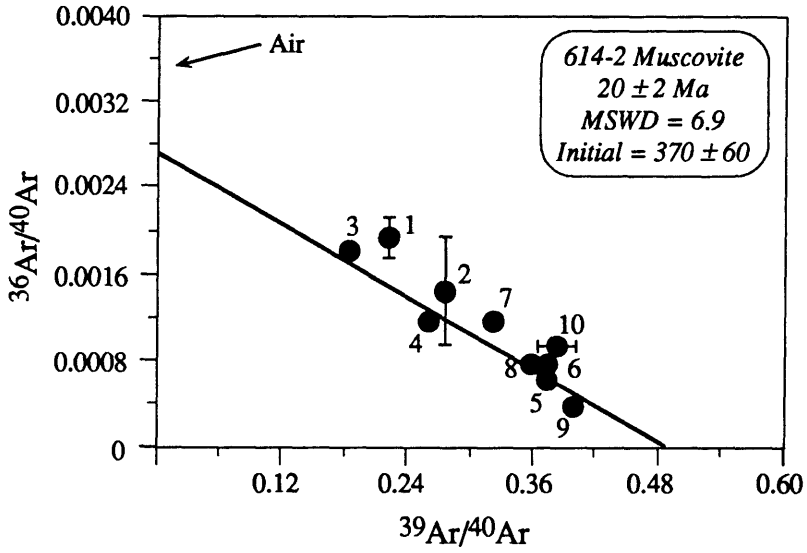
0.0040
0.0032
0.0024
0.0016
0.0008
0
$^{36}Ar/^{40}Ar$
Air
614-2 Muscovite
20 ± 2 Ma
MSWD = 6.9
Initial = 370 ± 60
1
2
3
4
5
6
7
8
9
10
0.12
0.24
0.36
0.48
0.60
$^{39}Ar/^{40}Ar$

Figure 4

d.

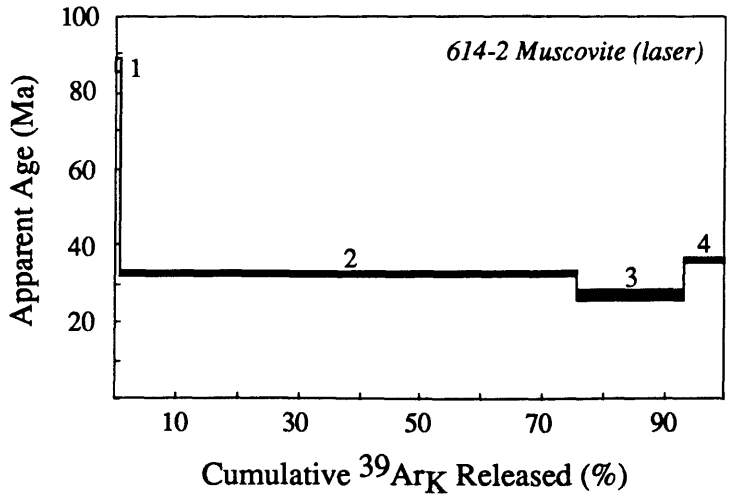
614-2 Muscovite (laser)
Apparent Age (Ma)
100
80
60
40
20
1
2
3
4
10
30
50
70
90
Cumulative $^{39}Ar_K$ Released (%)

e.

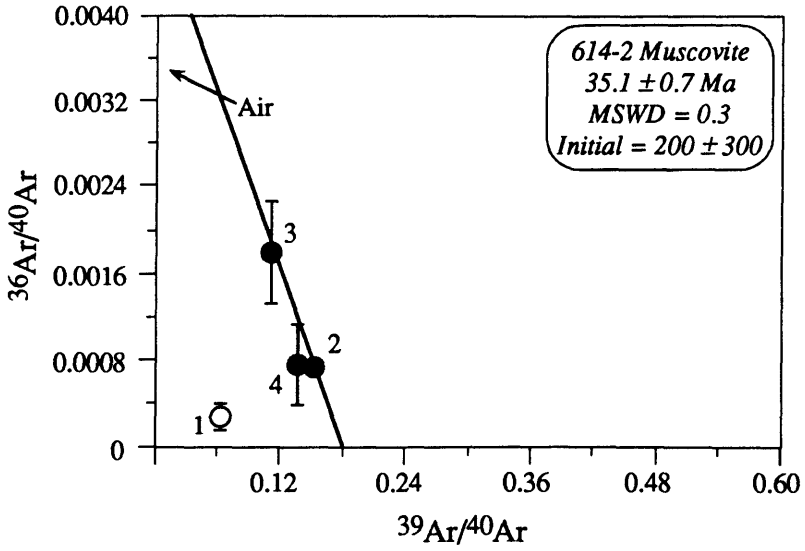
614-2 Muscovite
35.1 ± 0.7 Ma
MSWD = 0.3
Initial = 200 ± 300
Air
$^{36}Ar/^{40}Ar$
0.0040
0.0032
0.0024
0.0016
0.0008
0
1
2
3
4
0.12
0.24
0.36
0.48
0.60
$^{39}Ar/^{40}Ar$

Figure 4

f.

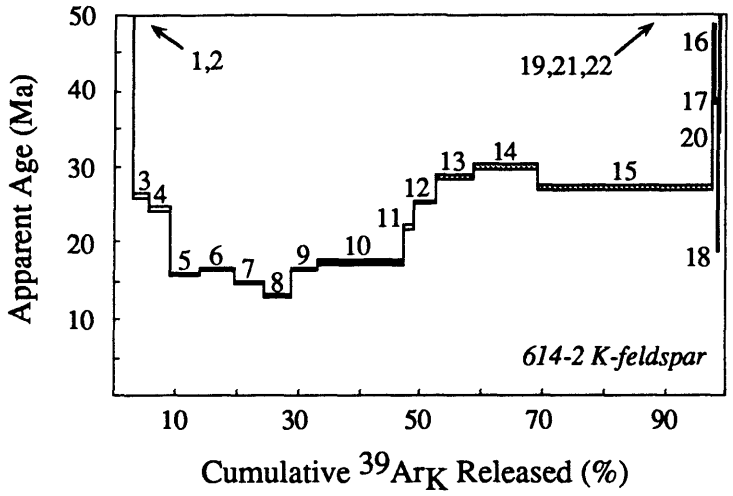
Apparent Age (Ma)
50
40
30
20
10
1,2
19,21,22
16
17
20
18
3
4
5
6
7
8
9
10
11
12
13
14
15
614-2 K-feldspar
10
30
50
70
90
Cumulative $^{39}Ar_K$ Released (%)

g.

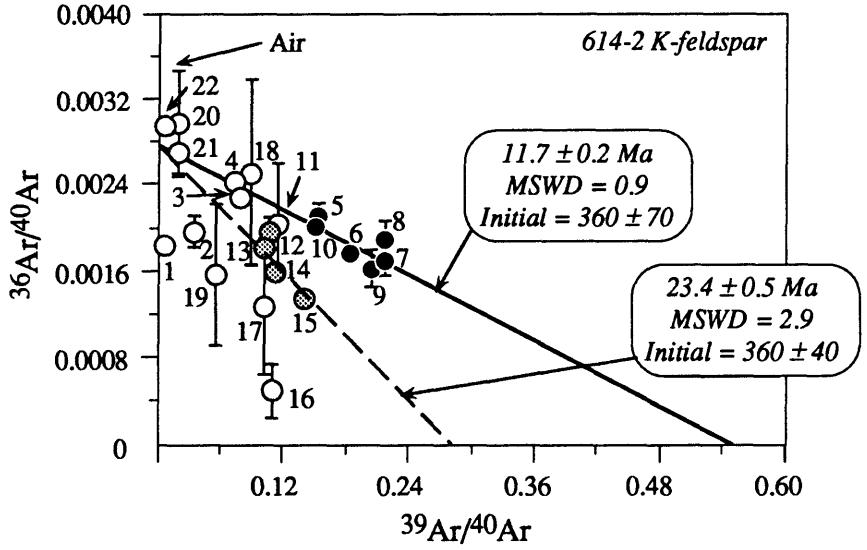
0.0040
0.0032
0.0024
0.0016
0.0008
0
$^{36}Ar/^{40}Ar$
Air
614-2 K-feldspar
11.7 ± 0.2 Ma
MSWD = 0.9
Initial = 360 ± 70
23.4 ± 0.5 Ma
MSWD = 2.9
Initial = 360 ± 40
0.12
0.24
0.36
0.48
0.60
$^{39}Ar/^{40}Ar$

Figure 4

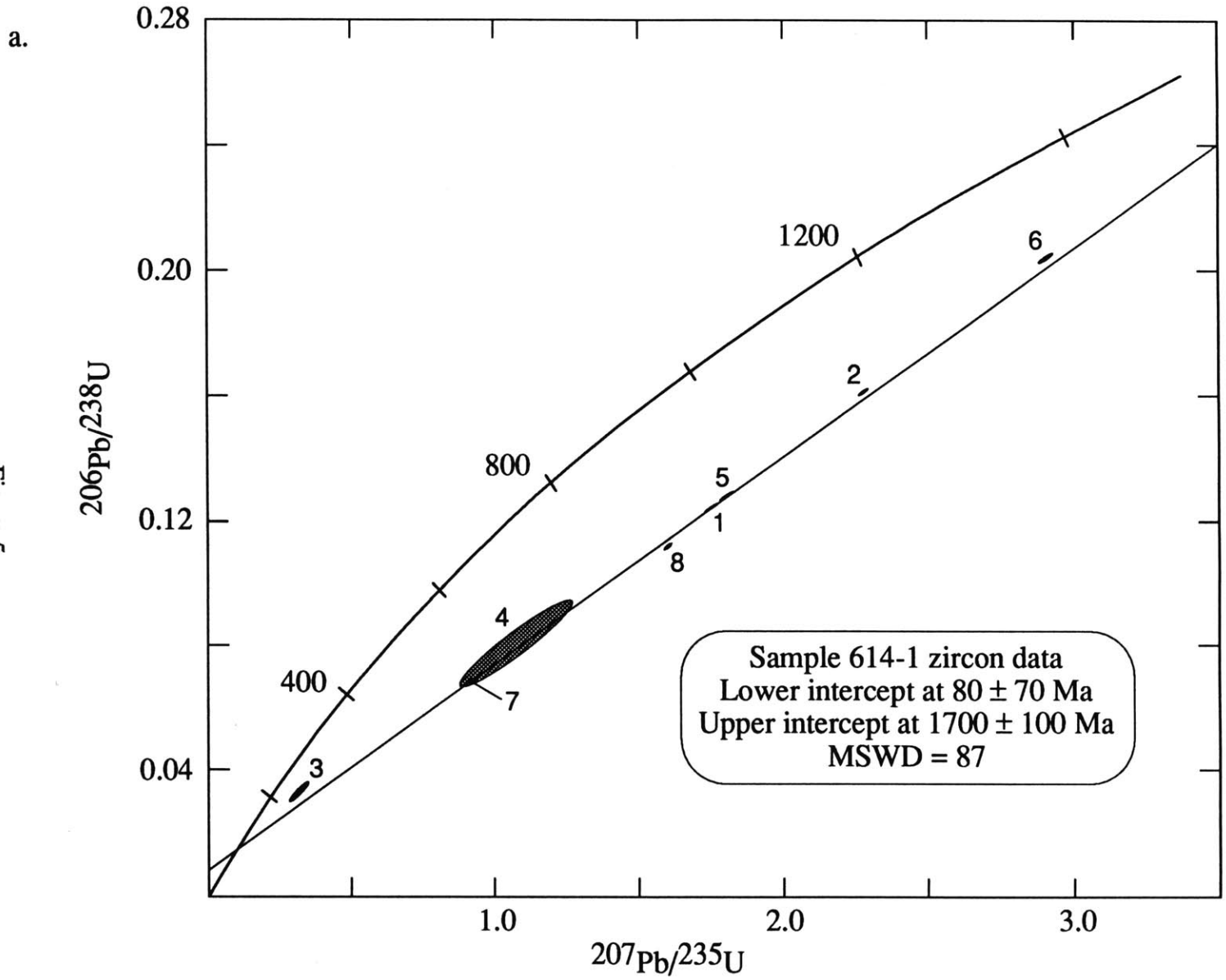
a.
0.28
0.20
0.12
0.04
206Pb/238U
1200
800
400
6
2
5
1
8
4
7
3
Sample 614-1 zircon data
Lower intercept at 80 ± 70 Ma
Upper intercept at 1700 ± 100 Ma
MSWD = 87
1.0
2.0
3.0
207Pb/235U

Figure 5

b.

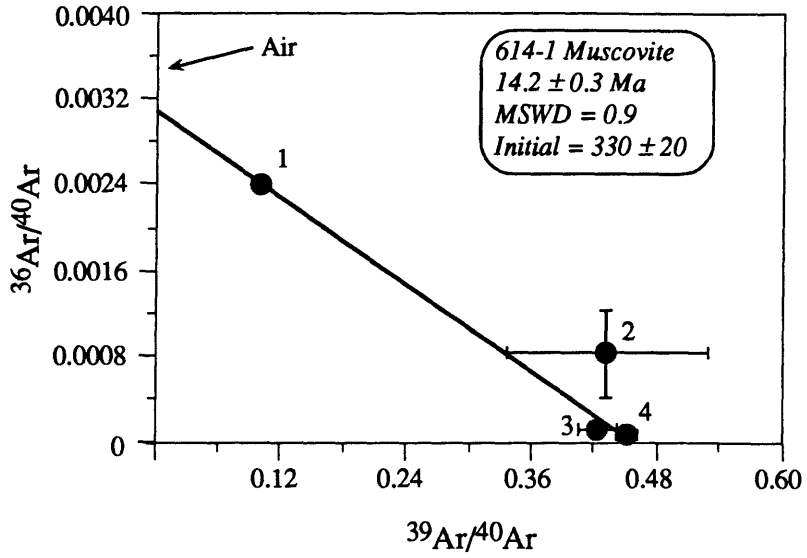
0.0040
0.0032
0.0024
0.0016
0.0008
0
Air
614-1 Muscovite
14.2 ± 0.3 Ma
MSWD = 0.9
Initial = 330 ± 20
1
2
3
4
0.12
0.24
0.36
0.48
0.60
36Ar/40Ar
39Ar/40Ar

Figure 5

c.

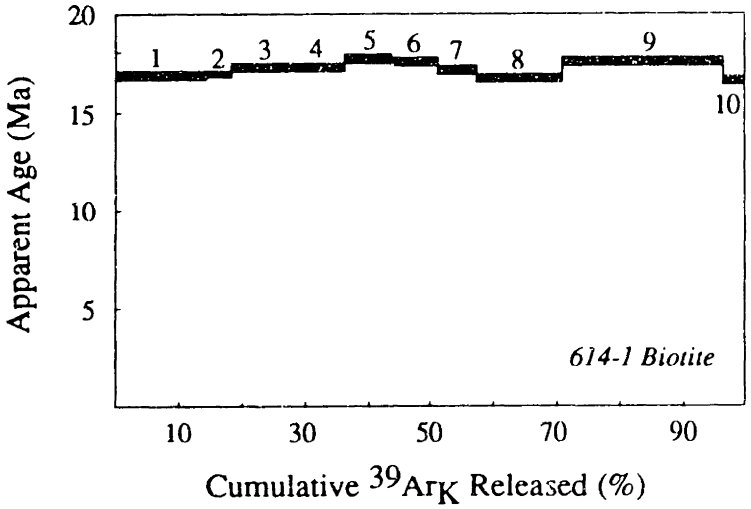
20
15
10
5
Apparent Age (Ma)
1
2
3
4
5
6
7
8
9
10
614-1 Biotite
10
30
50
70
90
Cumulative $^{39}Ar_K$ Released (%)

d.

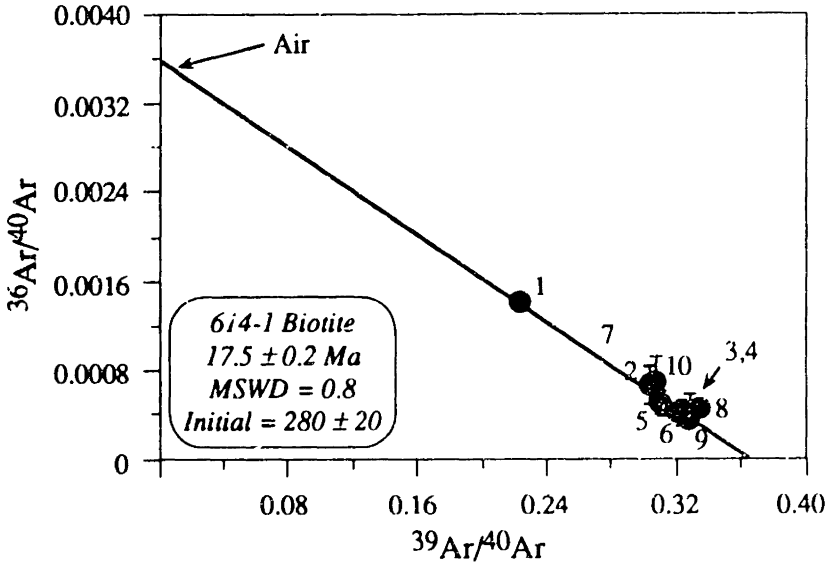
0.0040
0.0032
0.0024
0.0016
0.0008
0
$^{36}Ar/^{40}Ar$
Air
614-1 Biotite
17.5 ± 0.2 Ma
MSWD = 0.8
Initial = 280 ± 20
1
7
2
10
3,4
5
6
8
9
0.08
0.16
0.24
0.32
0.40
$^{39}Ar/^{40}Ar$

Figure 5

e.

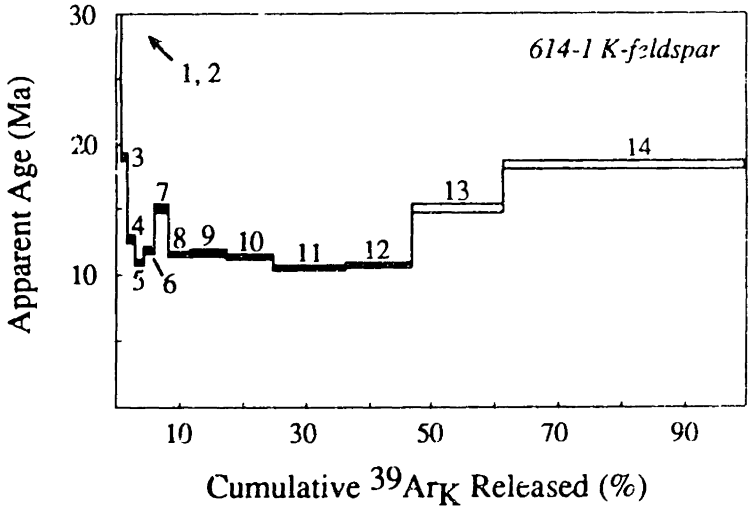
614-1 K-feldspar
Apparent Age (Ma)
30
20
10
1, 2
3
4
5
6
7
8
9
10
11
12
13
14
10
30
50
70
90
Cumulative $^{39}Ar_K$ Released (%)

f.

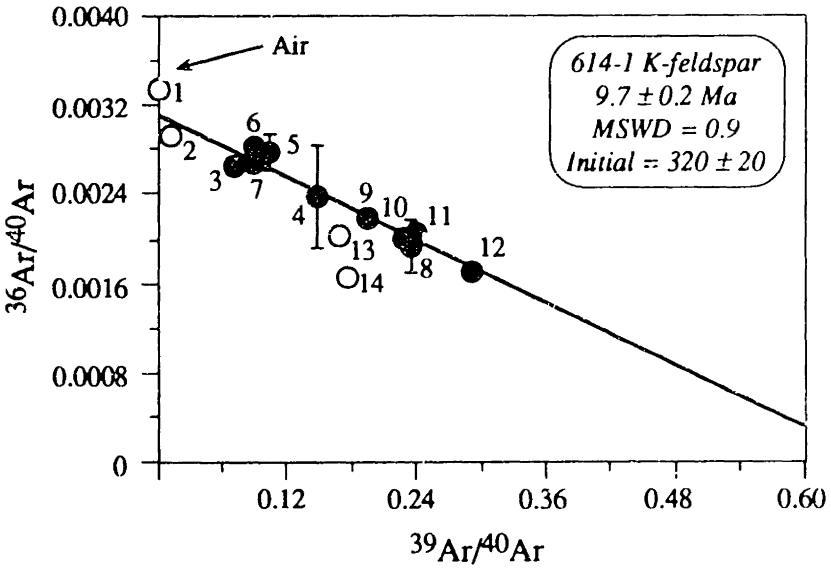
0.0040
0.0032
0.0024
0.0016
0.0008
0
Air
614-1 K-feldspar
9.7 ± 0.2 Ma
MSWD = 0.9
Initial = 320 ± 20
1
2
3
4
5
6
7
8
9
10
11
12
13
14
0.12
0.24
0.36
0.48
0.60
$^{36}Ar/^{40}Ar$
$^{39}Ar/^{40}Ar$

Figure 5

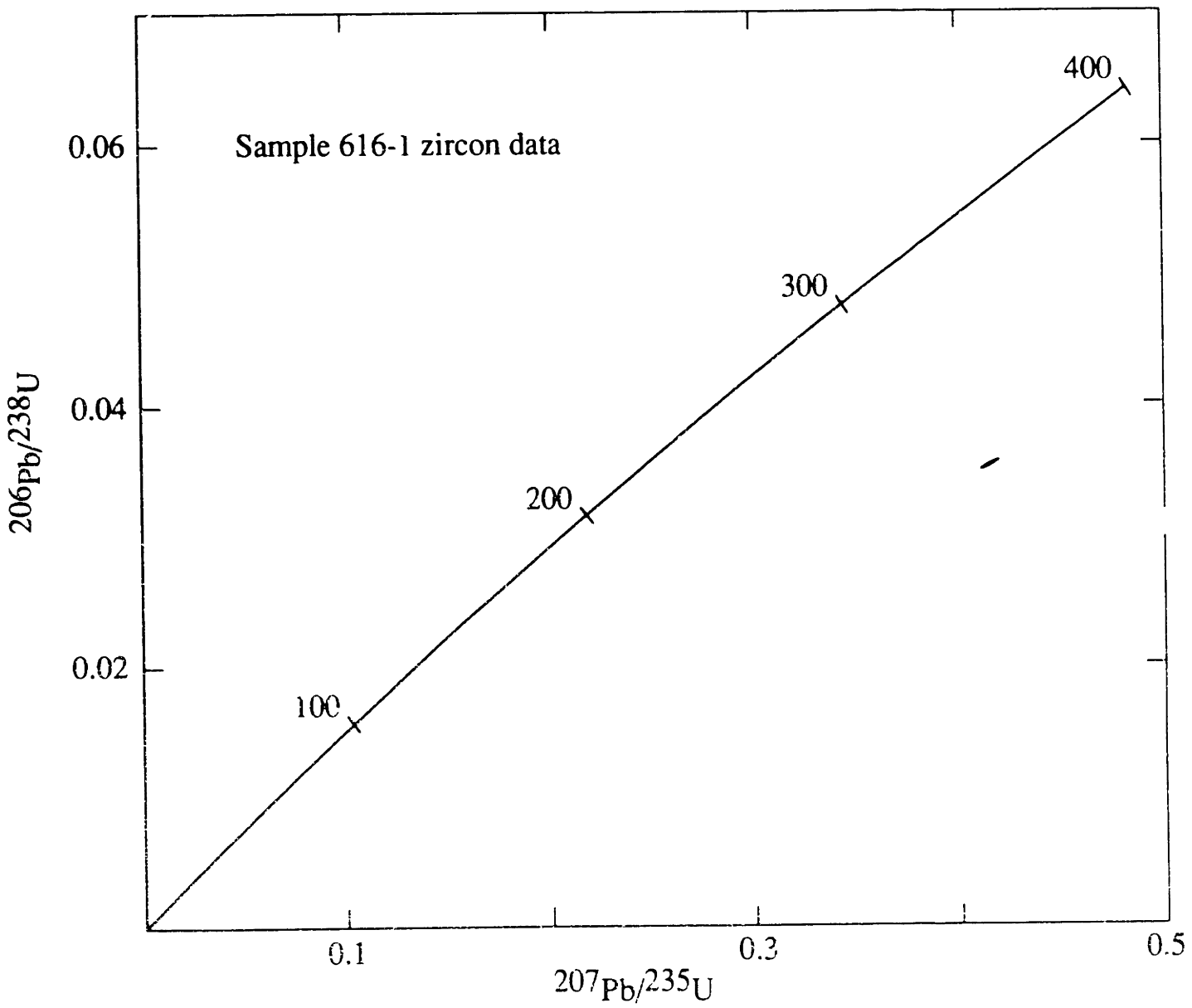
a.
Sample 616-1 zircon data
400
300
200
100
0.06
0.04
0.02
0.1
0.3
0.5
$^{206}Pb/^{238}U$
$^{207}Pb/^{235}U$

Figure 6

b.

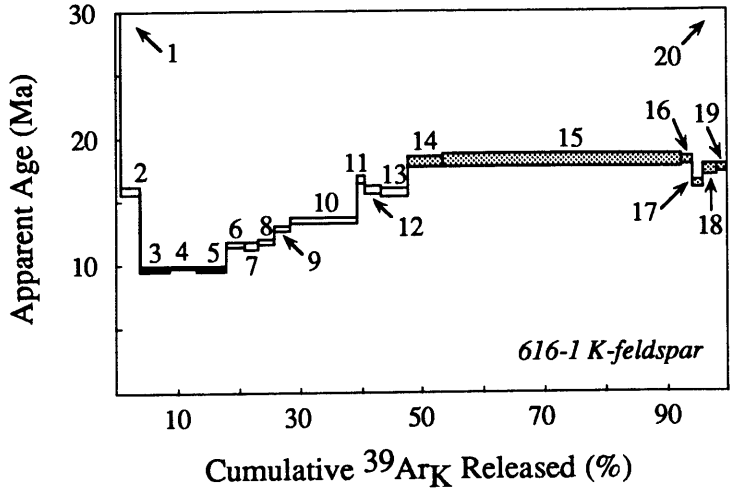
Apparent Age (Ma)
30
20
10
1
2
3 4 5
6 8
7
9
10
11
13
12
14
15
16
19
17
18
20
616-1 K-feldspar
10
30
50
70
90
Cumulative $^{39}Ar_K$ Released (%)

c.

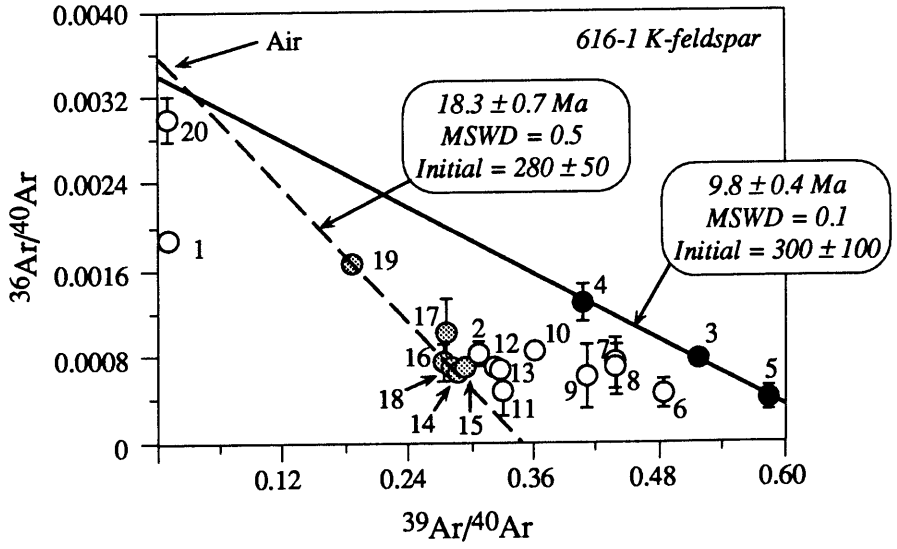
0.0040
0.0032
0.0024
0.0016
0.0008
0
$^{36}Ar/^{40}Ar$
Air
616-1 K-feldspar
18.3 ± 0.7 Ma
MSWD = 0.5
Initial = 280 ± 50
9.8 ± 0.4 Ma
MSWD = 0.1
Initial = 300 ± 100
0.12
0.24
0.36
0.48
0.60
$^{39}Ar/^{40}Ar$

Figure 6

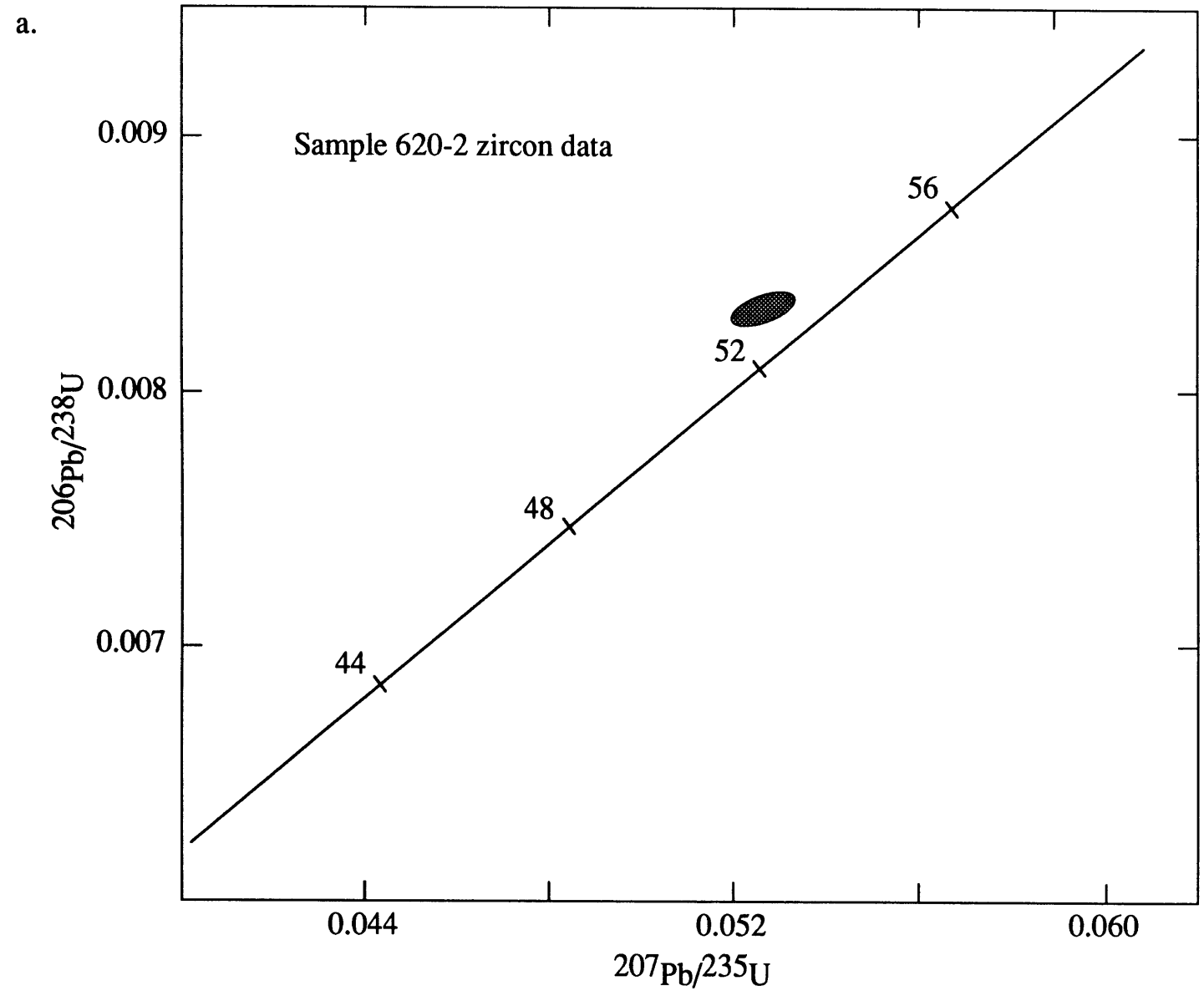
a.
Sample 620-2 zircon data
0.009
0.008
0.007
206Pb/238U
56
52
48
44
0.044
0.052
0.060
207Pb/235U

Figure 7

b.

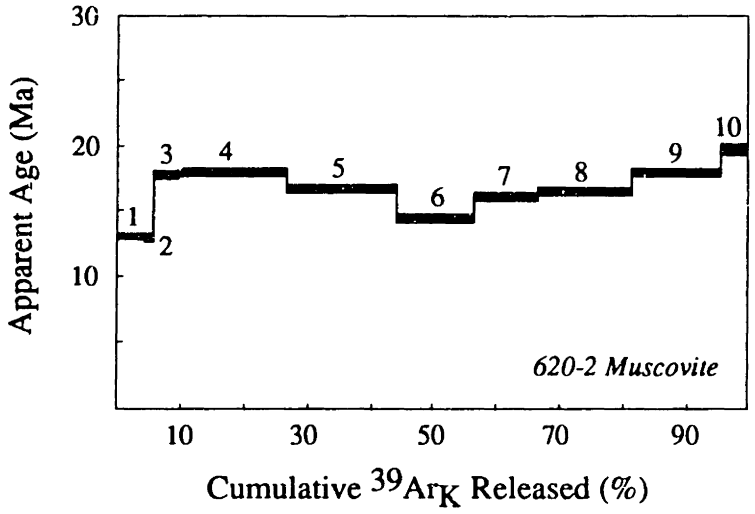
30
20
10
Apparent Age (Ma)
1
2
3
4
5
6
7
8
9
10
620-2 Muscovite
10
30
50
70
90
Cumulative $^{39}Ar_K$ Released (%)

c.

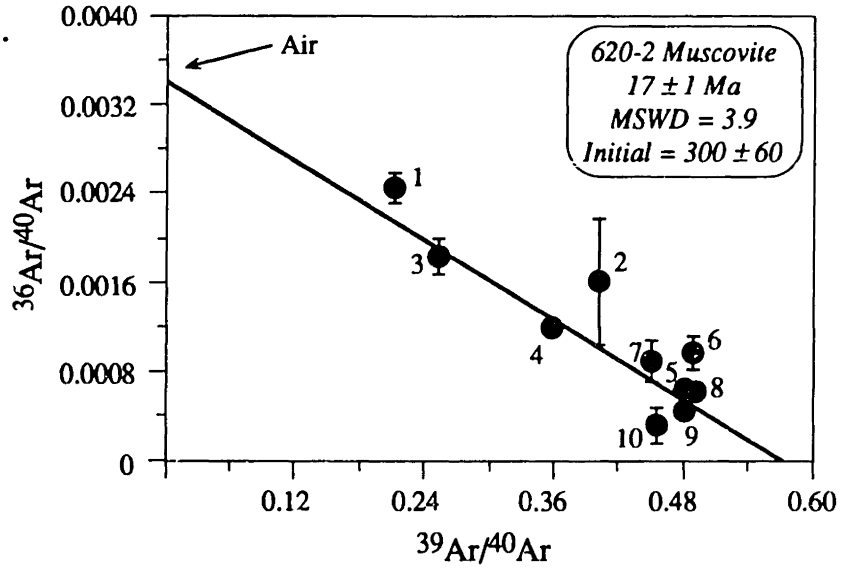
0.0040
0.0032
0.0024
0.0016
0.0008
0
$^{36}Ar/^{40}Ar$
Air
620-2 Muscovite
17 ± 1 Ma
MSWD = 3.9
Initial = 300 ± 60
1
2
3
4
5
6
7
8
9
10
0.12
0.24
0.36
0.48
0.60
$^{39}Ar/^{40}Ar$

Figure 7

d.

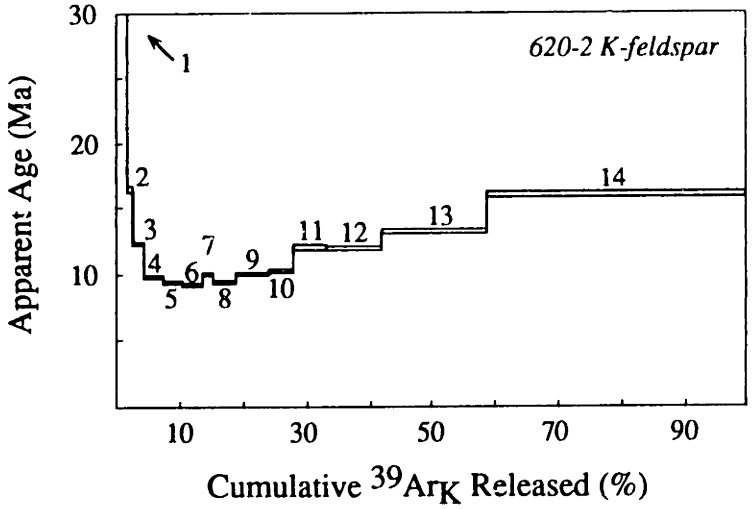
620-2 K-feldspar
Apparent Age (Ma)
30
20
10
10
30
50
70
90
Cumulative $^{39}Ar_K$ Released (%)

e.

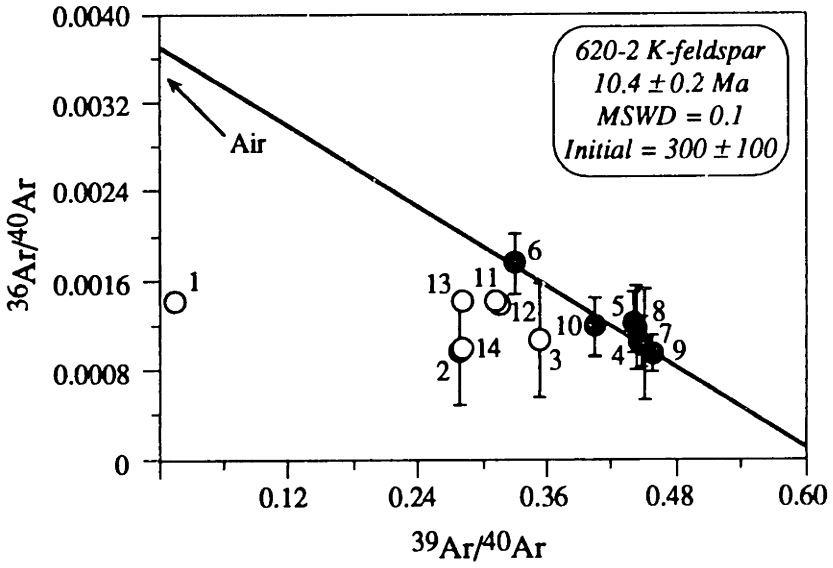
620-2 K-feldspar
10.4 ± 0.2 Ma
MSWD = 0.1
Initial = 300 ± 100
Air
$^{36}Ar/^{40}Ar$
0.0040
0.0032
0.0024
0.0016
0.0008
0
0.12
0.24
0.36
0.48
0.60
$^{39}Ar/^{40}Ar$

Figure 7

a.

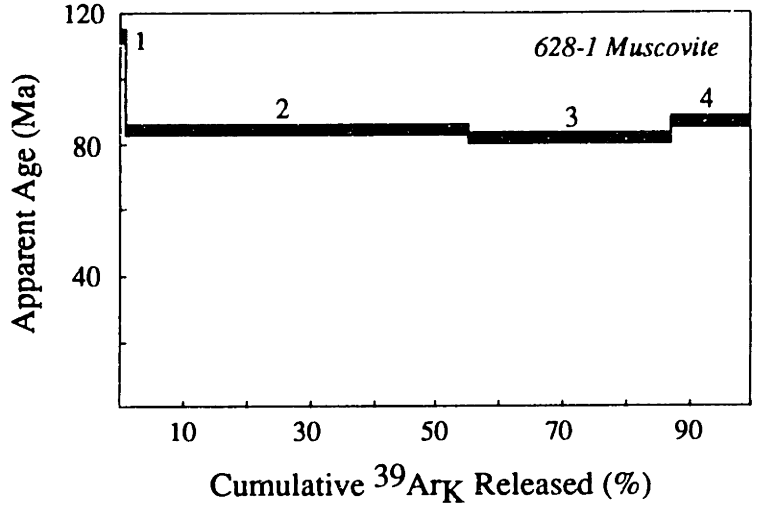
120
80
40
Apparent Age (Ma)
628-1 Muscovite
1
2
3
4
10
30
50
70
90
Cumulative $^{39}Ar_K$ Released (%)

b.

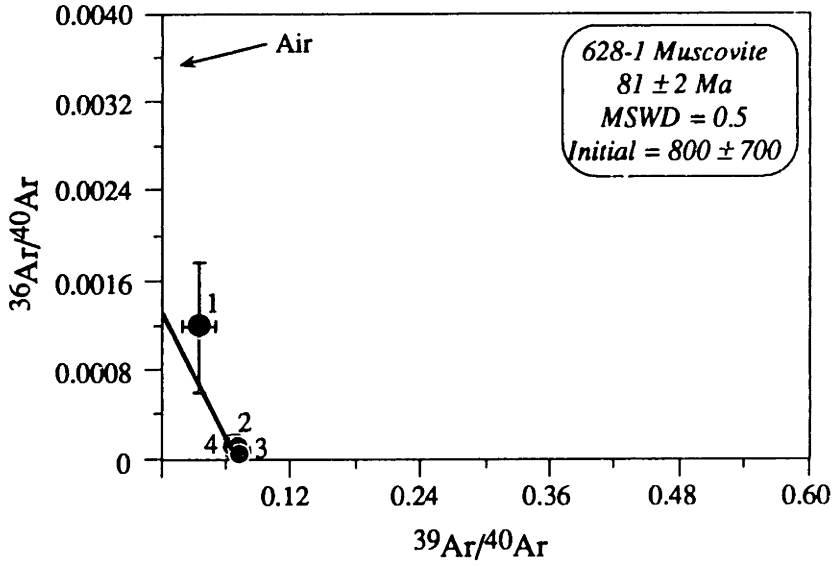
0.0040
0.0032
0.0024
0.0016
0.0008
0
$^{36}Ar/^{40}Ar$
Air
628-1 Muscovite
81 ± 2 Ma
MSWD = 0.5
Initial = 800 ± 700
1
2
3
4
0.12
0.24
0.36
0.48
0.60
$^{39}Ar/^{40}Ar$

Figure 8

a.

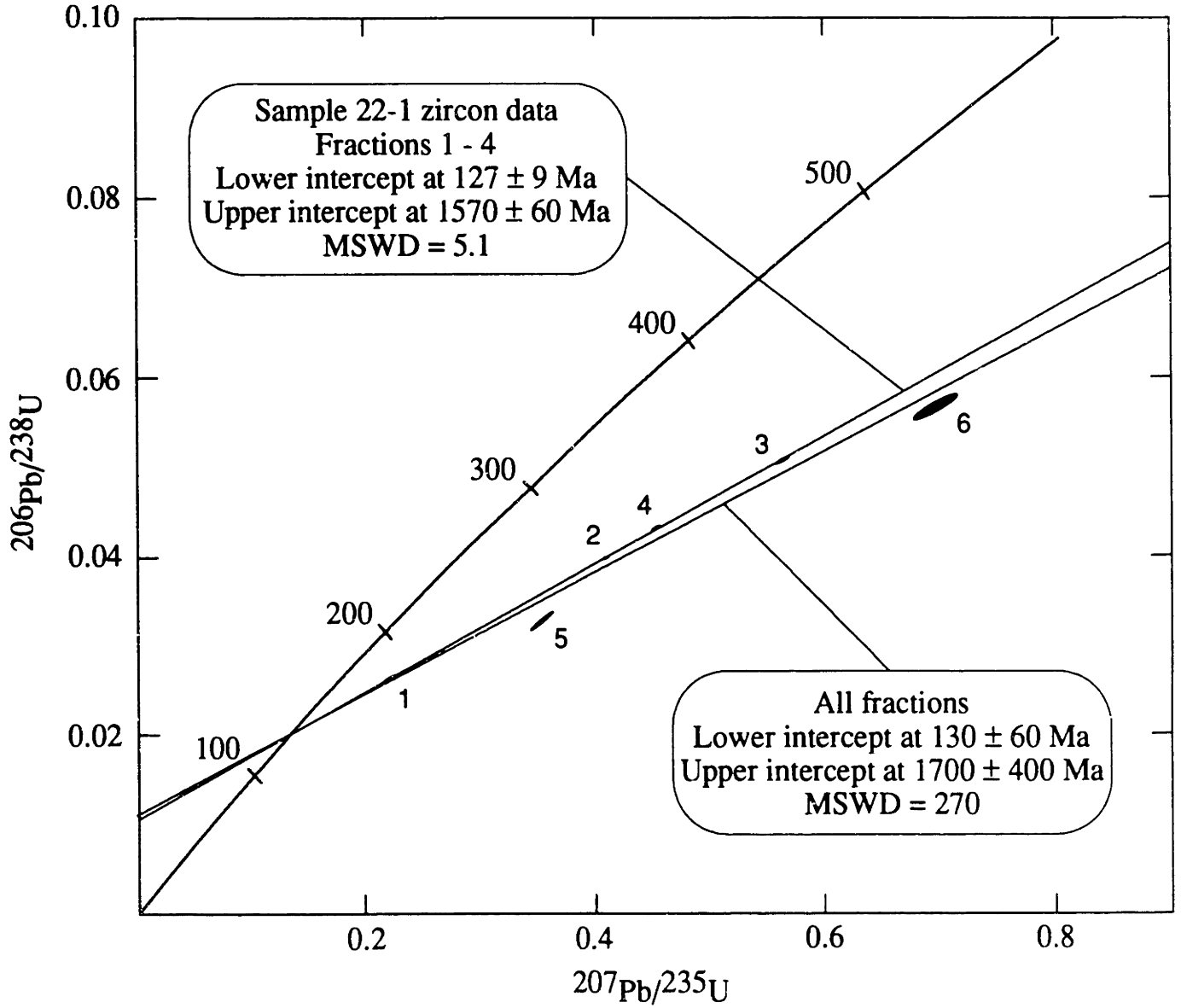
Sample 22-1 zircon data
Fractions 1 - 4
Lower intercept at 127 ± 9 Ma
Upper intercept at 1570 ± 60 Ma
MSWD = 5.1
All fractions
Lower intercept at 130 ± 60 Ma
Upper intercept at 1700 ± 400 Ma
MSWD = 270
100
200
300
400
500
1
2
3
4
5
6
0.10
0.08
0.06
0.04
0.02
0.2
0.4
0.6
0.8
206Pb/238U
207Pb/235U

Figure 9

b.

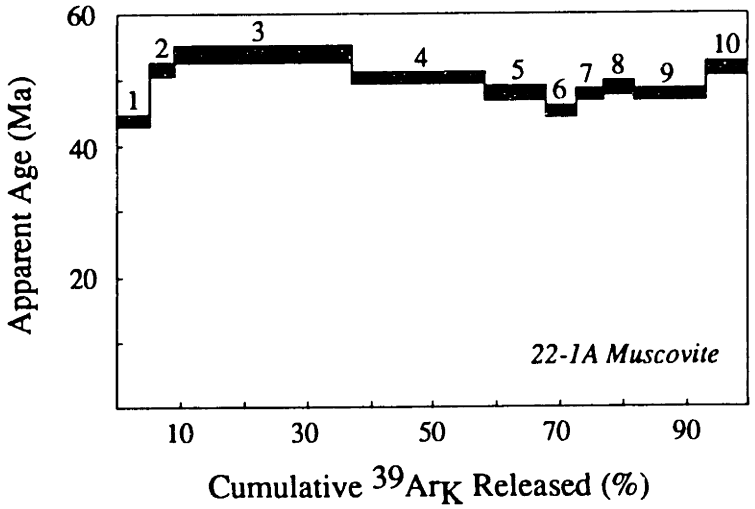
60
40
20
Apparent Age (Ma)
1
2
3
4
5
6
7
8
9
10
22-1A Muscovite
10
30
50
70
90
Cumulative $^{39}Ar_K$ Released (%)

c.

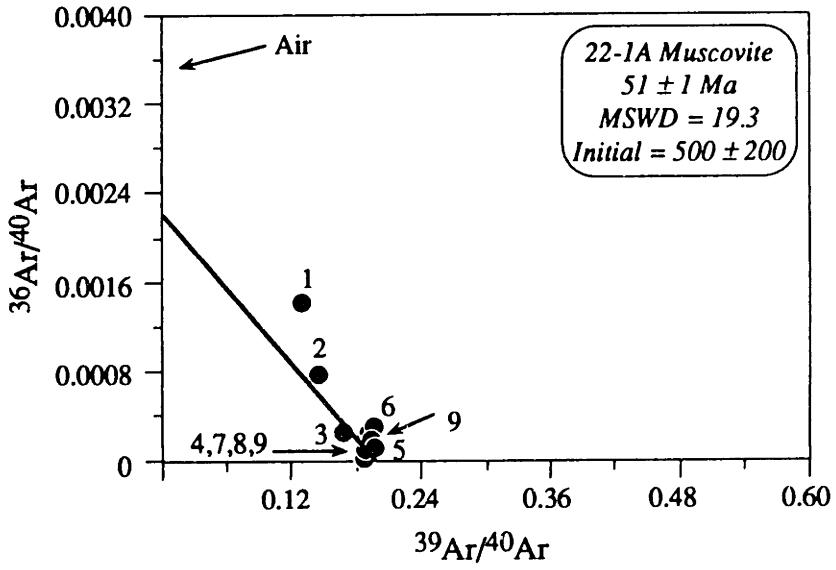
0.0040
0.0032
0.0024
0.0016
0.0008
0
$^{36}Ar/^{40}Ar$
Air
22-1A Muscovite
51 ± 1 Ma
MSWD = 19.3
Initial = 500 ± 200
1
2
3
4,7,8,9
5
6
9
0.12
0.24
0.36
0.48
0.60
$^{39}Ar/^{40}Ar$

Figure 9

d.

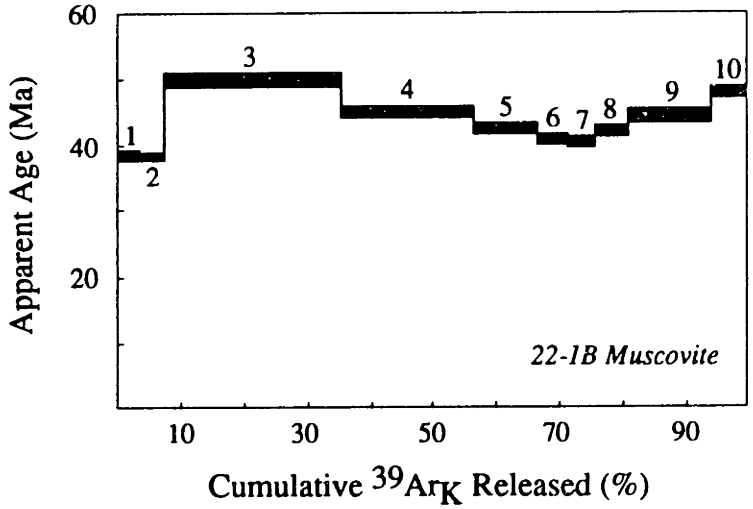
60
40
20
Apparent Age (Ma)
1
2
3
4
5
6
7
8
9
10
22-1B Muscovite
10
30
50
70
90
Cumulative $^{39}Ar_K$ Released (%)

e.

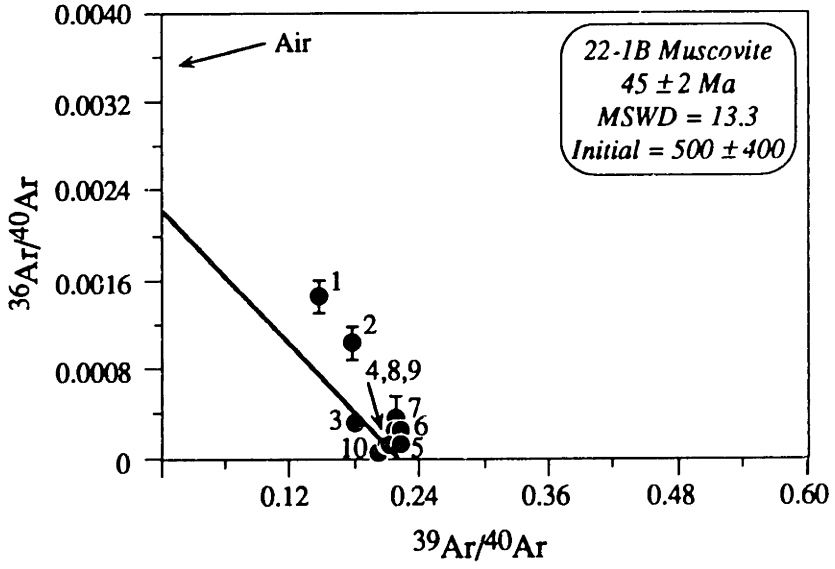
0.0040
0.0032
0.0024
0.0016
0.0008
0
$^{36}Ar/^{40}Ar$
Air
22-1B Muscovite
45 ± 2 Ma
MSWD = 13.3
Initial = 500 ± 400
1
2
4,8,9
3
7
6
10
5
0.12
0.24
0.36
0.48
0.60
$^{39}Ar/^{40}Ar$

Figure 9

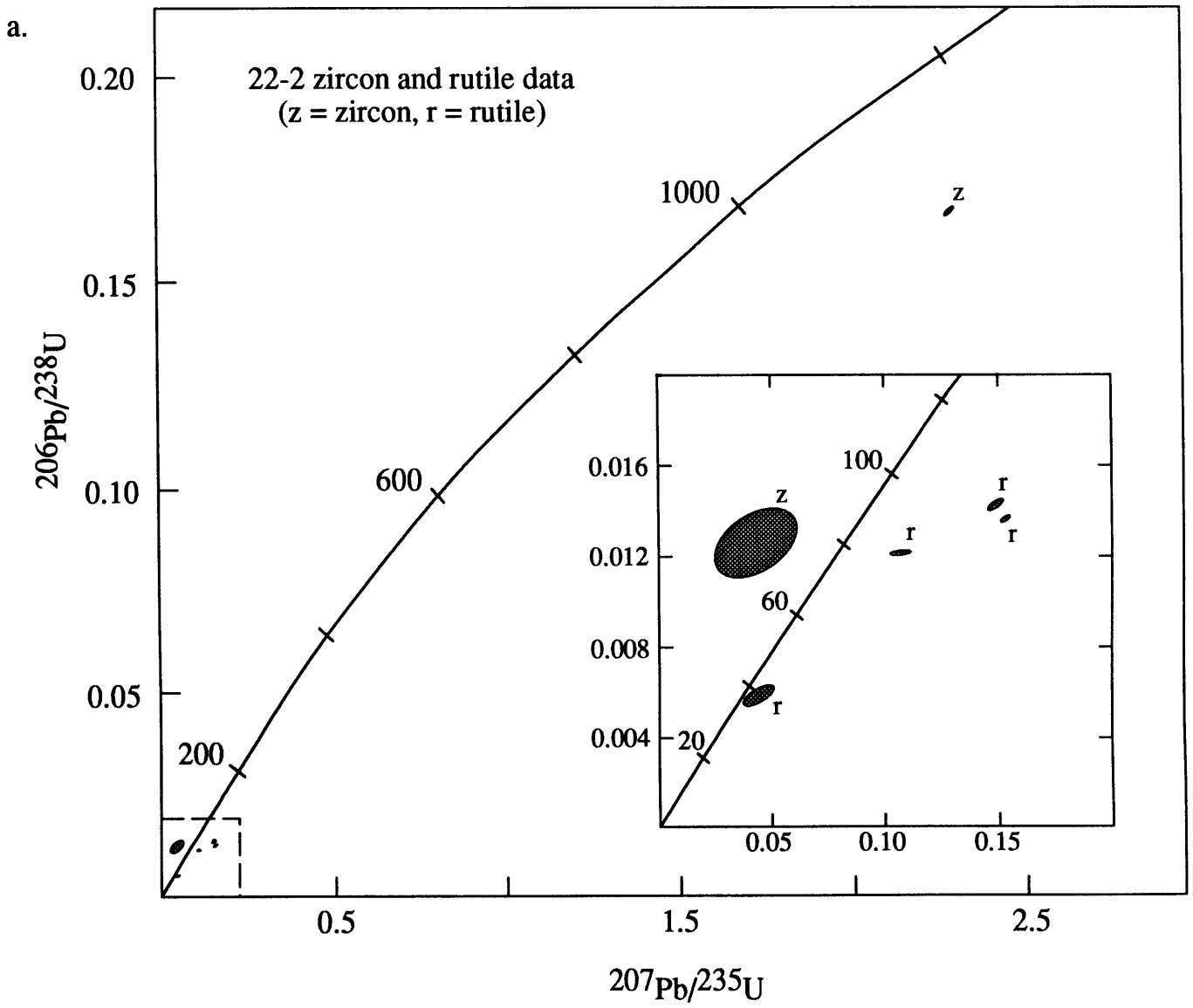
a.
22-2 zircon and rutile data
(z = zircon, r = rutile)
0.20
0.15
0.10
0.05
1000
600
200
z
0.016
0.012
0.008
0.004
100
60
20
r
0.05
0.10
0.15
0.5
1.5
2.5
$^{206}Pb/^{238}U$
$^{207}Pb/^{235}U$

Figure 10

b.

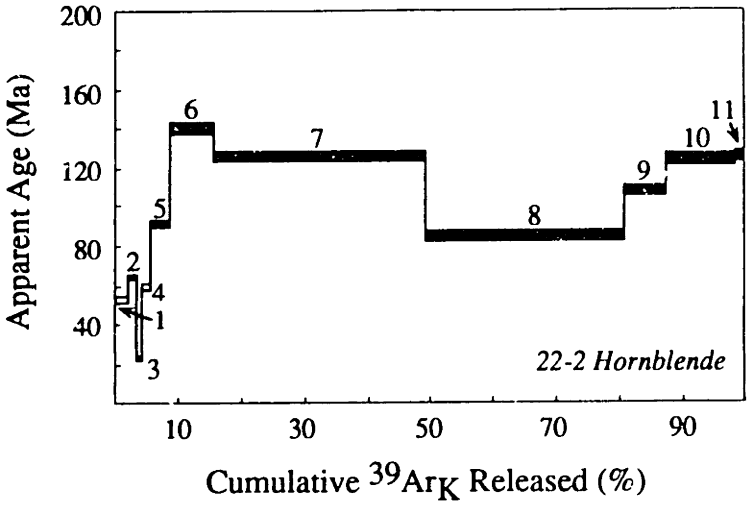
Apparent Age (Ma)
200
160
120
80
40
10
30
50
70
90
Cumulative $^{39}Ar_K$ Released (%)
22-2 Hornblende
1
2
3
4
5
6
7
8
9
10
11

c.

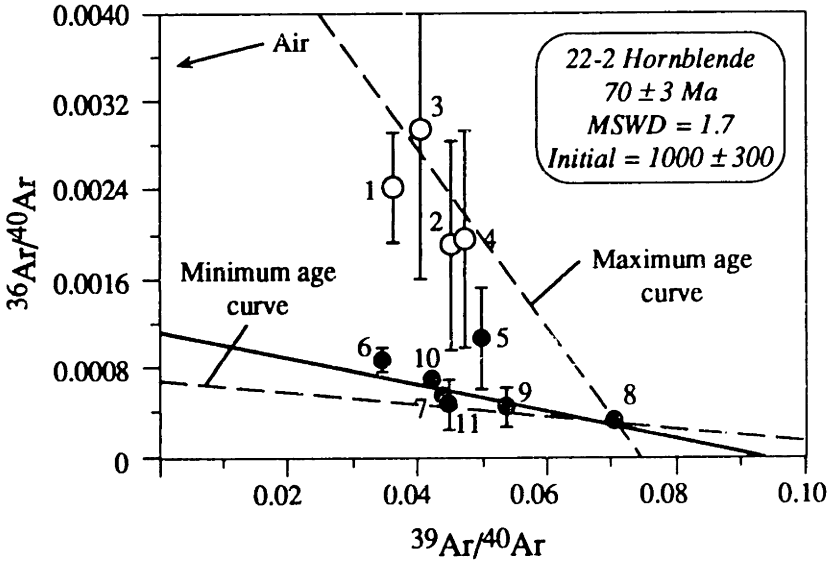
$^{36}Ar/^{40}Ar$
0.0040
0.0032
0.0024
0.0016
0.0008
0
0.02
0.04
0.06
0.08
0.10
$^{39}Ar/^{40}Ar$
Air
22-2 Hornblende
70 ± 3 Ma
MSWD = 1.7
Initial = 1000 ± 300
Minimum age curve
Maximum age curve
1
2
3
4
5
6
7
8
9
10
11

Figure 10

a.

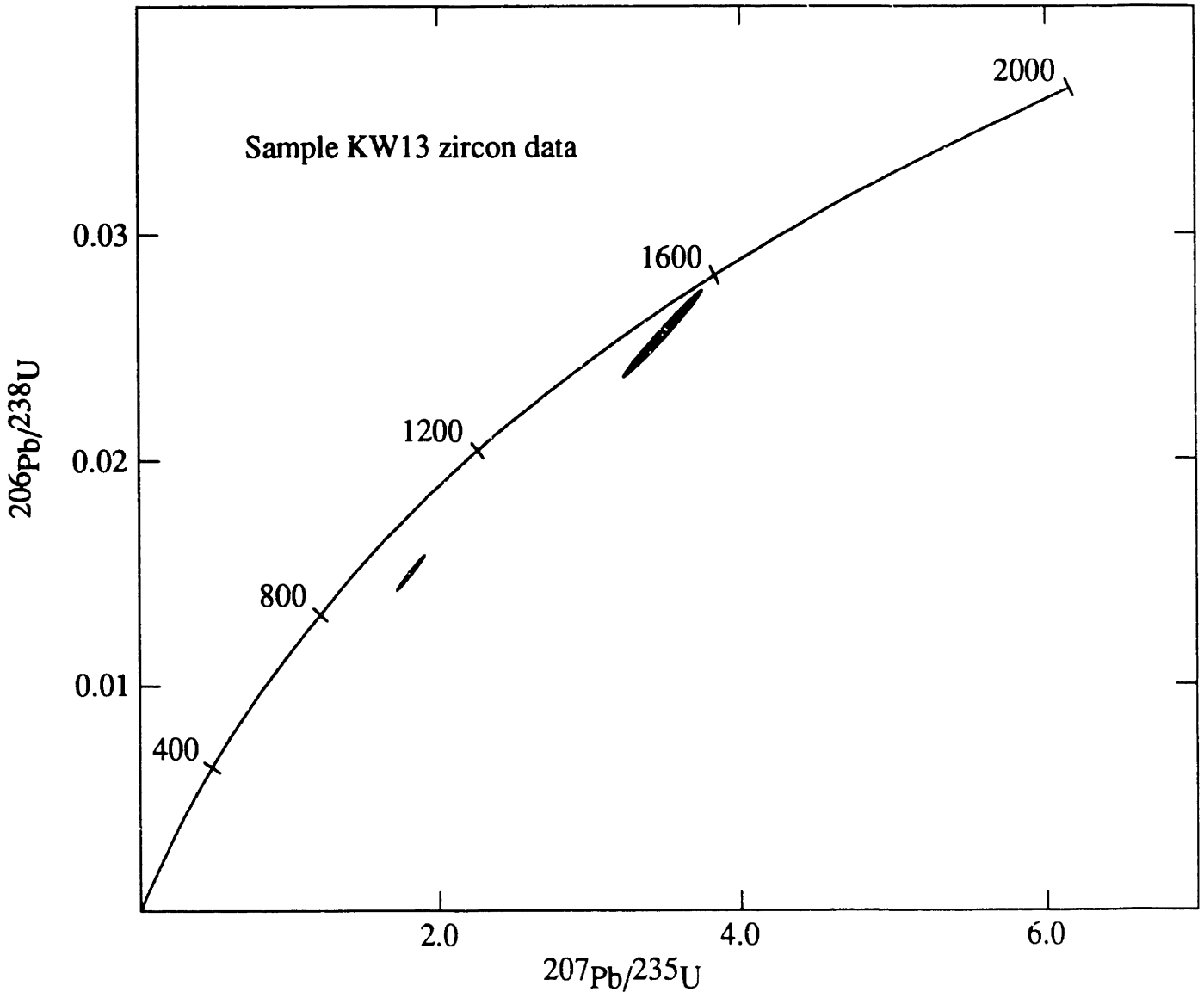
Sample KW13 zircon data
2000
1600
1200
800
400
0.03
0.02
0.01
206Pb/238U
2.0
4.0
6.0
207Pb/235U

b.

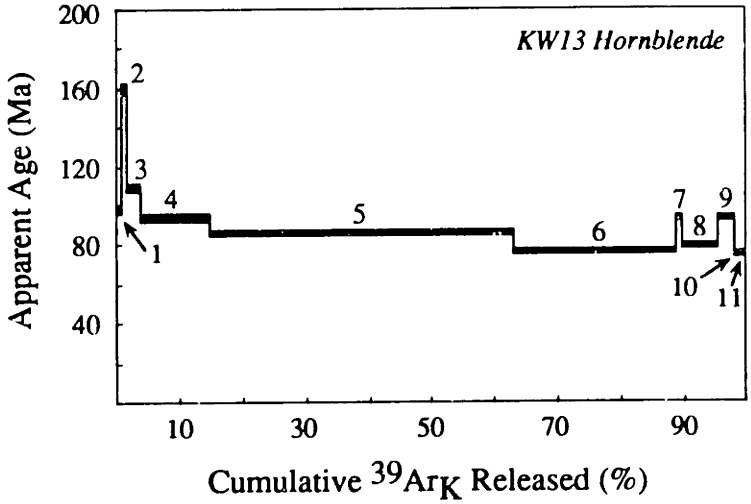
KW13 Hornblende
Apparent Age (Ma)
200
160
120
80
40
1
2
3
4
5
6
7
8
9
10
11
10
30
50
70
90
Cumulative $^{39}Ar_K$ Released (%)

c.

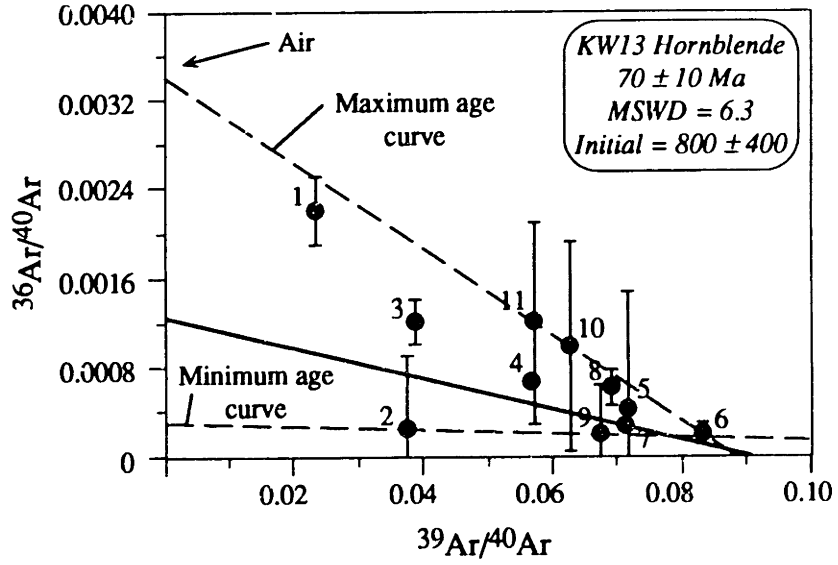
KW13 Hornblende
70 ± 10 Ma
MSWD = 6.3
Initial = 800 ± 400
Air
Maximum age curve
Minimum age curve
$^{36}Ar/^{40}Ar$
0.0040
0.0032
0.0024
0.0016
0.0008
0
0.02
0.04
0.06
0.08
0.10
$^{39}Ar/^{40}Ar$

Figure 11

a.

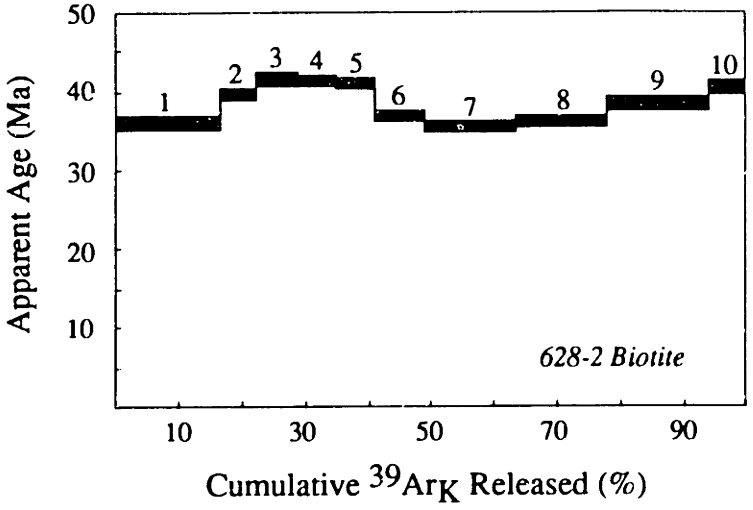
Apparent Age (Ma)
50
40
30
20
10
1
2
3
4
5
6
7
8
9
10
628-2 Biotite
10
30
50
70
90
Cumulative $^{39}Ar_K$ Released (%)

b.

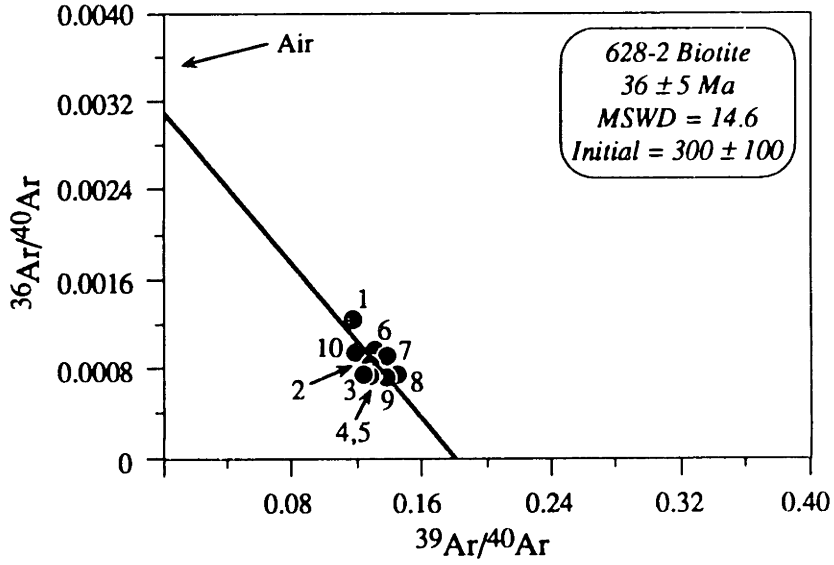
0.0040
0.0032
0.0024
0.0016
0.0008
0
Air
628-2 Biotite
36 ± 5 Ma
MSWD = 14.6
Initial = 300 ± 100
1
6
10
7
2
3
8
9
4,5
0.08
0.16
0.24
0.32
0.40
$^{36}Ar/^{40}Ar$
$^{39}Ar/^{40}Ar$

Figure 12

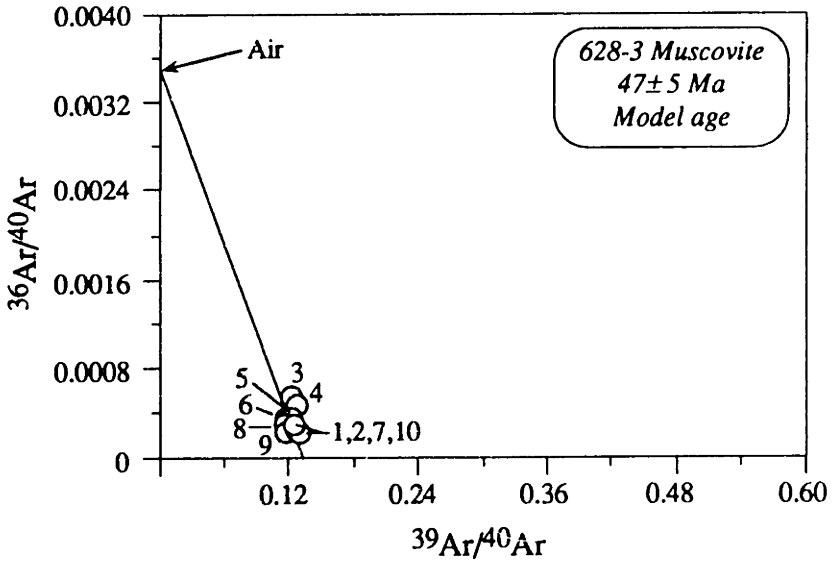
0.0040
0.0032
0.0024
0.0016
0.0008
0
36Ar/40Ar
Air
628-3 Muscovite
47± 5 Ma
Model age
5
3
4
6
8
9
1,2,7,10
0.12
0.24
0.36
0.48
0.60
39Ar/40Ar

Figure 13

a.

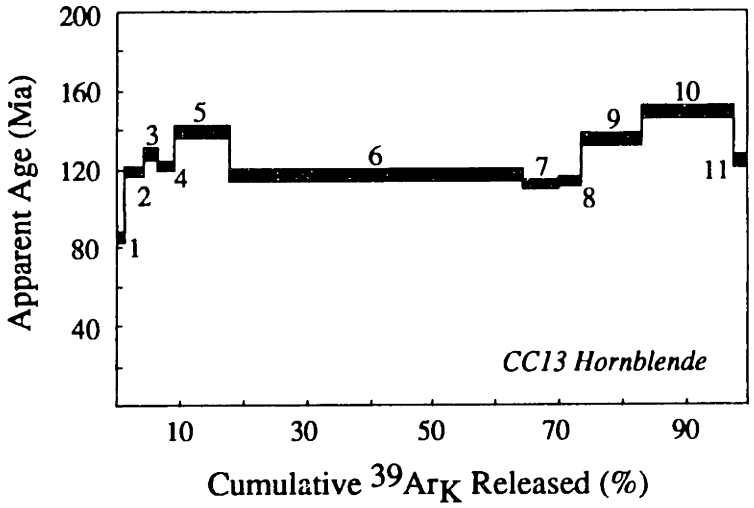
200
160
120
80
40
Apparent Age (Ma)
1
2
3
4
5
6
7
8
9
10
11
CC13 Hornblende
10
30
50
70
90
Cumulative $^{39}Ar_K$ Released (%)

b.

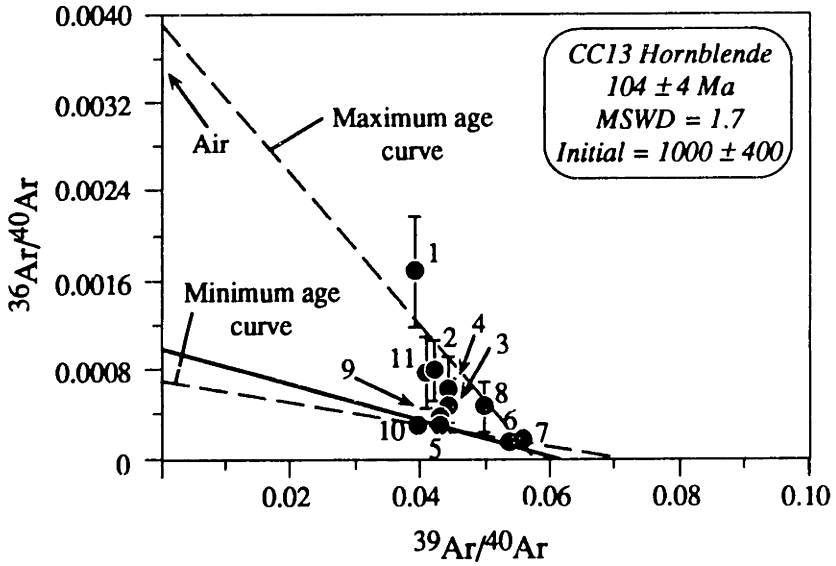
0.0040
0.0032
0.0024
0.0016
0.0008
0
$^{36}Ar/^{40}Ar$
Air
Maximum age curve
Minimum age curve
CC13 Hornblende
104 ± 4 Ma
MSWD = 1.7
Initial = 1000 ± 400
1
2
3
4
5
6
7
8
9
10
11
0.02
0.04
0.06
0.08
0.10
$^{39}Ar/^{40}Ar$

Figure 14

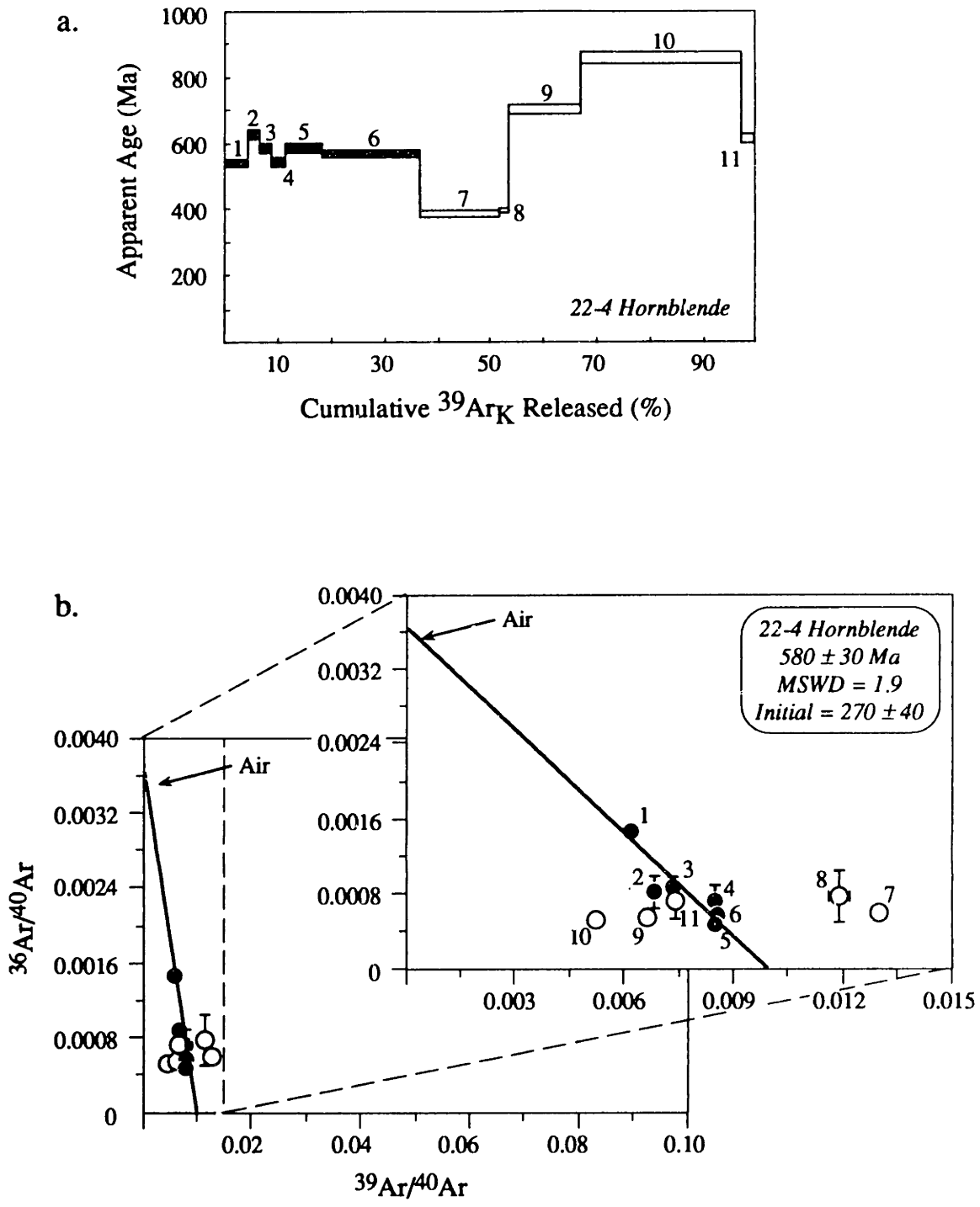
a.
Apparent Age (Ma)
1000
800
600
400
200
10
30
50
70
90
Cumulative $^{39}Ar_K$ Released (%)
22-4 Hornblende
b.
$^{36}Ar/^{40}Ar$
$^{39}Ar/^{40}Ar$
Air
22-4 Hornblende
580 ± 30 Ma
MSWD = 1.9
Initial = 270 ± 40
0.0040
0.0032
0.0024
0.0016
0.0008
0
0.02
0.04
0.06
0.08
0.10
0.003
0.006
0.009
0.012
0.015

Figure 15

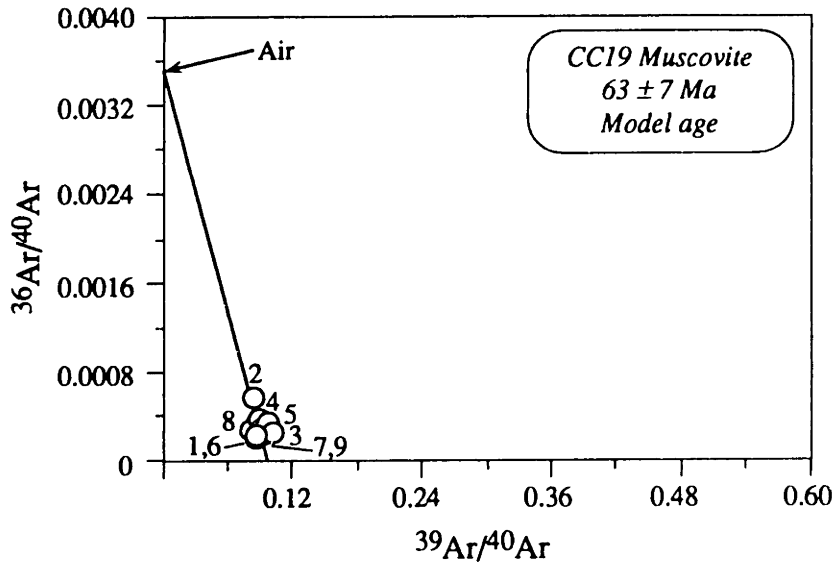
0.0040
0.0032
0.0024
0.0016
0.0008
0
36Ar/40Ar
Air
CC19 Muscovite
63 ± 7 Ma
Model age
2
4
5
8
3
1,6
7,9
0.12
0.24
0.36
0.48
0.60
39Ar/40Ar

Figure 16

a.

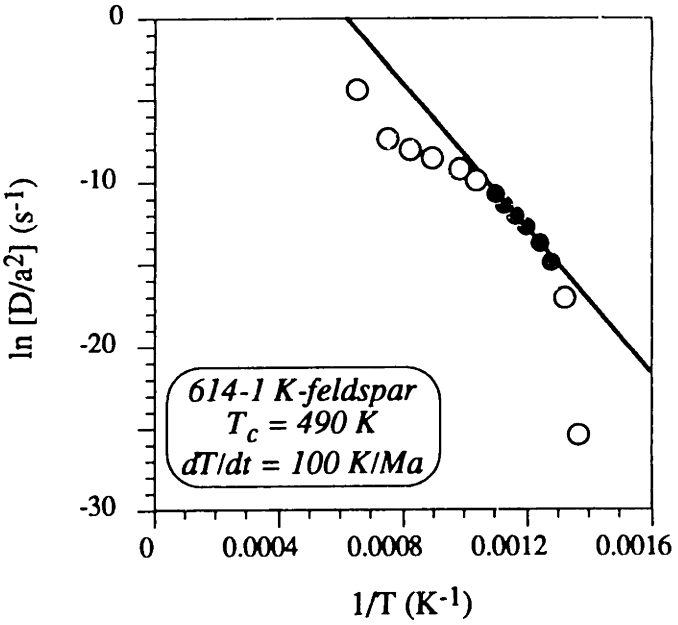
0
-10
-20
-30
ln [D/a²] (s⁻¹)
614-1 K-feldspar
T_c = 490 K
dT/dt = 100 K/Ma
0
0.0004
0.0008
0.0012
0.0016
1/T (K⁻¹)

b.

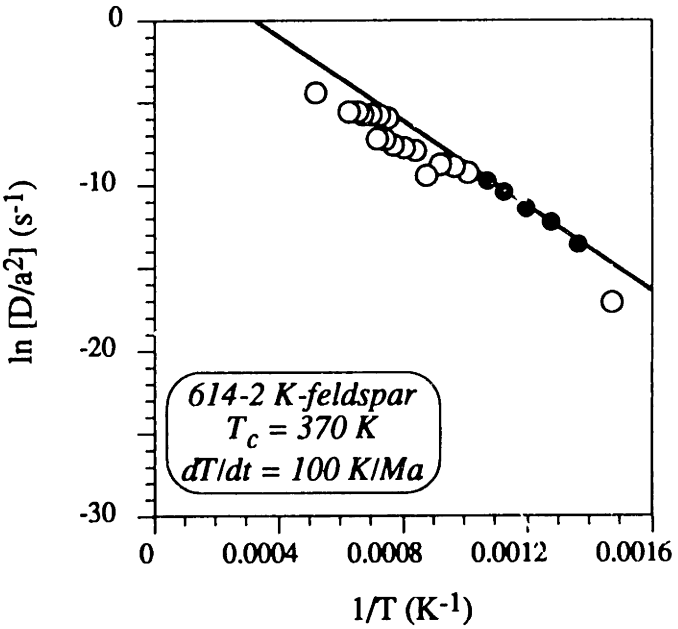
0
-10
-20
-30
ln [D/a²] (s⁻¹)
614-2 K-feldspar
T_c = 370 K
dT/dt = 100 K/Ma
0
0.0004
0.0008
0.0012
0.0016
1/T (K⁻¹)

Figure 17

c.

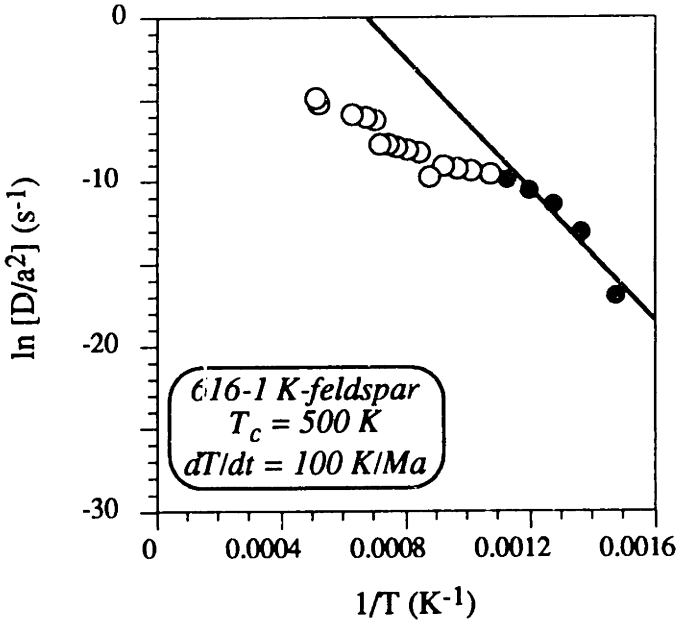
0
-10
-20
-30
ln [D/a²] (s⁻¹)
0
0.0004
0.0008
0.0012
0.0016
1/T (K⁻¹)
616-1 K-feldspar
T_c = 500 K
dT/dt = 100 K/Ma

d.

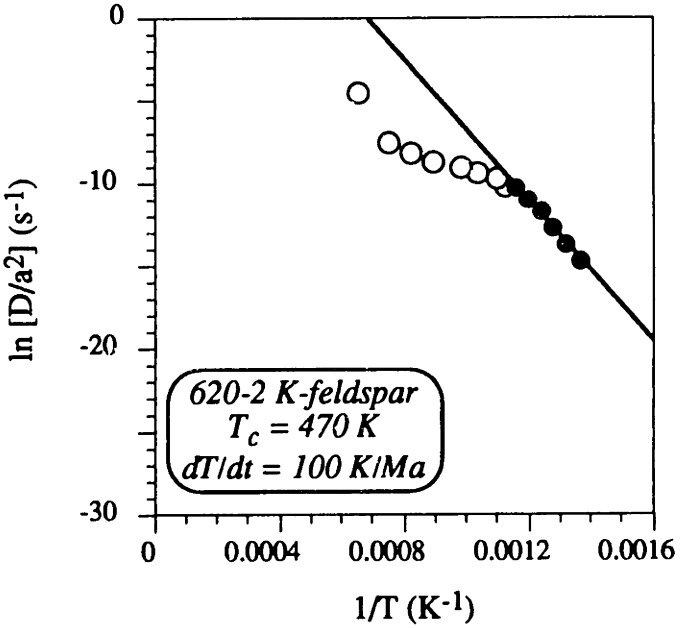
0
-10
-20
-30
ln [D/a²] (s⁻¹)
0
0.0004
0.0008
0.0012
0.0016
1/T (K⁻¹)
620-2 K-feldspar
T_c = 470 K
dT/dt = 100 K/Ma

Figure 17

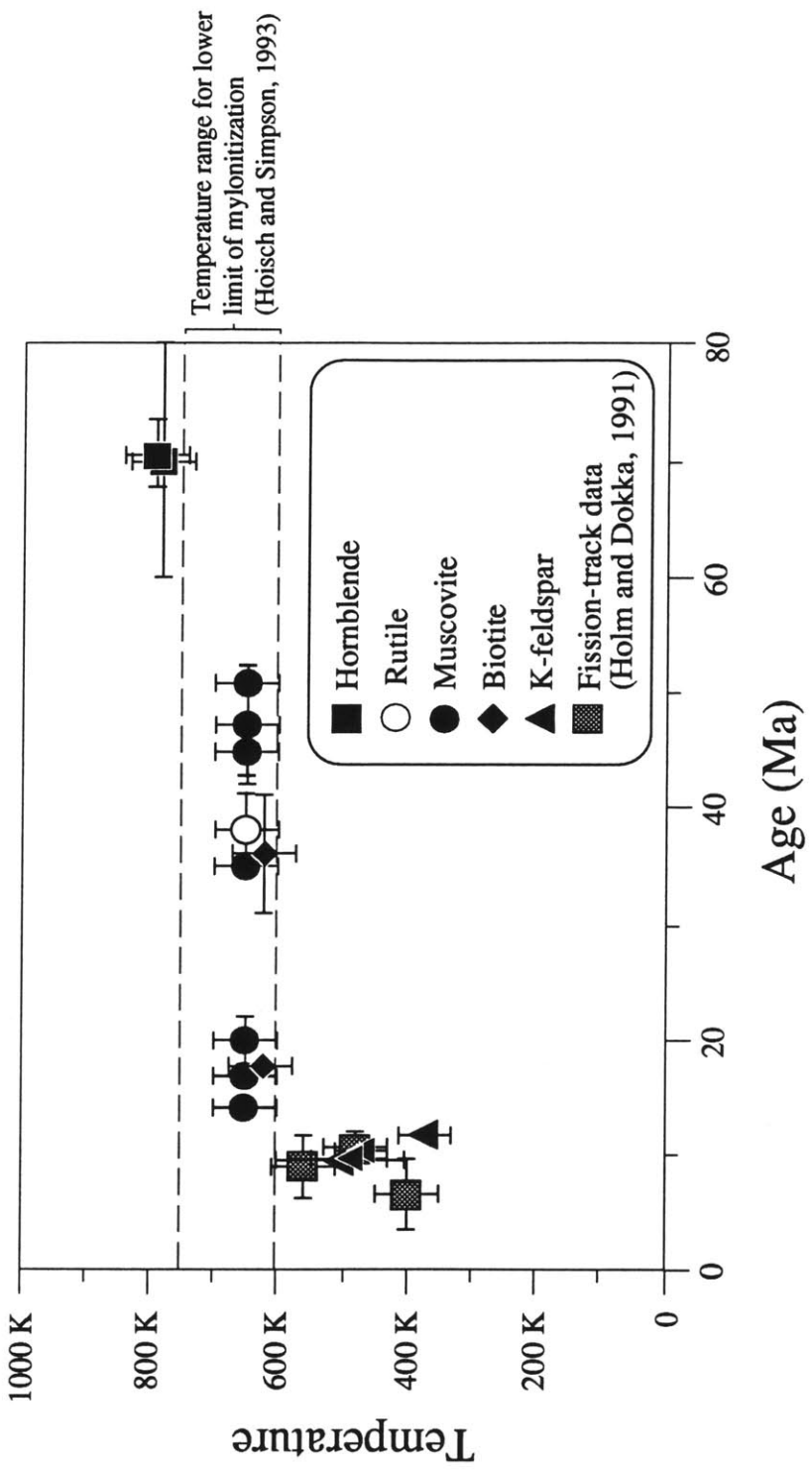
Temperature range for lower limit of mylonitization (Hoisch and Simpson, 1993)
Hornblende
Rutile
Muscovite
Biotite
K-feldspar
Fission-track data (Holm and Dokka, 1991)
1000 K
800 K
600 K
400 K
200 K
0
Temperature
0
20
40
60
80
Age (Ma)

Figure 18

CHAPTER 5

TRANSFORM-NORMAL EXTENSION ON THE NORTHERN DEATH VALLEY FAULT SYSTEM, CALIFORNIA–NEVADA

David Applegate
Department of Earth, Atmospheric, and Planetary Sciences
Massachusetts Institute of Technology

ABSTRACT

The Northern Death Valley fault zone is a major right-lateral structure in southeastern California that has accommodated 70 km or more of regional transtensional deformation in Tertiary to Recent time. Extension parallel to its northwest transport direction in the Death Valley region has produced "pull-apart" structures that are responsible for opening the central Death Valley rhombochasm. In several ranges along the length of the Northern Death Valley fault zone, there is also evidence for extension directed to the southwest, normal to strike-slip movement. Evidence from the Funeral, Grapevine, and Cottonwood Mountains suggests that a significant amount of down-dip slip has occurred on the Northern Death Valley fault zone and parallel structures (together referred to as the Northern Death Valley fault system) coeval with the majority of right-lateral slip. This oblique movement may be the result of a misorientation of the Northern Death Valley fault zone within the regional stress field over the past 6 My, a hypothesis supported by simple geometric calculations. Transform-normal extension on the Northern Death Valley fault zone may be responsible in part for opening northern Death Valley and for the present topography of the Funeral and Grapevine Mountains.

INTRODUCTION

Miocene to Recent extension in the central Basin and Range province parallels large strike-slip faults and is considered to be the result of an unstable transform boundary between the Pacific and North American plates that developed in middle Miocene time as the Mendocino triple junction migrated northward (Atwater, 1970; Wernicke, 1992). One of the characteristic manifestations of this transform-parallel extension is the presence of basins that opened in order to accommodate differential motion between two strike-slip faults. These basins are referred to as pull-apart basins, or rhombochasms, and a classic example is Death Valley in southeastern California (Figure 1; Burchfiel and Stewart, 1966). The central part of Death Valley is a basin bounded by two right-lateral, northwest-striking faults: the Southern Death Valley fault zone (SDF in Figure 1) and the Northern Death Valley fault zone (NDF in Figure 1; also referred to as the Furnace Creek fault zone). Stewart (1983) estimated that the Northern Death Valley fault zone accommodated 80 km of right-lateral slip in contrast to estimates of less than 10 km of slip on the Southern Death Valley fault zone (Wright and Troxel, 1967). The opening of the central Death Valley basin is the final stage in a process of Miocene to Recent extension that accommodated differential slip between these faults (Stewart, 1983). Earlier northwest-directed extension on the Amargosa fault transported the Panamint Mountains from a position on top of the Black Mountains before the later Death Valley fault (DVF in Figure 1) opened the actual basin (see Figure 1 for locations; Stewart, 1983).

A separate basin has developed in northern Death Valley that is not a pull-apart basin. The axis of this basin is oblique to that of central Death Valley and roughly parallels the Northern Death Valley fault zone (Figure 1). The opening of this basin has been attributed to northwest-directed extension on the Tucki Mountain detachment system at the northern end of the Panamint Mountains (Figure 2; Hodges et al., 1987; Snow and White, 1990), producing a basin that is deep at its southern end and shallows northward (Hunt and Mabey, 1966). The basin, however, is also deep adjacent to the Northern Death Valley

fault zone, suggesting a component of fault-normal extension on that structure. Evidence for such a component of down-dip, southwest-directed movement on the Northern Death Valley fault zone is present in the southern Funeral Mountains. In addition, structures that parallel the Northern Death Valley fault zone in the northern Funeral Mountains, the Grapevine Mountains, and the Cottonwood Mountains show evidence for oblique slip and southwest-directed normal slip (Locations in Figure 1). A Northern Death Valley fault system comprised of the Northern Death Valley fault zone and these related structures appears to be responsible for at least some of the opening of northern Death Valley.

Ben-Avraham (1985) has proposed a model for strike-slip-related basins that do not conform to the pull-apart model. These basins are bounded by both strike-slip and normal faults and form because of extension synchronous with strike-slip motion but normal to it. Ben-Avraham and Zoback (1992) suggest that transform-normal extension can be accounted for by a misorientation between the regional stress field and the transform structure. Such an explanation seems particularly appropriate for northern Death Valley, because the Northern Death Valley fault zone is a fairly long-lived structure, but the fault-normal extension is much younger, suggesting that a change in the regional stress field made simple, right-lateral motion on the Northern Death Valley fault zone unstable and required a component of extension as well.

This paper presents new evidence for young, southwest-directed extension in the northern Funeral Mountains and reviews other evidence from previously published mapping in the southern Funeral Mountains, Grapevine Mountains, and Cottonwood Mountains. The magnitude of this extensional component is then compared to that predicted by simple geometric calculations based on the strike of the Northern Death Valley fault zone and estimates of the regional extension direction.

NORTHERN DEATH VALLEY FAULT ZONE

The Northern Death Valley fault zone follows a northwest-southeast trend for 200 km from Fish Lake Valley in Nevada at the north end to the Resting Spring Range in California at the south end. Estimates of 45 km of right-lateral offset were made based on a displaced Jurassic pluton at its northern end (McKee, 1968) and on anomalous thickness differences in Paleozoic and Proterozoic formations (Stewart, 1967). These estimates were later increased to 80 km by Stewart (1983) based on offset facies and thickness trends of Proterozoic and Paleozoic units. Prave and Wright (1986) questioned this interpretation, arguing that the isopach trends only supported 50 km of offset. Subsequent reconstructions of the Mesozoic thrust belt support an intermediate number: Snow and Wernicke (1989) determined a right-lateral offset of ~ 70 km between the Cottonwood Mountains and southern Funeral Mountains. Displacement appears to be much smaller at the southern end of the Northern Death Valley fault zone beyond where it joins the Death Valley fault, as predicted by the pull-apart model for the two structures (Stewart, 1983; Wright and Troxel, 1967), and offset becomes negligible west of the Resting Spring Range (Figure 1). At its northern end, the Northern Death Valley fault zone curves towards a more northerly strike, and its displacement may be transferred to the Walker Lane fault system by normal faults (Kohler et al., 1993).

The Northern Death Valley fault zone appears to have initiated in Early Miocene time, and most of its movement is post- 14 Ma (Cemen et al., 1985). Extension between the Black Mountains and the Panamint Mountains has taken place since 11 Ma, with large lateral transport and the subsequent opening of central Death Valley taking place since 7 Ma (McKenna and Hodges, 1990). Because this extension is thought to be related to the accommodation of displacement on the Northern Death Valley fault zone, the majority of movement on the Northern Death Valley fault zone is inferred to be post- 7 Ma. Both the Death Valley fault and the Northern Death Valley fault zone show considerable evidence of Late Quaternary faulting and are currently active (Brogan et al., 1991). With a combined

length of over 300 km, these structures represent the second longest active fault system in California and are linked to the longer San Andreas fault system by the Garlock fault (Figure 1).

EVIDENCE FOR A SOUTHWEST-DIRECTED EXTENSIONAL COMPONENT ON THE NORTHERN DEATH VALLEY FAULT SYSTEM

Northern Funeral Mountains

The northern end of the Funeral Mountains is one of several metamorphic core complexes bordering Death Valley, including the Black Mountains (Figure 1; Holm and Wernicke, 1990) and the central and northern Panamint Mountains (Figure 1; Hodges et al., 1990; Hodges et al., 1987). Mid-crustal rocks in the Funeral Mountains have been brought to the surface in the footwall of low-angle extensional structures as the result of several episodes of extensional unroofing (Applegate et al., 1992). Early extension took place on extensional shear zones within the core in Late Cretaceous time (Figure 3; Applegate et al., 1992). A second episode of unroofing took place in Miocene time on the Boundary Canyon detachment (Figures 2 and 3), which separates the metamorphic core rocks from unmetamorphosed sedimentary rocks along the northern edge of the core complex (Wright and Troxel, 1994). The transport direction for both the Late Cretaceous and Miocene unroofing events is top-to-the-northwest (Reynolds et al., 1986; Applegate et al., 1992; Hoisch and Simpson, 1993).

The southwestern boundary of the core complex is defined by the Keane Wonder fault, a low-angle structure that parallels the Northern Death Valley fault zone (Figure 2). In the southern Funeral Mountains, the Keane Wonder fault shows a 5 km right-lateral offset of a large Mesozoic anticline in the hanging wall of the Schwaub Peak thrust (Figure 2; Cemen and Wright, 1990). The Keane Wonder fault does not offset the thrust; instead its motion appears to be taken up by a series of orthogonally oriented normal faults that connect it with the Northern Death Valley fault zone (Cemen et al., 1985).

Although the Keane Wonder fault shows evidence for right-lateral motion at its southern end, it parallels a number of low- to moderate-angle, southwest-dipping normal faults in the northern Funeral Mountains (Figure 3). These faults extend from the crest of the range towards Death Valley as first observed by Wright and Troxel (1994). Fault planes for 53 meso- and macroscale faults with a minimum 1 m offset were measured, all of which show evidence of down-dip motion. Poles to these fault planes are shown in Figure 4, and they cluster at a mean orientation of 70; N81E, corresponding to a plane oriented N19W; 20 SW. Cataclasis on these faults produced gouge zones that are several meters thick in places. The Big Bell fault runs continuously along the highest part of the range for several kilometers in an area around Chloride Cliff that is particularly disrupted by normal faults (Figure 3). The Big Bell fault shows a minimum down-to-the-southwest offset of 600 m. Faults with down-dip offset and similar orientation to the range-front faults are also found in the hanging wall of the core complex, and two of these structures cut the Boundary Canyon detachment between Boundary and Monarch Canyons (Figure 3).

Estimates on the displacement of the Keane Wonder fault and other normal faults are complicated by the complexity of earlier folding and other ductile deformation in the core complex and, in the case of the Keane Wonder fault, the absence of correlative rocks across it. A minimum estimate for the combined offset on these faults is 2 km based on the minimum stratigraphic separation exposed in the footwall of the Boundary Canyon detachment and the footwall of the Keane Wonder fault. A more reasonable minimum estimate is obtained by projecting the Keane Wonder fault and Boundary Canyon detachment to their intersection over the range. Accounting for doming, this approach suggests 4.6 km of apparent throw at a transect through Chloride Cliff. Since the Big Bell fault accounts for at least 600 m of this total, the minimum southwest-directed offset on the Keane Wonder fault itself is somewhat less than 4 km. None of the faults in the mapping area, including the Keane Wonder fault itself, show clear evidence of strike-slip movement.

Wright and Troxel (1994), however, suggest that in the northwest corner of the core, footwall rocks are bent westward to northwestward and attenuated as a result of right-lateral drag on the Keane Wonder fault.

These down-to-the-southwest normal faults are associated with asymmetric folds, a relationship first noted by Giaramita (1984). These folds formed as second-order folds to a large-scale anticline associated with doming of the core (Figure 3; Chapter 2). They are symmetric at the crest of the first-order anticline, which coincides with the range crest, but are increasingly asymmetric and inclined to the southwest closer to Death Valley. Although some of the asymmetry in these folds may be attributed to their position on the limb of a larger fold, many of these folds appear to have been dragged into an increased southwest inclination by movement on normal faults, causing the folds to "cascade" down the face of the range (Troxel, 1988). In places, the faults appear to parallel the southwestern limbs of outcrop-scale and macroscopic folds, forming discrete offsets on the steepened limb, whereas in other locations the faults clearly cut the folds, indicating that the folds formed earlier. Figure 5 is a photograph of a large, southwest-inclined anticline that appears to be entrained by the Keane Wonder fault, consistent with a component of southwest-directed movement on that fault.

Southern Funeral Mountains

The southern limit of the Northern Death Valley fault zone has been mapped by McAllister (1971) and Cemen (1983). Similar structures to those occurring in the northern Funeral Mountains are found here, including southwest-dipping normal faults that parallel the Northern Death Valley fault zone and Keane Wonder fault. Cemen et al. (1985) report the Northern Death Valley fault zone is represented in this area by faults that place rocks of the Miocene-Pliocene Furnace Creek Formation and Pliocene Funeral Formation against Paleozoic rocks of the Funeral Mountains. If one assumes that the underlying Miocene Artists Drive Formation is present in the subsurface, then a vertical, southwest-side down

displacement of more than 1200 m is indicated (Cemen et al., 1985). In addition to faulting, a number of northwest-axial folds are present at both macroscopic and outcrop scales which deform the Pliocene sediments as well as older rocks (McAllister, 1971). These folds are found in the hanging wall of the Northern Death Valley fault zone as well as its footwall, and in both the hanging wall and footwall of the Keane Wonder fault.

Grapevine Mountains

Reynolds (1969) mapped the southern Grapevine Mountains and found evidence for extensive down-to-the-southwest movement on normal faults both within the range and defining the range front. Normal faults within the range strike northwest or north-northwest and consistently show down-dip offsets to the southwest, except for a few antithetic east-dipping faults. Displacement on these faults varies from 50 to 400 m with a cumulative normal-sense offset of over 700 m toward Death Valley.

Reynolds (1969) refers to the range-front faults as the Grapevine fault zone (Figure 2). These closely-spaced normal faults strike N30W to N35W, sub-parallel to the Northern Death Valley fault zone, which is located 3 km southwest of the range front. The average dip on these faults and the faults within the range is 58°, and offsets on individual faults in the Grapevine fault zone are over 400 m (Reynolds, 1969). The bedrock-alluvium contact is itself a fault with potentially the greatest offset. Gravity data of Mabey (1963) indicate approximately 3000 m of Cenozoic rocks beneath northern Death Valley adjacent to the range front, and the steepest gradient in the gravity measurements is directly adjacent to the range front. Assuming that the basal Cenozoic rocks are equivalent to the base of the Titus Canyon Formation, which is exposed at an elevation of 1200 m, that implies a minimum down-to-the-southwest separation of over 4 km (Reynolds, 1969). Displacement on the Grapevine fault zone is accompanied by apparent dragging of rocks in the upright limb of an older recumbent syncline. Rocks in this limb are tilted westward and apparently dragged downward toward the valley with, in some cases, as much as 215° of rotation

(Reynolds, 1969). The amount of displacement on the Grapevine fault zone decreases to the north, where it is overlapped by Pliocene (?) rocks. This decrease correlates with a narrowing of northern Death Valley and of the distance between the Northern Death Valley fault zone and the Grapevine fault zone such that the range front of the northern Grapevine Mountains is bounded by the Northern Death Valley fault zone.

Hamilton (1988) noted that the range-front scarp on the Grapevine Mountains facing Death Valley trends southeastward into the Funeral Mountains detachment fault but does not cut it, being restricted to the upper plate. This interpretation is predicated on the assumption that the Keane Wonder fault represents part of the detachment system and not a later fault. The observation is equally compatible with the hypothesis that the Keane Wonder fault represents a continuation of the Grapevine fault zone.

Cottonwood Mountains

Across the Northern Death Valley fault zone from where displacement on the Grapevine fault zone decreases, a number of high-angle faults parallel the Northern Death Valley fault zone in the northern Cottonwood Mountains, displacing young sedimentary and volcanic rocks deposited in the Tertiary Ubehebe basin (Snow and White, 1990). Conglomerates in the basal part of the basin deposits resemble clasts from the Titus Canyon formation, and Snow and White (1990) correlate these deposits with those found in the southern Funeral Mountains (Cemen et al., 1985). Snow and White (1990) document significant eastward tilting of these deposits and relate the tilting to north-south-oriented rollover structures produced by motion above the northward projection of the Tucki Mountain detachment system (Figure 2). Because movement on the Tucki Mountain detachment system and hence tilting attributed to the rollover structures was over by ~ 3.7 Ma (Hodges et al., 1990), tilting of a younger sequence of Pliocene volcanics and marl and Pliocene-Pleistocene conglomerates is unrelated to the rollover, and Snow and White (1990) suggest that tilting of these units can be attributed to later faulting. The tilt axis for the basin

deposits trends N25W (Snow and White, 1990), which is similar to the N35W trend for the Northern Death Valley fault zone. Because the tilt axis was oblique to the west-northwest regional extension direction, Snow and White (1990) argued that the two were unrelated, but the closer similarity between the tilt axis and the trend of the Northern Death Valley fault zone suggests that at least the youngest tilting of the basin may be related to movement on these faults. In their cross-sections across the basin, Snow and White (1990) indicate that these faults have a normal offset with top-to-the-southwest sense of motion and over 100 m displacement.

Two other pieces of evidence suggest down-to-the-southwest normal motion across the Northern Death Valley fault zone. In their correlation of features across the Northern Death Valley fault zone between the southern Funeral Mountains and the Cottonwood Mountains, Snow and Wernicke (1989) base their reconstruction on the presence of a large Mesozoic backfold in the hanging walls of two closely spaced thrusts. In the Funeral Mountains, the Winters Peak anticline, which is offset by the Keane Wonder fault, is cored by rocks of the Johnnie Formation. In the Cottonwood Mountains, the correlative structure is the White Top Mountain backfold, which may be cored by rocks as old as the Ordovician Eureka Quartzite (Snow and Wernicke, 1989). If these structures are correlative, there is a stratigraphic offset of over 6 km between them (thicknesses from Wernicke et al., 1988). Although this offset may in part be related to movement on the Tucki Mountain detachment system, the juxtaposition of these structures across the Northern Death Valley fault zone requires a significant component of down-dip motion across that fault.

The lack of metamorphic rocks in the northern Cottonwood Mountains or ranges further north along the Northern Death Valley fault zone also suggests normal motion across the fault zone. The Boundary Canyon detachment system extends 30 km to the east of the Funeral Mountains into the Bullfrog Hills and Bare Mountains (Maldonado, 1990), but neither it nor rocks in its footwall are found across the Northern Death Valley fault zone, suggesting that the Cottonwood block has been dropped down to the west relative to

the Funeral Mountains. Because the Boundary Canyon detachment and the Northern Death Valley fault zone may have been moving in part contemporaneously, it is unlikely that the highest-grade rocks of the core complex would appear across the Northern Death Valley fault zone, but even the lower-grade rocks in the central Funeral Mountains are not found across the Northern Death Valley fault zone.

TIMING CONSTRAINTS ON THE NORTHERN DEATH VALLEY FAULT SYSTEM

The age of movement on the Boundary Canyon detachment, which is cut by the Keane Wonder fault and other structures, provides an upper age constraint for southwest-directed extension in the northern Funeral Mountains. Movement on the detachment is associated with rapid cooling of the metamorphic core rocks between 11 and 9 Ma based on $^{40}Ar/^{39}Ar$ cooling ages for K-feldspar and fission-track ages for titanite and zircon (Chapter 4; Holm and Dokka, 1991). Apatite fission-track ages indicate that the core rocks had cooled to ~ 380 K (Green et al., 1989) by 7 to 6 Ma (Holm and Dokka, 1991; Hoisch and Simpson, 1993), and Reynolds et al. (1986) state that rocks as young as 7 Ma are found in the hanging wall of the Boundary Canyon detachment. Thus, the detachment appears to have been active until at least 6 Ma, constraining the post-detachment faulting to be younger than 6 Ma. Obtaining a minimum age for southwest-directed extension in the northern Funeral Mountains is limited by the lack of younger sedimentary rocks.

In the southern Funeral Mountains, the Northern Death Valley fault zone and southwest-inclined folds affect sediments as young as Pliocene (Cemen et al., 1985). Faults within the Grapevine Mountains postdate deposition of the Oligocene-Miocene Titus Canyon formation and are postulated to be Pliocene in age because that is when significant relief developed between Death Valley and the Grapevine Mountains (Reynolds, 1969). Faults of the Grapevine fault zone cut Pliocene sediments and in places Pleistocene gravels, indicating that movement on these faults is quite young and may continue to the present

(Reynolds, 1969). The youngest sediments involved in southwest-directed normal faulting in the Cottonwood Mountains are Pleistocene conglomerates (Snow and White, 1990).

DISCUSSION

Southwest-directed deformation on the Northern Death Valley fault system has been active over the past 6 My and as such is coeval with movement on the Amargosa and Death Valley faults (McKenna and Hodges, 1990). Because movement on these latter faults is considered to be coeval with the majority of right-lateral movement on the Northern Death Valley fault zone, southwest-directed extension is not a separate "event" but represents the down-dip component of oblique slip on the Northern Death Valley fault system. Although this conclusion is consistent with evidence throughout the region that the overall extension direction during this time period was to the northwest, this example of transform-normal extension is anomalous since all of the other major extensional faults in the region after 10 Ma show transform-parallel movement (McKenna and Hodges, 1990).

Ben-Avraham (1985) described simultaneous strike-slip and transform-normal extension in asymmetric basins found in the southern part of the Dead Sea rift. These basins are bounded by transform faults on one side and by sub-parallel normal faults on the other. The equivalent normal faults across the basin from the Northern Death Valley fault zone are part of the Tucki Mountain detachment system. Although this system was active between 10 and 4 Ma and may have even younger motion related to the opening of Panamint Valley to the west (Hodges et al., 1990), it accommodated transform-parallel extension during this time. Instead, simultaneous transform-normal extension and strike-slip motion were both accommodated by the Northern Death Valley fault system on one side of the basin.

Although specific structures in northern Death Valley differ from the Dead Sea case, the overall kinematics of the extension may be the same. Ben-Avraham and Zoback (1992) argue that transform-normal extension can be explained by far-field stresses in a manner

analogous to transform-normal compression along the San Andreas fault in central California, which is manifested by folds and reverse faults that strike parallel to the San Andreas fault. Zoback et al. (1987) developed a model for a weak transform fault in strong crust which indicated that small obliquities between the maximum principal stress in the region and the transform could produce simultaneous strike-slip and compressional motion. Ben-Avraham and Zoback (1992) argue that this model, developed for a slightly convergent setting is equally applicable to a slightly divergent setting.

Some obliquity between the strike of the Northern Death Valley fault zone and the maximum principal stress is to be expected for a structure that developed in Early Miocene time but was most active in Late Miocene to Recent time. Numerous authors have pointed out that young fault zones may follow earlier structural trends and hence do not accurately reflect the orientation of the changing stress field (e.g. Wright, 1976). Its earlier history may have fixed the Northern Death Valley fault zone in an orientation favorable enough to the later stress field such that continued movement took place but oblique enough such that strike-slip movement was unstable, resulting in the need for transform-normal extension along the Northern Death Valley fault system. Although it is not possible to determine the paleo-stress field, one can obtain some estimate of the magnitude of a southwest-directed extensional component by comparing the strike of the Northern Death Valley fault zone to the regional extension vector.

The most straightforward estimate of a regional extension vector comes from Snow and Wernicke (1989), who determined a vector for offset of Mesozoic structures across the Northern Death Valley fault system of 68 ± 4 km oriented N48 ± 6W. This reconstruction assumes that a Mesozoic pluton in the Cottonwood Mountains did not overlap the Funeral Mountains block where no correlative pluton exists. If that pluton was rootless, however, then overlap of the two blocks is permissable, and a vector is obtained of similar magnitude oriented N60 ± 18W (Snow and Wernicke, 1989). The orientation of this vector is within uncertainty of the extension direction of N73 ± 12W determined for the entire Death Valley

extensional corridor by Wernicke et al. (1988). Adjacent to the Funeral Mountains, the Northern Death Valley fault zone is oriented approximately N45W. Further to the north, its strike changes to approximately N40W adjacent to the southern Grapevine Mountains and N30W adjacent to the northern Cottonwood Mountains. By comparing the extension vectors calculated by Snow and Wernicke (1989) with the strike of each segment of the Northern Death Valley fault zone, one can determine the angle of divergence for each segment of the fault and resolve a northwest-directed, right-lateral component and a southwest-directed, normal component. Assuming 68 km of displacement on a N48W vector, one obtains values for southwest-directed extension of 4 km adjacent to the Funeral Mountains, 9 km adjacent to the southern Grapevine Mountains, and 21 km adjacent to the northern Cottonwood Mountains (Figure 2 and Table 1). These values represent maximum estimates since the total offset measured by Snow and Wernicke (1989) probably includes some movement before 6 Ma. Using the N60W vector that allows for overlap of the blocks, one obtains much higher estimates for this extension: 18 km, 23 km, and 34 km from south to north (Figure 2 and Table 1). Within the uncertainty of these vectors, it is possible that northeast-directed compression could exist adjacent to the Funeral Mountains, but elsewhere the geometry consistently indicates a component of southwest-directed extension (Table 1).

This simple geometric argument accounts for the apparent increase in extension from the southern Funeral Mountains, where < 2 km is documented to the northern Funeral Mountains, where > 4 km is documented, to the southern Grapevine Mountains, where > 6 km is documented. The geometry, however, requires even greater extension adjacent to the northern Cottonwood Mountains, where displacements on faults parallel to the Northern Death Valley fault zone account for < 1 km of extension. Even if one considers the 6 km of apparent stratigraphic throw between the correlated Mesozoic anticlines, the amount is still much less than the 21 km indicated by the geometry. Furthermore, the northern Death Valley basin itself narrows to the north and becomes more shallow. One possible

explanation is that the rollover structures documented by Snow and White (1990) in the northern Cottonwood Mountains are related to normal movement on the adjacent Northern Death Valley fault zone and not to the Tucki Mountain detachment system, which is exposed over 40 km to the south. In that case, the extension would be taken up by distension of earlier Tertiary sediments. It is also possible that further to the north, the regional stress field has rotated, and the Northern Death Valley fault zone is no longer misaligned with it.

CONCLUSIONS

Much of the extension in the Death Valley region since Late Miocene time is related to movement on the Northern Death Valley fault zone. Although this extension is dominantly northwest-directed and transform-parallel, a significant component since 7 Ma is southwest-directed and transform-normal. This latter extension is coeval with the majority of right-lateral movement on the Northern Death Valley fault zone and can be explained by the divergence between the orientation of the long-lived Northern Death Valley fault zone and that of the regional stress field during this interval. The amounts of extension predicted are consistent with those documented in the Funeral and Grapevine Mountains, but substantially greater than predicted for the Cottonwood Mountains, suggesting the possibility that extension in that range attributed to the Tucki Mountain detachment system may be related to the Northern Death Valley fault system instead.

Because transform-normal extension in both the Funeral and Grapevine Mountains is associated with range-front structures, it may have some control on the present topography of these ranges. Both ranges show a steep western slope toward Death Valley and a more gradual eastern slope. This relationship suggests that the present topography of these ranges may be controlled by down-to-the-southwest faulting. The greater extensional component experienced by the Grapevine Mountains relative to the Funeral Mountains may explain in part the greater height of the Grapevine Mountains despite the fact that the highly

metamorphosed rocks in the northern Funeral Mountains have undergone much greater amounts of unroofing than the unmetamorphosed rocks in the Grapevine Mountains.

REFERENCES

Applegate, J. D. R., Walker, J. D. and Hodges, K. V., 1992, Late Cretaceous extensional unroofing in the Funeral Mountains metamorphic core complex, California: Geology, v. 20, p. 519-522.

Atwater, T., 1970, Implications of plate tectonics for the Cenozoic tectonic evolution of western North America: Geological Society of America Bulletin, v. 81, p. 3513-3536.

Ben-Avraham, Z., 1985, Structural framework of the Gulf of Elat (Aqaba), northern Red Sea: Journal of Geophysical Research, v. 90, p. 703-726.

Ben-Avraham, Z., and Zoback, M. D., 1992, Transform-normal extension and asymmetric basins: An alternative to pull-apart models: Geology, v. 20, p. 423-426.

Brogan, G. D., Kellogg, K. S., Slemmons, D. B. and Terhune, C. L., 1991, Late Quaternary faulting along the Death Valley-Furnace Creek fault system, California and Nevada: U.S. Geological Survey Bulletin, 23 pp.

Burchfiel, B. C. and Stewart, J. H., 1966, "Pull-apart" origin of the central segment of the Death Valley, California: Geological Society of America Bulletin, v. 77, p. 439-442.

Cemen, I., 1983, Stratigraphy, geochronology, and structure of selected areas of the northern Death Valley region, eastern California-western Nevada, and implications concerning Cenozoic tectonics of the region [Ph. D. thesis]: University Park, Pennsylvania State University, 235 pp.

Cemen, I. and Wright, L. A., 1990, Effect of Cenozoic extension on Mesozoic thrust surfaces in the central and southern Funeral Mountains, Death Valley, California, *in* Wernicke, B. P., ed., Basin and Range extensional tectonics near the latitude of Las Vegas, Nevada: Boulder, CO, Geological Society of America Memoir 176, p. 305-316.

Cemen, I., Wright, L. A., Drake, R. E. and Johnson, F. C., 1985, Cenozoic sedimentation and sequence of deformational events at the southeastern end of the Furnace Creek strike-slip fault zone, *in* Biddle, K. T. and Christie-Blick, N., ed., Strike-slip deformation and basin formation: Society of Economic Paleonologists and Mineralogists Special Publication 37, p. 127-141.

Giaramita, M. J., 1984, Structural evolution and metamorphic petrology of the Monarch Canyon area, northern Funeral Mountains, Death Valley, California [M.S. thesis]: Davis, University of California, 145 pp.

Green, P. F., Duddy, I. R., Laslett, G. M., Hegarty, K. A., Gleadow, A. J. W. and Lovering, J. F., 1989, Thermal annealing of fission tracks in apatite 4. Quantitative modeling techniques and extension to geological time scales: Chemical Geology (Isotope Geoscience Section), v. 79, p. 155-182.

Hamilton, W. B., 1988, Detachment faulting in the Death Valley region, California and Nevada: U.S. Geological Survey Bulletin, v. 1790, p. 51-85.

Hodges, K. V., McKenna, L. W. and Harding, M. B., 1990, Structural unroofing of the central Panamint Mountains, Death Valley region, southeastern California, *in* Wernicke, B. P., ed., Basin and Range extensional tectonics near the latitude of Las Vegas, Nevada: Boulder, Colorado, Geological Society of America Memoir 176, p. 377-389.

Hodges, K. V., Walker, J. D. and Wernicke, B. P., 1987, Footwall structural evolution of the Tucki Mountain detachment system, Death Valley region, southeastern California, *in* Coward, M. P., and others, eds., Continental Extensional Tectonics: Geological Society of London Special Publication 28, p. 393-408.

Hoisch, T. D. and Simpson, C., 1993, Rise and tilt of metamorphic rocks in the lower plate of a detachment fault in the Funeral Mountains, Death Valley, California: Journal of Geophysical Research, v. 98, p. 6805-6827.

Holm, D. K. and Dokka, R. K., 1991, Major Late Miocene cooling of the middle crust associated with extensional orogenesis in the Funeral Mountains, California: Geophysical Research Letters, v. 18, p. 1775-1778.

Holm, D. K. and Wernicke, B. P., 1990, Black Mountains crustal section, Death Valley extended terrain, California: Geology, v. 18, p. 520-523.

Hunt, C. B. and Mabey, D. R., 1966, Stratigraphy and structure, Death Valley, California: U.S. Geological Survey Professional Paper 494-A, 162 pp.

Kohler, G., Oldow, J. S., Sisson, V. B., and Donelick, R. A., 1993, Displacement transfer system linking the Furnace Creek and Walker Lane fault systems, west-central Nevada: Geological Society of America Abstracts with Programs, v. 25, p. 63.

Mabey, D. R., 1963, Complete Bouguer anomaly map of the Death Valley region, California, U. S. Geological Survey Geophysical Investigations map GP-305.

Maldonado, F., 1990, Structural geology of the upper plate of the Bullfrog Hills detachment fault system, southern Nevada: Geological Society of America Bulletin, v. 102, p. 992-1006.

McAllister, J. F., 1971, Preliminary geologic map of the Funeral Mountains in the Ryan Quadrangle, Death Valley region, Inyo County, California, scale 1: 62,500, U. S. Geological Survey Open-File Report, Scale 1:62,500.

McKee, E. H., 1968, Age and rate of movement on the northern part of the Death Valley-Furnace Creek fault zone, California: Geological Society of America Bulletin, v. 79, p. 509-512.

McKenna, L. W. and Hodges, K. V., 1990, Constraints on the kinematics and timing of late Miocene-Recent extension between the Panamint and Black Mountains, southeastern California, *in* Wernicke, B. P., ed., Basin and Range extensional tectonics near the latitude of Las Vegas, Nevada: Boulder, Colorado, Geological Society of America Memoir 176, p. 363-376.

Prave, A. R. and Wright, L. A., 1986, Isopach pattern of the Lower Cambrian Zabriskie Quartzite, Death Valley region, California-Nevada: Geology, v. 14, p. 251-254.

Reynolds, M. W., 1969, Stratigraphy and structural geology of the Titus and Titanothere Canyons area, Death Valley, California [Ph.D. thesis]: Berkeley, University of California, 310 pp.

Reynolds, M. W., Wright, L. A. and Troxel, B. W., 1986, Geometry and chronology of late Cenozoic detachment faulting, Funeral and Grapevine Mountains, Death Valley, California: Geological Society of America Abstracts with Programs, v. 18, p. 175.

Snow, J. K. and Wernicke, B., 1989, Uniqueness of geological correlations: An example from the Death Valley extended terrain: Geological Society of America Bulletin, v. 101, p. 1351-1362.

Snow, J. K. and White, C., 1990, Listric normal faulting and synorogenic sedimentation, northern Cottonwood Mountains, Death Valley region, California, *in* Wernicke, B. P., ed., Basin and Range extensional tectonics near the latitude of Las Vegas, Nevada: Boulder, Colorado, Geological Society of America Memoir 176, p. 413-445.

Stewart, J. H., 1967, Possible large right-lateral displacement along fault and shear zones in the Death Valley-Las Vegas area, California and Nevada: Geological Society of America Bulletin, v. 78, p. 131-142.

Stewart, J. H., 1983, Extensional tectonics in the Death Valley area, California: Transport of the Panamint Range structural block, 80 km northwestward: Geology, v. 11, p. 153-157.

Troxel, B. W., 1988, A geologic traverse of the northern Funeral Mountains, Death Valley, California, *in* Weide, D. L., and Faber, M. L., eds., This Extended Land, Geological Journeys in the Southern Basin and Range, Field Trip Guidebook: Las Vegas, Cordilleran Section, Geological Society of America, p. 45-49.

Wernicke, B., 1992, Cenozoic extensional tectonics of the U.S. Cordillera, *in* Burchfiel, B. C., and others, eds., The Cordilleran Orogen: Conterminous U.S., v. G-3, The Geology of North America: Boulder, Colorado, Geological Society of America, p. 553-581.

Wernicke, B., Axen, G.J., and Snow, J.K., 1988, Basin and Range extensional tectonics at the latitude of Las Vegas, Nevada: Geological Society of America Bulletin, v. 100, p. 1738-1757.

Wright, L. A., 1976, Late Cenozoic fault patterns and stress fields in the Great Basin and westward displacement of the Sierra Nevada block, discussion: Geology, v. 4, p. 489-494.

Wright, L. A. and Troxel, B. W., 1967, Limitations on right-lateral, strike-slip displacement, Death Valley and Furnace Creek fault zones, California: Geological Society of America Bulletin, v. 78, p. 933-950.

Wright, L. A. and Troxel, B. W., 1994, Geologic map of the central and northern parts of the Funeral Mountains and adjacent areas, Death Valley region, southern California, scale 1:48,000, U.S. Geol. Surv. Misc. Invest. Ser. I-2305, in press.

Zoback, M. D., et al., 1987, New evidence on the state of stress of the San Andreas fault system: Science, v. 238, p. 1105-1111.

Table 1. Estimates of southwest-directed extensional component of movement on the Northern Death Valley fault zone.

	Strike of Northern Death Valley fault zone					
	N45W (Funeral Mtns.)		N40W (S. Grapevine Mtns.)		N30W (N. Grapevine Mtns.)	
Direction of offset across NDF	Angle of obliquity (degrees)	SW extension* (km)	Angle of obliquity (degrees)	SW extension* (km)	Angle of obliquity (degrees)	SW extension* (km)
<u>No overlap between Funeral and Cottonwood Mountains allowed</u>						
N48W (N42 – 54W)	3 (-3 – 9)	4 (-4 – 11)	8 (2 – 14)	9 (2 – 16)	18 (12 – 24)	21 (14 – 28)
<u>Overlap between Funeral and Cottonwood Mountains allowed</u>						
N60W (N42 – 78W)	15 (-3 – 33)	18 (-4 – 37)	20 (2 – 38)	23 (2 – 42)	30 (12 – 48)	34 (14 – 51)

Numbers in parentheses indicate range of values produced by variation in direction of offset across the Northern Death Valley fault zone. Range of offset directions taken from Snow and Wernicke (1989).
*Assumes total offset of 68 km (Snow and Wernicke, 1989).

FIGURE CAPTIONS

Figure 1 Regional map of Death Valley extensional corridor including features described in text. Box in inset shows location of Figure 1. Dashed box on main figure shows location of Figure 2. Stippled pattern indicates outcrop of pre-Tertiary rock, and shaded pattern indicates outcrop of Funeral Mountains metamorphic core complex (FMMCC). Heavy lines show major Tertiary faults: strike-slip faults are shown with arrows, and normal faults are unornamented. Abbreviations refer to: AF–Amargosa fault, DVF–Death Valley fault, GF–Garlock fault, NDF–Northern Death Valley fault zone (also referred to as the Furnace Creek fault zone), PVF–Panamint Valley fault, RSR–Resting Spring Range, and SDF–Southern Death Valley fault zone. Map modified from Wernicke et al. (1988).

Figure 2 Location map for the northern Death Valley region, California and Nevada, modified from Wernicke et al.(1988). Note that Mesozoic structures have in many cases been reactivated along younger normal faults. Large arrows represent vectors of southwest-directed extensional component to movement on the Northern Death Valley fault zone predicted by calculations in Table 1. See text for explanation.

Figure 3 Simplified tectonic map of the northern Funeral Mountains.

Figure 4 Lower hemisphere, equal area stereonet plots of poles to brittle normal faults deforming the core rocks. (a) Scatter plot of poles to brittle faults with mean vector and great circle. A great circle and its pole are also shown for the Keane Wonder fault. (b) Contour plot of poles to brittle faults; contour interval = 4%/1% area.

Figure 5 Photograph of northwest-axial anticline that has been entrained by the Keane Wonder fault west of Monarch Canyon. Southwest is to the right in this photograph. Width of view is approximately 50 m. Anticline folds

Neoproterozoic marbles and schists. Keane Wonder fault is flat surface dipping to right, separating Neoproterozoic rocks from unmetamorphosed Tertiary strata.

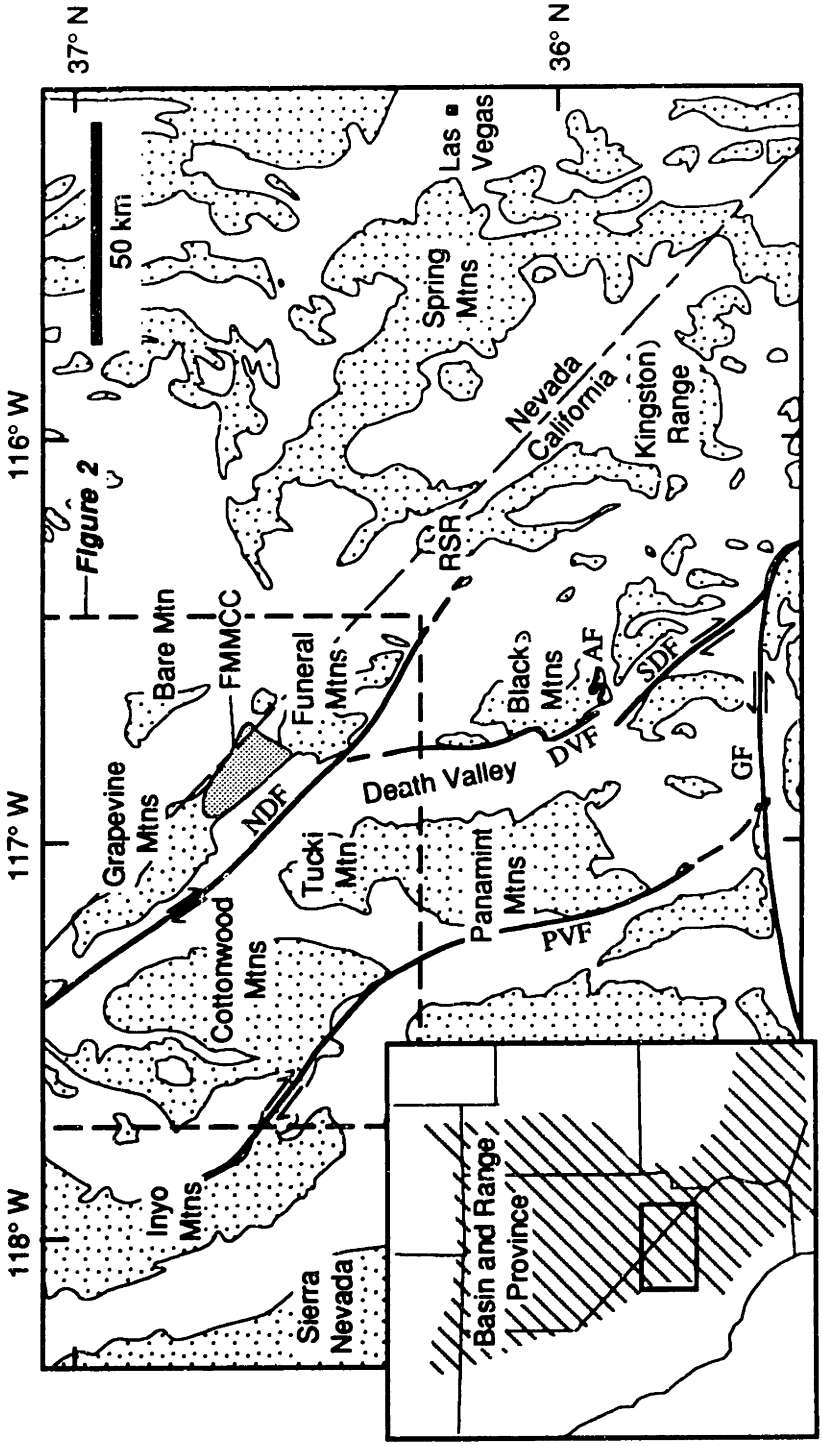
37° N
36° N
116° W
117° W
118° W
50 km
Figure 2
Las Vegas
Spring Mtns
Nevada
California
Kingston Range
RSR
Bare Mtn
FMMCC
Funeral Mtns
Black Mtns
AF
SDF
DVF
GF
Death Valley
NDF
Grapevine Mtns
Tucki Mtn
Panamint Mtns
PVF
Cottonwood Mtns
Inyo Mtns
Sierra Nevada
Basin and Range Province

Figure 1

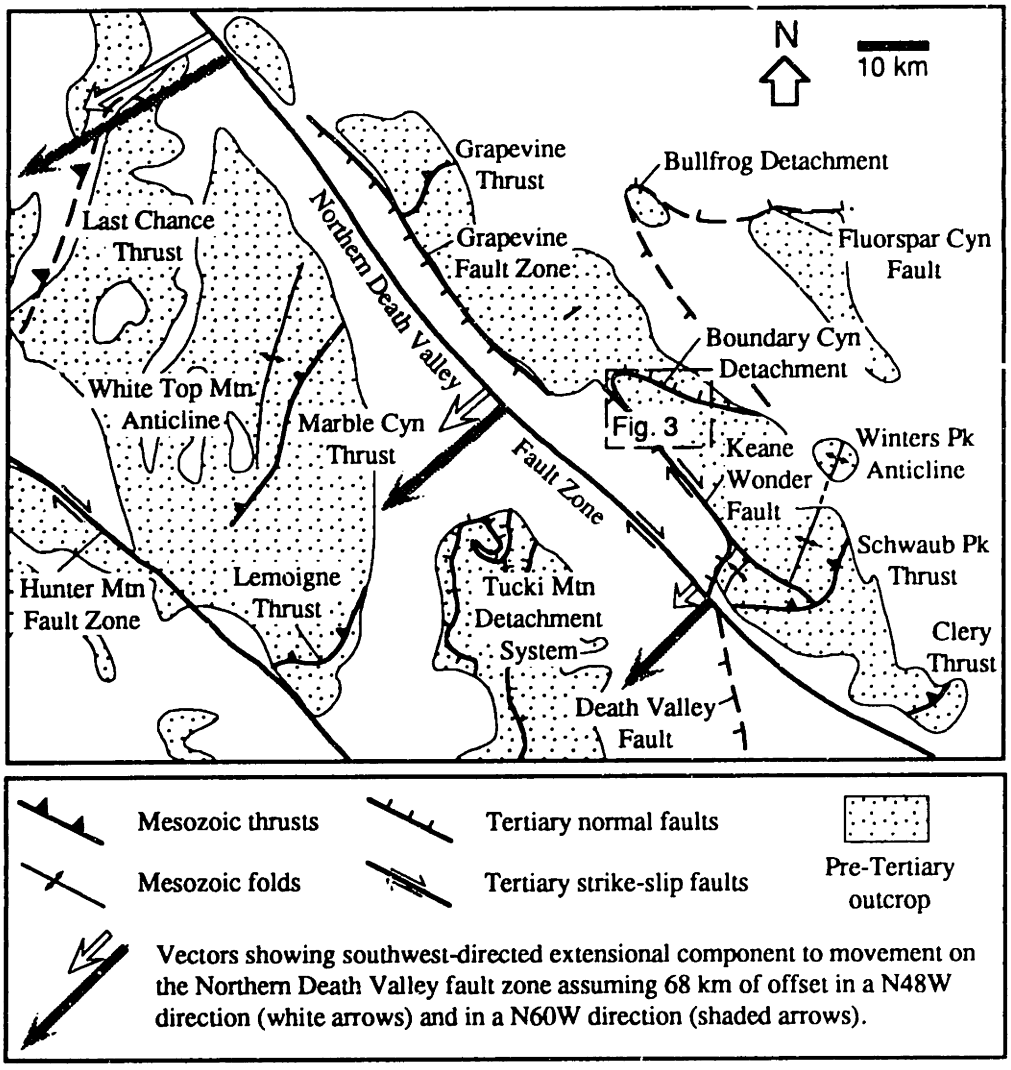
N
10 km
Grapevine Thrust
Grapevine Fault Zone
Bullfrog Detachment
Fluorspar Cyn Fault
Last Chance Thrust
Northern Death Valley
Boundary Cyn Detachment
White Top Mtn Anticline
Marble Cyn Thrust
Fig. 3
Keane Wonder Fault
Winters Pk Anticline
Fault Zone
Schwaub Pk Thrust
Hunter Mtn Fault Zone
Lemoigne Thrust
Tucki Mtn Detachment System
Clery Thrust
Death Valley Fault
Mesozoic thrusts
Tertiary normal faults
Pre-Tertiary outcrop
Mesozoic folds
Tertiary strike-slip faults
Vectors showing southwest-directed extensional component to movement on the Northern Death Valley fault zone assuming 68 km of offset in a N48W direction (white arrows) and in a N60W direction (shaded arrows).

Figure 2

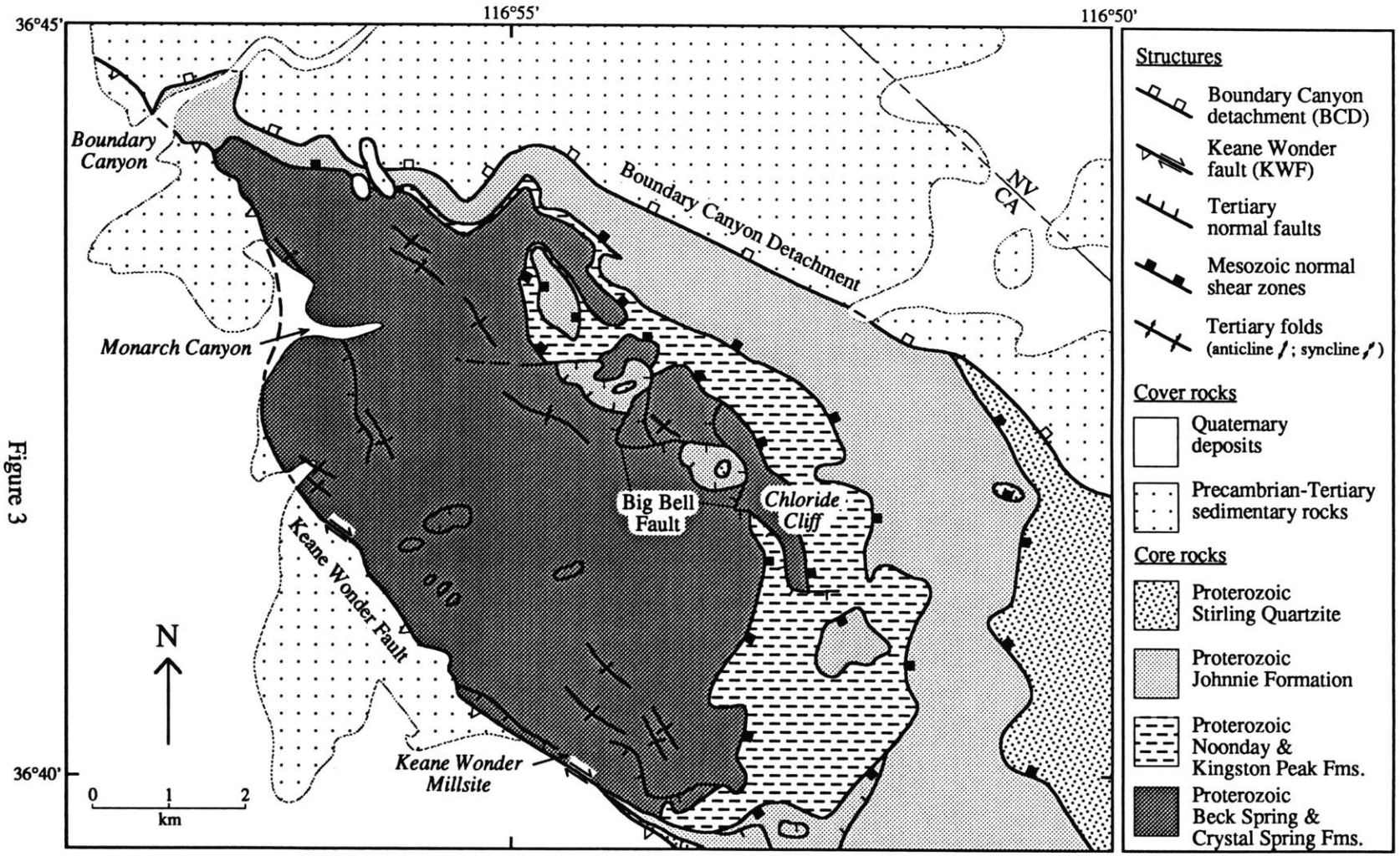
36°45'
116°55'
116°50'
36°40'
Boundary Canyon
Boundary Canyon Detachment
NV
CA
Monarch Canyon
Big Bell Fault
Chloride Cliff
Keane Wonder Fault
Keane Wonder Millsite
N
0 1 2
km
Structures
Boundary Canyon detachment (BCD)
Keane Wonder fault (KWF)
Tertiary normal faults
Mesozoic normal shear zones
Tertiary folds (anticline /; syncline /')
Cover rocks
Quaternary deposits
Precambrian-Tertiary sedimentary rocks
Core rocks
Proterozoic Stirling Quartzite
Proterozoic Johnnie Formation
Proterozoic Noonday & Kingston Peak Fms.
Proterozoic Beck Spring & Crystal Spring Fms.

Figure 3

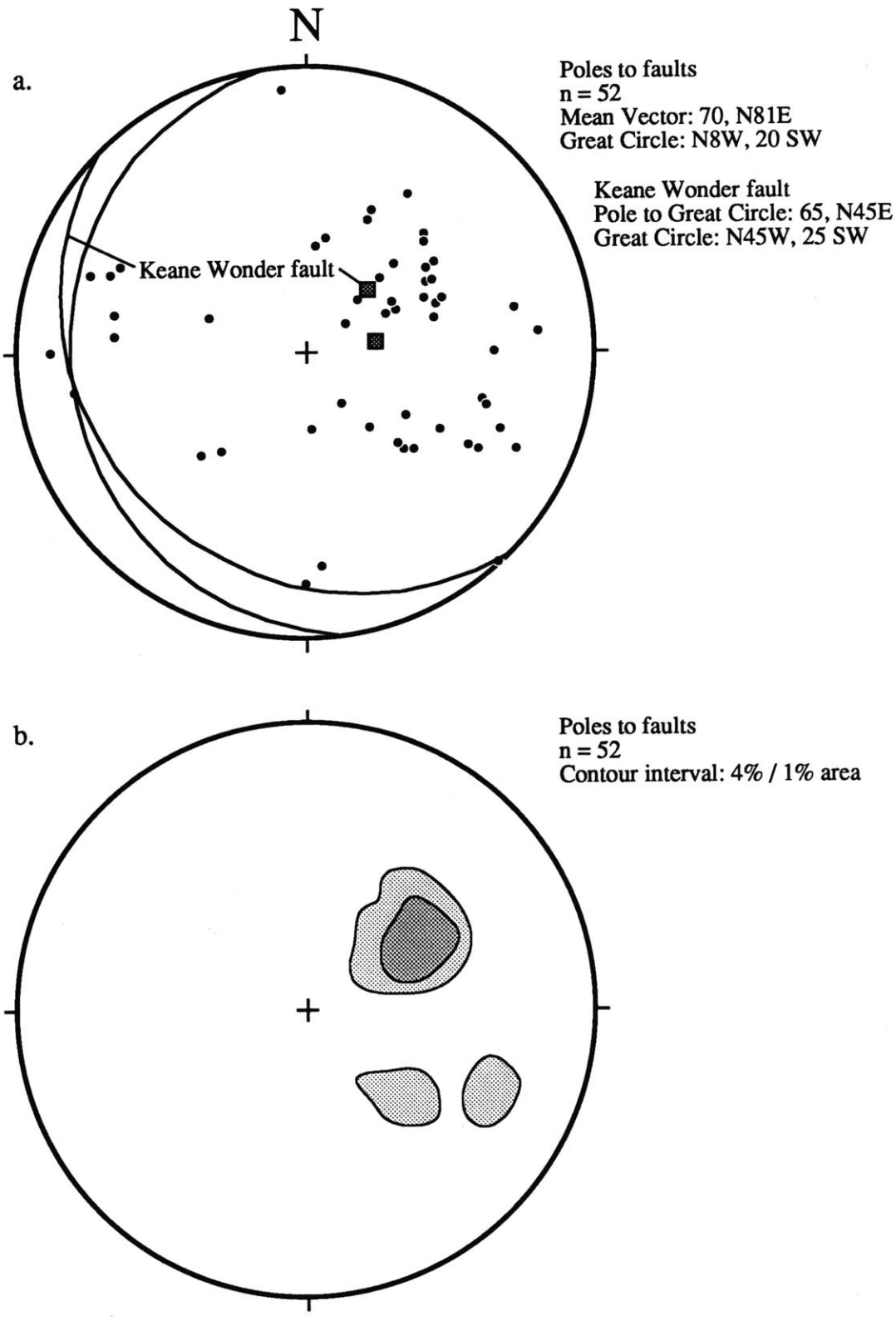
a.
N
Keane Wonder fault
Poles to faults
n = 52
Mean Vector: 70, N81E
Great Circle: N8W, 20 SW
Keane Wonder fault
Pole to Great Circle: 65, N45E
Great Circle: N45W, 25 SW
b.
Poles to faults
n = 52
Contour interval: 4% / 1% area

Figure 4

Figure 5

GEOLOGIC MAP OF THE NORTHERN FUNERAL MOUNTAINS, CALIFORNIA

SCALE 1 : 15,000

METAMORPHIC ROCKS

Neoproterozoic

- Zs — **Stirling Quartzite (basal member)** quartzite and minor schist
- Zj — **Johnnie Formation** pelitic schist, amphibolite, and quartzite
- Znsp — **Noonday Dolomite (Sentinel Peak member)** silty calcite marble

Mesoproterozoic

- Yku — **Upper Kingston Peak Formation** meta-diamictite
- Ykl — **Lower Kingston Peak Formation** pelitic schist, marble
- Yb — **Beck Spring Dolomite** calcite marble
- Ycu — **Upper Crystal Spring Formation** meta-arkose and metaquartzite
- Ycmg — **Middle Crystal Spring Formation (Grey marble member)** calcite marble
- Ycm — **Middle Crystal Spring Formation** silty calcite marble
- Ycl — **Lower Crystal Spring Formation** pelitic schist
- Ycb — **Basal Crystal Spring Formation** amphibolite gneiss, minor pelitic gneiss

SEDIMENTARY ROCKS (units from Wright and Troxel, 1994)

Quaternary

- Qa — **Alluvium** undifferentiated
- Ql — **Landslide deposits**

Tertiary

- Tfc — **Furnace Creek Formation** fanglomerates
- Tsa — **Arkosic sandstone, conglomerate, and siltstone**

Paleozoic/Neoproterozoic

- Cw — **Wood Canyon Formation** sandstone and siltstone
- Zsc — **Stirling Quatzite** dolomite and limestone

IGNEOUS ROCKS

- Td — **Tertiary diabase dikes**
- Kg — **Late Cretaceous granitoid dikes and sills**

MAP SYMBOLS

Contacts

- Depositional contact: accurately, approximately located, hidden
- Fault contact: accurately, approximately located, hidden

Fault Ornamentation

- Extensional shear zone with barbs on hanging wall
- Normal fault with barbs on hanging wall
- Oblique-slip fault with arrows showing sense of lateral movement and barbs on hanging wall

Attitudes

- Strike and dip of foliation
- Trend and plunge of lineation; filled head: stretching and mineral lineation; open head: crenulation hinge lineation
- Trend and plunge of minor fold: upright, overturned
- Trace of axial surface of: antiform, synform, overturned, with plunge

Cross-section Symbols

- Arrows indicate direction of fault movement; circle and cross symbols indicate that upper surface is moving away from the viewer

miles 0 1

kilometers 0 1

N

117°00' 116°45' 36°45' 36°30'

Plate 1

Chloride Cliff Quadrangle 1952 1:62,500

J. David R. Applegate

1994

Lindgren

Plate 1

CROSS SECTIONS TO ACCOMPANY GEOLOGIC MAP OF THE NORTHERN FUNERAL MOUNTAINS, CALIFORNIA

SCALE 1:20,000

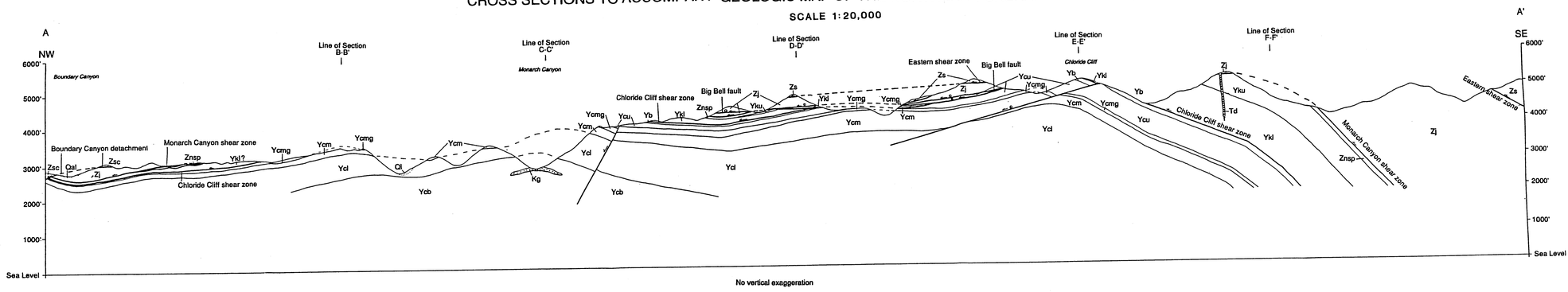

J. David R. Applegate

1994

Plate 2

Lindgren